This is to certify that the

dissertation entitled

Electrical and Magnetic Properties of Alkalides, Electrides and Related Materials and Their Structural and Molecular Dynamical Correlations

presented by

Michael James Wagner

has been accepted towards fulfillment
of the requirements for

Ph.D. degree in Chemistry

James L Dye
Major professor

Date 8/17/94

ELECTRICAL AND MAGNETIC PROPERTIES OF ALKALIDES, ELECTRIDES AND RELATED MATERIALS AND THEIR STRUCTURAL AND MOLECULAR DYNAMICAL CORRELATIONS

By

Michael James Wagner

A DISSERTATION

Submitted to

Michigan State University

in partial fulfillment of the requirements

for the degree of

DOCTOR OF PHILOSOPHY

Department of Chemistry

1994

ABSTRACT

ELECTRICAL AND MAGNETIC PROPERTIES OF ALKALIDES, ELECTRIDES AND RELATED MATERIALS AND THEIR STRUCTURAL AND MOLECULAR DYNAMICAL CORRELATIONS

By

Michael James Wagner

The magnetic and electrical properties of four electrides are presented that are shown to be consistent with that expected of electrons trapped in their cavities. It is shown that strength of the non-orthogonal overlap of electrons in neighboring traps can be directly related to the size and length of the channels which interconnect the cavities. Furthermore, it is shown that the magnetic interactions display dimensionality which is consistent with that of the channels. The electrical properties are shown to be consistent with thin band systems with strong Coulombic repulsions preventing the double occupancy of the cavities. So, while some electrides display high conductivity and small bandgaps, their conductivity is probably due to the hopping of defects.

The properties of four electrides are presented. These include an electride with large, antiferromagnetically coupled six-member electron rings ($[Cs^+$(15-crown-5)(18-crown-6)$e^-]_6$·(18-crown-6)), an electride with "ladderlike" one-dimensional, independent electron chains and what appears to be a spin-Peierls transition (Li^+(C211)e^-), an electride with a very unusual linear chain Heisenberg antiferromagnet (J/k = - 38.3(1) K) to Curie law paramagnetic, irreversible phase transition, and an electride with alternating Heisenberg linear chains.

The properties of electrides are shown to be highly dependent upon thermal history. Irreversible phase changes involving large changes in the physical properties can occur

with little or no decomposition. The changes in two of the electrides presented here are irreversible; however, these changes are probably related to the reversible phase change formerly seen in another electride (Cs^+(15-crown-5)$_2e^-$) whose transition can be quenched. The transitions are postulated to be closely related to the macrocyclic "merry-go-round" motions which are reported in the first section of this thesis.

The final section of this thesis is a report of the magnetic and electrical properties of $[Ru(bpy)_3]^0$. The magnetic properties are shown to be consistent with ligand localization of the HOMO electrons and antiferromagnetic alternating Heisenberg linear chain behavior. The material is highly conductive and probably due to 3-dimensional variable range hopping.

To my parents,
without whom all of this
would not have been possible.

ACKNOWLEDGMENTS

I would like to express my gratitude to Professor James L. Dye for his encouragement, guidance and support during my studies at Michigan State University. Perhaps the most valuable lesson he taught me was that science was fascinating enough to inspire enthusiasm even after forty years of research. I would also like to thank the members of Professor Dye's research group with whom I have worked, in particular Rui Huang, Eric Hendrickson, Jineun Kim, Songzhan Huang, Greggor Overney, Kuo Lih Tsai, Kerry Reidy, Guang Xu, Ching Tung Kuo, Pascal Cauliez, Judy Eglin and Kevin Moeggenborg. In addition, I would like to thank the Master Glassblowers at Michigan State University, Keki Mistry, Manfred Langer and Scott Bancroft, for their efforts in making and fixing the glassware used in my research. I am grateful to Kermit Johnson for assistance with the NMR, Professor Thomas Kaplan for discussions concerning magnetism and Bill Drapier for his patience with my persistent requests for immediate Photostats for publications. My numerous collaborators deserve special thanks; Dr. Dan Neuman, Dr. Julie Borchers, Professor Luis Echegoyen, Eduardo Pérez-Cordero and Rosanna Buigas.

I would like to extend my most sincere gratitude for the encouragement and guidance of Professor David Johnson. His faith in my ability, advise and the chance he gave me to discover the world of research were crucial to my success as a scientist. I would also like to express special thanks to Pat McCarthy for her support and understanding during the composition of this thesis.

I am grateful for the support of the National Science Foundation (Solid State Chemistry Grants DMR 87-14751, DMR 90-17292, INT. 86-19636 and B. P. (VRU)), Air Force Office of Scientific Research (AFOSR Grant F49620-92-J-0523). In addition, I am grateful to the Michigan State University Center for Fundamental Research for continuous research support as well as the Center for Materials Research Fellowship

(1989-1994), the Departmental First Year Fellowship (1989) and the Quill Fellowship (1990-1993) from the Department of Chemistry at Michigan State University , the Dupont Departmental Fellowship (1992) from the Dupont Corporation, the fellowship for full participation in the Workshop on Neutron and Synchrotron Radiation Studies of Materials from the Department of Energy and Brookhaven National Laboratory, and the Graduate Research Award (1994) from the Michigan State chapter of Sigma Xi.

TABLE OF CONTENTS

LIST OF TABLES

LIST OF FIGURES

INTRODUCTION

The study of alkali metal-ammonia solutions is a mature field, beginning nearly two centuries ago with the discovery of blue and bronze potassium-ammonia solutions by Sir Humphry Davy.[1] By contrast, the related crystalline compounds, alkalides and electrides, have been known for only about twenty years. The unusual species found in metal-amine solutions, alkali metal anions and solvated electrons, which have made their study of such an enduring field, both have stochiometric solid state counterparts in alkalides and electrides. The ability to study the unusual electronic and magnetic interactions of these species with each other and their surrounding media makes both of these fields fascinating areas of basic research. However, the presence of well-defined crystalline structures and the youth of the field lends hope that the study of alkalides and electrides will yield an even greater variety of materials with unusual and potentially useful properties.

The production of the vast majority of alkalides and electrides would not have been possible without the syntheses of macrocyclic (crown)[2] and macrobicyclic (cryptand)[3] cation complexants in the late 1960's. Both classes of materials rely on the unique ability of these complexants to strongly bind to the cation (the "macrocyclic effect"). These complexants are highly resistant to reduction, which allows them to bind even in the presence of the strongest reductant known in any given solvent, the solvated electron. Thus, the complexants not only dramatically enhanced the solubility of alkali metals in a number of solvents, but have allowed the production of solutions which are indefinitely stable when properly handled. Furthermore, even when stripped of the solvent, the complexants are not reduced nor do they decomplex when carefully handled. This is the

basis for the crystallization of alkalides and electrides, which are salts of complexed alkali metal cations, charge balanced by alkali metal anions and trapped electrons respectively.

The properties of alkalides and electrides are varied and fascinating. These properties have been the subject of a number of comprehensive review articles.[4-6] While it might appear that nearly twenty years of research would result in a rather complete understanding of these materials, this is not the case. Both classes of materials are highly reactive and thermally unstable. The handling techniques necessary for more or less routine crystal structure determination were developed less than a decade ago;[7] in fact, until then only a single alkalide structure[8] and no electride structures had been solved. Even the synthesis and characterization of polycrystalline electrides was fraught with difficulties in obtaining consistent results due to the inherent instability of these compounds. Thus, only recently have a sufficient number of alkalides and electrides been characterized reliably enough to confidently make generalizations about their structure-property relationships. It is the intent of this thesis to further the foundation with which to explore these relationships.

The body of this thesis is subdivided into four interrelated chapters. The first of these chapters consists of studies of the molecular dynamics of crown ethers in alkalides. The types of motion outlined in this chapter may have a profound effect on the properties electrides as will be pointed out in the second chapter. Taken as a whole, the second chapter is a study of the relation of the structure to the magnetic and electrical properties of four of the five electrides with known structure. The third of these chapters is the first study to be completed in a new thrust area of this laboratory; production of "expanded atoms"[9] or "synthetic bucky-balls". These materials, as is explained in the chapter, are closely related to electrides as well as to alkali metal doped fullerenes and hold great promise of novel properties. Following these three chapters is a summary of a few the projects which I have initiated that show great promise but which have not been sufficiently explored to warrant separate chapters.

The sections within the chapters of this thesis are written to be self-contained in order to ease their individual publication. Many of these sections are either published or are manuscripts ready for publication; others consist of material intended to be combined with the work of other lab members in manuscripts which are in preparation. A short introduction is included before each section in order to explain their origin or intended destination. Since the sections are largely self-contained, no discussion of theory or synthetic methods is included under separate headings. Sufficient theoretical background is included within each section and the citations therein (which are included at the end of each section) to fully comprehend the analysis presented. Further details of the synthetic methods employed can be found in previous publications.[10-13]

CHAPTER I

I.A Introduction

Alkalides and electrides may be considered to be salts with very large cations (8-10 Å diameter). The crystal structure of an individual alkalide or electride is largely determined by the packing of these cations; the anions, in most cases, merely fit into the vacancies left in the lattice of closest packed cations. However, the cations in these salts are not single atoms; they are alkali metal cations complexed by crown ethers or cryptands ("expanded cations"). This makes them rather different from "classical" salts in which the cation is a single atom. Expanded cations are not necessarily isotropic nor do questions about their conformation, rotations, internal vibrations or reorientations have obvious answers. Since the interactions of the cations and the anions are regulated by the intervening complexant, such questions may have great importance in understanding and eventually engineering the properties of these unusual salts. This chapter represents the first attempt to answer questions about the molecular dynamics of crown ether complexants in alkalides.

I.B NMR Study of Crown Ether Motion in Two Alkalides

This section is in the form of a paper entitled "NMR Study of Crown Ether Motion in Two Alkalides" which was published in *The Journal of Physical Chemistry*, volume 96, in the year 1992 and starting on page 9656. The study of NMR relaxation times was initiated by the co-authors and early experiments were carried out at Cambridge University in the laboratories of Dr. Peter Edwards. However , all of the final data reported in the paper were obtained by me at MSU. As a result, I was responsible for all data and analysis included in the paper. I also wrote the draft of this paper .

I.B.1 Introduction

Alkalides are salts formed from alkali metal cations encapsulated in either crown ethers or cryptands, charge balanced by alkali metal anions. Previous characterization techniques have included X-ray diffraction, optical spectroscopy, EPR, magnetic susceptibility, powder and single crystal NMR, powder and single crystal conductivity, photoelectron emission, photoluminescence, laser flash photolysis and differential scanning calorimetry[1].

Little is known about the dynamics of alkalides. Single crystal structures have given low temperature static structural information. The "fade-out" of the high angle powder diffraction pattern as temperature is raised above 203 K indicates that these structures are not conformationally locked at higher temperatures.[2] However, the nature of the motion in these compounds is not known.

Buchanan et al. have recently studied molecular motion in crown ether complexes. They concluded from ^{13}C CP/MAS NMR studies[3,4] of numerous model complexes that a large amplitude X-ray transparent motion was present at ambient temperatures. Further study by ^{2}H NMR lineshape analysis[5] identified the motion in 18-crown-6 (18C6)[6]

complexes to be a 6-site combined macrocyclic rotation and conformational adjustment. This motion was termed a "molecular merry-go-round" due to its similarity to the motion of the carnival ride.

The present investigation was undertaken to determine the nature of motion in sodides. NMR relaxation studies were chosen since they can measure both activation barriers and correlation times associated with slow molecular rotations.[7] The high sensitivity of ^{133}Cs and ^{23}Na NMR made these nuclei natural choices for study. Two alkalides with different complexing crown ethers, $Cs^+(18C6)_2Na^-$ and Cs^+(15-crown-5)$_2Na^-$ ($Cs^+(15C5)_2Na^-$),[8] were chosen to examine the effect of the crown ethers on the motion.

I.B.2 Experimental

$Cs^+(18C6)_2Na^-$ and $Cs^+(15C5)_2Na^-$ were synthesized by anaerobically dissolving stoichiometric amounts of cesium and complexant in dimethyl ether in the presence of approximately 50% excess sodium metal in a modified H-cell.[9] Care was taken to ensure that the temperature of the reaction mixture never exceeded -40 °C. By pouring the saturated solution through a frit, it was isolated from the excess sodium. Crystals were formed by the addition of trimethylamine and further cooling. Details of the purification of materials and of the synthetic methods used have been described in detail elsewhere.[10]

Preliminary ^{23}Na relaxation studies were carried out at both Michigan State University and Cambridge University.[11] These measurements demonstrated the general trends for $Cs^+(18C6)_2Na^-$, but had limited signal-to-noise ratios and some uncertainties in sample temperature. The results for $Cs^+(15C5)_2Na^-$ were further complicated by sample impurities and the limited temperature range over which the data were obtained.

The NMR spectra presented here for polycrystalline samples were obtained at the Max T. Rogers NMR facility at Michigan State University. All measurements were made

with a 9.3950 Tesla Varian VXR 400S NMR spectrometer equipped with a Varian variable temperature 5 mm wideline probe and a 1 kilowatt pulse amplifier. Temperature control was facilitated by a flow of dry, cold nitrogen gas. The sample temperature was taken to be that of a thermocouple placed near the sample. The temperature was allowed to equilibrate for at least ten minutes after the thermocouple indicated that the set point had been reached and stabilized. A saturation recovery pulse sequence was used to measure the nuclear spin-lattice relaxation times (T_1) of the central (+1/2 ´ -1/2) transitions. Ninety degree pulse lengths of 1.4 and 2.4 μs were employed for ^{133}Cs and ^{23}Na respectively. Chemical shifts are referenced to the appropriate aqueous cation at infinite dilution.

I.B.3 Results

The structures of $Cs^+(18C6)_2Na^-$ and $Cs^+(15C5)_2Na^-$ were previously determined[12,13]. Cs^+ is encapsulated ('sandwiched') by two crown ether molecules and strongly coordinated to the etheral oxygens. The crown ether protons tend to be oriented away from the central cation. The Na^- ion is located in the cavity between eight crown ether sandwiches and is therefore in the midst of a 'sea' of protons.

The central transition powder patterns for the ^{23}Na resonances were gaussian for both samples, centered at -62 and -61 ppm for $Cs^+(18C6)_2Na^-$ and $Cs^+(15C5)_2Na^-$ respectively (Figure 1). The ^{23}Na chemical shift is diagnostic for Na^-.[14-17] The gaussian lineshape is a result of the spherical nature of the spin 3/2 Na^- anion; the only significant contribution to the static line width is dipolar coupling with the crown ether protons.[12]

The ^{133}Cs central transition powder patterns showed evidence of anisotropy in the screening tensor in both samples. The ^{133}Cs central transition of $Cs^+(18C6)_2Na^-$ is nearly gaussian at low temperatures, centered near -61 ppm, a chemical shift that is characteristic of Cs^+ complexed by two 18C6 molecules in alkalides and model salts[18,19] At higher temperatures, dipolar contributions decreased, revealing dipolar-broadened, non-axial

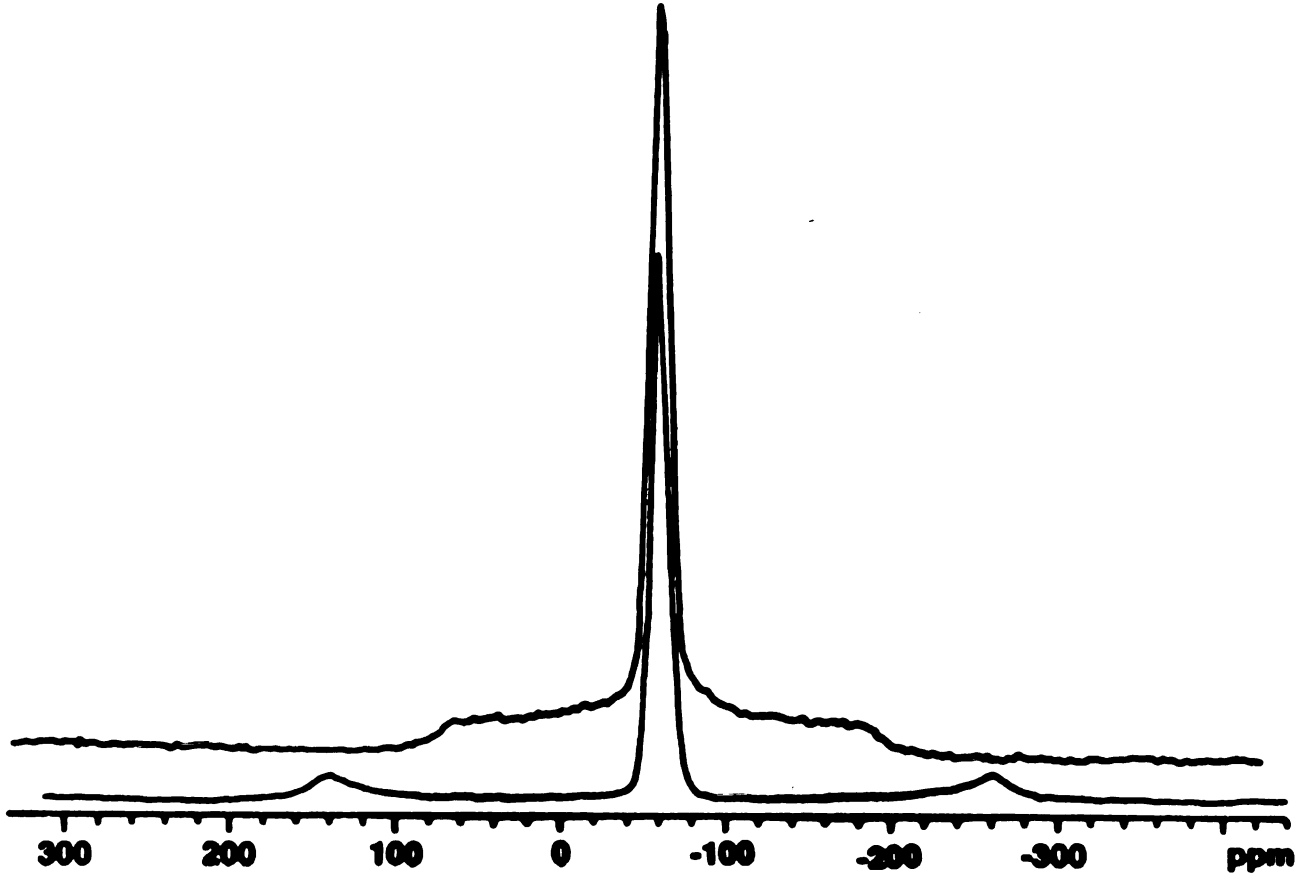

Figure 1: ^{23}Na spectrum of $Cs^{+}(18C6)_2Na^{-}$ at 273 K (lower curve) and $Cs^{+}(15C5)_2Na^{-}$ at 253 K (upper curve).

chemical shift anisotropy (CSA) and the presence of satellites from non-central transitions (Figure 2). The predominant mechanism that contributes to the static linewidth below 230 K was previously shown to be dipolar coupling to the crown ether protons.[12] The ^{133}Cs central transition of $Cs^+(15C5)_2Na^-$ displays non-axial chemical shift anisotropy over the entire temperature range, becoming very nearly axially symmetric as the temperature was raised above 291 K (Figure 3). The breadth of this transition caused experimental difficulties and its relaxation behavior is not discussed in this paper.

The spin-lattice relaxation behavior of the ^{133}Cs and ^{23}Na nuclei could be fit well by a single exponential at each temperature. As shown in Figure 4, the temperature dependence of the relaxation times can, in all cases, be fit to within experimental error by the equation

$$T_1^{-1} = aT^2 + b\exp(-E_a/RT), \qquad (1)$$

where the first term is associated with Raman type coupling to lattice vibrations or molecular librations and the second term is interpreted as arising from coupling to a thermally activated molecular rotation.[20] The parameters a, b and E_a are given in Table 1.

Rapid changes in the linewidth of the ^{23}Na resonances were also observed (Figure 5). The onset temperature for the linewidth change can be used to approximate an activation energy with the approximate formula of Waugh and Fedin[21] for the calculation of hindered-rotation barriers,

$$E_a \text{ (kJ mol}^{-1}) \approx 0.155T_c(K). \qquad (2)$$

The results are included in Table 1.

Satellites from other transitions were observed for the ^{23}Na spectra of both compounds and the ^{133}Cs spectra of $Cs^+(18C6)_2Na^-$, but analysis was carried out only on

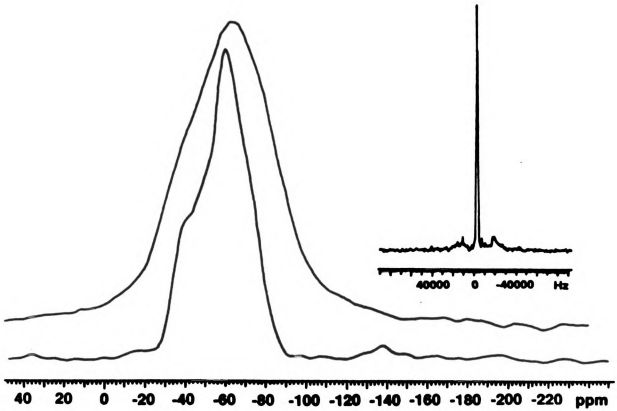

Figure 2: ^{133}Cs spectra of $Cs^{+}(18C6)_2Na^{-}$. Upper spectrum at 173 K, lower at 273 K, inset: complete spectrum at 273 K that shows satellites.

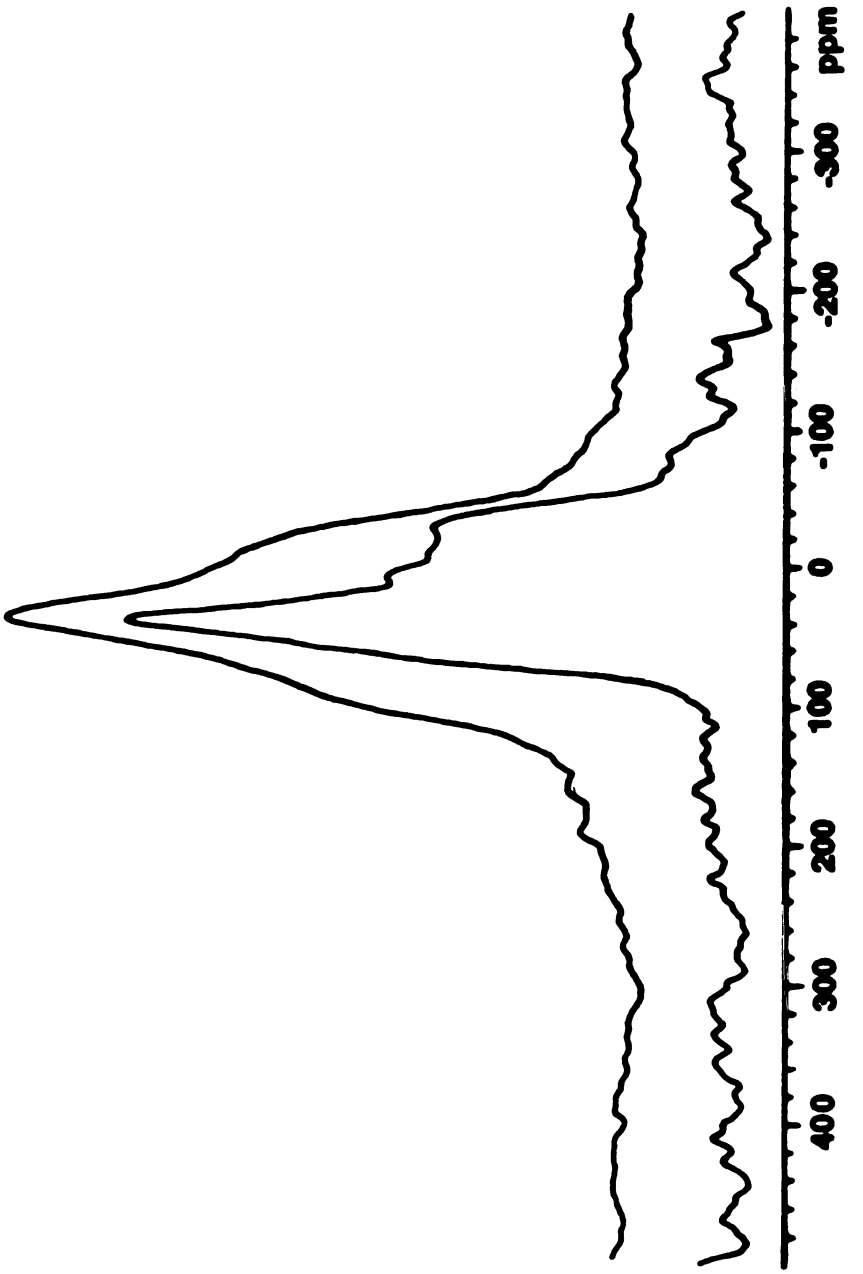

Figure 3: ^{133}Cs spectrum of $Cs^{+}(15C5)_2Na^{-}$. Upper spectrum at 173 K, lower at 291 K.

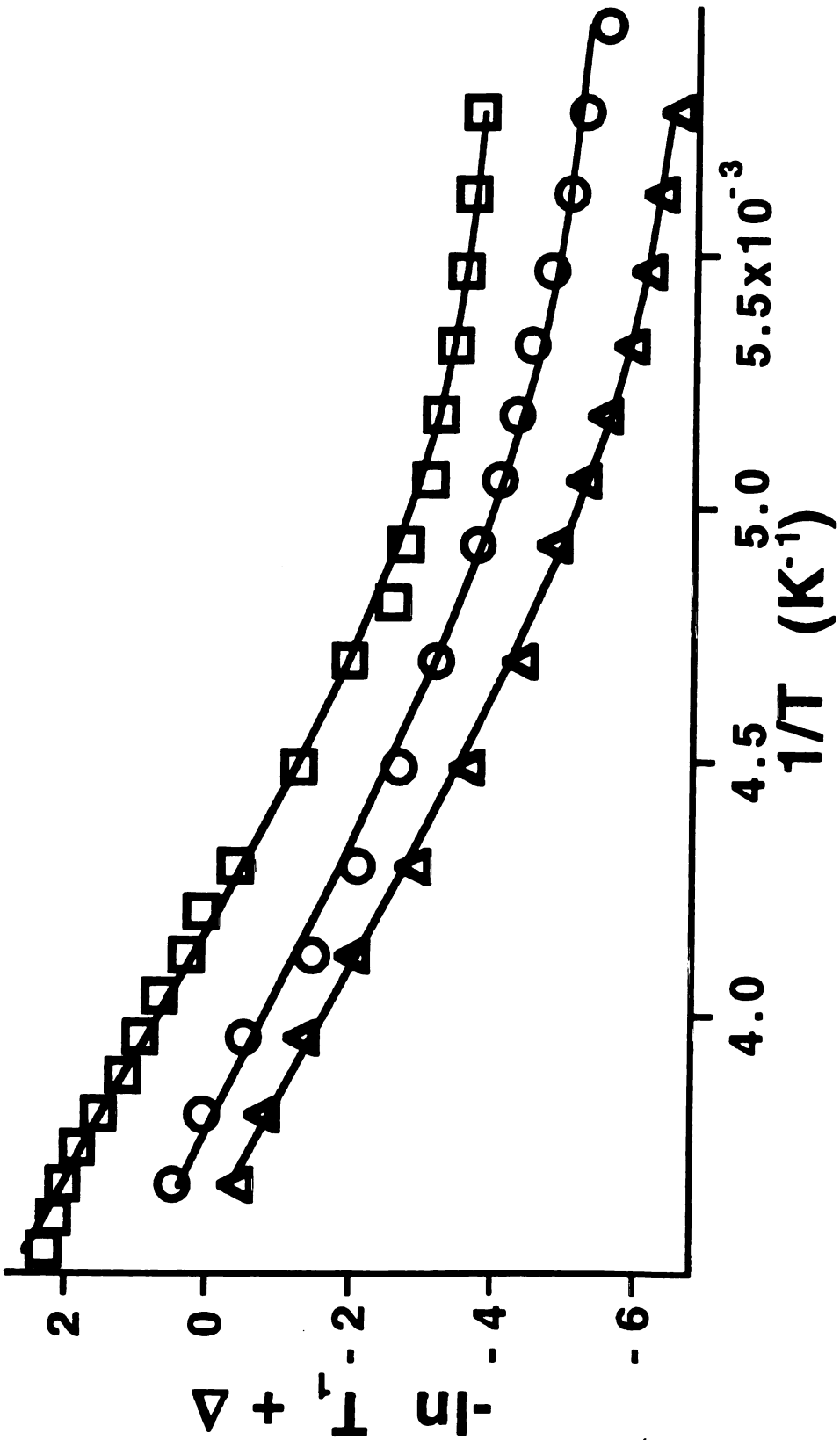

Figure 4: Fits of relaxation data by $T_1^{-1} = aT^2 + b\exp(-E_a/RT)$: $Cs^+(15C5)_2Na^-$ (^{23}Na NMR), $\Delta = 1$ (squares); $Cs^+(18C6)_2Na^-$ (^{23}Na NMR) $\Delta = 0$ (circles); $Cs^+(18C6)_2Na^-$ (^{133}Cs NMR), $\Delta = -1$ (triangles). The offset Δ has been added for graphical clarity.

Table 1: Fitting parameters from analysis of NMR data.

Compound	$Cs^+(18C6)_2Na^-$	$Cs^+(18C6)_2Na^-$	$Cs^+(15C5)_2Na^-$
nucleus	^{133}Cs	^{23}Na	^{23}Na
T1 analysis [a] E_a (kJ mol^{-1})	32.5(8)[b]	29.9(13)	35.4(7)
a ($s^{-1}K^{-2}$)	1.30(11) x 10^{-7}	1.70(17) x 10^{-7}	2.75(16) x 10^{-7}
b (s^{-1})	3.2(13) x 10^{+6}	7(5) x 10^{+5}	1.8(7) x 10^{+7}
Waugh analysis [c] E_a (kJ mol^{-1})	---	29.9 to 31.8	30.5 to 31.5
Correlation time [d] at T_M (s)	---	4.78(11) x 10^{-4} (222 K)	5.3(2) x 10^{-4} (211 K)

(a) Equation 1
(b) Standard deviation estimates of the last digit are given in parentheses.
(c) Equation 2
(d) Equation 7

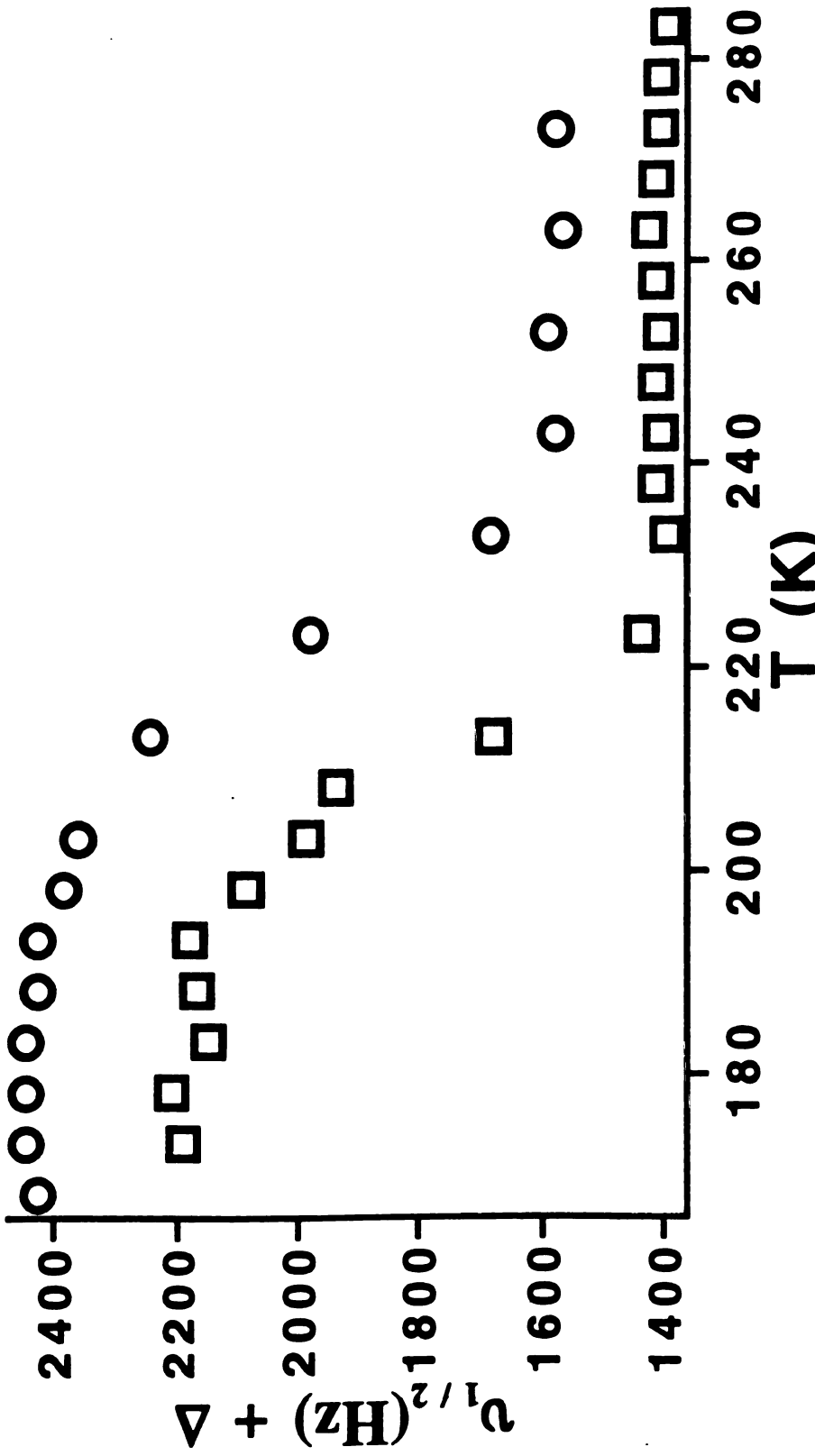

Figure 5: Dependence of the full width at half-height of the ^{23}Na central transition on temperature: $Cs^+(15C5)_2Na^-$, Δ = 0 Hz (squares); $Cs^+(18C6)_2Na^-$, Δ = 300 Hz (circles). The offset Δ has been added for graphical clarity.

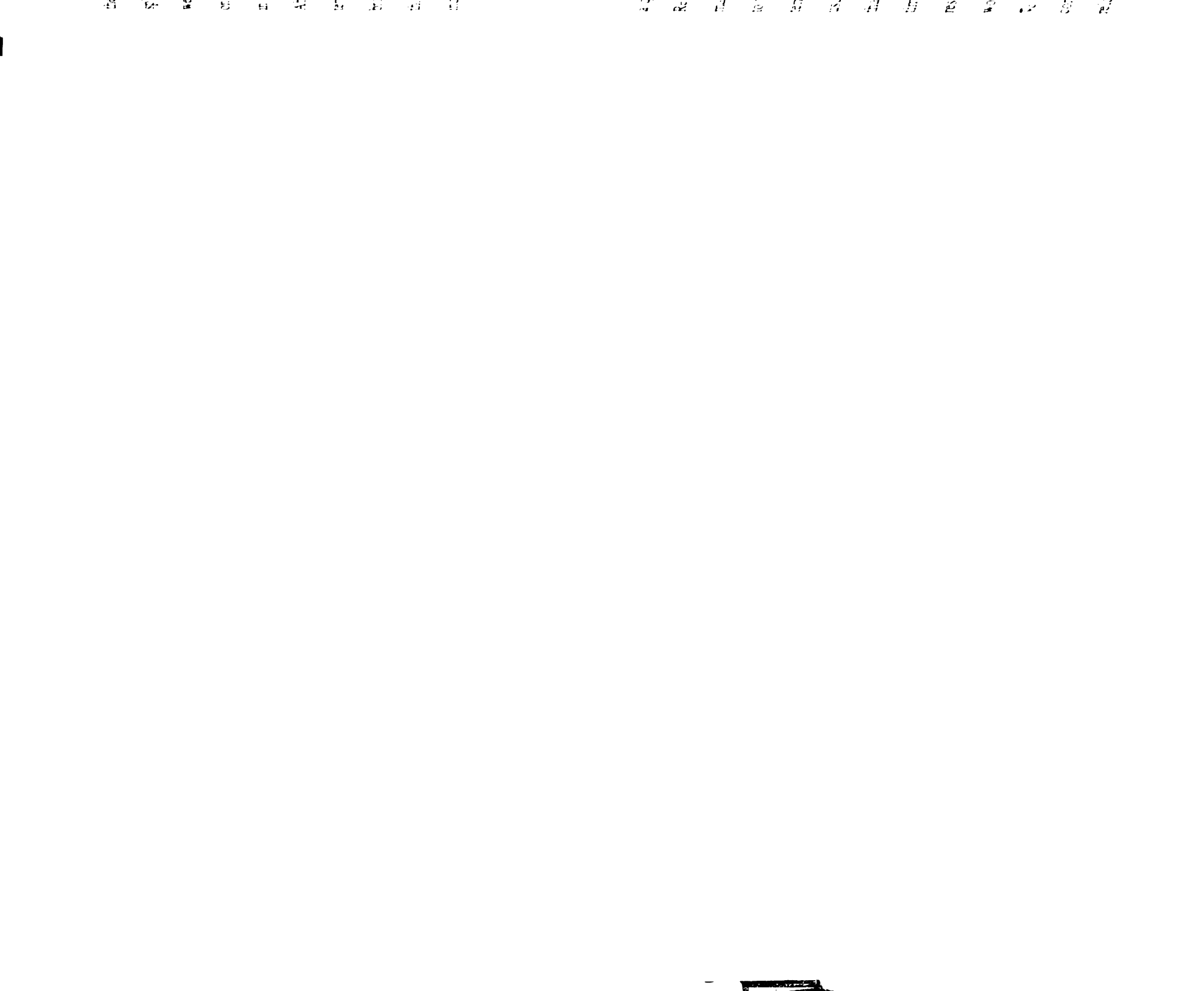

the former. The small value of the quadrupole coupling constant is further evidence of the spherical nature and the large size of the Na^- anion. The ^{23}Na satellites of $Cs^+(15C5)_2Na^-$ were observable from 173 to 283 K. The dependence of the ^{23}Na quadrupole frequency on temperature, as measured from satellite separation,[20] is shown in Figure 6. The scatter in the data at low temperatures reflects the increase in uncertainty as the pattern broadens. Above about 200 K, the observed quadrupole frequency, w_Q , changes linearly with temperature. The ^{23}Na satellites of $Cs^+(18C6)_2Na^-$ were only observed above 263 K; they broadened and became unobservable at lower temperatures. The quadrupole frequency in this case is also temperature dependent, but was only measured at two temperatures as indicated in Figure 6.

I.B.4 Discussion

Relaxation Mechanism. The relaxation of magnetization to equilibrium through a quadrupolar mechanism for $I > 1$ was shown by Hubbard to be multiexponential.[22] Relaxation can, however, be described by a single exponential when spin-spin interactions maintain a single spin temperature.[20] Strong homogeneous heteronuclear dipolar coupling to the crown ether protons is evidently responsible for the maintenance of a single spin-temperature for both ^{23}Na and ^{133}Cs in the compounds studied. We will assume, as is usually done, that the correlation function for the motion is exponential. It then follows that the spectral density, $J(\omega)$, is proportional to $\tau_c/(1+\omega_0^2\tau_c^2)$ where τ_c is the correlation time of the modulation of the electric field gradient (EFG). As we show later, the motion responsible for relaxation is probably an anisotropic rotation/re-orientation and thus one would expect a distribution of correlation times rather than a single, well defined value of τ_c. However, this treatment provides a rough comparison of quadrupolar and dipolar contributions to the spin-lattice relaxation. With these assumptions, the spin-lattice relaxation rate due to quadrupolar relaxation is described by[23]

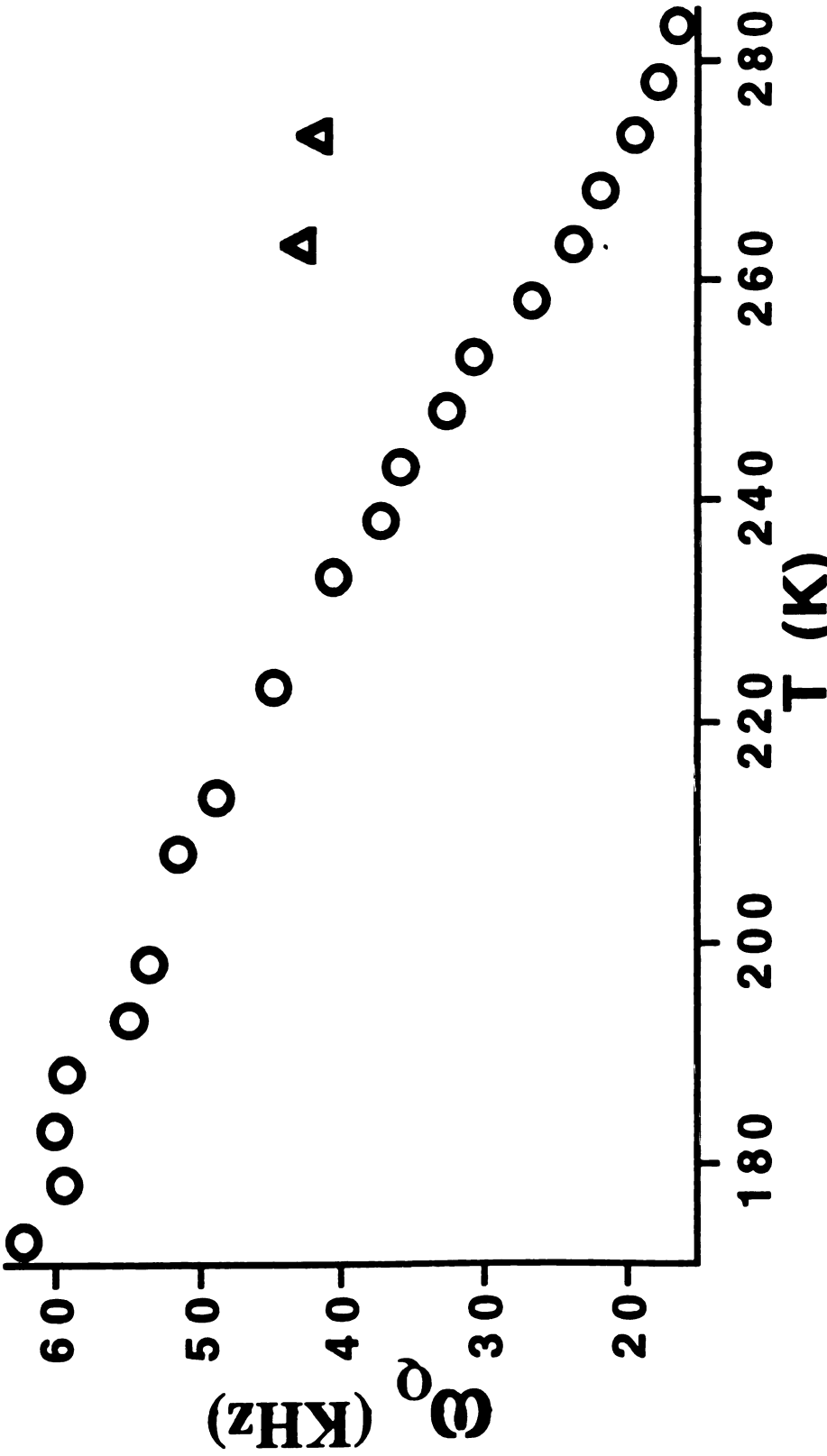

Figure 6: Dependence of the ^{23}Na quadrupole frequency on temperature: $Cs^+(15C5)_2Na^-$ (circles); $Cs^+(18C6)_2Na^-$ (triangles).

$$(1/T_1)_Q = C_Q[\tau_c/(1+\omega_o^2\tau_c^2) + 4\tau_c/(1+4\omega_o^2\tau_c^2)] \qquad (3)$$

where C_Q, the square of the interaction energy, can be approximated by $(1/25)(e^2qQ/h)^2(1+\eta^2/3)$, with e^2qQ/h being the rigid lattice quadrupole coupling constant(QCC) and η being the asymmetry parameter.

Relaxation by a heteronuclear dipolar mechanism is also expected to be bi-exponential in general.[20] As in the quadrupolar case, magnetization may decay as a single exponential when a single spin temperature is maintained. Again, we assume that a single τ_c describes the modulation of the dipolar interactions although one might expect a distribution depending on the orientation of the various internuclear vectors and on the diffusion coefficients.[24] We will only consider rotations; the description does not necessarily apply to the dipolar relaxation of ^{23}Na nuclei by protons since the motional model proposed involves changes in both angles and individual internuclear distances . Changes in internuclear distances in the case of the ^{133}Cs nuclei, however should be negligible and appear in the quadradic term of equation 1. The relaxation of a nucleus of spin I by nuclei of spin S, assuming an exponential correlation function, is described by[25]

$$1/T_1 = C_D\{3\tau_c/(1+\omega_I^2\tau_c^2) + \tau_c/[1+\tau_c^2(\omega_I-\omega_S)^2] + 6\tau_c/[1+\tau_c^2(\omega_I+\omega_S)^2]\} \qquad (4)$$

where ω_I and ω_S are the Larmor frequencies of the indexed spins; C_D is analogous to C_Q and is equal to $(2/15)\gamma_I^2\gamma_S^2h^2S(S+1)\sum r_{IS}^{-6}$. The second moment of a resonance line broadened by heteronuclear dipolar interactions with nuclei at distance r_{IS} is[20]

$$M_2=(4/15)\gamma_I^2\gamma_S^2h^2S(S+1)\sum r_{IS}^{-6} \qquad (5)$$

If all nuclei contributing to the second moment are involved in the motion, C_D is simply equal to one half of the second moment.

The contributions to spin-lattice relaxation from electronic and magnetic interactions with lattice motion are, to a first approximation, proportional to the squares of their interaction energies.[26] In the case of the ^{23}Na nuclei in $Cs^+(18C6)_2Na^-$, the two strongest interactions are heteronuclear dipolar coupling to the neighboring protons and the coupling of its quadrupole moment to the EFG. The square of the dipolar interaction energy may be approximated by one half of the second moment, which is equal to $(\upsilon_{1/2}/2.36)^2$ for a gaussian line, in which $\upsilon_{1/2}$ is the full width at half-height.[20] The rigid lattice linewidth associated with heteronuclear dipolar coupling was previously calculated to be 2520 Hz using known crystallographic information and all protons within 7.0 Å.[12] The rigid lattice QCC is not known; however, the motionally averaged QCC at 263 K is known from the observed satellite separation(for I = 3/2, QCC = $2\omega_Q$). The rigid lattice QCC should be much larger than this.[27] Even the rigid lattice QCC may understate the importance of a quadrupole mechanism, since motion may give rise to a time dependent EFG which is larger than one might expect from the rigid lattice EFG, as for example, in ionic crystals where the nuclei have cubic symmetry.[26] The motionally averaged QCC however, may be used as a lower limit estimate of the quadrupole interaction energy. Comparing one half of the second moment(0.57 MHz^2) to 1/25 of the square of the motionally averaged QCC at 263 K(74.5 MHz^2 assuming $\eta = 0$) shows that the quadrupole contribution to T_1 is more than 130 times more important than the dipolar contribution. The dominance of a quadrupolar relaxation mechanism for ^{23}Na in $Cs^+(15C5)_2Na^-$ can be demonstrated by a similar argument.

The relaxation of ^{133}Cs in $Cs^+(18C6)_2Na^-$ is also due to a quadrupolar mechanism. This can be seen by estimating the interaction energy necessary to effect the observed relaxation and comparing it to an estimate of the dipolar interaction energy. Normally, one would simply calculate C_Q or C_D by finding the T_1 minimum experimentally. The thermal

instability of the studied alkalides prevented us from making measurements at a sufficiently high temperature to find such a minimum in the nuclear relaxation times. Thus we must turn to the linewidth data to calculate correlation times.

The rotational motion responsible for the modulation of the EFG is the same one which modulates the dipolar interactions leading to motional narrowing. The similarity of the activation barriers as calculated by T_1 relaxation data and linewidth data is strong evidence for this. The motional narrowing takes place at long correlation times when T_1 relaxation caused by the molecular rotation is just beginning to dominate that caused by lattice vibrations. Motional narrowing begins when the inverse of the correlation time of the modulation of the local dipolar field is on the order of the static linewidth and is complete when $1/\tau_c$ is much larger than the static linewidth. The correlation times can be calculated by[28,29]

$$\delta w^2 = \delta w''^2 + (\delta w'^2 - \delta w''^2)(2/\pi)\tan^{-1}[\alpha\delta w\tau_c], \qquad (6)$$

where δw is the measured linewidth, $\delta w''$ is the motionally averaged linewidth, $\delta w'$ is the linewidth of the rigid lattice and α is a numerical factor on the order of unity. Setting α to unity, the correlation time at the temperature (T_M) at which point one half the total narrowing has been completed is[30]

$$\tau_c(T_M) = 0.41/(\delta w' - \delta w''). \qquad (7)$$

Values calculated for each compound are included in Table 1. Assuming that the dipolar field is modulated at the same frequency as the EFG, insertion of the correlation time calculated by Equation 6 into the equations for spin-lattice relaxation times (3 and 4) gives estimates of C_Q and C_D.

Comparison of the value of C_D estimated by using the linewidth calculated from crystallographic information (1350 Hz so 1/2 M_2 = 0.16 MHz^2)[12] to the C_D estimated above (31 GHz^2) shows that the dipolar field is more than 400 times too weak to account for the observed relaxation times of ^{133}Cs in $Cs^+(18C6)_2Na^-$. The relaxation must therefore be due to quadrupolar interactions. This is to be expected since, although analysis of the satellites was not attempted, they show that the quadrupolar interaction is clearly much larger than the dipolar interaction near 273 K; furthermore, the rigid lattice quadrupolar interaction should be much larger than that seen at 273 K. Rough estimates of the rigid lattice QCC's, using the approximation for C_Q given above, assuming that the entire EFG is modulated by the motion and that $\eta = 0$, yields a value near 1 MHz for Cs in $Cs^+(18C6)_2Na^-$ and 2 MHz for Na in both compounds.

Motional Model. Relaxation, linewidth and quadrupole frequency data all indicate the influence of a molecular rotation. Low temperature relaxation is dominated by quadrupolar coupling to lattice vibrations or molecular librations while above 200 K it appears to be dominated by coupling to some molecular rotation. The reduction of linewidth occurs when the correlation time for this rotation is comparable to the static linewidth.[20] The decrease in ω_Q is indicative of motional averaging of the electric field gradient due to a rotation.[20]

Further evidence for a molecular rotation is provided by the ^{133}Cs lineshape for $Cs^+(15C5)_2Na^-$. At low temperatures, when the rotational correlation time is long, the lineshape is a non-axially symmetric CSA pattern as expected from the crystal structure. As the correlation time shortens (higher temperature), the lineshape changes towards an axial pattern, until at 291 K, the lineshape corresponds to a very nearly axially symmetric interaction. These data are consistent with a rotation of the encapsulating crown ethers. The lack of complete axial symmetry could result from remaining anisotropies even in the presence of rotational motion.

Recent powder X-ray diffraction studies of 15C5 sandwich alkalides and electrides suggest that the 'locked' crystalline structures seen in single crystal studies become fluctional at temperatures above 203 K.[2] With the exception of a few low angle peaks, the well defined peak structure fades into an amorphous background as temperature is increased. In most cases, including $Cs^+(15C5)_2Na^-$, the process is reversible. Single crystal studies performed at 213 K show no sign of large amplitude motion even though motional narrowing begins at about 200 K.[12,13] This is consistent with a macrocyclic rotation in which the crown ether molecules hop from one crystallographic conformation to an equivalent one. At low temperatures (long τ_c), the time spent hopping is much shorter than the residence time in a given conformation. As the temperature is raised, the time spent in motion becomes more significant and the average structure becomes more disordered. This could explain the fade out of the powder X-ray pattern. Furthermore, torsional oscillations of the individual -O-CH_2-CH_2- groups, which could account for the low temperature relaxation behavior, would also contribute to a fade out of the pattern.

I.B.5 Conclusions

Ratcliffe et. al. have characterized motion in crown ether model complexes.[5] They concluded that the motion was a combined macrocyclic rotation and conformational adjustment, involving the jumping of individual -O-CH_2-CH_2- groups to adjacent crystallographic sites. Their model for motion in these complexes is also consistent with the evidence presented in this paper for motion in two "sandwich type" sodides. The motion would be X-ray transparent when the time spent in motion is small compared to the time spent in the equilibrium positions. The wash out of high angle powder X-ray peaks, leaving a few low angle peaks intact, occurs as the correlation time shortens with rising temperature. Such a process should be reversible, and it is found to be so.

In light of the conclusion that rotation of the macrocycle is responsible for the sharp changes in linewidth, quadrupole frequency, spin-lattice relaxation, lineshape and powder X-ray patterns, the vibrations causing low temperature relaxation can be identified. These vibrations are almost certainly torsional oscillations of the individual $-O-CH_2-CH_2-$ units. Oscillations of this type would certainly be expected since the high temperature motion involves this type of conformational adjustment. The high frequency modulation of the electric field gradient by these librations induces relaxation through a Raman-type indirect process. At temperatures above 200 K, the modulation of the EFG by the macrocyclic rotation/conformational adjustment dominates the T_1 relaxation of both ^{133}Cs and ^{23}Na.

I.B.6 Acknowledgments

This research was supported by NSF Grants DMR 87-14751, DMR 90-17292, INT. 86-19636 and B. P.(VRU). We would also like to express our gratitude to the Michigan State University Center for Fundamental Materials Research for some of the instrumentation used in this work. We thank Professor James Yesinowski for helpful discussion.

REFE

1 F
P
A
&
D

2 D

3 B

4 B
S

5 R
C

6 I
a

7 F

8 I
1

9 K

10

11

12

13

14

15

16

17

18

REFERENCES

(1) For reviews and references see Dye, J. L.; Jackson, J. E.; Cauliez, P. in Proceedings of the Fifth International Kyoto Conference on New Aspects of Organic Chemistry, in press; Dye, J. L. *Science* **1990**, *247*, 663; Dye, J. L.; DeBacker, M. G. *Ann. Rev. Phys. Chem.* **1987**, *38*, 271; Dye, J. L. *Prog. Inorg. Chem.* **1984**, *32*, 327.

(2) Doeuff, S.; Tsai, K.-L.; Dye, J. L. *Inorg. Chem.* **1991**, *30*, 849.

(3) Buchanan G. W.; Kirby, R. A. *Tetrahedron Lett.* **1987**, *28*, 4783.

(4) Buchanan, G. W.; Morat, C.; Ratcliffe C. I.; Ripmeester, J. A. *J. Chem. Soc., Chem. Commun.* **1989**,1306.

(5) Ratcliffe, C. I.; Ripmeester, J. A.; Buchanan G. W.; Denike, J. K. *J. Am. Chem. Soc.*, **1992**, *114*, 3294.

(6) IUPAC name: 18-crown-6; 1,4,7,10,13,16-hexaoxacyclooctadecane, abbreviation 18C6.

(7) Fyfe, C. A. Solid State NMR for Chemists, C. F. C. Press, Ontario, 1983.

(8) IUPAC name: 15-crown-5; 1,4,7,10,13-pentaoxacyclopentadecane, abbreviation 15C5.

(9) Kim, J., PhD. Dissertation, Michigan State University, 1989.

(10) Dye, J. L. *J. Phys. Chem.* **1984**, *88*, 3842.

(11) McMills, L. E., PhD. Dissertation, Michigan State University, 1989.

(12) Dawes, S. B.; Ward, D. L.; Fussa-Rydel, O.; Huang R. H.; Dye, J. L. *Inorg. Chem.* **1989**, *28*, 2132.

(13) Huang R.; Dye, J. L., unpublished results.

(14) Ellaboudy, A.; Tinkham, M. L.; VanEck, B.; Dye, J. L.; Smith, P. B. *J. Phys. Chem.* **1984**, *88*, 3852.

(15) Ellaboudy A.; Dye, J. L. *J. Magn. Reson.* **1986**, *66*, 491.

(16) Dye, J. L.; Andrews C. W.; Ceraso, J. M. *J. Phys. Chem.* **1975**, *79*, 3076.

(17) Edwards, P. P.; Ellaboudy, A.; Holton D. M.; Pyper, N. C. *Ann. Reports on NMR Spect.* **1988**, *20*, 315.

(18) Dawes, S. B.; Ellaboudy, A. S.; Dye, J. L. *J. Am. Chem. Soc.* **1987**, *109*, 3508.

(19) Ellaboudy A.; Dye, J. L. *J. Am. Chem. Soc.* **1983**, *105*, 6490.

(20) Abragam, A. Principles of Nuclear Magnetism, Oxford University Press, London, 1986.

(21) Waugh J. S.; Fedin, E. I. *Sov. Phys. Solid State* **1963**, *4*, 1633.

(22) Hubbard, P. S. *J. Chem. Phys.* **1970**, *53*, 985.

(23) Bobel, D.; Muller-Warmuth, W.; Olyschlager, H. *J. Magn. Reson.* **1979**, *36*, 371.

(24) Woessner, D. E. *J. Chem. Phys.* **1962**, *37*, 647.

(25) Farrar T. C.; Becker, E. D. Pulse and Fourier Transform NMR, Chapt. 4, Academic Press, New York, 1971.

(26) Cohen M. H.; Reif, F. *Solid State Phys.* **1957**, *5*, 321.

(27) Chihara H.; Nakamura, N. in Advances in Nuclear Quadrupole Resonance, Volume 4, 1980.

(28) H. S. Gutowsky and G. E. Pake, J. Chem. Phys. **18**, 162(1950)

(29) Andrew E. R.; Eades, R. G. *Proc. Roy. Soc. (London)* **1953,** *A216*, 405.

(30) Das, T. P. *J. Chem. Phys.* **1957**, *27*, 763.

I.C Evidence for correlated rotations in $Li^+(18C6)(CH_3NH_2)_2Na^-\cdot(18C6)_3$

The following section is in the form of a draft of a paper entitled "Evidence for correlated rotations in $Li^+(18C6)(CH_3NH_2)_2Na^-\cdot(18C6)_3$." to be submitted for publication in *The Journal of Physical Chemistry*. I am responsible for the writing of this draft.

I.C.1 Introduction

The crystal structure of $Li^+(18C6)(CH_3NH_2)_2Na^-\cdot(18C6)_3$, as implied by the single crystal X-ray diffraction measurements of Dye and Huang,[1] contains some rather unusual features. Lithium is normally found to be four coordinate. The complexed Li cation in this structure however, is apparently in the center of a nearly planar 18-crown-6 ring and is coordinated to two methylamine molecules, the coordination sphere being completed by the six complexant oxygens but at unreasonably long distances. The apparent Li-N distances are only 1.733 Å, much less than the expected ~2 Å. The apparent Li-O distances are also rather unusual, 2.764 Å, which is much longer than the expected contact distance of ~2 Å. The lithium cation was assigned a position on a 3-fold symmetry axis which is perpendicular to the complexant plane ($R\bar{3}$ symmetry). The two methylamines are situated on either side of the cation; both their nitrogens and carbons lie on the 3-fold axis. This leads to an unusual 180° N-Li-N bond angle. The anion, Na^-, is also located on the 3-fold axis, well isolated as is usual. There are additionally three other "free" 18-crown-6's which have the usual conformation of alternating oxygens and carbons and are located about the 3-fold axis. A stereoscopic view of the apparent molecular structure is given in Figure 1. The authors[1] were aware of the unusual nature of the

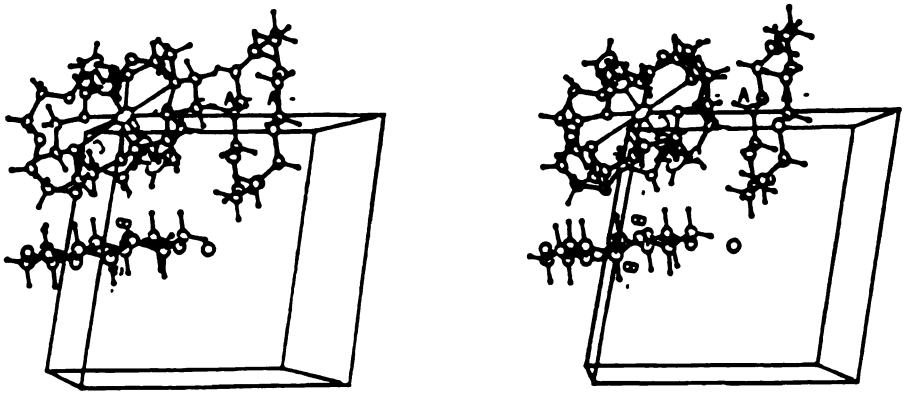

Figure 1. Stereoscopic view of $Li^{+}(18C6)(CH_3NH_2)_2Na^{-}\cdot(18C6)_3$.

structure and suggested an alternative fluxional model but the X-ray diffraction data did not agree well with the alternate model.

The apparent nature of the lithium bonding in the crystal structure is so unusual that it warranted further study. A single crystal was choosen from newly synthesized material and the structural determination was repeated. The structural details were identical to those previously determined.[1] The remainder of the synthesis was used in the following static, variable temperature, multinuclear, solid state NMR study.

I.C.2 Results and Discussion

Typical ^{7}Li and ^{23}Na NMR spectra, obtained with a 9.8950 T Varian VXR 400S NMR spectrometer and a 1 kW amplifier with a 5 mm wideline static probe, are shown in Figures 2 and 3. The chemical shifts are referenced to the respective aqueous cation at infinite dilution. The spectra were measured with a spin-echo method to minimize baseline distortion. The powder patterns are typical of S = 3/2 nuclei with a first-order quadrupolar perturbation and dipolar broadening.[2] The quadrupole satellites are clearly visible, distributed symmetrically about the central transition as expected. The separation between the satellites is the quadrupole frequency (ν_Q) for S=3/2 systems.

The temperature dependence of the ^{7}Li quadrupole frequency is displayed in Figure 4. The quadrupole frequency is, within experimental error, independent of temperature. In contrast, the ^{23}Na quadrupole frequency displays a smooth decrease with increasing temperature as can be seen in Figure 5.

The temperature dependence of the full-width at half intensity ($\nu_{1/2}$) of the ^{7}Li and ^{23}Na central transitions are shown in Figures 6 and 7. In both cases, the linewidth shows a sharp decrease over a narrow temperature range. The lineshape and width are primarily determined by chemical shift anisotropy (CSA), quadrupolar and dipolar interactions. Of these interactions, it is expected that dipolar contributions will dominate in this system.

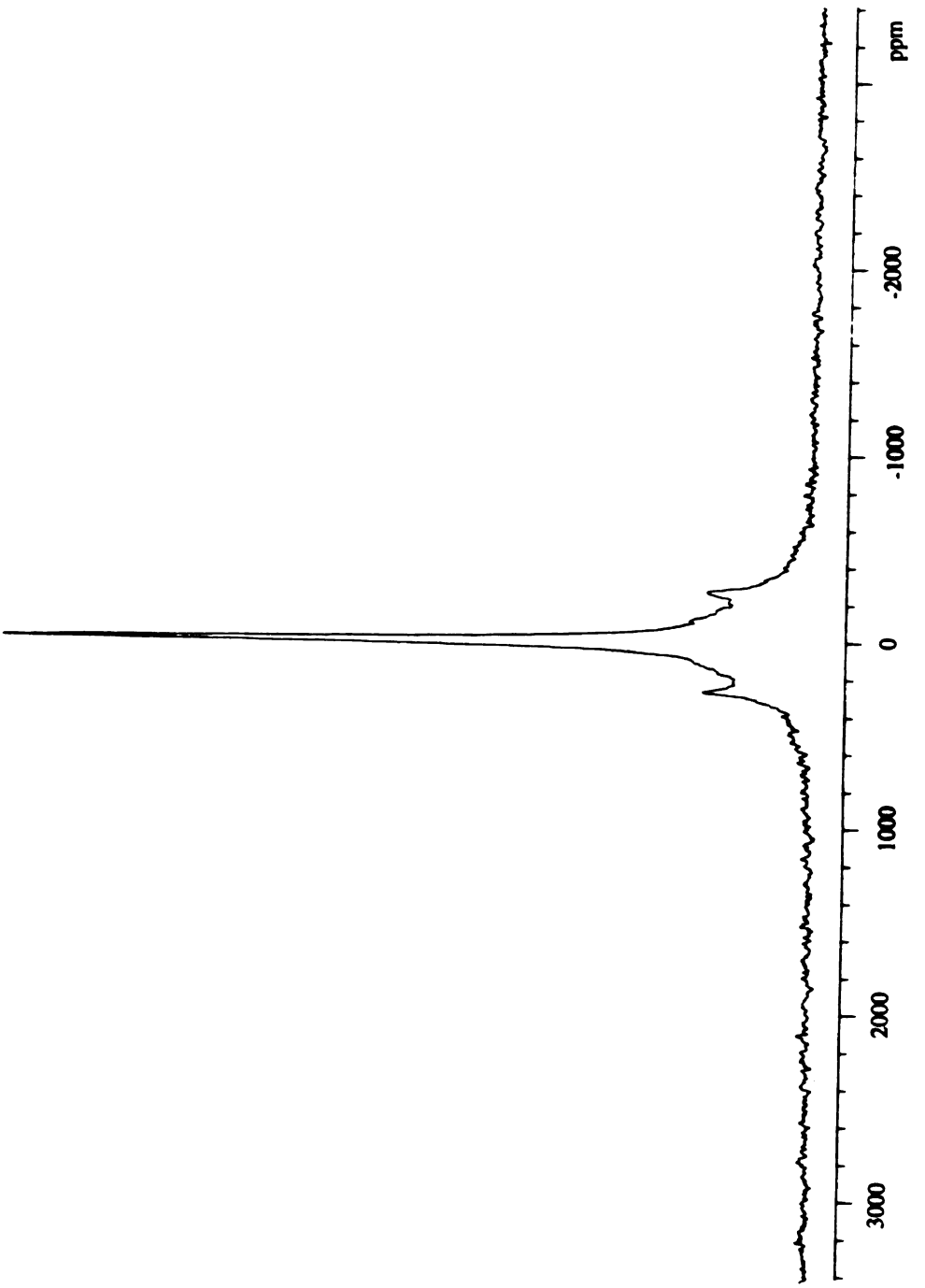

Figure 2. ^{7}Li NMR powder pattern showing quadrupole satellites.

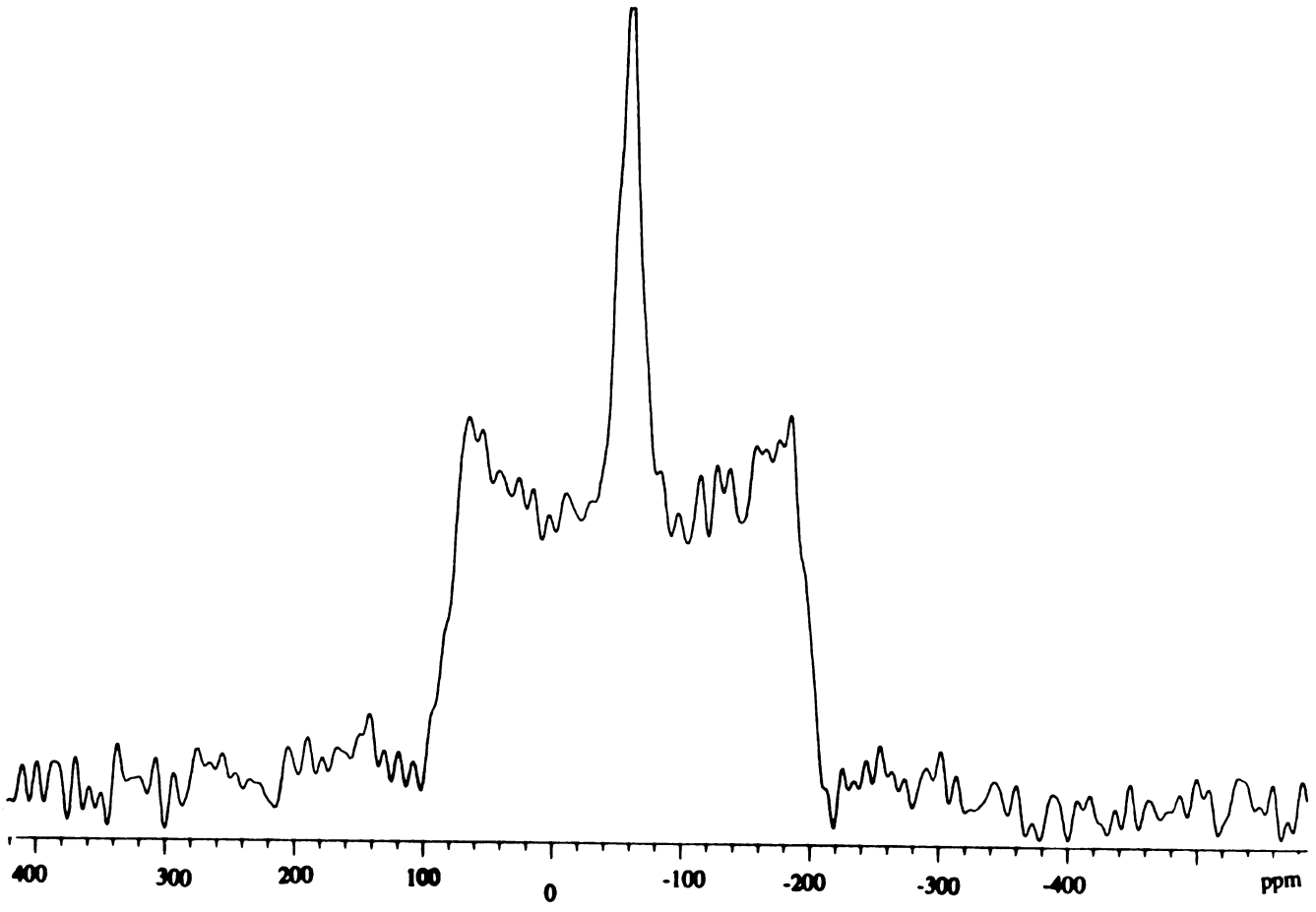

Figure 3. ^{23}Na NMR powder pattern showing quadrupole satellites.

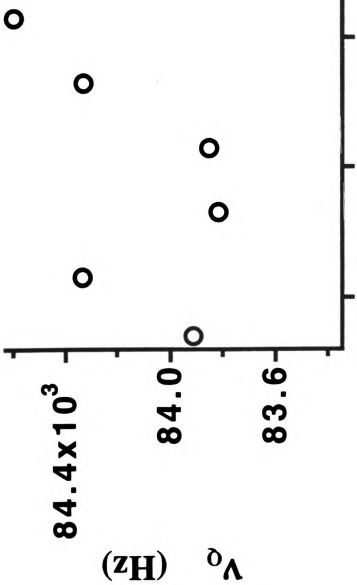

Figure 4. The temperature dependence of the ^{7}Li quadrupole frequency.

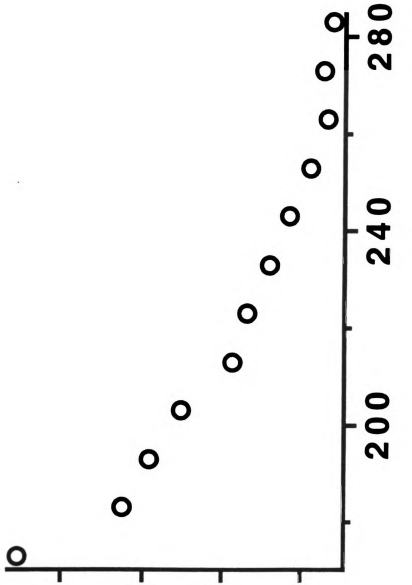

Figure 5. The temperature dependence of the ^{23}Na quadrupole frequency.

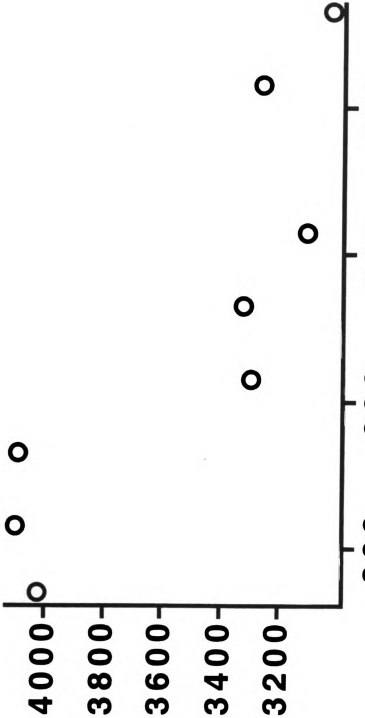

Figure 6. The temperature dependence of the full-width at half intensity of the ^{7}Li resonance.

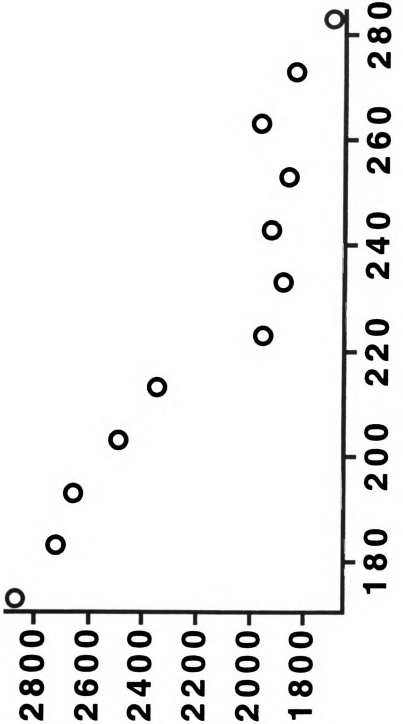

Figure 7. The temperature dependence of the full-width at half intensity of the ^{23}Na resonance.

The chemical shift range and the quadrupole coupling constant of lithium are small, limiting the size of these interactions. The large size and spherical nature of the sodium anion likewise limits the effectiveness of the first two broadening mechanisms.[3] Dipolar contributions, on the other hand, are expected to be quite large since the system can be characterized as have both the cation and anion immersed in a "sea of protons", which along with the methylamine nitrogens, should interact strongly to broaden the observed resonances.

The rigid lattice dipolar contribution to the second moment (M_2) of the NMR resonance of spin I by unlike spins can be calculated by a summation of the pairwise interactions using the Van Vleck equation[2]

$$M_2 = \frac{1}{3}\left[\frac{\mu_o}{4\pi}\right]\hbar^2\gamma_I\gamma_S S(S+1)\sum_k \frac{(1-3\cos^2\theta_{j.k})^2}{r_{j.k}^6} \qquad (1)$$

in which the summation is over all spins S^k interacting with spin I^j. This equation can be simplified for a microcrystalline powder sample, assuming a random distribution of crystallite orientations, by averaging $(1-3\cos^2\theta_{j.k})^2$ over all directions with the following result:

$$M_2 = \frac{4}{15}\left[\frac{\mu_o}{4\pi}\right]\hbar^2\gamma_I\gamma_S S(S+1)\sum_k r_{j.k}^{-6}. \qquad (2)$$

The lineshape of a dipolar broadened solid state powder spectrum is expected to be Gaussian.[2] The full width at half intensity of a Gaussian curve is related to the second moment by

$$\nu_{1/2} = \sqrt{(2\ln 2)M_2}. \qquad (3)$$

In the absence of molecular rotations or translations, the second moment calculated from equation 2 represents a good approximation of the linewidth one expects to find experimentally for systems broadened only by dipolar coupling to unlike spins. Motions which do not affect the mean displacement of the spins (ie lattice vibrations) will have very little effect on the linewidth. By contrast, molecular rotations or translations whose correlation times (τ_c) are on the order of the inverse rigid lattice linewidth are expected to effectively narrow the resonance. This type of molecular motion lessens the time averaged local field experienced by the spins and thus the broadening interaction. In other words, the average position and angle with respect to the applied field becomes time dependent. Only quasi-adiabatic components of the local field are effective in linebroadening. Fourier components of the local field with frequencies near the rigid lattice linewidth (in the rotating frame) will still contribute to the linewidth, but as the motional correlation time shortens, these will no longer be quasi-adiabatic and thus the line will narrow. The motional correlation times of rotations and translations are expected to be temperature dependent. Thus as one raises temperature, the linewidth of a solid should narrow from the rigid lattice value in a stepwise fashion as the correlation times of the various available rotations and translations pass though the narrowing criterion.

The linewidth of the ^{7}Li and ^{23}Na resonances of $Li^{+}(18C6)(CH_3NH_2)_2Na^{-}\cdot(18C6)_3$ both show stepwise reduction of their linewidths with onset temperatures of approximately 210 and 180 K respectively (Figures 6 and 7). The rigid lattice linewidths of the ^{7}Li and ^{23}Na resonances calculated from crystallographic data and all protons and nitrogens within 9 Å (using equations 2 and 3) are 12.33 and 2.89 kHz respectively. The latter value agrees well with the low temperature linewidth of the ^{23}Na resonance, however, the low temperature ^{7}Li resonance is only ~ 4 kHz. It is clear that either the structure is incorrect or the line is narrowed by a substantial, large amplitude molecular rotation or cationic/molecular diffusion.

One model of this compound that is consistent with the NMR data and can also be considered to be compatible with the x-ray data, is one in which the lithium is four coordinate but is hopping from site to site around the ring at low temperatures. The coordination would probably be much like that seen in the related compound $Li^+(18C6)(CH_3NH_2)_2Na^-$ shown in Figure 8.[1] Such a coordination, if rigid, would have a linewidth associated with dipolar interactions with the complexing crown ether and methylamines of 28.15 kHz. While this is more than three times that of $Li^+(18C6)(CH_3NH_2)_2Na^-\cdot(18C6)_3$, hopping of the cation between the six equivalent sites would decouple these dipolar interactions and dramatically reduce their contributions to the observed linewidth. To be effective, such a hopping motion must have a very low activation barrier and a very short correlation time at the temperature at which the x-ray data were gathered (near 200 K). This model was also considered earlier,[1] but did not appear to agree with the x-ray data. Two test refinements, which were published with the structure and based on site disordered cations, could not account for the high electron density found at the center of the 18C6 ring.[1] However, it has since been pointed out to us that site disorder around an axis of symmetry can result in the "pile up" of electron density on that axis which is unresolvable by refinement.[4] Fast hopping of the cation around the symmetry axis, which runs through the middle of the complexing crown and perpendicular to its plane, could thus yield an average lithium position in the center of the ring as observed.

The motion associated with the linewidth reduction observed in both ^7Li and ^{23}Na resonances above ~ 200 K is undoubtly not due to intra-crown cationic hopping. The ^7Li linewidth has already been substantially reduced at 200 K; the correlation time of the hopping must be much faster than the reciprocal rigid lattice linewidth even at 200 K. The motion associated with the reduction of the linewidth is probably a macrocyclic rotation of the three free crown ethers. The ^{23}Na linewidth calculated from only methylamine and free crown protons within 9 Å of the anion is 2.84 kHz; in other words, motion of the

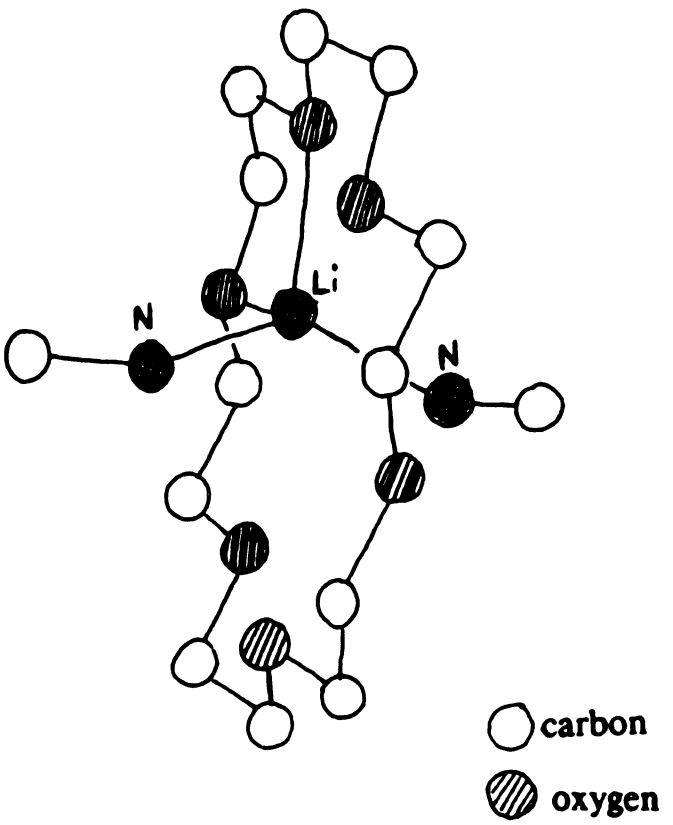

Figure 8. View of the bonding in of the complexed lithium cation in $Li^{+}(18C6)(CH_3N_2)_2Na^{-}$.

com

the

acc

acc

of t

co

sno

res

ima

sin

stu

freq

fie

qu

hav

ob

tim

one

bet

an

bar

mea

complexing crown would have a negligible effect on the observed linewidth. Furthermore, the dipolar contribution associated with the free crown ether hydrogens alone would account for a linewidth of 2.59 kHz; thus, motion of the methylamine alone could not account for the observed reduction. Macrocyclic rotation and conformational adjustment of the free crowns, such as that seen in the complexing crowns of two other sodides,[5] could easily account for the observed narrowing. The motion would be x-ray transparent since it would involving fast hopping between equivalent equilibrium sites with an average residence time in the equilibrium positions which is much longer than the intersite hopping time. This motion would also account for the decrease in the ^{7}Li linewidth above 200 K since the dipolar contribution of the free crown protons (~ 2.28 kHz according to the structure) would be modulated. Furthermore, the smooth decrease of the ^{23}Na quadrupole frequency with increasing temperature is evidence of time averaging of the anion's electric field gradient while no decrease is seen for the cation. Thus, the motion responsible for the quadrupolar effects must change the time averaged local structure of the anion without having much effect on that of the cation. Motion of the free crowns could account for this observation due to their proximity to the anion and remoteness from the cation.

By using the approximate formula of Waugh and Fedin for the calculation of hindered-rotation barriers from linewidth data,[6]

$$E_a \text{ (kJ mol}^{-1}) \approx 0.155 T_c \text{ (K)} \qquad (4)$$

one finds an activation energy (E_a) for the macrocyclic rotation of the free crowns of between 28 and 31 kJ mol^{-1}; the wide range of this value is due to the difficulty in picking an onset temperature (T_c) with the limited data available. The magnitude of this activation barrier is in good accord with that seen previously in two other sodides.[5] The values measured in this case are slightly smaller; one might expect this to be the case since the

crown ethers in the previous study were "sandwiched" around the cation and intercrown steric hinderance to the macrocyclic rotation might lead to a larger barrier.

It is likely that the lithium cations are undergoing rapid intra-crown, 6-site diffusional hopping even at very low temperatures and that the three free crown ethers undergo macrocyclic rotations at higher temperatures. It is not totally clear, however, whether the methylamine and complexing crown ethers undergo rotational or translational motion at these temperatures. In order to account for the observed linewidth of the ^{23}Na resonance, the methylamine must be static on an NMR timescale (ms) at $T < \sim 180$ K. The linewidth observed below this temperature corresponds well to that due to dipolar coupling to the free crown *and* the methylamine protons (2.84 kHz calculated, 2.87 kHz measured). Complete decoupling of the methylamine protons would result in a linewidth which is too small (2.59 kHz) to account for the data. Methylamine motion would certainly result in a substantial reduction in the linewidth, and the absence of this reduction makes it unlikely that it is undergoing significant rotation or translational motion below ~ 180 K. On the other hand, the data yield no clues as to whether the complexing crown ether is undergoing macrocyclic rotations. It does, however, seem likely that such motion does occur with an activation barrier that is on the order of that seen in the free crowns and in previous studies of sodides[5] and model complexes.[7-9]

I.C.3 Conclusions

The unusual coordination of the lithium cation in $Li^+(18C6)(CH_3NH_2)_2Na^-\cdot(18C6)_3$, initially implied by the single crystal x-ray diffraction data, is probably an artifact of rapid lithium intra-crown hopping. This hopping between symmetry equivalent equilibrium sites results in the artificial build-up of apparent electron density on the symmetry axis, resulting in an apparent ring centered lithium cation. The more likely

coordination of the cation in this structure is four-coordinate, similar to that seen in the related compound $Li^+(18C6)(CH_3NH_2)_2Na^-$.

It is apparent from ^7Li and ^{23}Na NMR linewidth and quadrupole coupling frequency measurements that the three free crown ethers are undergoing a combined macrocyclic rotation and conformational adjustment, similar to that seen in previous sodides.[5] The correlation time of this motion is on the NMR timescale above 200 K. The approximate activation barrier associated with this motion is between 28 and 31 kJ mol^{-1}.

I.C.4 Acknowledgements

This research was supported by NSF Solid State Chemistry Grants DMR 87-14751 and DMR 90-17292 and by the Michigan State University Center for Fundamental Materials Research.

I.C.5 References

(1) Dye, J. L.; Huang, R. H. *Pure & Appl. Chem.* **1993**, *65*, 435.

(2) Abragam, A. *Principles of Nuclear Magnetism*; Clarendon Press: Oxford, 1986.

(3) Dye, J. L.; Ellaboudy, A. S.; Kim, J. In *Modern NMR Techniques and Their Application in Chemistry*; A. I. Popov and K. Hallenga, Eds.; Marcel Dekker: New York, 1991; pp 217.

(4) Coppens, P., Distinguished Professor of Chemistry, State University of New York at Buffalo, private communication.

(5) Wagner, M. J.; McMills, L. E. H.; Ellaboudy, A. S.; Eglin, J. L.; Dye, J. L.; Edwards, P. P.; Pyper, N. C. *J. Phys. Chem.* **1992**, *96*, 9656.

(6) Waugh, J. S.; Fedin, E. I. *Sov. Phys. Solid State* **1963**, *4*, 1633.

(7) Buchanan, G. W.; Kirby, R. A. *Tetrahedron Lett.* **1987**, *28*, 4783.

(8) Buchanan, G. W.; Morat, C.; Ratcliff, C. I.; Ripmeester, J. A. *J. Chem. Soc., Chem. Commun.* **1989**, 1306.

(9) Ratcliffe, C. I.; Ripmeester, J. A.; Buchanan, G. W.; Denike, J. K. *J. Am. Chem. Soc.* **1992**, *114*, 3294.

CHAPTER II

II.A Introduction

The "excess" electrons in electrides are confined to the void spaces in the lattice as demonstrated by theory and experiment.[4,14-16] The magnetic and electronic properties, which are largely determined by these trapped electrons, will undoubtably be highly dependent on the cavity and channel structure in which they are confined. These electrons are not confined to just the cavities, but they extend into all void space and, to some extent onto the molecules which form the void walls, to minimize their kinetic energy. The kinetic energy of a wave function in any void space is dependent on the size of that void. Assuming equivalent channel potential energies, the electron density will extend further into the wider channels than into the more narrow channels. By measuring the width and length of the channels between the cavities, one can judge the relative strength of the overlap of the neighboring trapped electrons' wave functions. Knowing the important exchange pathways is crucial in modeling both the magnetic and electronic properties of electrides.

Recently, the channel and cavity structure of the five electrides with known crystal structure has been studied extensively.[17] The space void of atoms was determined by defining a minimum distance from any point in the lattice to the nearest van der Waals surface. Iterative testing of all lattice points results in an "isosurface" depicting the cavities and channels. Varying the allowed distance from large to small causes the minimum allowable void size to shrink, making thinner channels and smaller cavities visible. By studying a number of these isosurfaces, the relative sizes of the cavities and channels were judged and absolute minimum widths measured.

This chapter consists of the study of four electrides with known structures. Special attention is paid to relating the properties of these electrides to their individual channel and cavity structures. Included in this chapter are two publications which are in print, two

which will soon be submitted and two sections which are to be converted into sections of papers in preparation.

II.B An electride with a large six electron ring

The following section is in the form of a paper entitled "An Electride with a Large Six Electron Ring" which was published in *Nature (London)*, volume 368, in the year 1994 and starting on page 726. The paper was written by Professor Dye in consultation with Dr. Rui Huang and myself; all co-authors participated in the final editing of the manuscript. Dr. Huang was responsible for the x-ray crystallography and Professor Judith Eglin the differential scanning calorimetry and some preliminary characterization. I was responsible for the measurement and analysis of magnetic susceptibility, DC and AC conductivity and ^{133}Cs NMR.

II.B.1 Letter to *Nature*

ELECTRIDES are crystalline salts that contain complexed alkali metal cations and trapped electrons.[1] Theory[2,3] and experiment[4,5] indicate that the excess electron distribution is concentrated in cavities and channels formed by close-packing of the large complexed cations. Thus, electrides might serve as models of confined electron lattice gases. The new electride, $[Cs^+(15C5)(18C6)\cdot e^-]_6\cdot(18C6)$, crystallizes in the $R\bar{3}$ space group and has a central 18-crown-6 (18C6) molecule surrounded by six Cs^+ ions, each sandwiched between a 15-crown-5 (15C5) and an 18C6 molecule. The six electrons released when Cs metal interacts with the crown ethers are presumably trapped in six cavities, forming a puckered ring with three cavities above and three below the plane of the central crown molecule. As expected for a ring of six electrons the ground state is diamagnetic. The electron distribution in rings contrasts with the chain-like connections of cavities observed in three other electrides.[6-8] Polycrystalline samples are ~ 10^6 times more conductive than either $Cs^+(15C5)_2\cdot e^-$ or $Cs^+(18C6)_2\cdot e^-$.

The new mixed-sandwich electride has the empirical formula $[Cs(15C5)(18C6)]_6 \cdot 18C6$ (although it also contains some excess caesium). It was synthesized by anaerobically dissolving caesium metal and about a 10% excess of a 1:1 mixture of 15C5 and 18C6 in dimethyl ether (sometimes with methylamine) in a modified H-cell.[6] The temperature was kept below 220 K to prevent thermal decomposition. Crystals were grown by slow cooling after adding trimethylamine to reduce the solubility, or by slowly evaporating dimethyl ether from the mixture. Rapid crystallization gave mixtures with $Cs^+(15C5)_2 \cdot e^-$ and $Cs^+(18C6)_2 \cdot e^-$.

The phase purity of polycrystalline samples was checked by differential scanning calorimetry. The "parent" electrides, $Cs^+(15C5)_2 \cdot e^-$ and $Cs^+(18C6)_2 \cdot e^-$, show characteristic endothermic peaks at 266 K and 312 K, respectively, and the onset of exothermic decomposition peaks at 299 K and 315 K. The mixed sandwich endotherm is at 284 K (ΔH = 7 kJ mol^{-1}) and decomposition begins at 308 K; both temperatures are between those of the parent compounds.

Two crystals from separate syntheses were selected for X-ray structure determination and were mounted anaerobically at ~ 220 K by previously described techniques.[9] The crystal structure is complex but highly symmetric. The $R\bar{3}$ space group yields a 3-fold rotation axis (the *c* axis) perpendicular to the plane of, and through the center of a "free" 18C6 molecule, as well as inversion symmetry through its center. Table 1 gives some structural data.

Six mixed sandwich complexes of Cs^+, centered 5.4 Å from the plane of the free crown ring, are grouped around the central 18C6 molecule in the shape of a double three-bladed propeller. Each of the three "blades" above the ring makes an angle of 60° with respect to the plane of the central ring. The three below the ring are equivalent but tilted in the opposite direction. Figures 1-3 show two views of the central 18C6 ring and the six 15C5-Cs^+-18C6 sandwiches. These complete units pack together efficiently, but leave empty cavities and channels in which we expect to find the excess electrons.

Table 1. Crystal Data for $[Cs^+(15C5)(18C6)\cdot e^-]_6\cdot(18C6)$ at 180 K.

Space Group	$R\bar{3}$ (148)		
Cell parameters	$a = b = 33.108(6)$ Å		
	$c = 16.266(5)$ Å		
	$z = 18$		
Range of 2θ	3.5° to 45°		
No. of reflections used in refinement $3.0(F_o^2)$	2905 with $F_o^2 >$		
No. of variables	333		
Unweighted agreement factor	0.050		
Weighted agreement factor	0.031		
High peak in final diff. map	0.48 e Å^{-3}		
Selected positional parameters (inversion center at 0.0, 0.0, 0.5)			
Sandwiched Cs^+	0.2803	0.0324	0.8336
Defect Cs^+ (multiplicity 0.047)	0.0	0.0	0.3876
Trap center	0.170	0.215	0.660

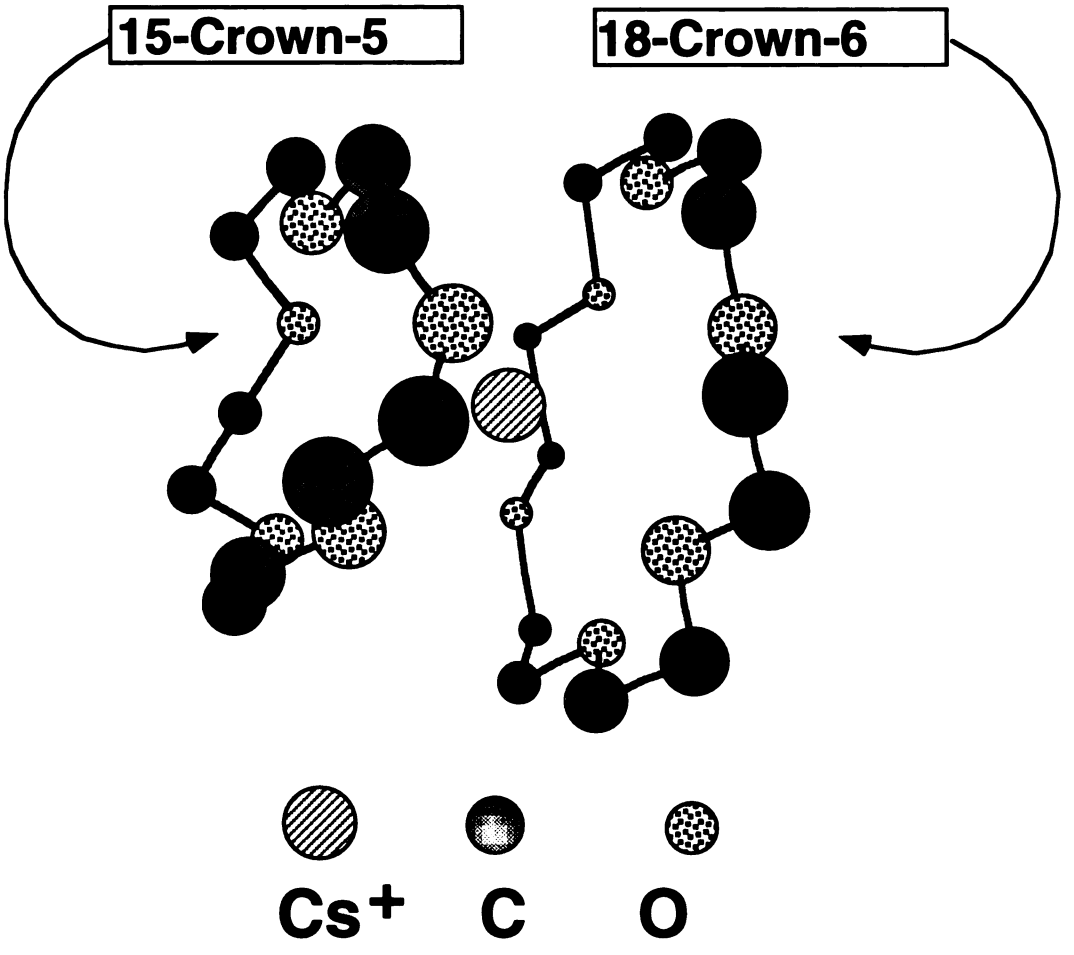

Figure 1. "Ball and stick" model of one of the six 15C5-Cs^+-18C6 sandwich units.

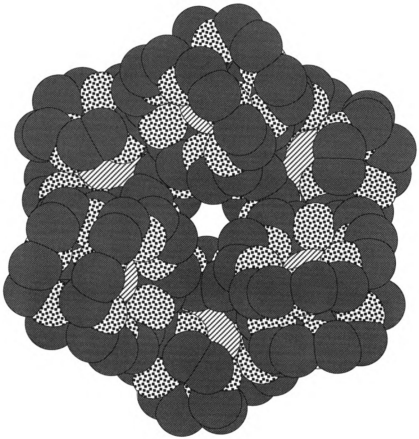

Figure 2. Space-filling model of the central $[Cs^{+}(15C5)(18C6)\cdot e^{-}]_6\cdot(18C6)$ unit (down the c-axis), constructed from the X-ray coordinates. Note that the central "free" 18C6 molecule is hidden in this view. The hydrogens have been deleted for clarity.

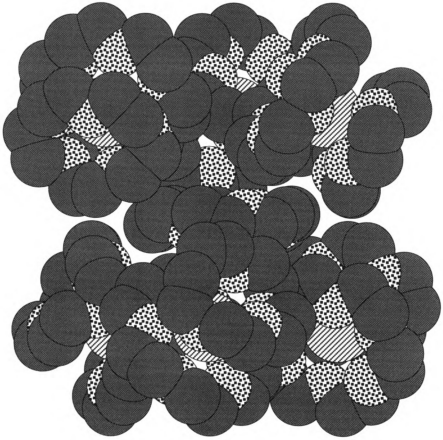

Figure 3. Space-filling model of the central $[Cs^{+}(15C5)(18C6)\cdot e^{-}]_6\cdot(18C6)$ unit (perpendicular to the c-axis), constructed from the X-ray coordinates. The hydrogens have been deleted for clarity.

The irregularly shaped cavities may be approximated as ellipsoids (~ 5 Å along *c* and 2.5 Å in diameter). The collection of six cavities, with the overall symmetry of the space group, forms a puckered six-member ring as shown schematically in Figure 4. The cavities are alternately above and below the plane of the central 18C6 molecule and each is connected to its two neighbors by rather open channels with center-to-center distances of ~ 8 Å. In addition, each cavity has two longer channels to neighboring 6-cavity rings. The "top" cavities connect to "top" cavities of neighboring rings via both channels with center-to-center distances of about 10 Å, and similarly for the bottom cavities. We presume that one electron occupies each cavity and that intra-ring electron-electron coupling is the strongest . Inter-ring coupling could, however, provide a three-dimensional conducting network of cavities and channels.

Although the structure was essentially solved on the basis of the description given above, the difference map of electron density showed distinct spherical peaks about 1.8 Å above and below the central 18C6 ring that were ~ 10 times the background level. The diameter of each of these spherical regions was ~ 2 Å, large enough to accommodate a Cs^+ ion. A likely location for excess Cs^+ would be in contact with the free 18C6 molecule at its center with a Cs-O distance of about 3.5 Å and located about 1.6 Å above the center of the crown ether ring. This is close to the position of the excess electron density (1.8 Å). By including partial occupancy of Cs^+ at these positions, the excess electron density was removed and the agreement factor was improved from R = 0.069 and R_w = 0.050 to R = 0.050 and R_w = 0.031. The refined occupancies for two separately synthesized crystals correspond to 4.5 ± 0.2 and 4.7 ± 0.2 mole percent excess caesium, so that about one in four of the central 18C6 molecules is coordinated to one Cs^+ ion. Unless a corresponding number of sandwich sites for Cs^+ were empty, the electrons released by the inclusion of excess caesium would be added to the "pool" of trapped electrons. Thus, caesium acts as an n-dopant.

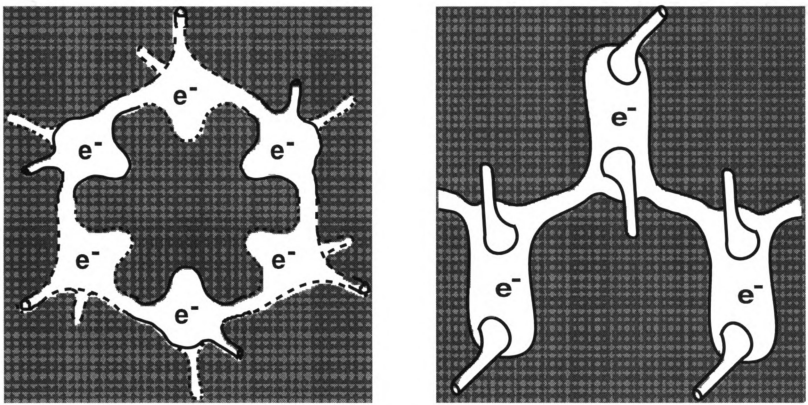

Figure 4. Schematic diagram of the cavities and channels in the central unit of the electride. (left) Top view (the solid outline is above the plane of the central "free" 18C6 molecule while the dashed outline is below). The "outside" channels connect to adjacent rings. (right) Side view of three out of the six cavities and channels in the ring. The actual shapes of the cavities and channels are somewhat more complex than this diagram indicates.

The electronic contribution to the magnetic susceptibility was measured from 2 K to 230 K with an SHE SQUID susceptometer. It is strikingly different from those of $Cs^+(15C5)_2 \cdot e^-$ and $Cs^+(18C6)_2 \cdot e^-$, which both show Curie-Weiss behavior at high temperatures and weak antiferromagnetism, with maxima in the susceptibilities at 4.5 K and 50 K, respectively.[7,10] By contrast, the mixed-sandwich electride exhibits weak field-independent paramagnetism that indicates strong inter-electron coupling. The paramagnetism increases with temperature to 3% and 13% of the value expected for free spins at 80 K and 200 K, respectively. The susceptibility below about 50 K increases rapidly with decreasing temperature, indicating the presence of up to 4 - 5 % of excess electrons. The $T^{-0.6}$ dependence of the "paramagnetic tail" of a sample with only 0.7% unpaired spins is reminiscent of quasi-one dimensional behavior.[11,12]

The magnetic susceptibility data are qualitatively in accord with a model of diamagnetic six-electron rings weakly coupled together, with "extra" electrons required to balance the charges of the defect Cs^+ ions on the central 18C6 rings. As expected, the magnitude of this effect varies from sample to sample. Also, the number of unpaired electrons need not be the same as the number of excess Cs^+ ions. Some regions might contain two defects with paired excess electrons, some sandwich cation trapping sites might be empty, and partial decomposition could remove unpaired electrons.

The ^{133}Cs NMR chemical shift of +17 ppm at 210 K is far smaller than the values of +547 ppm and +132 ppm for $Cs^+(15C5)_2 \cdot e^-$ and $Cs^+(18C6)_2 \cdot e^-$, respectively, and the temperature dependence has the opposite slope. This behavior is expected from the small value of the paramagnetic susceptibility and its increase with temperature. Even accounting for the low percentage of unpaired spins, however, it is clear that the electron contact density at the caesium nucleus is orders of magnitude lower than in the parent electrides; the mixed-sandwich complex of Cs^+ is much more effective at excluding unpaired electron density.

Both *dc* and *ac* powder conductivities show that the mixed-sandwich electride is at least 10^6 times more conductive than the parent compounds. Impedance spectroscopy with potassium-coated electrodes (to reduce polarization and the Schottky barrier[13]) over the temperature range 80 K to 230 K yielded an apparent activation barrier of 0.064 ± 0.002 eV, but, as shown in Figure 5, a better fit can be obtained with the equation

$$\sigma = \sigma_o \exp[-(T_o/T)^{1/2}]. \quad (1)$$

This result, and the low-temperature magnetic susceptibility, suggest that a variable-range hopping mechanism is responsible for the observed conductivity.[14,15]

This electride, and the three with published structures,[6-8] demonstrate the extreme diversity in the structures and properties of electrides. Both $Cs^+(15C5)_2 \cdot e^-$ and $Cs^+(18C6)_2 \cdot e^-$ have electron-trapping cavities that are strung out like beads on a chain, some 8.5-9 Å apart, connected by narrow but open channels. They have low electronic conductivities (~ 10^{-10} $ohm^{-1}cm^{-1}$ at 200 K[13]) and relatively weak antiferromagnetic coupling. By contrast, K^+(cryptand [2.2.2])$\cdot e^-$ has spin-paired electrons in elongated traps[8] and shows high (but thermally activated) conductivity (~ 10 $ohm^{-1}cm^{-1}$ at 200 K[13]) and strong antiferromagnetic pair-wise coupling.[8]

It is remarkable that seemingly minor changes in the complexant(s) used to encapsulate the cation can have such dramatic effects. Evidently, the size, shape and connectivities of the cavities and channels are of critical importance to the structures and properties of electrides.

We acknowledge support from the U.S. National Science Foundation under Grant No. DMR 90-17292.

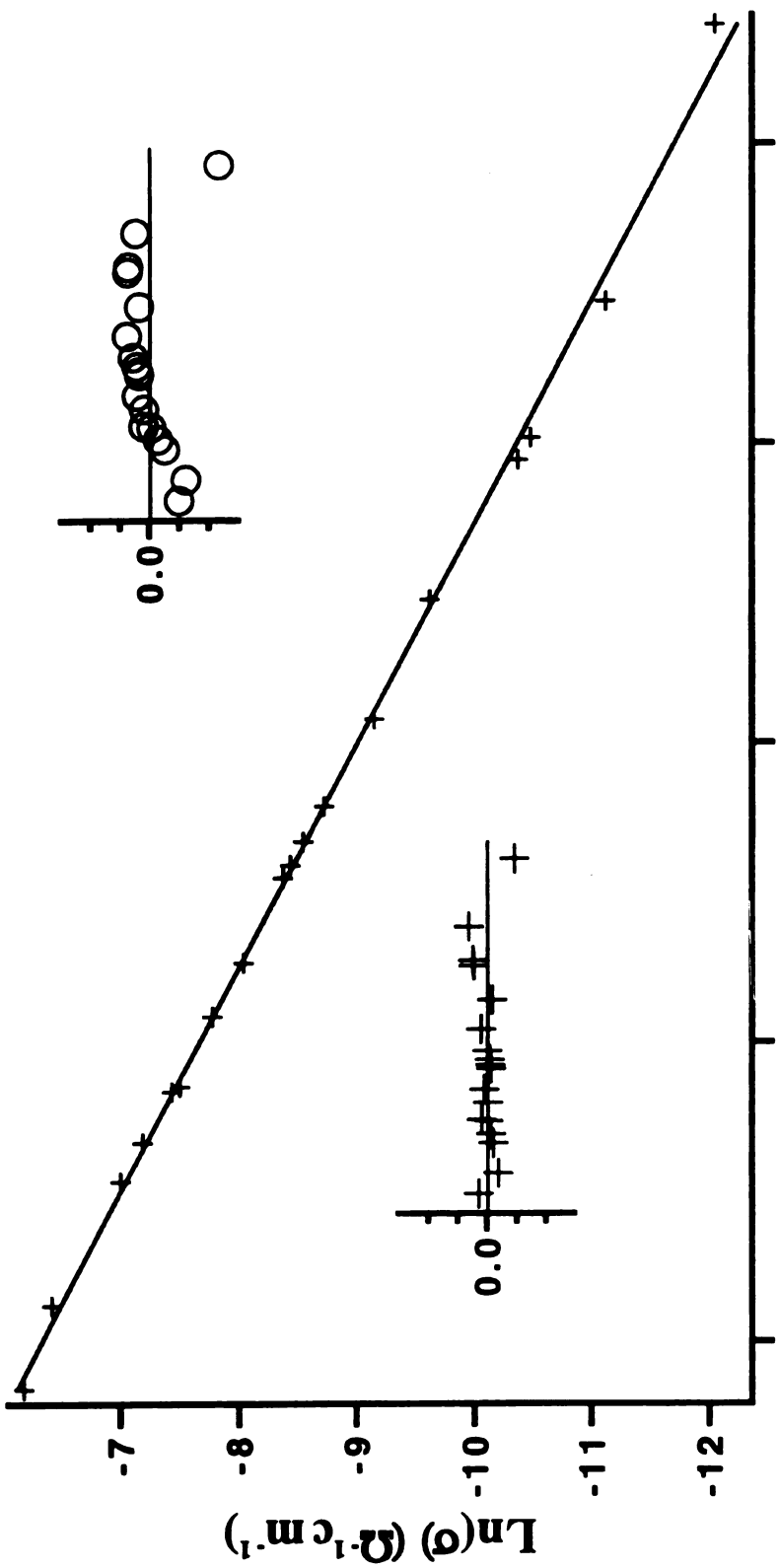

Figure 5: Least-squares fit to the low-frequency intercept of impedance spectroscopy data by equation (1) (see text). The residuals (calculated - observed)in the upper-right diagram are for a fit of $\ln(\sigma)$to $1/T$ while those in the lower-left diagram are for a fit of $\ln(\sigma)$ to $1/T^{0.5}$. The least-squares fit by this equation yielded only random deviations with σ_o=22.2(7) Ω^{-1} cm^{-1} and To=1.80(2) x10^4 K.

П.В.

1.

2.

3.

4.

5.

6.

7.

8.

9.

10.

11.

12.

13.

14.

15.

II.B.2 REFERENCES

1. Wagner, M.J. & Dye, J.L. *Annual Review of Materials Science* **23**, 223-253 (1993).

2. Singh, D.J., Krakauer, H., Haas, C. & Pickett, W.E. *Nature (London)* **365**, 39-42 (1993).

3. Dye, J.L. *Nature (London)***365**, 10-11 (1993).

4. Dye, J.L. *Science* **247**, 663-668 (1990).

5. Shin, D.H., Dye, J.L., Budil, D.E., Earle, K.A. & Freed, J.H. *Journal of Physical Chemistry* **97**, 1213-1219 (1993).

6. Dawes, S.B., Ward, D.L., Huang, R.H. & Dye, J.L. *Journal of the American Chemical Society* **108**, 3534-3535 (1986).

7. Dawes, S.B., Eglin, J.L., Moeggenborg, K.J., Kim, J. & Dye, J.L. *Journal of the American Chemical Society* **113**, 1605-1609 (1991).

8. Huang, R.H., Faber, M.K., Moeggenborg, K.J., Ward, D.L. & Dye, J.L. *Nature (London)* **331**, 599-601 (1988).

9. Ward, D. L., Huang, R. H. & Dye, J. L. *Acta Crystallogr.* **C44**, 1374-1376 (1988).

10. Wagner, M.J., Huang, R.H. & Dye, J.L. *Journal of Physical Chemistry* **97**, 3982-3984 (1993).

11. Bulacvskii, L.N., Zvarykina, A.V., Karimov, Y.S., Lyubovskii, R.B. & Shchegolev, I.F. *Soviet Physics JETP* **35**, 384-389 (1972).

12. Soos, Z.G. & Bondeson, S.R. *Molecular Crystals and Liquid Crystals* **85**, 19-31 (1982).

13. Moeggenborg, K.J., Papaioannou, J. & Dye, J.L. *Chemistry of Materials* **3**, 514-520 (1991).

14. Efras, A.L. & Shklovskii, B.I. *Journal of Physics C* **8**, L49-L51 (1975).

15. Brenig, W., Döhler, G.H. & Heyszenau, H. *Philosophical Magazine* **27**, 1093-1103 (1973).

II.C $[Cs^+(15\text{-crown-}5)(18\text{-crown-}6)e^-]_6 \cdot$ (18-crown-6): Properties of the First Mixed Crown Electride.

The following section is in the form of a draft of a paper entitled "$[Cs^+(15\text{-crown-}5)(18\text{-crown-}6)e^-]_6 \cdot$(18-crown-6): Properties of the First Mixed Crown Electride" to be submitted as an invited oral presentation as a part of the symposium "Synthesis, Structure, and Properties of Metastable Compounds" at the 208th American Chemical Society National Meeting. In addition, it will be submitted for publication in a refereed conference proceedings to be published in the *Journal of Solid State Chemistry*. I am responsible for the writing of this draft.

II.C.1 Introduction

Electrides are salts that consist of complexed alkali metal cations charge balanced by stochiometrically trapped electrons. Electrides in which the cation is complexed by two crown ethers ("sandwiched") have been extensively studied.[1-3] Specifically, $Cs^+(18\text{-crown-}6)_2e^-$ (abbreviated $Cs^+(18C6)_2e^-$) and $Cs^+(15\text{-crown-}5)_2e^-$ (abbreviated $Cs^+(15C5)_2e^-$), have been well characterized; the former by single crystal x-ray crystallography,[4] NMR,[5] EPR,[6-8] powder conductivity,[9-11] optical absorption spectroscopy,[9,12] DSC[5] and magnetic susceptibility,[13-15] the latter by all the aforementioned techniques except EPR.[16,17] The possibility of the existence of an electride with cations "sandwiched" by two different crown ethers became apparent when $Cs^+(18C6)_2e^-$ was mixed with $Cs^+(15C5)_2e^-$ as a temperature reference during a ^{133}Cs NMR experiment; a third peak not due to either pure $Cs^+(18C6)_2e^-$ or $Cs^+(15C5)_2e^-$ appeared which was attributed to a mixed-crown electride formed by solid state reaction in the NMR rotor.[17]

The structure and physical properties of the deliberately synthesized mixed crown electride have proven to be quite different from those of either parent compound [$Cs^+(18C6)_2e^-$ or $Cs^+(15C5)_2e^-$]. The properties of this mixed-crown electride caused us to conclude that it is not a mixture of the two parent compounds but rather a new compound. Later, single crystal x-ray diffraction studies showed that this was indeed the case; each cesium cation is sandwiched between one 18-crown-6 *and* one 15-crown-5. Six such sandwiches are arranged around a central 18C6 molecule. In addition, the packing of the complexed cations leaves 6-member rings of cavities, which theory[18,19] and experiment[8,20] have indicated are the electron trapping sites in electrides. This is rather surprising since the trapping sites in electrides are normally isolated as is the case in the parent electrides, although electron pairs do occur in $K^+(C222)e^-$.[21] The structure and properties of this fascinating new electride with six-member electron rings, which has the empirical formula $[Cs(15C5)(18C6)]_6 \cdot 18C6$, have been discussed in a brief communication elsewhere;[22] this paper describes the properties in full detail.

II.C.2 Experimental

$[Cs^+(18C6)(15C5)e^-]_6 \cdot (18C6)$ was synthesized by anaerobically dissolving cesium and approximately 10% excess of a 1:1 mixture of 18-crown-6 and 15-crown-5 in dimethyl ether in a modified H-cell.[23] The reaction vessel was cooled in dry ice during evacuation to prevent the loss of the more volatile 15-crown-5. Care was taken to ensure that the reaction mixture never exceeded 220 K to prevent thermal decomposition. Crystals were formed by addition of trimethylamine, further cooling to dry ice temperature and slowly reducing the volume of primary solvent (~ 1 - 2 weeks). Crystals were dried in vacuum, collected in inert atmosphere and stored in liquid N_2. Due to the extreme sensitivity of this electride to thermal and oxidative decomposition, sample manipulation was always performed in an inert atmosphere on aluminum supports

immersed in liquid N_2. Details of the purification of materials and of the synthetic methods used have been described elsewhere.[24]

The ^{133}Cs spectra were measured at the Max T. Rogers NMR facility at Michigan State University on a 9.3950 Tesla Varian VXR 400S NMR spectrometer utilizing a Doty dual bearing VT-MAS probe. Samples were spun at 4 KHz, a 2.4 ms pulse length was employed with 5 to 15 second post-acquisition delay times and the signal was averaged over 64 transients. The rotors were loaded into the precooled probe in a nitrogen filled glove bag. A dewar of liquid nitrogen was utilized not only to store the sample but also to limit the humidity in the bag. Sample temperature was calibrated with a thermocouple attached to the brass rotor guide pin while spinning an empty rotor at the same speed and gas pressures as had been used in obtaining the spectra.

Magnetic susceptibility measurements were made with an S.H.E. 800 Series SQUID susceptometer. Samples were run in Kel-F buckets and transferred to the SQUID in a nitrogen-filled glove bag. A large copper block was cooled to liquid nitrogen temperature and inserted into the loading mechanism immediately prior to loading the liquid nitrogen-cooled sample. The block acted as a heat sink to ensure that the sample's temperature did not rise much above liquid N_2 temperature during evacuation and back-filling of the anti-chamber. The electronic contribution to the susceptibility was calculated by subtracting the diamagnetic contribution of the decomposed sample and the bucket.

Pressed powder and pellet dc conductivity measurements were made as a function of temperature and voltage with a Keithley 617 programmable electrometer. Impedance spectroscopy measurements were made with a Hewlett-Packard 4192A-LF impedance analyzer over the frequency range of 5 Hz to 13 MHz. Application of potassium metal to the electrodes was accomplished in a helium-filled glove box; the sample and conductivity cell were kept below 200 K in a cold well during the loading. Samples for

measurements that did not require alkali metal electrodes were loaded in a nitrogen filled glove bag. Further details of the methods employed are published elsewhere.[10,11]

II.C.3 Results and Discussion

The crystal structure has been described elsewhere[22] so only a review of the general features will be presented here. It crystallizes in the ($R\bar{3}$) space group. Each cesium cation is complexed by an 18C6 and a 15C5 molecule. These "sandwiched" cations pack alternately above and below the plane of a central "free" (ie non-complexing) 18C6 molecule. A three fold symmetry axis runs through the middle and perpendicular to the plane of the free crown. The "sandwiched" cations form a double three-bladed propeller about this axis; they are tilted 60° with respect to the plane of the free crown, the upper three tilted in the opposite sense of the lower three (see Figures II.B.1 - II.B.3).

The packing of the molecules leaves cavities arranged around and alternately above and below the plane of the free crown. The cavities are approximately ellipsoidal, being ~ 5 Å in length (along the c-axis, i. e. perpendicular to the plane of the free crown) and ~ 2.5 Å in diameter. These cavities form a 6-member ring about the free crown with a short (~ 8 Å center-to-center), open channel connecting each cavity with its two nearest neighbors in the ring. Each cavity is connected to two neighboring 6-member rings by long (~ 10 Å) more constricted channels. Additionally, there are two smaller and more spherical cavities located above and below the plane of the free crown which serve as the sites of the approximately 4.5 mole percent excess cesium (in the form of the cation) that was observed in the crystal structure. This dopant level corresponds to one in four free crowns being coordinated to a Cs^+ ion. More narrow, bent channels connect these central cavities with each of the ring cavities. The cavity and channel structure can be seen in the isosurfaces displayed in Figure 1.[25] Not clear from the figure is that there

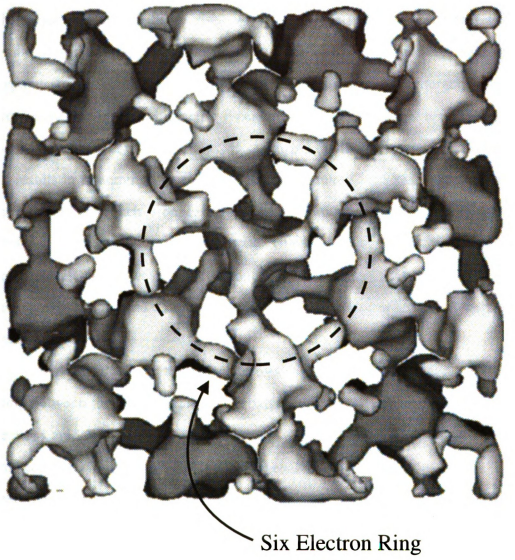

Figure 1. Depiction of the cavities and channels in the mixed crown electride (similar to those to be published in reference 25).

are also infinite, albeit rather long and narrow, straight channels down the c-axis that interconnect the central cavities of the rings.

The electronic contribution to the molar magnetic susceptibility for $[Cs^+(15C5)(18C6)e^-]_6 \cdot 18C6$ is shown in Figure 2. It is field independent between 0.5 and 7 KG. The data display no maximum and rather than tending toward Curie-Weiss law behavior, its susceptibility rises with increasing temperature after reaching a minimum of what appears to be an impurity tail. The high temperature susceptibility corresponds to less than 13 % and 3 % of the number of non-interacting unpaired electrons expected in a stochiometric F-center salt at 200 and 80 K respectively. This behavior is reminiscent of $K^+(C222)e^-$.[21] Allowing the temperature to rise above about 230 K results in a seemingly irreversible change to more Curie-like behavior. Multiple warmings result in a much stronger signal, perhaps through thermally created defect sites or a order-disorder transition. The magnetic behavior of $[Cs^+(15C5)(18C6)e^-]_6 \cdot 18C6$ is in sharp contrast to the two parent compounds which are antiferromagnets with maxima in their susceptibilities and a nearly stochiometric number of independent spins at high temperatures.[14,17]

The structure of the mixed crown electride suggests that the dominant coupling between the trapped electrons is within the six-member rings. The inter-ring connections are long (~ 10 Å) and constricted. Within the rings, the nearest neighbors are connected by short open channels which should afford strong non-orthogonal overlap. Neglecting inter-ring and second nearest neighbor intra-ring interactions, the Hamiltonian representing the exchange interaction of a six member Heisenberg ring is given by

$$\mathcal{H} = -2J\left(\sum_{i=1}^{5} \hat{S}_i \bullet \hat{S}_{i+1} + \hat{S}_6 \bullet \hat{S}_1\right) - g\beta\sum_{1}^{6} H \bullet \hat{S}_i \qquad (1)$$

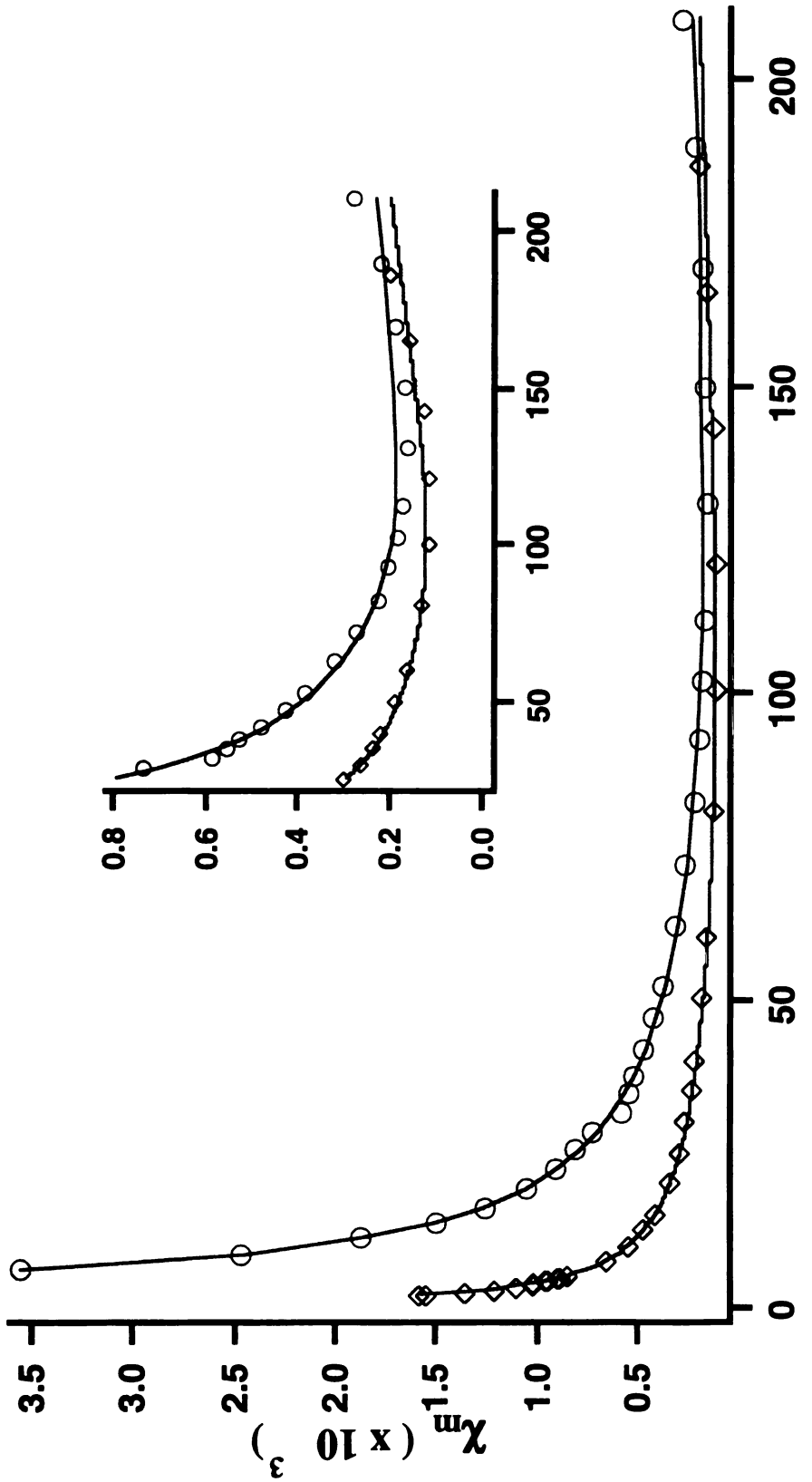

Figure 2: The temperature dependence of the electronic molar susceptibility for two separate syntheses with different concentrations of "excess" cesium. The solid lines are non-linear least squares fits by an independent six-electron ring model (equation 4). The inset is an expansion of the high temperature region.

The energy levels for S=1/2 six-member rings governed by this Hamiltonian have appeared in print.[26] Using the published energy levels, the temperature dependence of the zero field susceptibility is

$$\chi_m = \frac{Ng^2\beta^2}{6kT}\left\{\frac{\begin{array}{l}28+20\exp(x)+4\exp(1.4385x)+2\exp(2x)\\+2\exp(2.7639x)+20\exp(3x)+10\exp(4x)\\+4\exp(5x)+4\exp(5.5616x)+2\exp(7.2361x)\end{array}}{\begin{array}{l}7+10\exp(x)+\exp(1.3945x)+6\exp(1.4385x)\\+3\exp(2x)+3\exp(2.7639x)+10\exp(3x)\\+7\exp(4x)+6\exp(5x)+6\exp(5.5616x)\\+\exp(6x)+3\exp(7.2361x)+\exp(8.6056x)\end{array}}\right\} \qquad (2)$$

where $x = -J/kT$. In addition to the magnetic moment due to the six electron rings, allowance must be made for contributions to the susceptibility from paramagnetic trapped electrons from the excess cesium and for uncorrected diamagnetism and temperature independent paramagnetism (TIP). The trapped electrons are assumed to be largely uncorrelated and to follow a Curie-like law

$$\chi_{para} = \frac{C}{T^n}. \qquad (3)$$

The total susceptibility of this model can then be represented by the sum of the three terms

$$\chi = \chi_m + \chi_{para} + \chi_{dia} \qquad (4)$$

where χ_{dia} is a small temperature independent term to account for any uncorrected diamagnetism and TIP. Non-linear least-squares fitting of the data by equation 4 resulted

in excellent fits for two separately synthesized samples as shown in Figure 2. In each case, the spectroscopic g value was held at that of the free electron. The fitting parameters for the sample with the more paramagnetic tail are C = 0.0211(6), n = 1.01(2), J/k = -400(20) and χ_{dia} = -3(2) x 10^{-5}. (The numbers in parenthesis are standard deviation estimates of the last digit.) The value of n indicates that the defect electrons obey the Curie law (are uncorrelated) and the value of C indicates that the tail can be accounted for by approximately 5.6 mole percent unpaired spins. The fitting parameters for the sample with the smaller tail (Figure 3) are C = 0.00240(1), n = 0.62(1), J/k = -410(10) and χ_{dia} = -3(1) x 10^{-5}.

The size of the Curie tail is preparation dependent as one would expect for defect electrons. In most samples, the low temperature data could be fit well by the Curie law plus a temperature independent diamagnetic correction and the value of the Curie constant corresponded to up to 4 - 5% excess electrons. This number is in good agreement with the observed excess Cs^+ level seen in the x-ray structure and is therefore likely to be due to the electron released by the excess cesium. The sub-Curie law value of the exponent in the case of the sample with a much smaller tail than the others (Figure 2) is characteristic of linear chain systems.[27] This behavior has been explained in two different ways; the REHAC model[28] and the segment model.[29] The former model explains the phenomenon by invoking a random distribution of exchange values which effectively divides the chain into weakly interacting segments, resulting in a low temperature increase in χ which is weaker than T^{-1}. The latter explanation proposes that the behavior is the result of interspersed paramagnetic odd and diamagnetic even length chains. It seems likely that the electrons released by the excess Cs^+ localize in the cavities left open on the opposite side of the free crown but with significant delocalization along the c axis channels. Overlap via the channel with the next nearest dopants' electrons might then lead to the chain-like behavior seen in the low temperature

susceptibility. However, it is unclear to us why the chain-like sub-Curie tail is only seen at a very small dopant level.

The ^{133}Cs NMR chemical shift of $[Cs^+(15C5)(18C6)e^-]_6 \cdot 18C6$ is very different from that of either of the other two electrides; it is by far the smallest of the three, more than 115 and 530 ppm smaller than those of $Cs^+(18C6)_2e^-$ and $Cs^+(15C5)_2e^-$ respectively at 210 K.[5,17] The chemical shift of the mixed crown electride shifts paramagnetically with increasing temperature (Figure 3), the *opposite* trend of that observed for either of the parent compounds. The shift depends linearly on temperature with a slope of 0.235(6) ppm K^{-1} and an intercept of -32(1) ppm. Allowing the temperature to rise above ~ 250 K resulted in a slow, but significant and irreversible paramagnetic change of the chemical shift and irreproducible behavior.

$[Cs^+(15C5)(18C6)e^-]_6 \cdot 18C6$, like $Cs^+(18C6)_2e^-$ and $Cs^+(15C5)_2e^-$, exhibits a ^{133}Cs contact (Knight) shift due to interaction with the electride electrons.[5,17] The unpaired electron contact density at the cation nucleus($\langle|\psi(0)|^2\rangle$) is related to the Knight shift ($K(T)$) by

$$K(T) = (\frac{8\pi}{3N_{av}})\langle|\psi(0)|^2\rangle\chi(T) \qquad (5)$$

where $\chi(T)$ is the electronic contribution to the magnetic susceptibility and all other symbols have their usual meanings.[30] $K(T)$ is approximately proportional to T since, in the limited temperature range studied by NMR, $\chi(T)$ is approximately proportional to T. $K(T)$ can therefore be closely approximated by

$$K(T) = \sigma(T) - \sigma(\infty) = 0.235 ppm K^{-1} \cdot T. \qquad (6)$$

The electronic part of the molar susceptibility at 210 K is 2.80 x 10^{-3} emu/mol. Using these data and the method more fully described elsewhere,[5] the atomic character can be

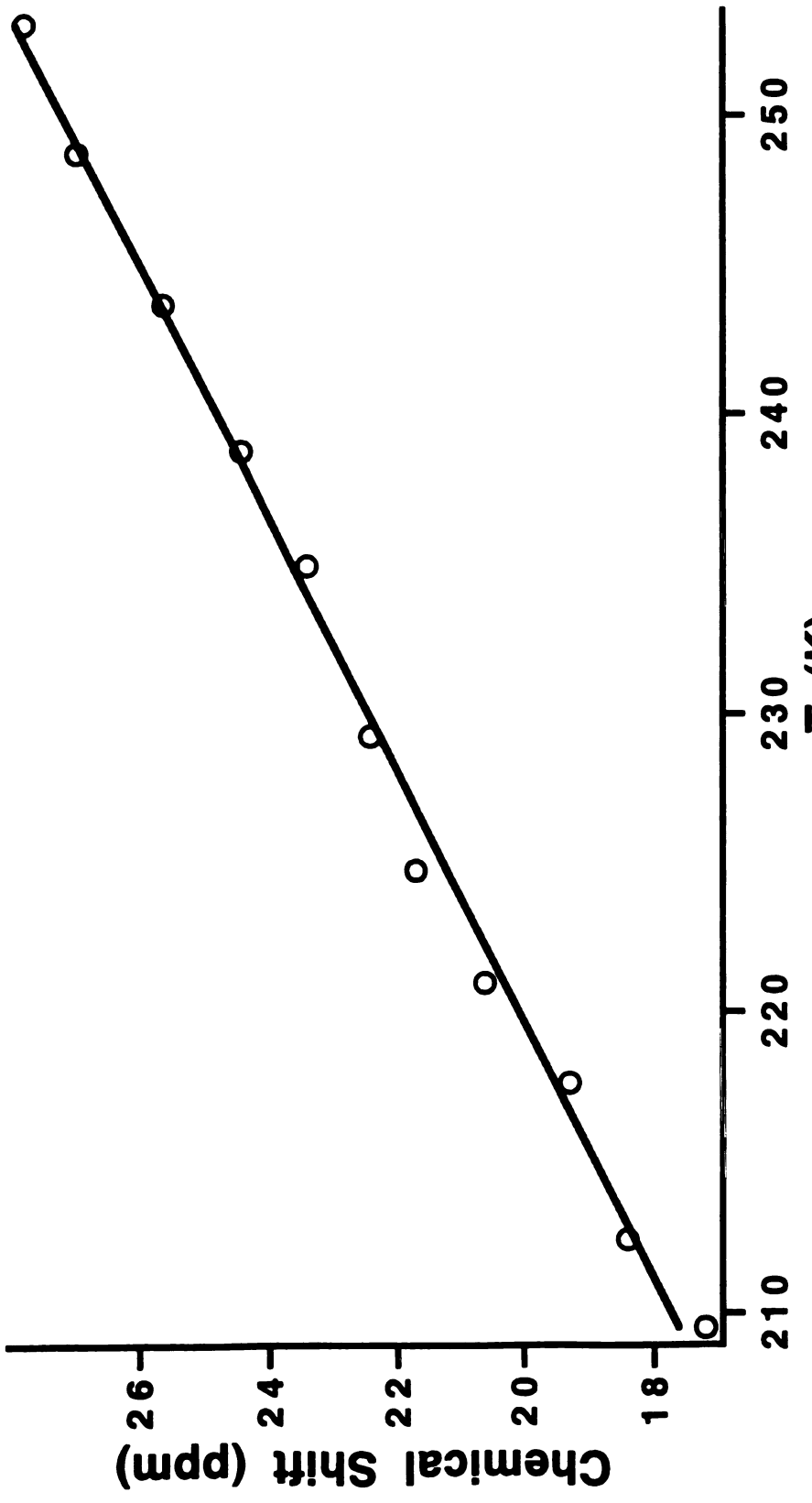

Figure 3. ^{133}Cs NMR chemical shift plotted as a function of temperature. The solid line is a least-squares fit by equation 6.

calculated at 210 K to be 4.79 x 10^{-3} %. This value is an order of magnitude smaller than that calculated for $Cs^+(18C6)_2e^-$ and $Cs^+(15C5)_2e^-$.[5,17] It must be noted that thermal expansion of the compound may cause longer average Cs-O distances as the temperature is raised resulting in a diamagnetic change in the Ramsey[31] shift which will also be linear in temperature. This would in effect reduce the overall paramagnetic Knight shift with increasing temperature resulting in an erroneously small calculated atomic character. However, the temperature dependence due to the change in the Ramsey shift is expected to be small; a temperature independent chemical shift is seen in all $Cs(18C6)_2$ and $Cs(15C5)_2$ salts and alkalides except $Cs^+(18C6)_2Cs^-$, an exception due to the effect of the structural perturbation caused by the large size of the cesium anion.[5] Thus, the calculated atomic character of the trapped electron should be a good approximation, although it is a lower limit. Its exceedingly small value demonstrates an extraordinary exclusion of the electride electron from the Cs nucleus and is testament to the tighter complexation or "fit" provided by the mixed crown system vs. the single crown systems.

As with the other physical properties, the electrical conductivity of $[Cs^+(15C5)(18C6)e^-]_6 \cdot 18C6$ is very different from the parent electrides, which exhibit very low electronic conductivities (~ 10^{-10} Ω^{-1} cm^{-1} at 200 K).[11] Packed powder DC conductivity data were collected from 81 K to room temperature (Figure 4). The apparent activation energies (E_a) can be calculated from the familiar Arrehenius relation

$$\sigma = \sigma_o \exp[-E_a/kT] \qquad (7)$$

where σ is the measured conductivity. A fit to the low temperature (81 - 125 K) behavior yields an apparent activation energy of 0.06 eV. The data between 125 and 192 K show two other linear regions with somewhat smaller apparent activation energies. Above 192 K the resistivity rises, reaching a maximum value at 226 K followed by a sharp decrease to 259 K where the resistivity again rises, the final rise presumably due to decomposition.

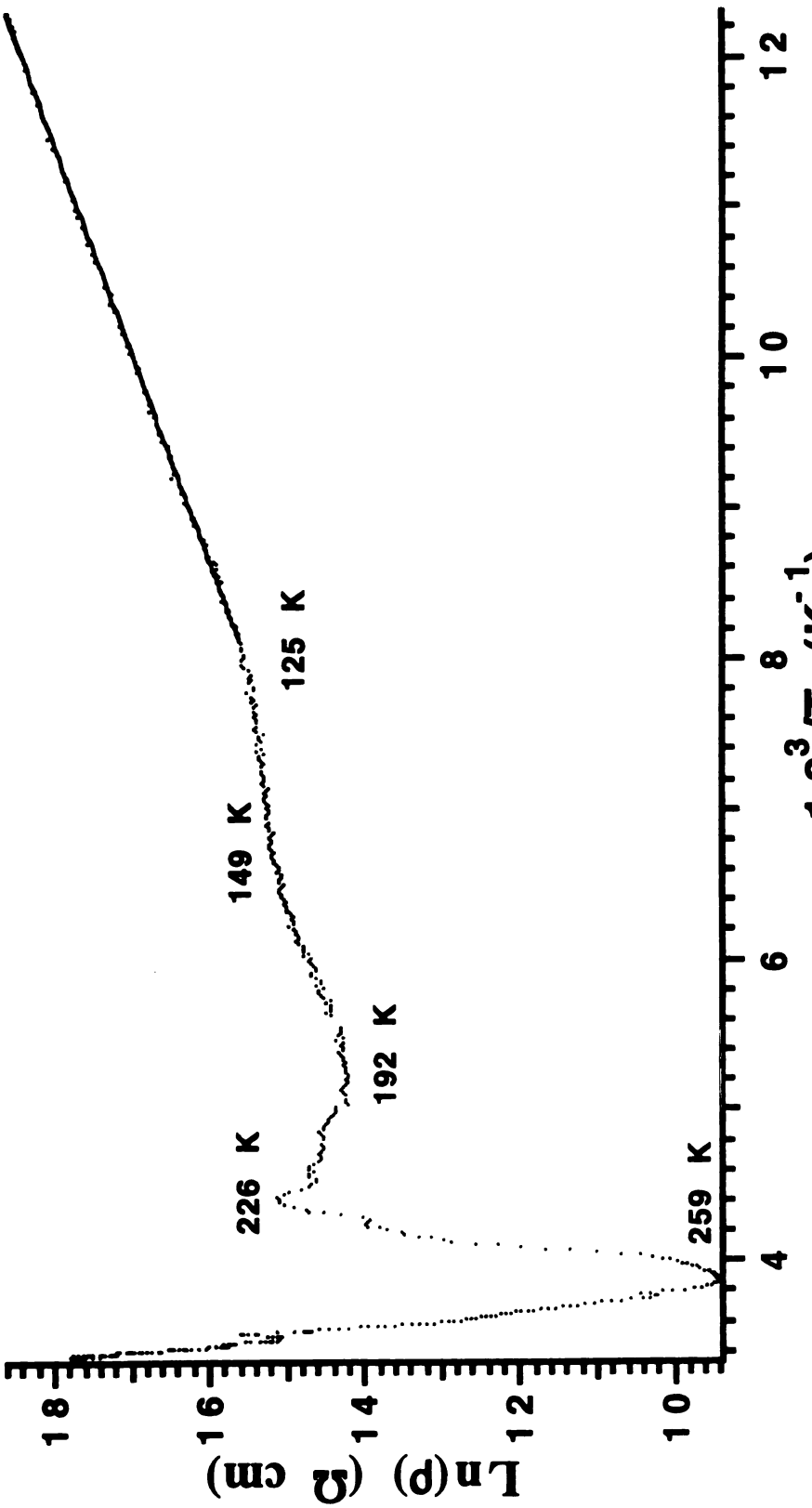

Figure 4. The natural log of the packed powder resistance plotted against inverse temperature. The superimposed line is a fit of the low temperature data to equation 7.

The initial rise is unlikely to be due to a semiconductor-metal transition since such a transition is not indicated by any other measurement including impedance spectroscopy outlined below. The rise and fall in resistivity may be due to electrode contact effects and is similar to that seen in $Cs^+(18C6)_2e^-$.[11]

The DC conductivity is markedly non-Ohmic as seen in Figure 5. This fact and the rather large resistance seen in the 2-probe DC conductivity measurements indicate the possibility of a Schottky barrier or oxide layer at the contacts. Complex AC 2-probe impedance measurements (Figure 6) with bare steel electrodes show at least two resolvable arcs. The higher impedance (lower frequency) arc is strongly bias dependent also indicating an electrode effect. The electrodes were coated with potassium metal and the impedance spectroscopy repeated on pressed pellets. This resulted in a much lower resistance and a smaller dependence on the applied bias voltage (Figure 7). This indicates that the outer arc and much of the resistance seen is due to a Schottky barrier, since the work function of potassium is expected to more closely match that of the electride. In addition, measurements with potassium-coated electrodes indicate only one arc with a zero frequency resistance at least an order of magnitude smaller than the smaller of the two seen with bare steel electrodes. Instrumental limitations prevented us from checking for the existence of higher frequency arcs. The measured arc may be from intergrain transport and contact resistances, in which case the intrinsic resistance of the sample would be lower than our measurements show. The temperature dependence of the zero frequency resistance, measured with potassium coated electrodes, is shown in Figure II.B.5. It should be noted that allowing the temperature to rise above 230 K resulted in an irreversible increase in the resistance. The data can be fit with a single exponential with an apparent activation barrier of 0.064(2) eV. The fit of the data by this model of simple activated charge transport across a well defined-bandgap appears to be good at first glance, but examination of the residuals clearly shows that it has systematic deviations. A much better fit, without systematic deviations, can be made by the equation

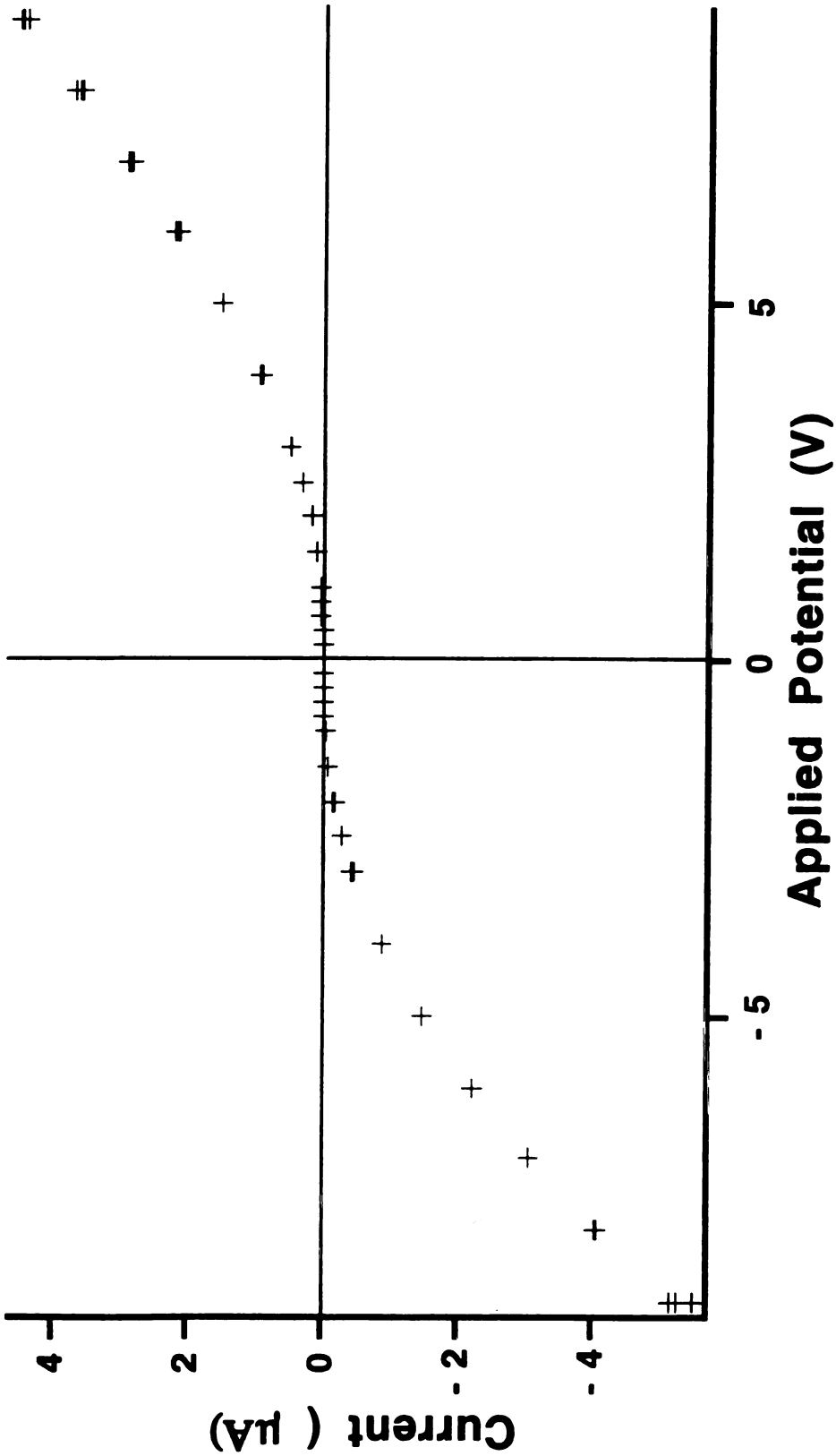

Figure 5. I-V curve of packed powder at 162 K showing non-ohmic behavior.

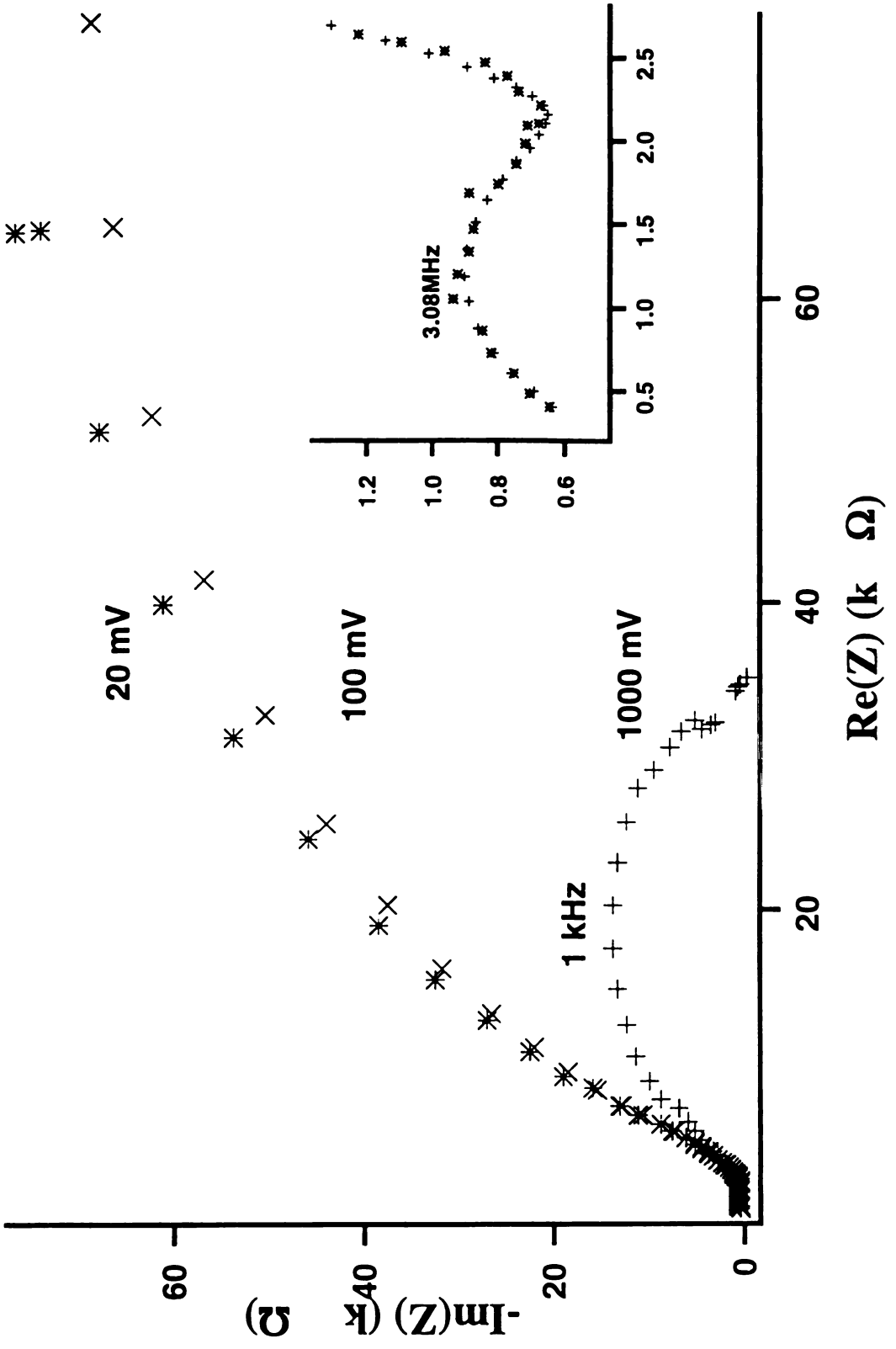

Figure 6. Impedance spectroscopy arcs of packed powders between bare steel electrodes at 160 K. The applied voltage and frequency of arc maxima are indicated on the figure. The inset is an expansion of the high frequency arc.

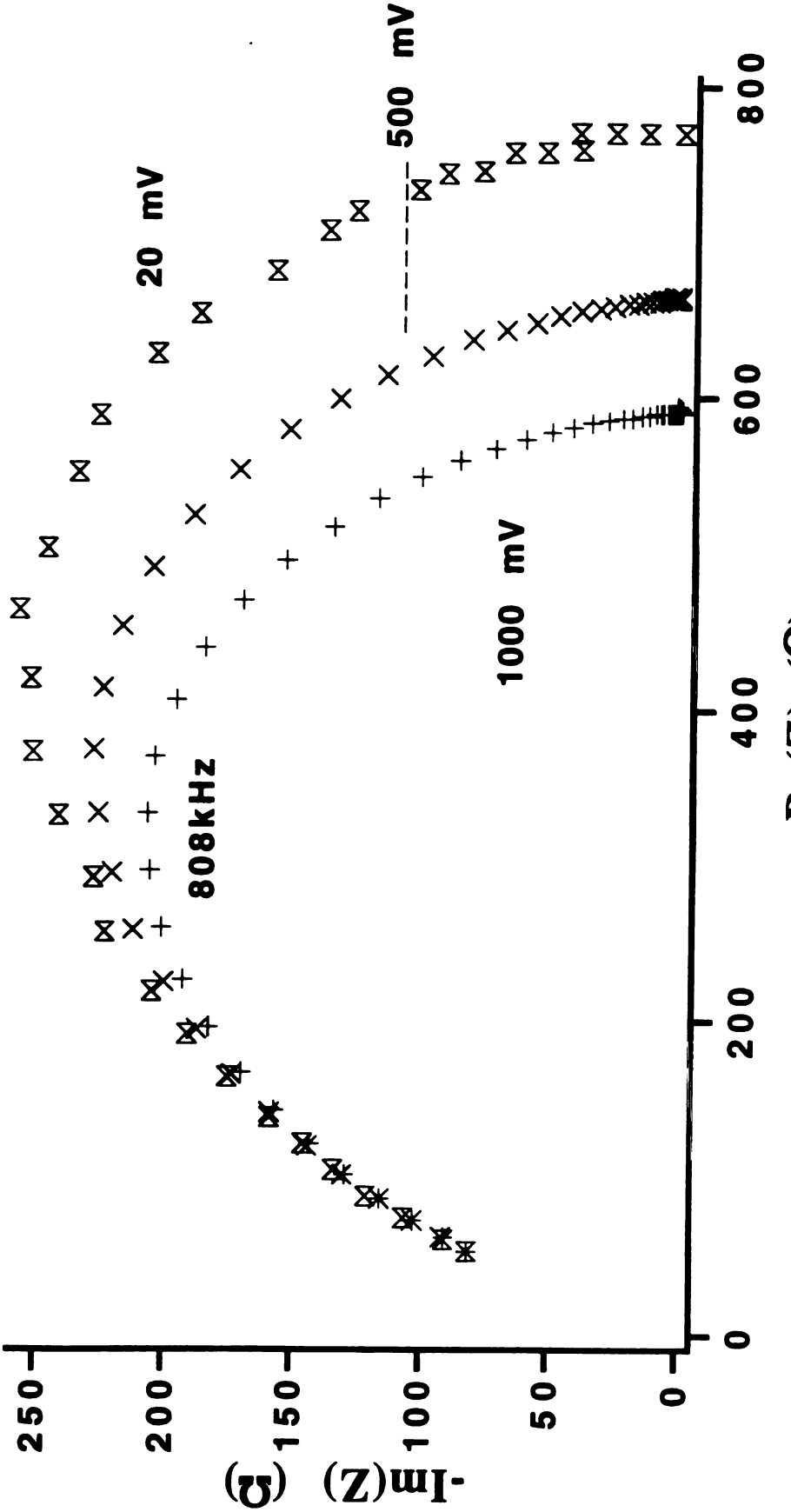

Figure 7. Impedance spectroscopy arcs of a pressed pellet between potassium coated electrodes at 137 K.

$$\sigma=\sigma_o exp[-(T_o/T)^{0.5}] \quad (8)$$

with σ_o = 22.2(7) Ω^{-1} cm^{-1}, T_o = 1.80(2) x 10^4 K, as shown in Figure II.B.5. This is indicative of one of three general transport mechanisms; granular metallic[32-34], variable-range hopping in the presence of a Coulomb gap[35] and quasi-one-dimensional variable-range hopping.[36]

The granular metallic mechanisms require a non-vanishing density of states at the Fermi level. Our susceptibility data indicate that there is a gap at the Fermi level and thus the granular metallic models are inappropriate. Therefore the conductivity is most likely to be due to a variable-range hopping mechanism, where the parameter T_o depends inversely on the carrier localization length. The conductivity may be due to hopping of the defect electrons between the central crown cavities through the c-axis channels, along which the wavefunctions of these electrons are expected to extend. In addition, the conductivity of other electrides has been shown to be largely due to defects;[10,11,37] large coulombic repulsions are expected to inhibit the mobility of the intrinsic electride electrons.[18]

II.C.4 Conclusions

$[Cs^+(15C5)(18C6)e^-]_6 \cdot 18C6$ exemplifies the diversity of structural possibilities that can be found in electrides. The simple combination of crown ethers which results in this electride and its remarkable six-electron ring is testament to further diversity one might find with other, as yet undiscovered, electrides. The dramatic difference in the properties between this electride and its two parent compounds demonstrates the wide variation of properties that can occur with seemingly minor alterations of the complexants

used. Further exploration of this young field through the use of other complexants and combinations of complexants promises to yield other structures with novel properties.

II.C.5 Acknowledgments

This research was supported by NSF Solid State Chemistry Grants DMR 87-14751 and DMR 90-17292 and by the Michigan State University Center for Fundamental Materials Research.

II.C.6 References

(1) Wagner, M. J.; Dye, J. L. In *Molecular Recognition: Receptors for Cationic Guests*; G. W. Gokel, Ed.; Pergamon Press: in press; Vol. I.

(2) Wagner, M. J.; Dye, J. L. *Ann. Rev. Mat. Sci.* **1993**, *23*, 223.

(3) Dye, J. L. *Chemtracts-Inorganic Chemistry* **1993**, *5*, 243.

(4) Dawes, S. B.; Ward, D. L.; Huang, R. H.; Dye, J. L. *J. Am. Chem. Soc.* **1986**, *108*, 3534.

(5) Dawes, S. B.; Ellaboudy, A. S.; Dye, J. L. *J. Am. Chem. Soc.* **1987**, *109*, 3508.

(6) Ellaboudy, A. Ph.D. Dissertation Thesis, Michigan State University, East Lansing, 1984.

(7) Shin, D. H. Ph.D. Dissertation Thesis, Michigan State University, East Lansing, 1992.

(8) Shin, D. H.; Dye, J. L.; Budil, D. E.; Earle, K. A.; Freed, J. H. *J. Phys. Chem.* **1993**, *97*, 1213.

(9) Ellaboudy, A.; Dye, J. L.; Smith, P. B. *J. Am. Chem. Soc.* **1983**, *105*, 6490.

(10) Moeggenborg, K. J. Ph.D. Dissertation Thesis, Mich. State Univ., East Lansing., 1990.

(11) Moeggenborg, K. J.; Papaioannou, J.; Dye, J. L. *Chem. Mater.* **1991**, *3*, 514.

(12) Ellaboudy, A.; Tinkham, M. L.; VanEck, B.; Dye, J. L.; Smith, P. B. *J. Phys. Chem.* **1984**, *88*, 3852.

(13) Dawes, S. B. Ph.D. Dissertation Thesis, Michigan State University, East Lansing, 1986.

(14) Wagner, M. J.; Huang, R. H.; Dye, J. L. *J. Phys. Chem.* **1993**, *97*, 3982.

(15) Issa, D.; Ellaboudy, A.; Janakiraman, R.; Dye, J. L. *J. Phys. Chem.* **1984**, *88*, 3847.

(16) Ward, D. L.; Huang, R. H.; Kuchenmeister, M. E.; Dye, J. L. *Acta Crystallogr.* **1990**, *C46*, 1831.

(17) Dawes, S. B.; Eglin, J. L.; Moeggenborg, K. J.; Kim, J.; Dye, J. L. *J. Am. Chem. Soc.* **1991**, *113*, 1605

(18) Singh, D. J.; Krakauer, H.; Haas, C.; Pickett, W. E. *Nature* **1993**, *365*, 39.

(19) Dye, J. L. *Nature* **1993**, *365*, 10.

(20) Dye, J. L. *Sci.* **1990**, *247*, 663.

(21) Huang, R. H.; Faber, M. K.; Moeggenborg, K. J.; Ward, D. L.; Dye, J. L. *Nature* **1988**, *331*, 599.

(22) Wagner, M. J.; Huang, R. H.; Eglin, J. L.; Dye, J. L. *Nature(London)* **1994**, *368*, 726.

(23) Kim, J. Ph.D. Dissertation Thesis, Michigan State Univ., East Lansing, 1989.

(24) Dye, J. L. *J. Phys. Chem.* **1984**, *88*, 3842.

(25) Overney, G.; Nagy, T. F.; Wagner, M. J.; Dye, J. L. , *submitted to Angew. Chem. Int. Ed. Engl.*

(26) Orbach, R. *Phys. Rev.* **1959**, *115*, 1181.

(27) Hatfield, W. E.; ter Haar, L. W. *Ann. Rev. Mater. Sci.* **1982**, *12*, 177.

(28) Bulaevskii, L. N.; Zvarykina, A. V.; Karimov, Y. S.; Lyubovskii, B. B.; Shchegolev, I. F. *Sov. Phys. JETP* **1972**, *35*, 384.

(29) Soos, Z. G.; Bondeson, S. R. *Mol. Cryst. Liq. Cryst* **1982**, *85*, 19.

(30) Knight, W. D. *Physical Review* **1944**, *76*, 1259.

(31) Ramsey, N. F. *Phys. Rev.* **1952**, *86*, 243.

(32) Sheng, P.; Abeles, B.; Arie, Y. *Phys. Rev. Lett.* **1973**, *31*, 44.

(33) Adkins, C. J. *J. Phys. C* **1987**, *20*, 235.

(34) Li, Q.; Cruz, L.; Phillips, P. *Phys. Rev. B* **1993**, *47*, 1840.

(35) Efros, A. L.; Shklovskii, B. I. *J. Phys. C* **1975**, *8*, 149.

(36) Mott, N. F.; Daveh, M. *Adv. Phys.* **1985**, ***34***, 329.

(37) Hendrickson, J. E.; Wagner, M. J.; Dye, J. L. *manuscript in preparation.*

II.D The First Crystalline Electride Revisited: New Magnetic Susceptibility Studies of $Cs^+(18\text{-crown-}6)_2e^-$

The following section is in the form of a paper entitled "The First Crystalline Electride Revisited: New Magnetic Susceptibility Studies of $Cs^+(18\text{-crown-}6)_2e^-$" which was published in The Journal of Physical Chemistry, volume 97, in the year 1993 and starting on page 3982. Rui Huang, with my assistance, is responsible for the single-crystal X-ray crystallography. I am responsible for all other measurements and analysis as well as writing the draft.

II.D.1 Introduction

In 1983, $Cs^+(18\text{-crown-}6)_2e^-$ [$Cs^+(18C6)_2e^-$], the first of an entirely new class of crystalline materials, electrides, was reported.[1] Since that time, this compound has been extensively characterized by single crystal x-ray crystallography,[2] NMR,[3] EPR,[4] powder conductivity,[1] optical absorption spectroscopy,[1,5] and magnetic susceptibility[2,6,7] Recently, new conductivity[8,9] and EPR measurements[10,11] gave significantly different results than were previously obtained. The difference was attributed to a low level of excess cesium doping in the previous samples, formally as the ceside, but the identity of the species responsible has not been verified. These results raised the question of what effect such doping may have had on the other measured properties of this electride, a question made all the more important by the significant theoretical interest in calculating its properties.[12-14] Specifically, could such doping, rather than partial decomposition or lack of correct stoichiometry of the polycrystalline samples, be responsible for the low free spin count (never exceeding about 80% of that expected)[2,6,7] as measured by magnetic susceptibility?

wer

pre

The

cou

exc

for

con

X-r

pre

me

wer

sus

sub

mo

Fig

-7(

Vie

II.D.2 Experimental

To determine the reason for the low spin count, undoped samples of $Cs^+(18C6)_2e^-$ were required. The earlier measurements had been made with polycrystalline samples prepared from solutions that were nominally stochiometric in both complexant and metal. Thus the equilibrium

$$2\ Cs^+(18C6)_2e^- \quad \Leftrightarrow \quad Cs^+(18C6)_2Cs^- + 2(18C6)$$

could lead to a mixture of e^- and Cs^- in solution. For later investigations, a 10 to 20% excess of complexant was used to drive the reaction toward electride formation. Samples for susceptibility were crystallized by utilizing slow (1 to 2 weeks) solvent removal at constant temperature (190 K). A crystal was selected from the synthesis and single crystal X-ray crystallographic measurements proved that it had the same structure as had been previously published.[2] Enough large (mm scale) single crystals for susceptibility measurements were selected and pulverized under liquid nitrogen. Magnetic susceptibilities were measured with an S. H. E. computer-controlled variable-temperature SQUID susceptometer. The electronic contribution to the susceptibility was determined by subtracting the diamagnetic signal of the sample after decomposition.

II.D.3 Results and Discussion

Susceptibility measurements. A typical plot of the temperature dependence of the molar susceptibility, which is field independent between 0.05 and 0.7 T, is shown in Figure 1. The susceptibility can be well fit by the Curie-Weiss law at temperatures above ~70 K. Least-squares fitting of the high temperature data (>70 K) to the Curie-Weiss law yielded 107(2)% unpaired electrons and a Weiss constant of -82(3) K. (Numbers in

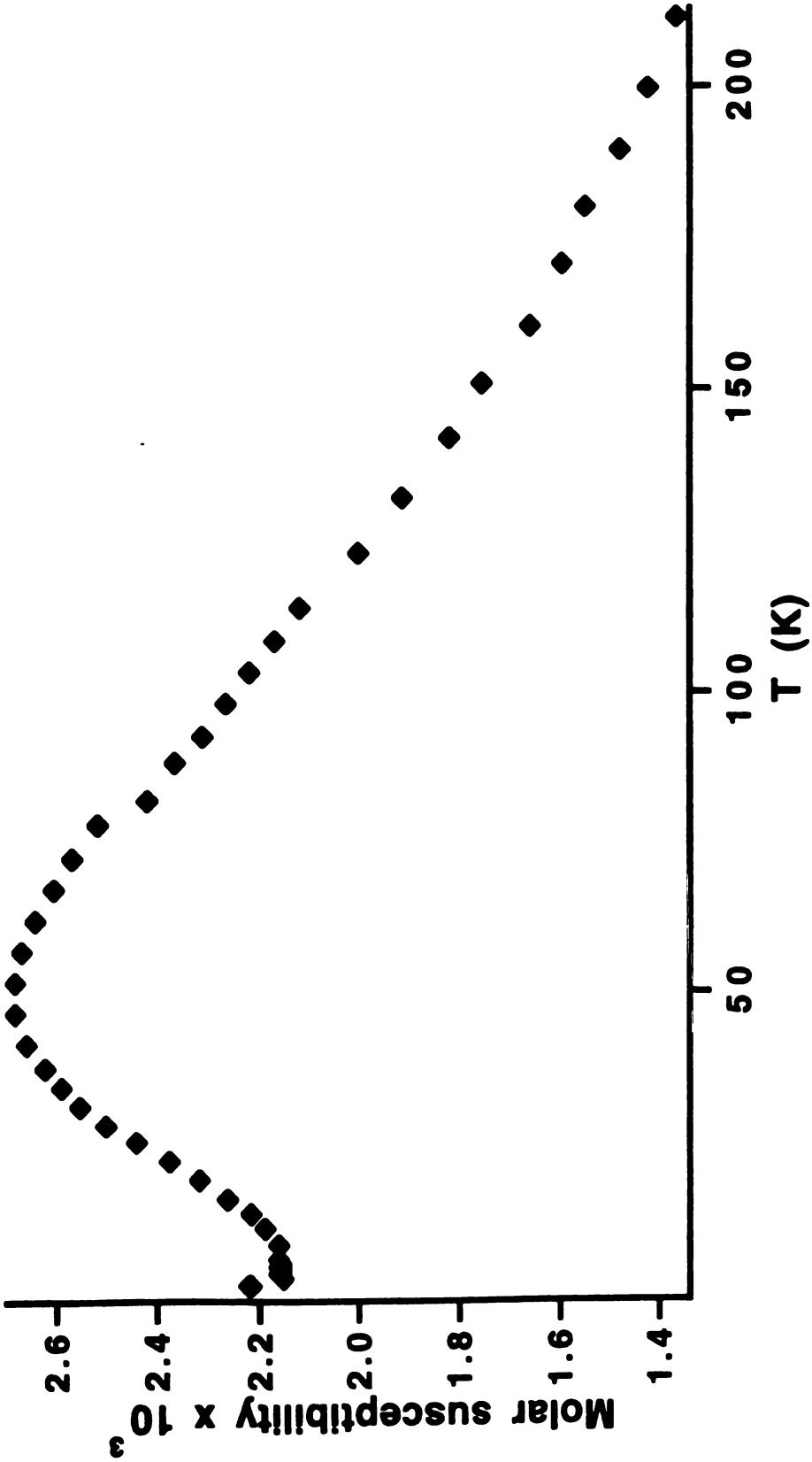

Figure 1. Temperature dependence of the molar electronic magnetic susceptibility of $Cs^+(18C6)_2e^-$ that has never been heated above 230K, showing evidence of antiferromagnetic order.

parentheses are estimated standard deviations of the last digit for a single run.) It should be noted that these numbers represent an upper limit since the high temperature susceptibility of an antiferromagnet is expected to approach Curie-Weiss behavior asymptotically.[15] A maximum in the susceptibility occurred at ~50 K with a gradual decrease below this temperature. At very low temperatures, what appeared to be a "Curie tail" from a very small amount of paramagnetic impurities could be seen whose magnitude was synthesis dependent. Simple extrapolation of the low temperature behavior to 0 K after subtraction of a 0.4% Curie tail gave an intercept of about 2/3 of the maximum susceptibility, as would be expected for a 3D antiferromagnet. The reproducibility of these data was confirmed with two other samples; a high temperature Curie-Weiss law fit yielded 107(1)% and 106(2)% unpaired electrons and Weiss constants of -84(2) K and -85(4) K respectively.

Although these new measurements clearly showed that the crystalline electride is an antiferromagnet, the subsequent behavior was highly dependent on the thermal history of the sample. Allowing the sample to warm briefly above about 230 K caused a seemingly irreversible change in the susceptibility to behavior reminiscent of a ferrimagnet.[15] (Neither annealing samples at 190 K for 16 hrs nor at 230 K for 12 hrs resulted in reversion to antiferromagnetic behavior.) Repeated warming above 230 K caused further deviation from antiferromagnetism, finally resulting in behavior which can be well fit to the Curie-Weiss law. Least-squares fitting of the entire temperature range (1.5 to 240 K) yielded 90.6(2)% unpaired electrons and a Weiss constant of -2.3(2) K. The lower spin count does not necessarily represent significant decomposition due to the thermal cycling since, as previously mentioned, the high temperature Curie-Weiss fitting of the antiferromagnetic data is expected to overestimate the number of unpaired spins. The susceptibility of samples that had not undergone a complete conversion are well fit by a linear combination of the antiferromagnetic data points and the best fit Curie-Weiss law behavior. The dependence of sample magnetic susceptibility on thermal history is illustrated in Figure 2.

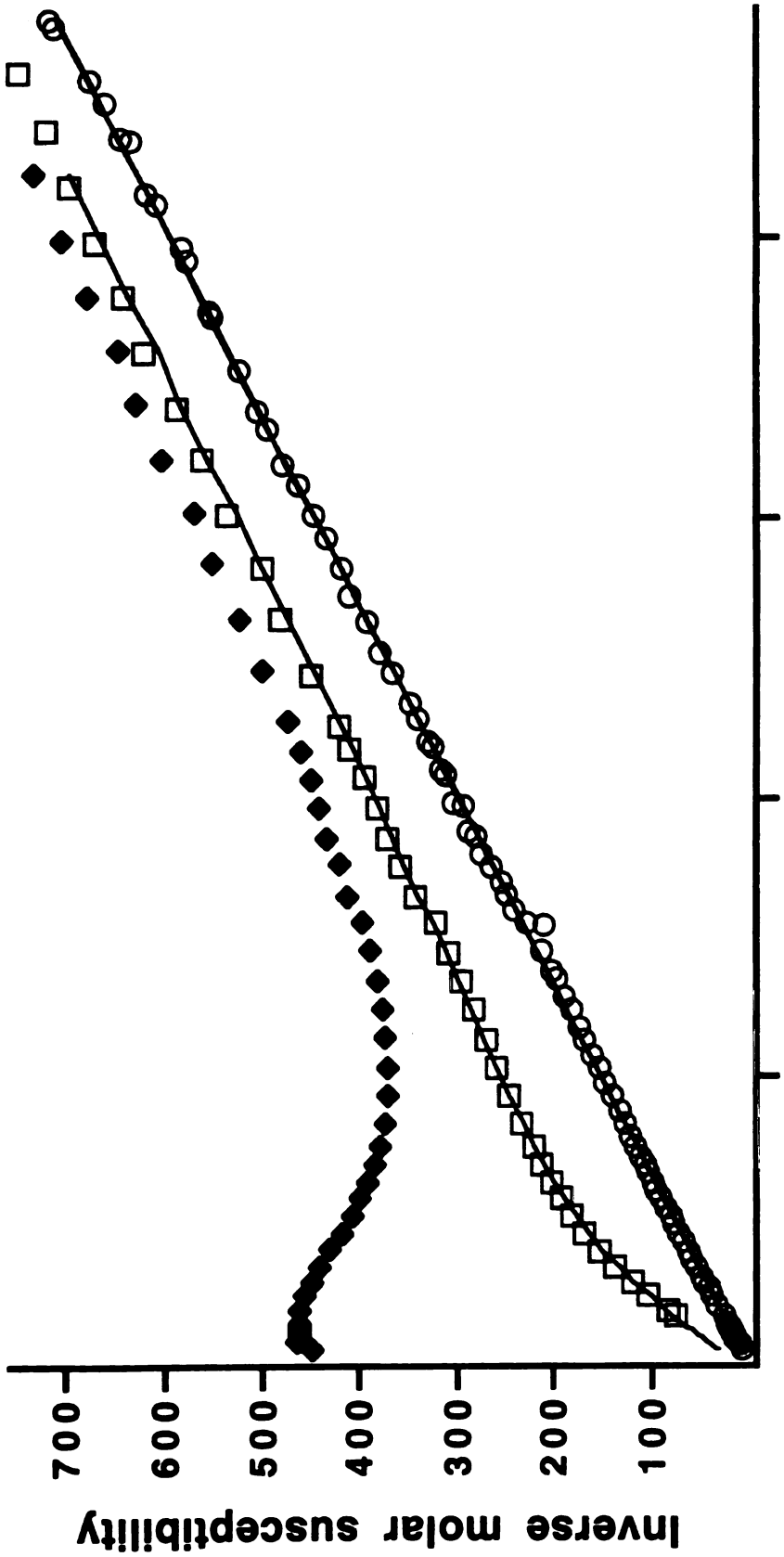

Figure 2. Temperature dependence of the inverse molar electronic magnetic susceptibility of $Cs^{+}(18C6)_2e^{-}$. The uppermost plot is that of a sample that has never been heated above 230 K (diamonds). The middle plot is the behavior observed after a brief excursion above 230 K (squares); the line through the data is a linear combination of the upper data and the Curie-Weiss law fit of the lower plot. The lower plot is the behavior observed after repeatedly heating the sample above 230 K (circles); the line through the data is the least-squares Curie-Weiss law fit.

The nature of the change in susceptibility that occurs above about 230 K is unknown. The known low temperature crystal structure shows the presence of two chemically equivalent but magnetically inequivalent complexed cesium cations as well as two such vacant anionic sites.[2] There is a large body of evidence that the unpaired electron density is centered at the vacant anionic site.[16] The high temperature phase shows the presence of two chemically distinct Cs^+ cations in MAS NMR[3] and two major inequivalent electron trapping sites were found in recent EPR studies.[11] DSC studies show no evidence of a first order transition between the two phases. Recent conductivity measurements indicate that the electride is primarily an ionic conductor in this temperature region, with Cs^+ as the migrating species.[8,9] Substantial crown ether motion has been observed in the isostructural sodide $Cs^+(18C6)_2Na^-$.[17] Perhaps motion-assisted migration of Cs^+ into the channels to form Cs atoms at elevated temperatures causes significant, irreversible disorder. Such disorder might distort the lattice in such a way as to create two chemically inequivalent Cs^+ cations and trapping sites, and lead to the Curie-Weiss behavior indicated by the magnetic susceptibility measurements.

Comparison with previous results. These results are in contrast to the previous results, which had found $Cs^+(18C6)_2e^-$ to fit the Curie-Weiss law, but with only up to about 80% of the expected free electrons and a Weiss constant of only -1 to -2 K, indicating weak electron-electron interactions.[2,6,7] In order to confirm that the behavior depended on sample preparation, polycrystalline samples were produced by recrystallizing $Cs^+(18C6)_2e^-$ in the presence of a small amount of $Cs^+(18C6)_2Cs^-$. The susceptibility behavior of these samples was similar to that obtained in the earlier investigations. Polycrystalline samples made in a similar fashion but with an excess of complexant present during synthesis always showed evidence of antiferromagnetic order.

The previously calculated unpaired electron contact density at the Cs^+ nucleus obtained from ^{133}Cs NMR spectra should be corrected in light of the new susceptibility data. It had been reported that the unpaired electron density at Cs^+ was 8.75×10^{21} cm^{-3},

leading to 0.033% atomic character at 250 K as calculated from the Knight shift measured by NMR techniques.[3] Recalculating both values yields 9.6 x 10^{21} cm^{-3} and 0.036%. While these values are somewhat different, they are still very small compared to the contact densities observed for cesium solutions in ammonia, amines, and other solvents, thus demonstrating the small occupancy of the 6s orbital of the complexed cesium cation in $Cs^+(18C6)_2e^-$.[3]

II.D.4 Conclusions

This new study of $Cs^+(18C6)_2e^-$ has shown that the magnetic properties of samples with the published structure are significantly different from those previously ascribed to it. We found that this electride has stochiometric trapped electrons that display antiferromagnetic order and which can undergo a gradual transition to Curie-Weiss law behavior, still retaining more than 90% of the stochiometric spin count. This is contrary to previous studies which characterized the electride as a Curie-Weiss paramagnet with never more than 80% unpaired electrons. The behavior seen in previous studies can be reproduced by rapidly harvesting polycrystalline samples from solutions that contain a slight excess of cesium.

While doping with excess cesium is a likely cause of the differences in the measured properties of $Cs^+(18C6)_2e^-$, one cannot exclude other possibilities. Poor loading technique resulting in significant decomposition as well as loss of all evidence of antiferromagnetic order is possible, however, highly unlikely. The measurements were repeated several times by several different investigators who were well acquainted with the need to keep electrides as cold as possible to prevent decomposition. It is also possible that polycrystalline samples made in the presence of near stochiometric reactants may not have the same structure as that reported for the electride. The published structure of the electride was obtained from single crystals that were grown slowly. The rapid harvesting of

polycrystalline samples from near stochiometric solutions could yield a highly disordered system which might even include some solvent in the structure.

Interesting questions still remain about this electride. What is the nature of the magnetic transition above 230 K? Could the properties of the electride be so drastically altered by a small percentage of excess cesium doping and, if so, how? If one can dope the electride with cesium, does a superlattice form? These questions are currently being investigated by powder x-ray diffraction, NMR, and additional SQUID measurements.

II.D.5 Acknowledgements

This research was supported by NSF grant DMR 90-17292 and the MSU Center for Fundamental Materials Research. The X-ray diffractometer system was provided by NSF grant CHE 8403823.

II.D.6 References

1. Ellaboudy, A. S.; Dye, J. L.; Smith, P. B. *J. Am. Chem. Soc.* **1983**, *105*, 6490.

2. Dawes, S. B.; Ward, D. L.; Huang, R. H.; Dye, J. L. *J. Am. Chem. Soc.* **1986**, *198*, 3534.

3. Dawes, S. B.; Ellaboudy, A.; Dye, J. L. *J. Am. Chem. Soc.* **1987**, *109*, 3508.

4. Ellaboudy, A. S., Ph.D. Dissertation, Michigan State University, **1984**.

5. Ellaboudy, A. S.; Tinkham, M. L.; Van Eck, B.; Dye, J. L.; Smith, P. B. *J. Phys. Chem.* **1984**, *88*, 3852.

6. Issa, D.; Ellaboudy, A.; Janakiraman, R.; Dye, J. L. *J. Phys. Chem.* **1984**, *88*, 3847.

7. Dawes, S. B., Ph.D. Dissertation, Michigan State University, **1986**.

8. Moeggenborg, K. J., Ph.D. Dissertation, Michigan State University, **1990**.

9. Moeggenborg, K. J.; Papaioannou, J.; Dye, J. L. *Chem. Mater.* **1991**, *3*, 514.

10. Shin, D. H., Ph.D. Dissertation, Michigan State University, **1992**.

11. Shin, D. H.; Dye, J. L.; Budil, D. E.; Earle, K. A.; Freed, J. H. *J. Phys. Chem.* **1993**, in press.

12. Rencsok, R.; Kaplan, T. A.; Harrison, J. F. *J. Chem. Phys.* **1990**, *93*, 5875.

13. Allan, B.; DeBacker, M. G.; Lannoo, M.; Lefebvre, I. *Europhys. Lett.* **1990**, *11*(1), 49.

14. Golden, S.; Tuttle, T. R. Jr. *Phys. Rev. B* **1992**, *45*, 913.

15. Goodenough, J. B. Magnetism and the Chemical Bond, John Wiley & Sons, **1963**.

16. Wagner, M. J.; Dye, J. L. *Ann. Rev. Mat. Sci.* **1993**, in press.

17. Wagner, M. J.; McMills, L. E. H.; Ellaboudy, A. S.; Eglin, J. L.; Dye, J. L.; Edwards, P. P.; Pyper, N. C. *J. Phys. Chem.* **1992**, in press.

II.E $Cs^+(18\text{-crown-}6)_2e^-$: A Linear Chain Heisenberg Antiferromagnet With Interesting Phase Transitions.

The following section is in the form of a draft of a paper entitled "$Cs^+(18\text{-crown-}6)_2e^-$: A Linear Chain Heisenberg Antiferromagnet With Interesting Phase Transitions" to be submitted for publication in *The Journal of Physical Chemistry*. I am responsible for the writing of this draft.

II.E.1 Introduction

One of the most intriguing examples of the particle/wave duality of the electron is in their role as the anions of electrides. In electrides, the wavefunctions of the anionic electrons are localized in vacancies which serve as the alkali metal anion sites in the more conventional salts termed alkalides.[1-3] This situation is analogous to the well known F-center salts except that in the case of electrides, the salt has a *stochiometric* number of anionic electrons! It is common for chemists to draw a strong distinction between the wave like nature of atoms and electrons, thinking of the former in strictly particle terms and the latter as a wave. Electrides remind the chemist that the distinction is less than clear; electrons, which are normally thought of as satellites of the atomic cores, take the place of atomic ions while, of course, still retaining those properties unique to electrons.

Electrides have received considerable experimental and theoretical attention.[1-3] They hold the potential for novel electronic and magnetic properties as well as being model systems of confined electron gases. The simplicity of the electronic structure near the Fermi level makes them excellent systems with which to study metal-insulator transitions.[4]

The first crystal structure of an electride, $Cs^+(18\text{-crown-}6)_2e^-$ (abbreviated $Cs^+(18C6)_2e^-$), was published less than a decade ago.[5] Prior to and since that time, it has been characterized by NMR,[6] EPR,[7] powder conductivity,[8] optical absorption

spectroscopy,[8,9] and magnetic susceptibility.[5,10,11] More recent conductivity,[12,13] EPR[14,15] and susceptibility measurements[16] have called into question whether the formally studied samples had been "doped" with ceside, drastically altering the properties. The recent theoretical interest in electrides in general[4,17] and $Cs^+(18C6)_2e^-$ in particular,[18-23] makes it imperative that the questions surrounding the true properties which are attributable to the material with the published crystal structure are resolved. This article presents the properties of the electride with the published crystal structure and shows that these properties can be irreversibly altered by thermal history.

II.E.2 Experimental

$Cs^+(18C6)_2e^-$ was synthesized by anaerobically dissolving cesium metal in dimethyl ether in the presence of 10-20% excess complexant in a modified H-cell.[24] Addition of a co-solvent (trimethylamine or diethylether) and slow solvent removal (1-2 weeks) at constant temperature (190 K) resulted in large (millimeter scale) crystals. This procedure results in single crystals with the same crystal structure as previously published.[5,16] Single crystals were selected and pulverized under liquid nitrogen to yield the high quality polycrystalline samples used in all measurements. Care was taken to ensure that the temperature of the samples never rose above 190 K. All sample manipulation was performed in N_2 glove bags in the presence of an open liquid N_2 dewar to limit humidity. Further details of the purification of materials and of the synthetic methods used have been described in detail elsewhere.[25]

The NMR spectra were obtained at the Max T. Rogers NMR facility at Michigan State University. Measurements were made with a 9.8950 T Varian VXR 400S NMR spectrometer equipped with a 1 kW pulse amplifier. Variable temperature magic angle spinning (VT-MAS) spectra were obtained by using a Varian probe equipped with a pressurized bearing gas cooling system; dry N_2 was used for both the bearing and drive

gases. The probe head was protected by a N_2 glove bag containing an open liquid N_2 dewar to reduce humidity prior to pre-cooling to 153 K with a strong stream of bearing gas. The sample was then loaded directly from liquid N_2 in the glove bag. This procedure resulted in no visible condensation on the probe or the rotor even on humid days and consequently, sample spinning was assured. Sample temperature was calibrated with methanol in a capillary tube inserted down a tight fitting hole drilled in the center of the rotor cap. Samples were found to consistently spin at between 1.5 and 5.5 kHz in silicon nitride rotors with this set-up. Sample temperature was determined by using the known temperature dependence of the methanol proton spectra;[26] ^1H spectra were obtained with the decoupler channel. Thermal equilibrium was verified by waiting 10 minutes after the thermocouple in the bearing gas stream had equilibrated to the set temperature and by taking ^1H MeOH spectra both before and after the ^{133}Cs spectra of the sample. ^{133}Cs chemical shifts are referenced to the aqueous cesium cation at infinite dilution.

Powder x-ray diffraction spectra were obtained by using a Rigaku RU 200B powder x-ray spectrometer with low temperature attachment. Samples were run on aluminum holders and loaded in a glove bag directly from liquid N_2 into the precooled sample chamber.

Differential thermal analysis (DTA) was carried out with a Shimadzu DSC-50 calorimeter equipped with a low temperature attachment. Samples were hermetically sealed in aluminum pans using a liquid N_2 cooled press. The calorimeter was set-up and run in a N_2 glove bag and was precooled to 130 K prior to loading. A steady flow of helium gas was maintained in the sample cell prior to and during the measurements.

II.E.3 Results

The temperature dependence of the ^{133}Cs NMR shift is shown in Figure 1. A previous study of $Cs^+(18C6)_2e^-$ had found there to be a single peak at temperatures above

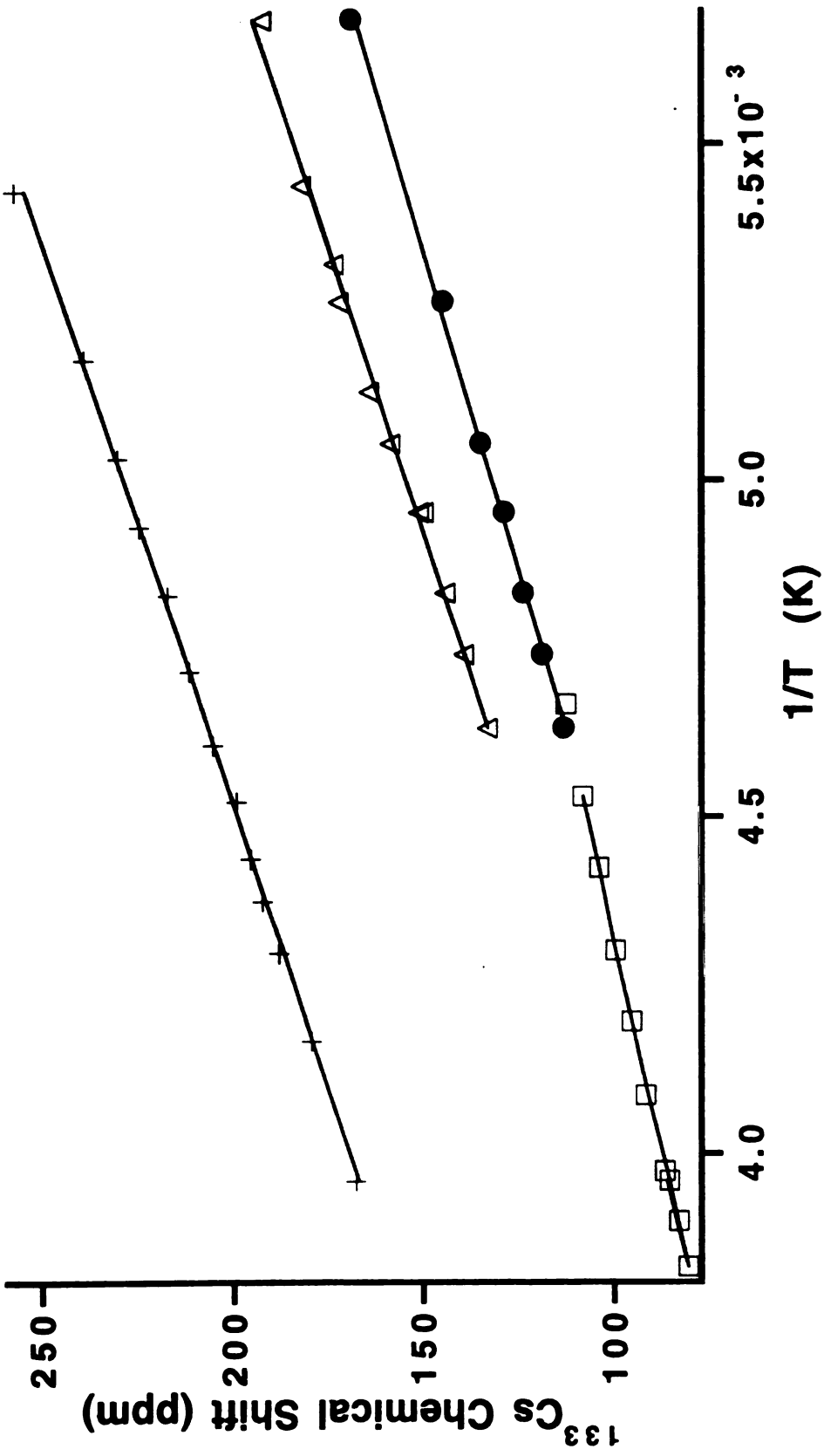

Figure 1. The temperature dependence of the NMR chemical shift of $Cs^+(18C6)2e^-$: LT peak (crosses), the HT peak (squares), the HT2a peak (filled circles) and the HT2b peak (triangles). The linear least-squares fits by equation 5 are shown as solid lines.

225 K; below this temperature a second peak paramagnetically shifted by about 20ppm appeared.[6] The chemical shifts were found to depend inversely upon temperature and this dependence was attributed to a contact (Knight) shift due to interaction with the trapped electrons. The Knight shift was found to be identical for both peaks in the temperature range studied. The existence of two chemically inequivalent peaks at low temperatures was surprising since the crystal structure indicates that there is only one chemically and magnetically equivalent cesium.[5] In the present study, it has been found there is only one peak if the sample is rigorously kept below ~ 230 K. The peak is shifted about 100 ppm from that seen in the previous study and has a similar temperature dependence. Upon warming past ~ 230 K, a second peak can be seen to grow near the chemical shift of the high temperature peak seen in the previous study. The growth is slow and its rate is temperature dependent; as the new peak grows, the peak due to the "low temperature phase" (LT phase) diminishes. The transformation can be made to go to completion to the high temperature phase (HT phase) by waiting for a sufficient period of time as can be seen in Figure 2. Cooling the sample does not result in the reappearance of the "low temperature phase" but rather the peak shifts paramagnetically in very much the same way as seen in the previous study and splits into two peaks separated by about 20 ppm at ~ 220 K (the HT2 phase). The transition from two peaks to one peak is rapid upon warming and the reverse is somewhat slower upon cooling. Upon completion at low temperature, the ratio of the intensities of the two peaks is approximately 3 to 2 (more paramagnetic peak, HT2b, to less paramagnetic peak, HT2a).

An attempt was made to observe the transitions seen in the NMR spectra by using DTA. Upon warming from low temperature, no transitions were observed from 150 K to 265 K. However, upon cooling, a small exotherm (ΔH = - 0.21 kJ mol^{-1}) appeared with an onset temperature of 219.7 K (Figure 3). Rewarming the sample resulted in the observation of an endotherm (ΔH = 0.33 kJ mol^{-1}) with an onset temperature of 217.7 K (Figure 4). The relatively larger heat of enthalpy of the endotherm as compared to the

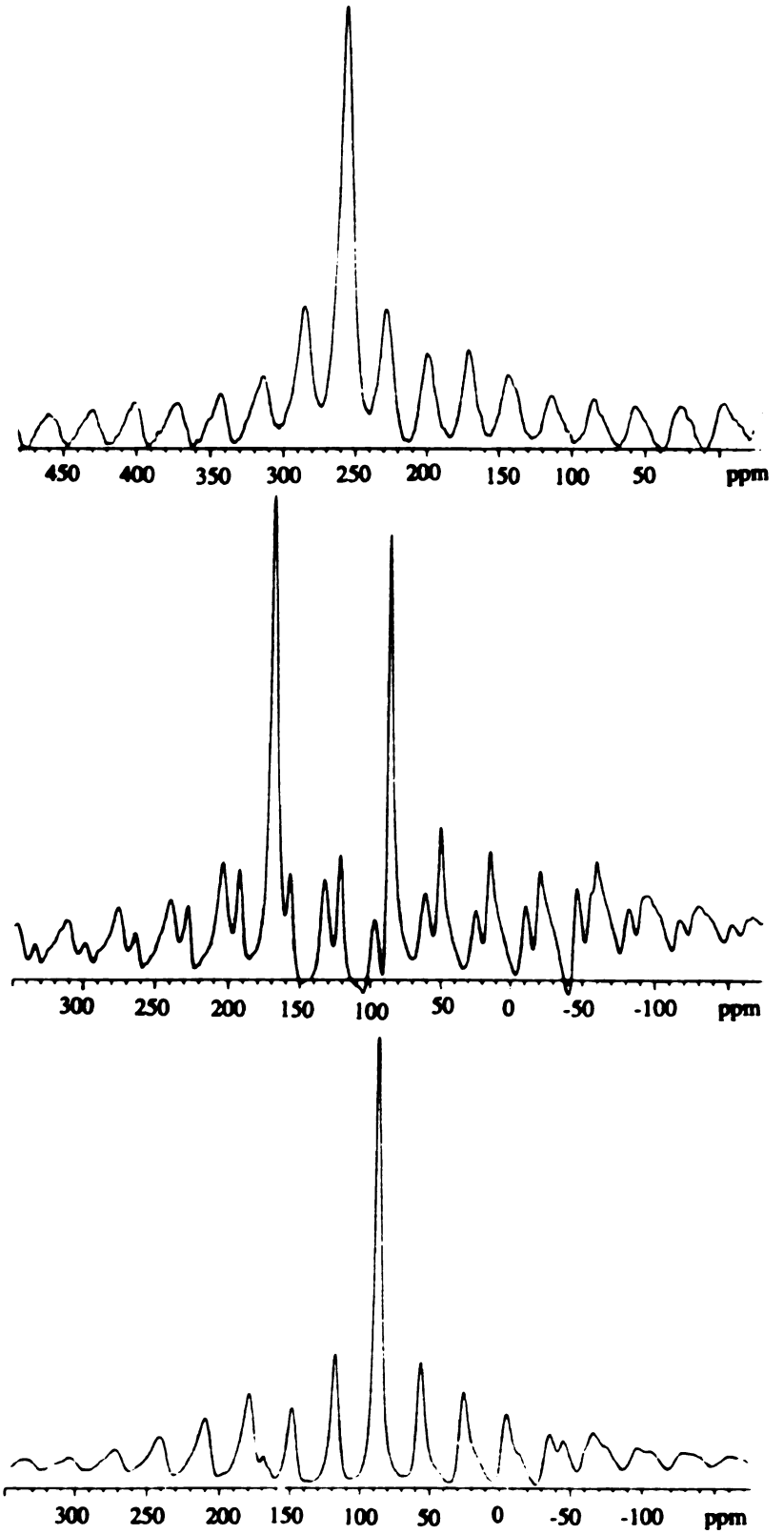

Figure 2. 133Cs NMR spectra: LT phase, 184 K (top), mixture of LT and HT phases, 253 K (middle), HT phase, 252 K (bottom).

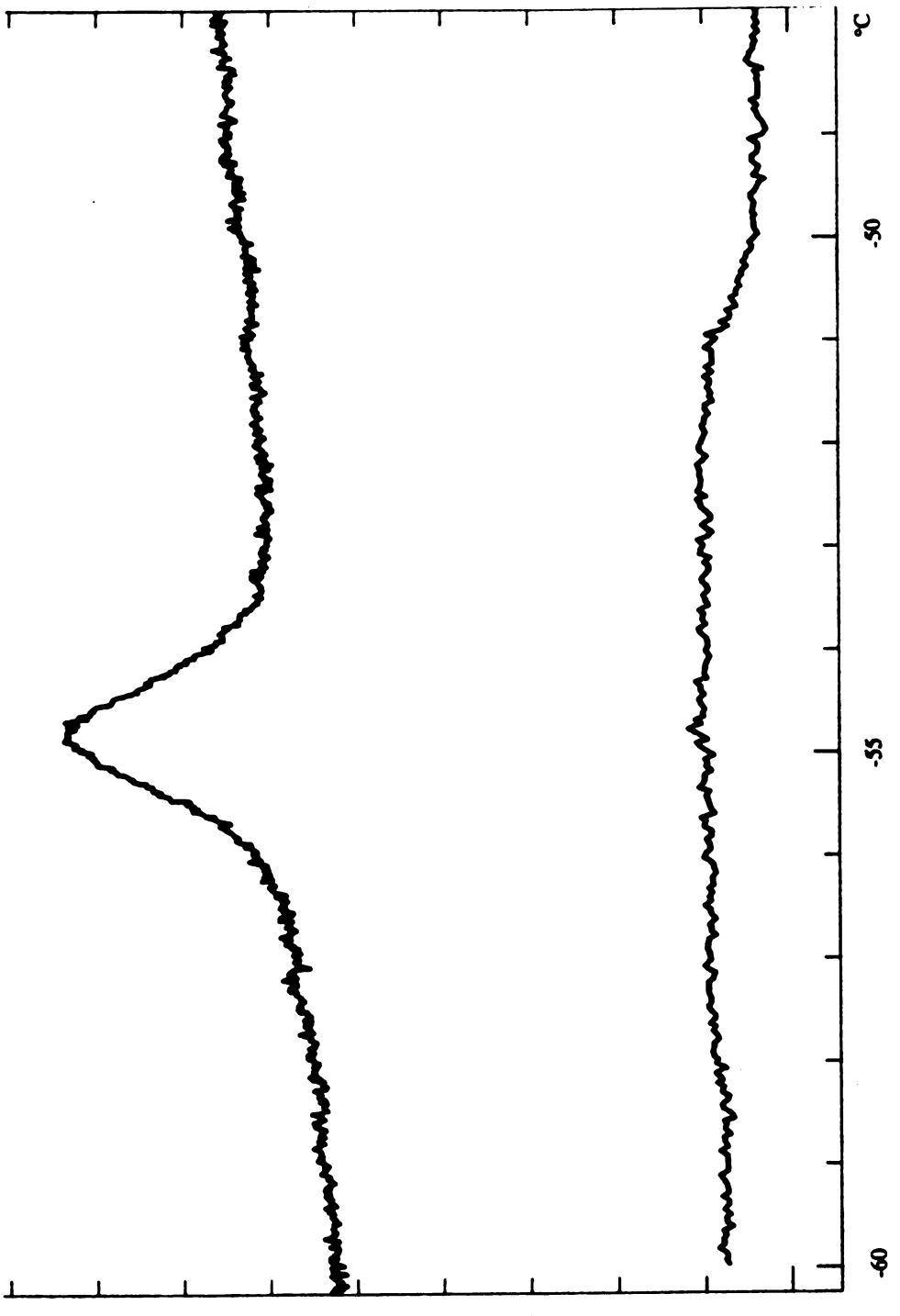

Figure 3. DTA trace showing a lack of features during first warming (bottom) and an exotherm upon subsequent cooling (top).

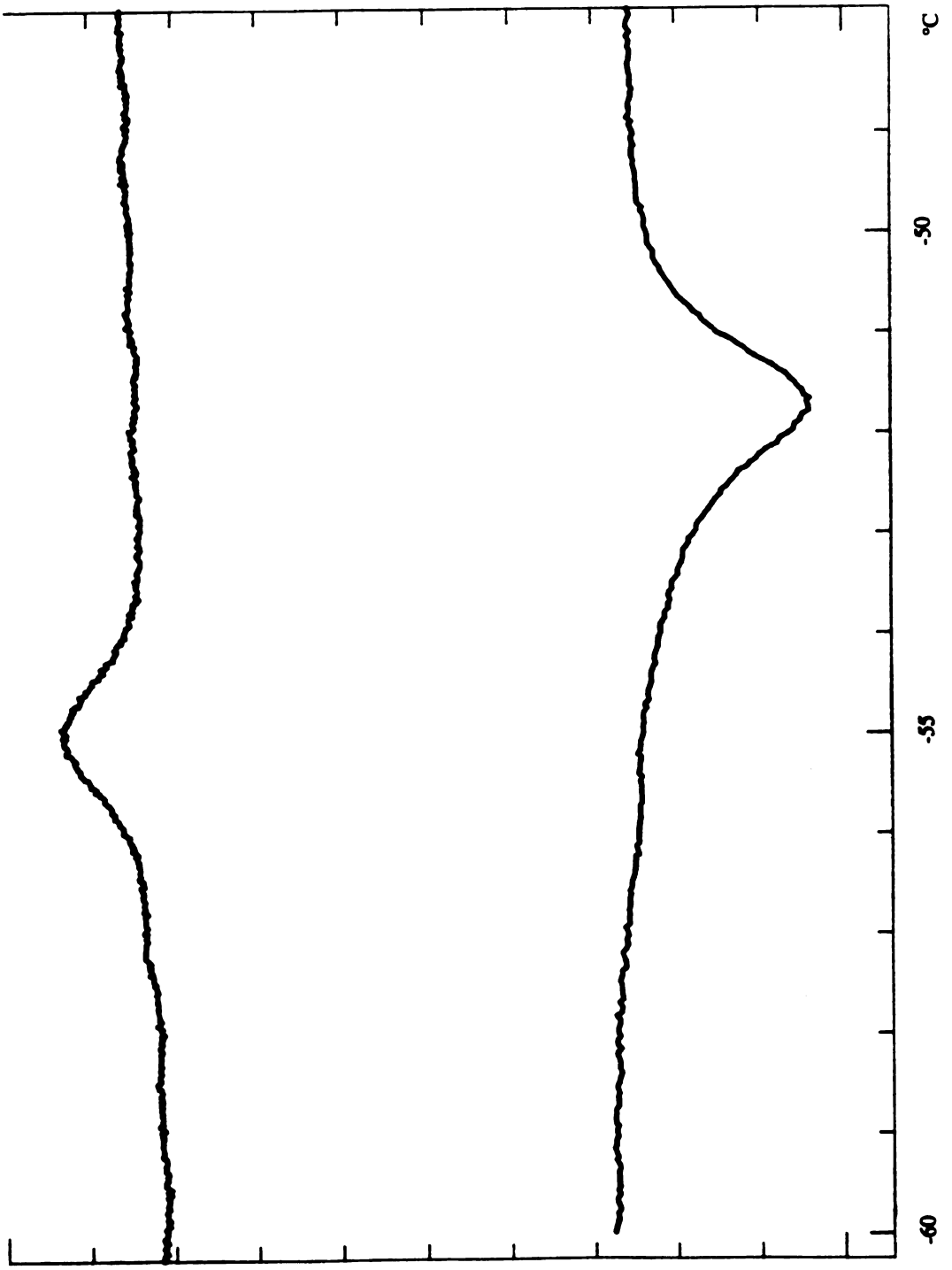

Figure 4. DTA trace showing an endotherm upon warming (bottom) which is larger than the exotherm upon cooling (top).

exotherm was consistently observed upon repeated cycling. The enthalpy change of the endotherm was consistently between 0.32 to 0.34 kJ mol^{-1}; however the change in enthalpy of the cooling transition varied between - 0.21 and - 0.30 kJ mol^{-1}. This is indicative of undercooling.

A variable temperature powder x-ray diffraction study was undertaken to assess the crystallinity of the HT phase. The initial diffraction pattern of a freshly synthesized polycrystalline sample displayed the sharp features expected. Repeated warming to ~ 240 K resulted in the irreversible broadening of the peaks until only a few low angle peaks were resolvable above an amorphous background (Figure 5). The irreversibility of this broadening is in contrast to many alkalides which show reversible behavior.[27]

II.E.4 Discussion

The structure of $Cs^{+}(18C6)_2e^{-}$ can be described as a closest-packed arrangement of "expanded" cations with the charge balancing anions (electrons) occupying the vacancies left in the lattice. Each cesium cation is complexed by two 18-crown-6 complexant molecules in a "sandwich" fashion. While these "expanded" cations pack efficiently, they do leave considerable void space in the form of cavities and interconnecting channels. The cavities are elliptical, elongated down the c-axis. They are connected together along the c-axis (monoclinic space group C2/c) at the ends by extremely short and open channels; the cavity-center to cavity-center distance is 8.68 Å; however, since the cavities themselves are approximately 7 Å in length the effective channel length is less than 2 Å. The cavities are connected to four other cavities in the a-b plane by long, narrow channels; the center to center distance is 10.27 Å and the cavity radius is approximately 2 Å so the effective channel length is more than 6 Å. These features can be seen in the depictions of the cavities and channels in Figure 6, which were constructed from the x-ray structure.[28] Since the electrons are confined to lattice voids, the interactions of neighboring electrons are

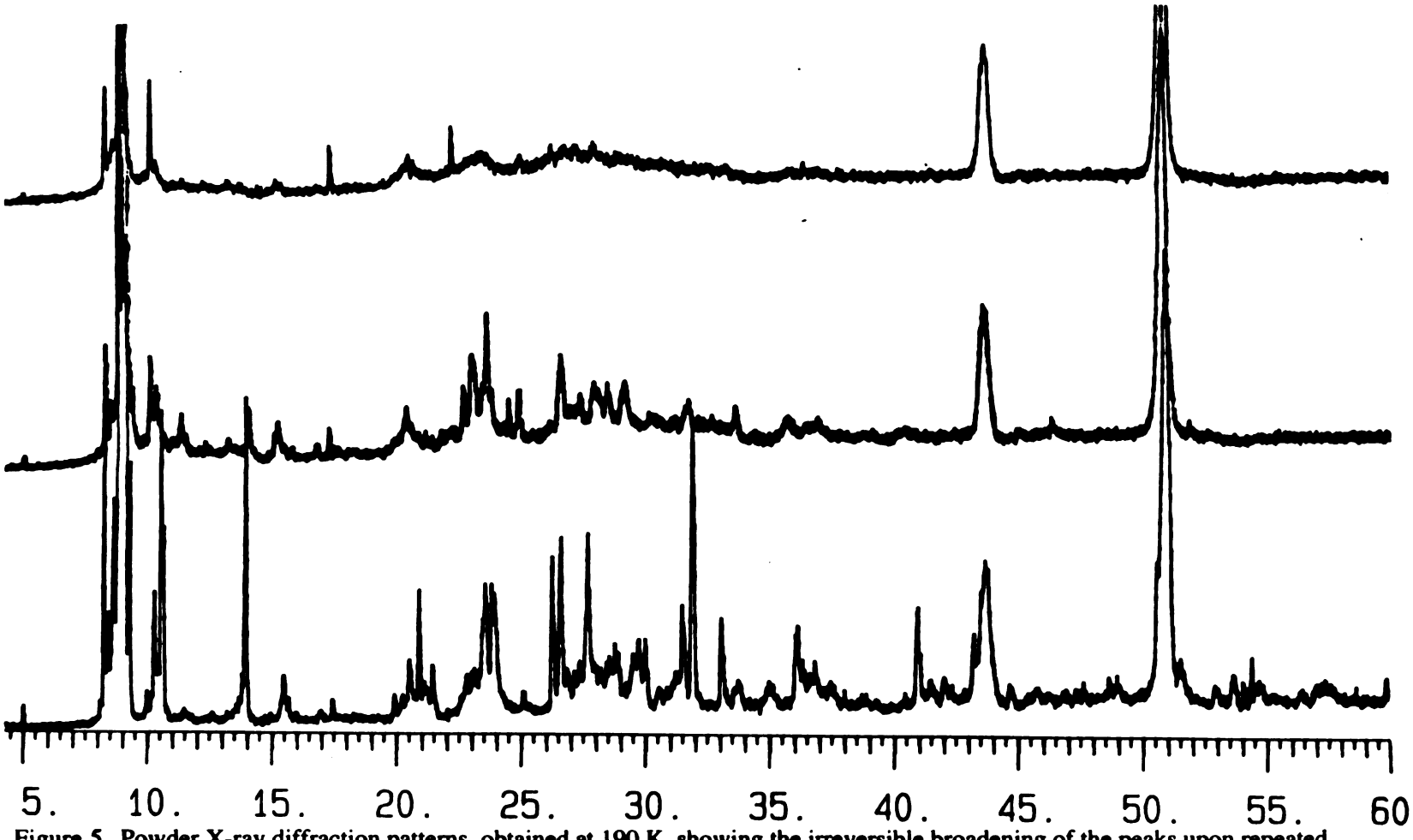

Figure 5. Powder X-ray diffraction patterns, obtained at 190 K, showing the irreversible broadening of the peaks upon repeated warming to above ~ 240 K (bottom -prior to warming, middle - after brief warming and top - after repeated warming). The two large peaks at ~ 43 and 50° (2 theta) are due to the aluminum sample holder.

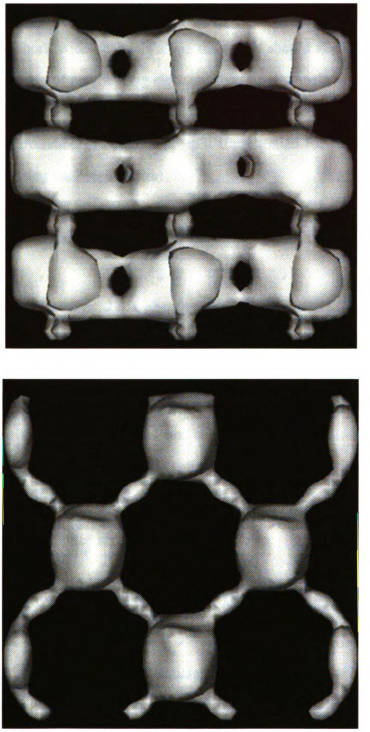

Figure 6. Isosurface showing the cavities and channels of $Cs^{+}(18C6)_2e^{-}$ in the a-b plane (bottom) and along the c-axis (top)..

regulated by the size and length of the interconnecting channels. From this perspective, one would expect $Cs^+(18C6)_2e^-$ to be describable as a quasi-one-dimensional system.

From the cavity and channel structure, we can construct a model of the magnetic interactions. The short, wide channels along the c-axis should allow for a much larger non-orthogonal overlap of neighboring electrons than the channels in the a-b plane. The spin anisotropy has been shown to be small[15] so we expect the system to behave as an infinite isotropic (Heisenberg) chain. The spin Hamiltonian for such a system can be expressed as (neglecting the Zeeman term)

$$\mathcal{H} = -2J\sum_i \hat{S}_i\hat{S}_{i+1} \qquad (1)$$

where the coupling parameter J is negative for antiferromagnetic interactions. The published susceptibility for the carefully crystallized (and never warmed above about 230 K) electride shows a broad maximum at about 50 K, indicating strong antiferromagnetic interactions.[16] While the temperature dependence of the susceptibility for a spin-1/2 linear chain Heisenberg antiferromagnet has not been solved as a closed form analytical expression, extrapolations of infinite chain behavior from finite size ring calculations have been published.[29] The results of these calculations have been fit to the convenient analytic expression

$$\chi_m = \frac{Ng^2\beta^2}{kT}\left[\frac{0.25 + 0.14995x + 0.30094x^2}{1 + 1.9862x + 0.68854x^2 + 6.0626x^3}\right] \qquad (2)$$

where $x = kT/|J|$.[30,31] Nonlinear least-squares fitting of the previously published data by equation 2 resulted in an excellent fit with $J/k = -38.3(1)K$ and 93.7(3)% of the expected number of spins (see Figure 7). (The numbers in parenthesis are standard deviation estimates of the last digit.) The data for the fit was truncated below 19 K;

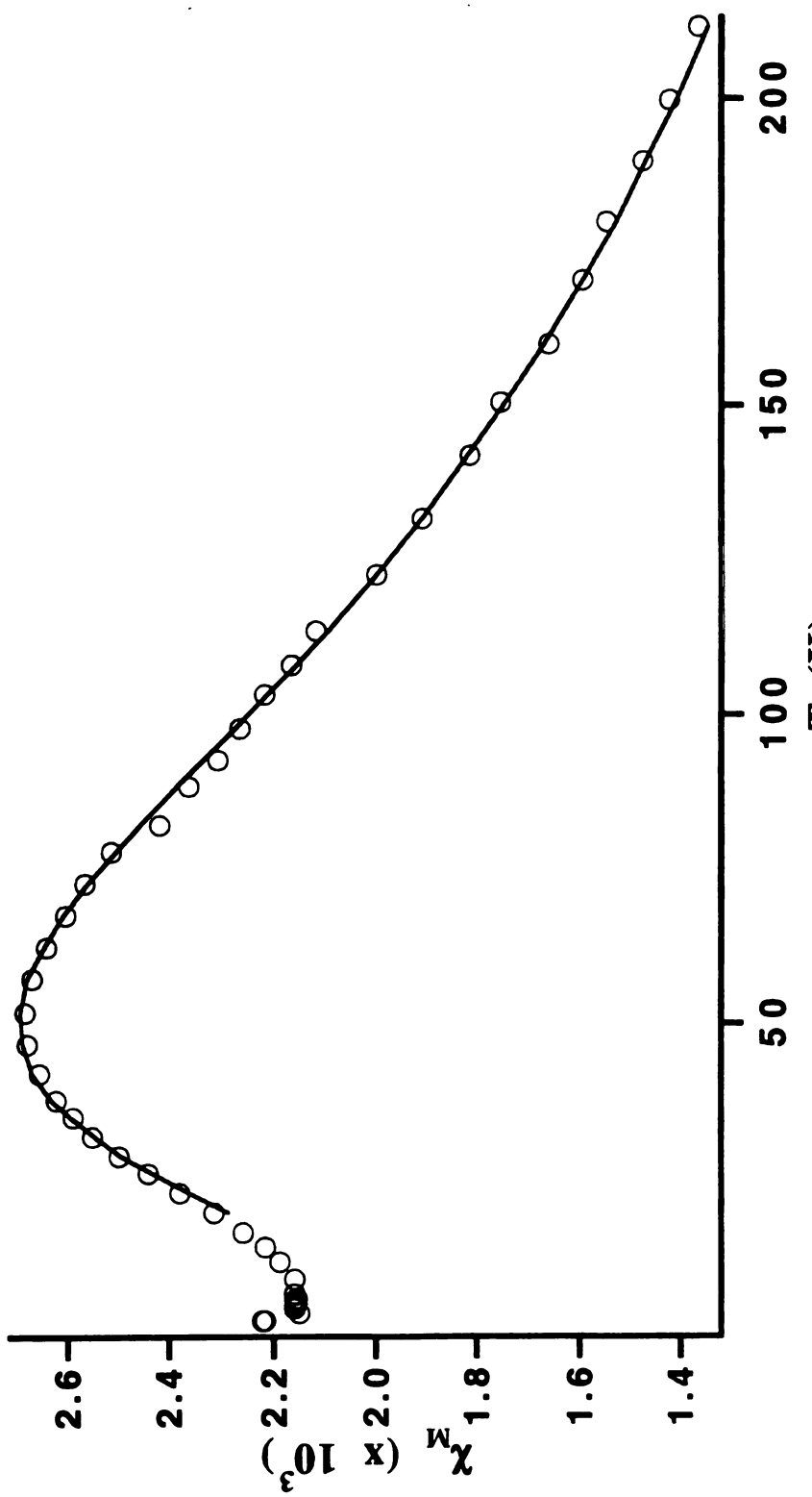

Figure 7. Least-squares fit of the magnetic susceptibility data to the linear chain Heisenberg antiferromagnetic model (equation 2).

deviations from linear chain behavior can be seen in the low temperature data. These deviations might be in part due to the presence of some of the high temperature phase which behaves as a Curie law paramagnet, however, this is may not be the entire reason, since addition of a Curie law term to equation 2 did not result in a wholly satisfactory fit. The presence of finite length chains may contribute a sub-Curie law term.[32] Interchain coupling could also result in low temperature deviations; however, the data could not be adequately fit by the addition of a meanfield correction to equation 2. Of course, there is the possibly of 3-D long range ordering (a Néel transition) when zJ', where J' is the interchain coupling strength and z is the number of contributing neighbors, is on the order of kT.[33] Additionally, any finite spin anisotropy results in the splitting of the parallel and perpendicular susceptibilities at sufficiently low temperatures.[29] Studies of the single crystal susceptibilities and the magnetic heat capacity are needed to resolve questions about the very low temperature behavior. However, it is clear that the magnetic data are in accord with that expected from the cavity and channel structure. The coupling between nearest neighbors in the electron chains is *at least* eight times that between the neighbors in the a-b plane as one would expect from the relatively shorter and more open channels along the c-axis.

The slow, irreversible transition from the LT phase to the HT phase seen in the NMR, in which the ^{133}Cs peak shifts diamagnetically by ~ 100ppm, coincides well with that seen in the susceptibility,[16] in which the material changes from a linear chain antiferromagnet to a Curie law paramagnet. The temperature dependence of the chemical shift of each of the 3 phases seen in NMR is largely determined by the contact (Knight) shift due to interaction with the electride electrons.[6] The contact density at the cation nucleus $\langle|\psi(0)|^2\rangle$ is related to the Knight shift ($K(T)$) by

$$K(T) = (\frac{8\pi}{3N_{av}})\langle|\psi(0)|^2\rangle\chi(T) \qquad (3)$$

where $\chi(T)$ is the electronic contribution to the magnetic susceptibility and all other symbols have their usual meanings.[34] Calculation of the contact density allows one to calculate the fractional atomic character because

$$F = \langle|\psi(0)|^2\rangle \Big/ \langle|\psi(0)|^2\rangle_{atom} \qquad (4)$$

where $\langle|\psi(0)|^2\rangle_{atom}$ is the contact density of a gaseous atom, which for cesium has been estimated to be 2.645 x 10^{25} e cm^{-3}.[35] Since the susceptibility is proportional to 1/T for all phases in the temperature region in which NMR data are available, the Knight shift can be related to the chemical shift as

$$K(T) = \sigma(T) - \sigma(\infty). \qquad (5)$$

Using equations 3-5 and the measured susceptibility, the chemical shift at infinite temperature, the Knight shift, the contact density and the fractional atomic character have been calculated and are tabulated in Table 1.

The Knight shift and fractional atomic character of the HT phase are in good agreement with the previously published measurements; however, the present study shows that the HT and HT2 phases do not exhibit identical contact densities as previously assumed from the limited data.[6] The previous study calibrated the temperature of only four of the NMR spectra, two above and two just below the transition. The shifts at these temperatures agree well with those found in the present study in which all the NMR spectra were calibrated; however, the previous assumption that all other points lie on the least-squares straight line constructed from the four calibrated points is incorrect. The major conclusion of the previous study that the trapped electron density at the nucleus is extremely low *is* confirmed by this study; in fact, the density is extremely low in all the phases of the electride.

Table 1: Parameters and results of contact shift calculations.

NMR peak	χ	$\sigma(\infty)$ (ppm)	$K(T)\cdot T$ (x 10^4ppm)	$\langle\lvert\psi(0)\rvert^2\rangle$	F
LT	1.37 x 10^{-3} (T = 211 K)	- 67(3)	5.92(7)	1.47 x 10^{22}	5.6 x 10^{-4}
HT	1.40 x 10^{-3} (T = 239 K)	- 71(3)	3.98(7)	8.55 x 10^{21}	3.2 x 10^{-4}
HT2a	1.65 x 10^{-3} (T = 206 K)	-129(5)	5.2(1)	1.10 x 10^{22}	4.2 x 10^{-4}
HT2b	1.65 x 10^{-3} (T = 206 K)	-139(7)	5.9(1)	1.25 x 10^{22}	4.7 x 10^{-4}

The thermally induced transition from the LT phase to the HT phase does not answer all the questions concerning the differences between previous and more recent studies. Previous magnetic susceptibility studies found Curie law behavior[5,10,11] similar to that seen in what are now known to be the HT phases. However, a thermally induced transition to the HT phase could not be responsible for the low spin counts observed (never exceeding about 80% of the expected free spins). It has since been found that this behavior could be reproduced by recrystalling the pure electride in the presence of a small percentage of $Cs^+(18C6)_2Cs^-$.[16] Additionally, the inconsistencies in the previous and most recent conductivity and EPR studies were found to be resolvable by the "ceside doping" explanation. The chemical shifts of coprecipated $Cs^+(18C6)_2e^-$ and $Cs^+(18C6)_2Cs^-$ prove that the HT phase NMR behavior can also be reproduced with ceside doping.[6]

The earlier ceside doping is understandable since in the more recent studies, $Cs^+(18C6)_2e^-$ has been made with a slight excess of the complexant to drive the equilibrium

$$2Cs^+(18C6)_2e^- \Leftrightarrow Cs^+(18C6)_2Cs^- + 2(18C6) \qquad (6)$$

to the left. Previously, the electride was typically made with stochiometric solutions which could have resulted in the inclusion of a small percentage of cesium in the lattice, formally as ceside.

The fact that both a small percentage of ceside doping and a thermally induced transition result in similar behavior may not be coincidental. The large size (~ 3.5 Å radius) of the cesium anion prevents closest packing of the complexed cations in the ceside structure.[36] Ceside doping in the electride would certainly result in a local distortion of the electride structure; the strain created by the local distortion might be relieved by long range structural rearrangement when kT is sufficiently high to overcome potential barriers to the shifting of the complexed cations. The cesium anion dopant, even at fairly high doping

levels, would be very difficult to detect by NMR since coupling with the neighboring paramagnetic trapped electrons would provide a very efficient relaxation mechanism. A structural distortion similar to that caused by ceside doping in the electride might occur in the pure electride through release of cesium cations from the complexant into a small percentage of the cavities. It is known that the dominant conduction mechanism of $Cs^+(18C6)_2e^-$ is cationic in the temperature range in which the LT to HT transition is observed.[12,13] The release of cations into the cavities (where they would reside as ceside or cesium metal) might accompany an expansion of the lattice as described above. Unlike the case of ceside doping, this release would not necessarily have a significant effect on the spin count seen in susceptibility. The irreversibility of the temperature induced transition is easily understood since recomplexation and recrystallization may be extremely slow in the solid state.

Although the powder x-ray diffraction data indicate that the high temperature phases have a large degree of disorder, some conclusions about their general structural features can be drawn from the NMR data. The calculated chemical shift at infinite temperature for both the LT and the HT phases agree well with those seen in $Cs(18C6)_2$ alkalides. The infinite temperature chemical shift is mainly determined by the Cs-O overlap.[6] The conformations of the sandwiched cations must therefore be quite similar in the LT and HT phases. The difference in the chemical shift between the LT and the HT phase is mainly due to a decrease in the contact density in the HT phase. The chemical shifts at infinite temperature of the two peaks of the HT2 phase are the same within experimental error, however, they are paramagnetically shifted by ~ 60 ppm from that of the LT and HT phase. This indicates that the HT2 phase has stronger Cs-O overlap. In addition, the contact densities are intermediate to those of the LT and HT phases.

The previous NMR study had found that the HT phase of the electride could be doped with sodium to make mixed electride-sodide systems. The ^{133}Cs spectra exhibited five peaks, one each at the shifts expected for the HT phase of the electride and the pure

sodide and 3 others which were spaced at intervals of 1/8th of the distance between the peaks. These peaks were interpreted as being due to the successive substitution of diamagnetic sodium anion into the cavities surrounding the complexed cesiums, thus eliminating the interaction of one trapped electron and its contribution to the Knight shift for each substitution. This indicates that each trapped electron in the HT phase contributes equally to the Knight shift, otherwise the peaks would not be equally spaced. This probably would not be the case for isolated electrons in the known crystal structure since the eight trapping sites which surround each complexed cation are at different radii and it seems unlikely that access to the cesium through the crown would coincidentally equalize the contact densities. This suggests that the transition from the LT to the HT phase involves a rearrangement of the complexed cations which, while retaining the complexation conformation as indicated by the values of the chemical shift at infinite temperature, results in trapping sites which are at a more nearly uniform distance from the cation.

One model of the transition from the HT to the LT phase which is consistent with all the data is one in which the complexed cations rearrange from their uniformly canted rows to a more nearly cubic arrangement about the cavities. This rearrangement would involve a slight lattice expansion which might be termed a "lattice melting" and the formation of more spherical cavities with a less anisotropic channel structure; creating larger and more spherical cavities that would better accommodate ceside dopant or cesium which has decomplexed. A more spherical cavity and reduction in the canting in the rows would ensure that each trapped electron is equidistant from all eight of the cations which surround it. This would also account for the transition from quasi-one-dimensional antiferromagnetism to Curie paramagnetism observed since it would result in two effects which would tend to minimize the electronic overlap; firstly, the electrons could withdraw from the channels into the more spacious cavities and secondly, there would be no preferentially wide, short channels.[16] One could think of the electron in the LT phase as being "squeezed" out of the cavities and down the wide, short channels by the elongated

nature of the cavities; widening the cavities to a more spherical shape would relieve the "pressure" (i.e. lower the kinetic energy) on the electrons while narrowing and lengthening the short channels would raise the kinetic energy within them and thus limit their electron density.

The amorphous character of the powder X-ray spectra can be understood in terms of crown ether disorder. It is known that the isostructural sodide's crown ethers undergo rapid "merry-go-round" reorientations in the temperature region in which the LT to HT transition is observed.[37] Similar motions in the electride would account for the loss of crystallinity as observed by powder x-ray diffraction; the irreversibility of the loss of crystallinity could be accounted for by randomness in the repacking of the complexant upon "lattice freezing" to the HT2 phase.

Within the model presented, a speculative description of the general structural features of the HT2 phase can be made. The paramagnetic shift of the infinite temperature chemical shift upon the transition from the HT to HT2 phases could be accounted for by tighter complexation in the HT2 phases. The isolated cavities of the HT form are retained however, since no discontinuity in the magnetic susceptibility is observed. The overall lattice volume would decrease, however, perhaps due to tighter complexation and packing. The contact densities of the HT2 phase would then be intermediate to those of the LT and HT phases as observed, since the lattice volume would be intermediate and thus the average Cs^+-e^- distance would be intermediate. The HT2 phase may be more closely related to the structure of $Cs^+(18C6)_2Cs^-$ between 230 and 285 K which also displays two cation peaks (separated by ~ 10 ppm) in the ^{133}Cs NMR.[6] Unfortunately, no X-ray structural data are available for this compound either.

II.E.5 Conclusions

The model of the phase changes presented above, while being consistent with all the experimental data, is admittedly highly speculative. These phase changes are certainly intriguing and should alert the reader to the possibilities of polymorphism in molecular-ionic crystals such as alkalides and electrides. However, the main purpose of this study was to establish the properties of the phase of $Cs^+(18C6)_2e^-$ which has a published crystal structure. It is clear from this study that the magnetic properties are consistent with those expected from electrons confined to the cavities and channels in the structure, as has been found for other electrides.[38] In addition, measurement of the electron contact density at Cs^+ of the crystalline electride confirm that, while it is slightly higher than previously reported, it is still extraordinarily small and consistent with exclusion of the electride electron from the cesium core and into the trapping sites. So, while the $Cs^+(18C6)_2e^-$ system is much more complex and intriguing than previously thought, it can in all its forms be called a "stochiometric F-center salt".

II.E.6 Acknowledgements

This research was supported by NSF Solid State Chemistry Grants DMR 87-14751 and DMR 90-17292 and by the Michigan State University Center for Fundamental Materials Research.

II.E.7 References

(1) Wagner, M. J.; Dye, J. L. In *Molecular Recognition: Receptors for Cationic Guests*; G. W. Gokel, Ed.; Pergamon Press: in press; Vol. I.

(2) Wagner, M. J.; Dye, J. L. *Ann. Rev. Mat. Sci.* **1993**, *23*, 223.

(3) Dye, J. L. *Chemtracts-Inorganic Chemistry* **1993**, *5*, 243.

(4) Singh, D. J.; Krakauer, H.; Haas, C.; Pickett, W. E. *Nature* **1993**, *365*, 39.

(5) Dawes, S. B.; Ward, D. L.; Huang, R. H.; Dye, J. L. *J. Am. Chem. Soc.* **1986**, *108*, 3534.

(6) Dawes, S. B.; Ellaboudy, A. S.; Dye, J. L. *J. Am. Chem. Soc.* **1987**, *109*, 3508.

(7) Ellaboudy, A. Ph.D. Dissertation Thesis, Michigan State University, East Lansing, **1984**.

(8) Ellaboudy, A.; Dye, J. L.; Smith, P. B. *J. Am. Chem. Soc.* **1983**, *105*, 6490.

(9) Ellaboudy, A.; Tinkham, M. L.; VanEck, B.; Dye, J. L.; Smith, P. B. *J. Phys. Chem.* **1984**, *88*, 3852.

(10) Issa, D.; Ellaboudy, A.; Janakiraman, R.; Dye, J. L. *J. Phys. Chem.* **1984**, *88*, 3847.

(11) Dawes, S. B. Ph.D. Dissertation Thesis, Michigan State University, East Lansing, **1986**.

(12) Moeggenborg, K. J. Ph.D. Dissertation Thesis, Mich. State Univ., East Lansing., **1990**.

(13) Moeggenborg, K. J.; Papaioannou, J.; Dye, J. L. *Chem. Mater.* **1991**, *3*, 514.

(14) Shin, D. H. Ph.D. Dissertation Thesis, Michigan State University, East Lansing, **1992**.

(15) Shin, D. H.; Dye, J. L.; Budil, D. E.; Earle, K. A.; Freed, J. H. *J. Phys. Chem.* **1993**, *97*, 1213.

(16) Wagner, M. J.; Huang, R. H.; Dye, J. L. *J. Phys. Chem.* **1993**, *97*, 3982.

(17) Rencsok, R.; Kaplan, T. A.; Harrison, J. F. *J. Chem. Phys.* **1993**, *98*, 9758.

(18) Allan, G.; DeBacker, M. G.; Lannoo, M.; Lefebvre, J. *Europhys. Lett.* **1990**, *11*, 49.

(19) Rencsok, R.; Kaplan, T. A.; Harrison, J. F. *J. Chem. Phys.* **1990**, *93*, 5875.

(20) Kaplan, T. A.; Rencsok, R.; Harrison, J. F. *Phys. Rev. B.* **1993**, , *submitted.*

(21) Golden, S.; Tuttle, T. R., Jr. *Phys. Rev. B.* **1992**, *45*, 913.

(22) Golden, S.; Tuttle, T. R., Jr. *Phys. Rev. B.* **1991**, *44*, 7828.

(23) Golden, S.; Tuttle, T. R., Jr. *Journal of the Chemical Society Faraday Transactions* **1988**, *84*, 1913.

(24) Kim, J. Ph.D. Dissertation Thesis, Michigan State Univ., East Lansing, **1989**.

(25) Dye, J. L. *J. Phys. Chem.* **1984**, *88*, 3842.

(26) English, A. D. *J. Magn. Reson.* **1984**, *57*, 491.

(27) Doueff, S.; Tsai, K.; Dye, J. L. *Inorg. Chem.* **1991**, *30*, 849.

(28) Overney, G.; Nagy, T. F.; Wagner, M. J.; Dye, J. L. , *to be submitted to Angew. Chem. Int. Ed. Engl.*

(29) Bonner, J. C.; Fisher, M. E. *Phys. Rev.* **1964**, *135*, A640.

(30) Estes, W. E.; Gavel, D. P.; Hatfield, W. E.; Hodgson, D. *Inorg. Chem.* **1978**, *17*, 1415.

(31) Hall, J. W. Ph.D. Dissertation Thesis, University of North Carolina, Chapel Hill, 1977.

(32) Soos, Z. G.; Bondeson, S. R. *Mol. Cryst. Liq. Cryst* **1982**, *85*, 19.

(33) Bonner, J. C. In *Magneto-Structural Correlations in Exchange Coupled Systems*; R. D. W. e. al., Ed.; D. Reidel Publishing Company: Dordrecht, Holland, 1985; pp 157.

(34) Knight, W. D. *Phys. Rev.* **1944**, *76*, 1259.

(35) Edwards, P. P. *Adv. Inorg.Chem. RadioChem.* **1982**, *25*, 135.

(36) Huang, R. H.; Ward, D. L.; Kuchenmeister, M. E.; Dye, J. L. *J. Am. Chem. Soc.* **1987**, *109*, 5561-5563.

(37) Wagner, M. J.; McMills, L. E. H.; Ellaboudy, A. S.; Eglin, J. L.; Dye, J. L.; Edwards, P. P.; Pyper, N. C. *J. Phys. Chem.* **1992**, *96*, 9656.

(38) Wagner, M. J. Ph.D. Dissertation Thesis, Mich. State Univ., East Lansing., **1994**.

II.F $Li^+(C211)e^-$: A One-Dimensional Heisenberg Antiferromagnet with a Ladderlike Spin Configuration

The following section is in the form of a draft of a paper intended to be combined with the crystal structure determined by Rui Huang and to be submitted for publication in *The Journal of the American Chemical Society* with minor modifications. I am responsible for the work and analysis presented here as well as writing this draft.

II.F.1 Introduction

Although the first report of the optical and magnetic properties of powders and films of $Li^+(C211)e^-$ appeared in 1981, it was only recently, more than a decade later, that the structure of this electride was determined by Rui Huang in our laboratory. This electride is the least thermally stable of those with known structure; handling at temperatures in excess of 230 K can result in rapid decomposition. The solutions from which the crystals are grown are even more unstable, decomposing even at 210 K. Special crystallization procedures had to be developed before successful growth of single crystals for x-ray determination could be accomplished.

$Li^+(C211)e^-$ is structurally similar to $Li^+(C211)Na^-$. The cavities have an estimated diameter of 4.3 Å. Open, short (7.91 Å center-to-center) channels connect the nearest neighbor cavities to form a zig-zag chain. Narrower and slightly longer (8.15 A) channels connect the nth cavity with the n+2 and n-2 cavities of the chain as shown in Figure 1.[1] These zig-zag chains are only weakly connected to each other by long, constricted channels.

The earliest study of the magnetic susceptibility, optical absorption and EPR properties of $Li^+(C211)e^-$ was performed on powders of stochiometry $(Li)_x(C211)$, where x ranged from 0.6 to 2. The samples were made by rapid evaporation of ammonia from

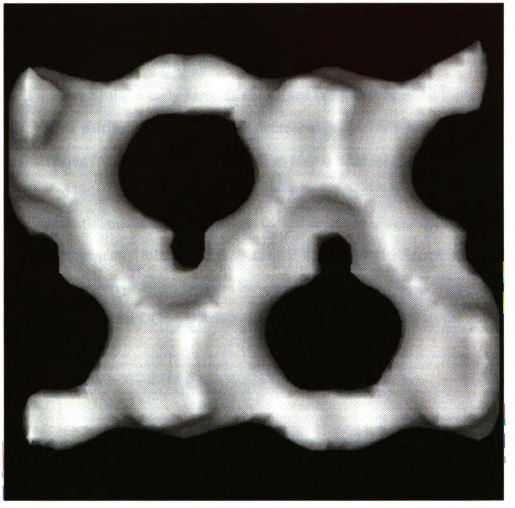

Figure 1. Isosurface showing the cavities and the channels which connect the nearest and next nearest cavities in $Li^{+}(C211)e^{-}$ to form infinite zig-zag chains.

solutions of Li and C211 in liquid ammonia at 195 K.[2] The susceptibility was found to be inversely proportional to temperature at high temperatures, with a broad maximum and apparent drop to zero as the temperature approached 0 K.

Optical spectra obtained in the 1981 study showed a broad absorption in the near IR with a tail into the visible. Samples with $x \leq 1$ showed two peaks and a shoulder which suggests that the excess electrons may have multiple trapping sites. Samples with $x = 1.57$ showed considerably more homogeneous behavior. Spectra of samples with $x = 2$ featured a plasma type edge which is similar to that of metallic metal-ammonia solutions.

EPR spectra of these early samples confirmed the presence of multiple trapping sites and the spin pairing as temperature is decreased. The lines were quite narrow, gradually increasing from less than 1 G to 1-2 G as temperature was lowered to 3 K. The g-values indicated little interaction between the excess lithium and the complexed cation.

The synthetic method employed in the 1981 study resulted in powders of questionable homogeneity; following the successful solution of the crystal structure, the properties of pure polycrystalline samples have been measured. This section describes DSC, NMR, packed powder DC conductivity and magnetic susceptibility studies.

II.F.2 Experimental

Polycrystalline samples of $Li^+(C211)e^-$ were synthesized in three-chamber quartz cells like the one depicted in Figure 2. Transfer of starting materials was done in a helium filled glovebox equipped with a nitrogen scrubber. Lithium metal, in slight excess, and C211, were loaded in chambers 1 and 3 respectively. After cell evacuation to ~ 10^{-6} torr, the lithium was dissolved in ammonia at 195 K and poured through the frit to chamber 2, leaving behind any insoluble impurities. The constriction in the connecting tube was rinsed by distilling solvent onto it until it no longer turned blue, indicating that all lithium had been washed from the constriction. The ammonia was then distilled away leaving finely divided

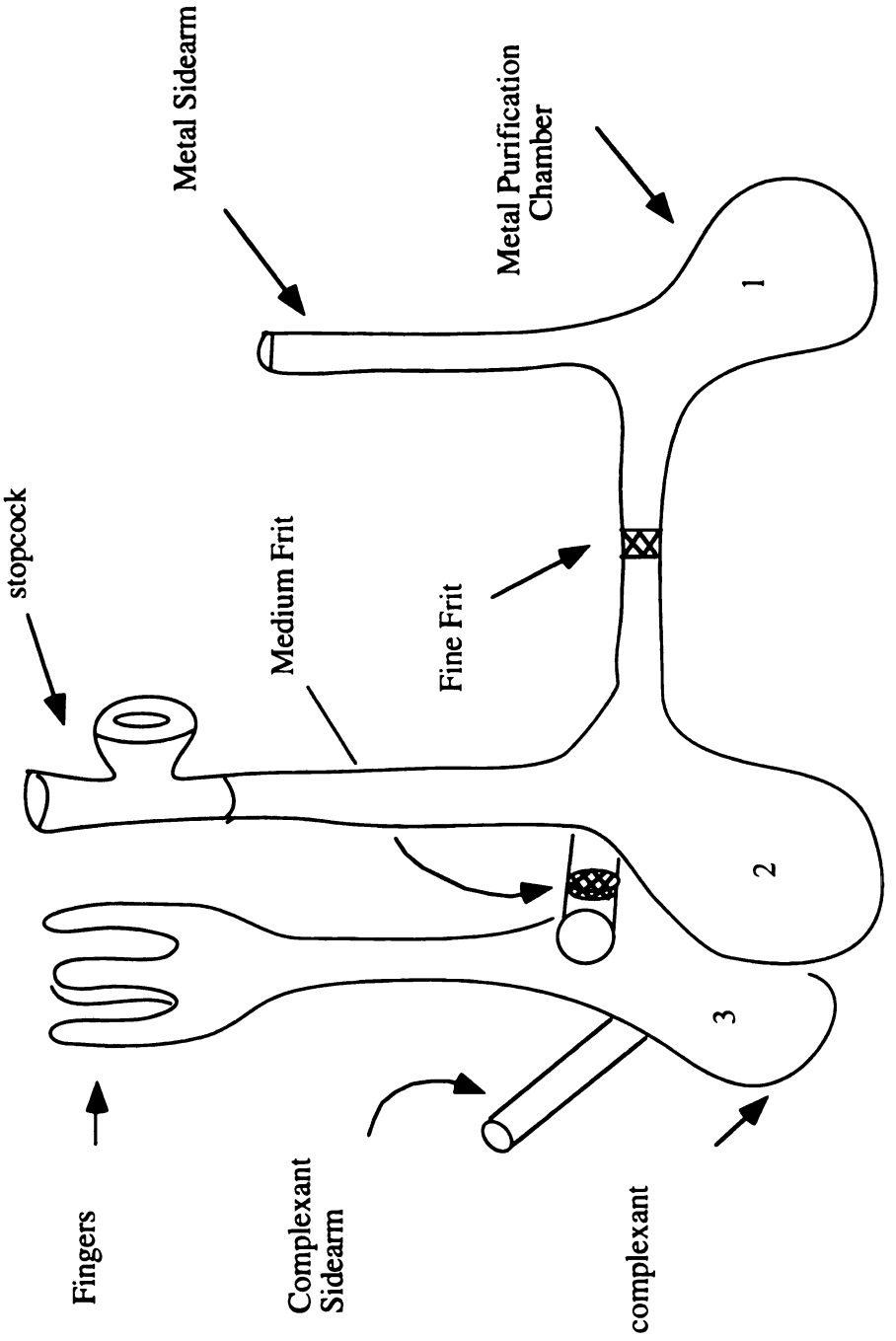

Figure 2. Three-chamber quartz cell ("cow").

lithium particles in chamber 2. Chamber 1 was then removed by torch. A few milliliters of methylamine was distilled into chamber 2 (195 K); the lithium was dissolved and poured through the frit to chamber 3. The solution was periodically stirred for about 2 hours to allow for complexation, then the methylamine was distilled away leaving a black polycrystalline material (the electride). To ensure complete removal of the methylamine, dimethyl ether was added, allowed to stand, then removed. The electride was then dissolved in dimethyl ether (~ 15-20 ml) with a small fraction of diethyl ether (~ 2-3 ml) as a co-solvent. The solution was poured through the frit, leaving a small amount of lithium in chamber 3, and the solvent was slowly (~ 2 days), isothermally (195 K) removed until a few milliliters remained. Pouring off the solvent revealed small black crystals which were dried and collected. Further details of material purification, reaction vessel preparation and synthetic procedures have been previously published elsewhere.[3-6]

Differential thermal analysis (DTA) was carried out with a Shimadzu DSC-50 calorimeter in hermetically sealed aluminum pans. All manipulations of the sample, prior to and after sealing, were performed in N_2 glove bags. Open liquid nitrogen dewars were maintained to limit glovebag humidity and prevent condensation during the brief time the samples were exposed. The sample crimper was precooled in liquid nitrogen prior to sealing. The DTA cell was precooled below 173 K prior to loading. Measurements were made under a constant flow of helium through the sample cell.

The pressed powder dc conductivity measurements were made as a function of temperature with a Keithley 617 programmable electrometer. Alternating polarity, rectangular, 100 mV voltage pulses of 10 seconds duration were applied and the current was measured during each pulse. Temperature was controlled by suspending the conductivity cell in a "soft" 30 liter dewar which had been precooled with liquid nitrogen. Temperature was measured with a carbon-glass four probe thermometer (Lakeshore Cryotronics, Inc. model CGR-1-100) suspended on the exterior of the cell at the sample height and within 1 cm of the sample horizontally. A N_2 gas flow was used to maintain a

positive pressure inside the dewar and adjusted such that the temperature slowly rose to room temperature over a 48 hour period. Further details of the methods used are described elsewhere.[7,8]

The ^7Li NMR spectra were measured at the Max T. Rogers NMR facility at Michigan State University on a 9.3950 Tesla Varian VXR 400S NMR spectrometer utilizing a Varian VT-MAS probe. Samples were spun at 5.5 kHz; a 3.5 μs pulse length was employed with a 0.5 second post-acquisition delay time and the signal was averaged over 128 transients. A sealed glass capillary tube (1.7 mm OD) filled with MeOH was axially fixed in the rotor. The known temperature dependence of the dipolar splitting of the hydroxyl and methyl protons was used to calibrate temperature immediately before and after ^7Li acquisitions.[9] Ten minutes of equilibration time was allowed after the thermocouple in the bearing gas stream stabilized at the set point; the sample temperature was assumed to be equilibrated when temperature calibration measurements prior to and after acquisition agreed. The rotors were loaded into the precooled probe in a N_2 glove bag, a dewar of liquid N_2 was utilized to not only store the sample but also to limit the humidity in the bag. Chemical shifts are referenced to $Li^+(aq)$ at infinite dilution.

II.F.3 Differential Thermal Analysis

No phase transitions were observed between 173 K and the decomposition temperature (onset ~ 0 K). The decomposition is rapid once initiated and highly exothermic. This caused the sample to heat faster than the programmed ramp rate as can be seen in Figure 3. This is similar to $K^+(C222)e^-$ for which an autocatalytic reaction mechanism has been proposed.[7]

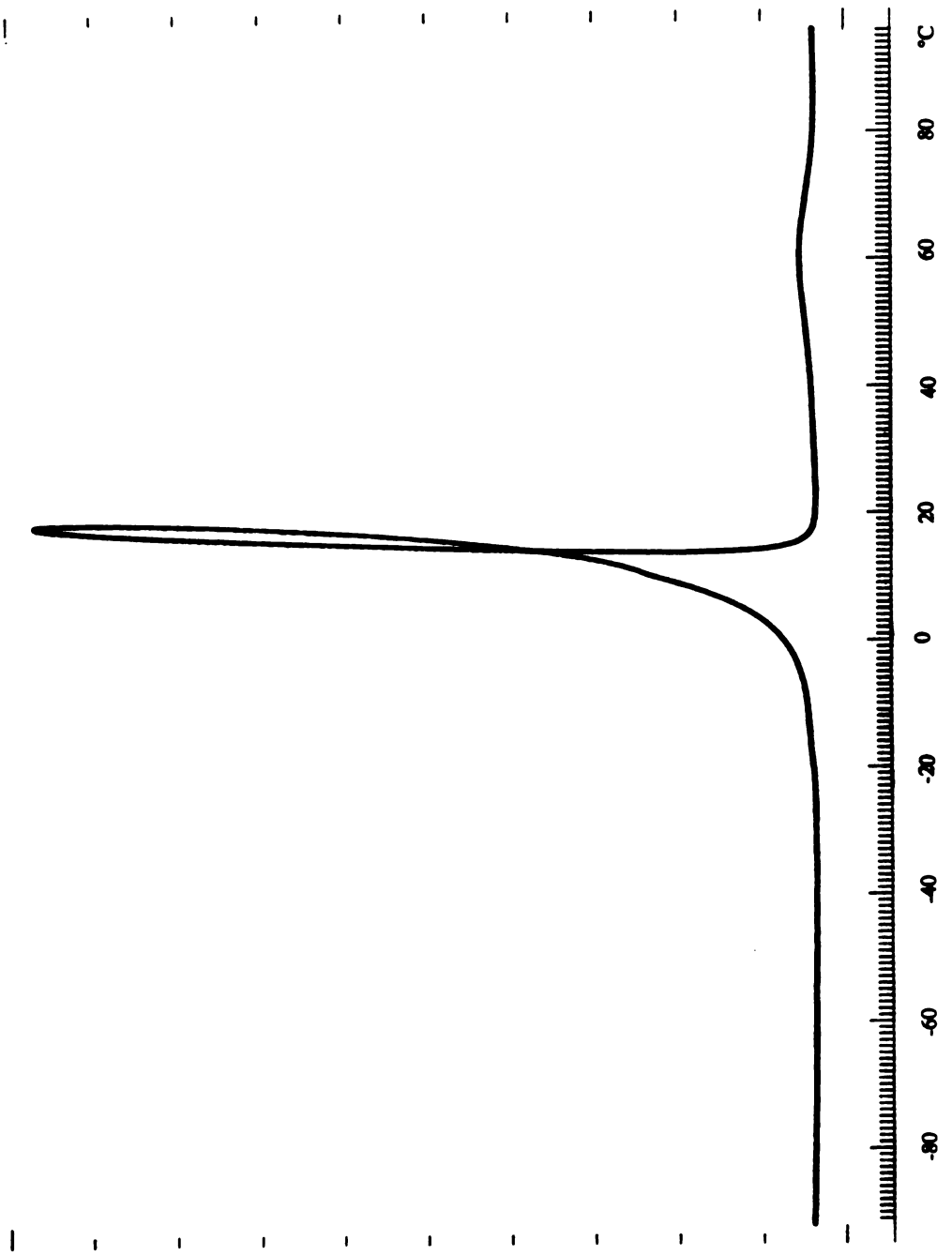

Figure 3. DTA trace of $Li^{+}(C211)e^{-}$. Note the temperature overshoot caused by rapid and highly exothermic decomposition.

II.F.4 DC Conductivity

The temperature dependence of the measured resistance is shown in Figure 4. The slope of the low temperature data yields an apparent bandgap of ~ 4.4 eV. The sharp rise in resistance at high temperature is due to irreversible decomposition of the sample. The conductivity data show this electride to be a rather poor conductor. The magnitude of the resistance is reminiscent of $Cs^+(18C6)_2e^-$ and $Cs^+(15C5)_2e^-$. It has been suggested that the poor conductivity of these electrides, even though they have half-filled bands, is due to Coulombic repulsions which prevent the double occupancy of a single trap and thus charge transport.[10] In fact, it may be that the conductivity of this and other electrides is largely due to defects and that the "pure" electrides are insulators.

II.F.5 Magnetic Susceptibility

The temperature dependence of the magnetic susceptibility of a polycrystalline sample (run by Rui Huang) is displayed in Figure 5 (crosses). It is qualitatively similar to that seen for the rapidly precipitated sample of stochiometry $(Li)_{1.57}(C211)$ measured in the 1981 study, with a broad maximum at about 20 K and tending to zero at 0 K. The data cannot be adequately fit by mean field theory or the theoretical treatment of antiferromagnetism by Ohya-Nishiguchi.[11] This is not surprising since the cavity and channel structure suggest that one should expect one-dimensional chain behavior; neither theory takes chain correlations into account. The broad maximum in the susceptibility, which cannot be reproduced by the aforementioned models, is indicative of the low dimensional magnetic interactions that are expected from the structure.

Neglecting all interactions other than those between each trapped electron and its two nearest neighbors results in a magnetic model of $Li^+(C211)e^-$ as independent, infinite,

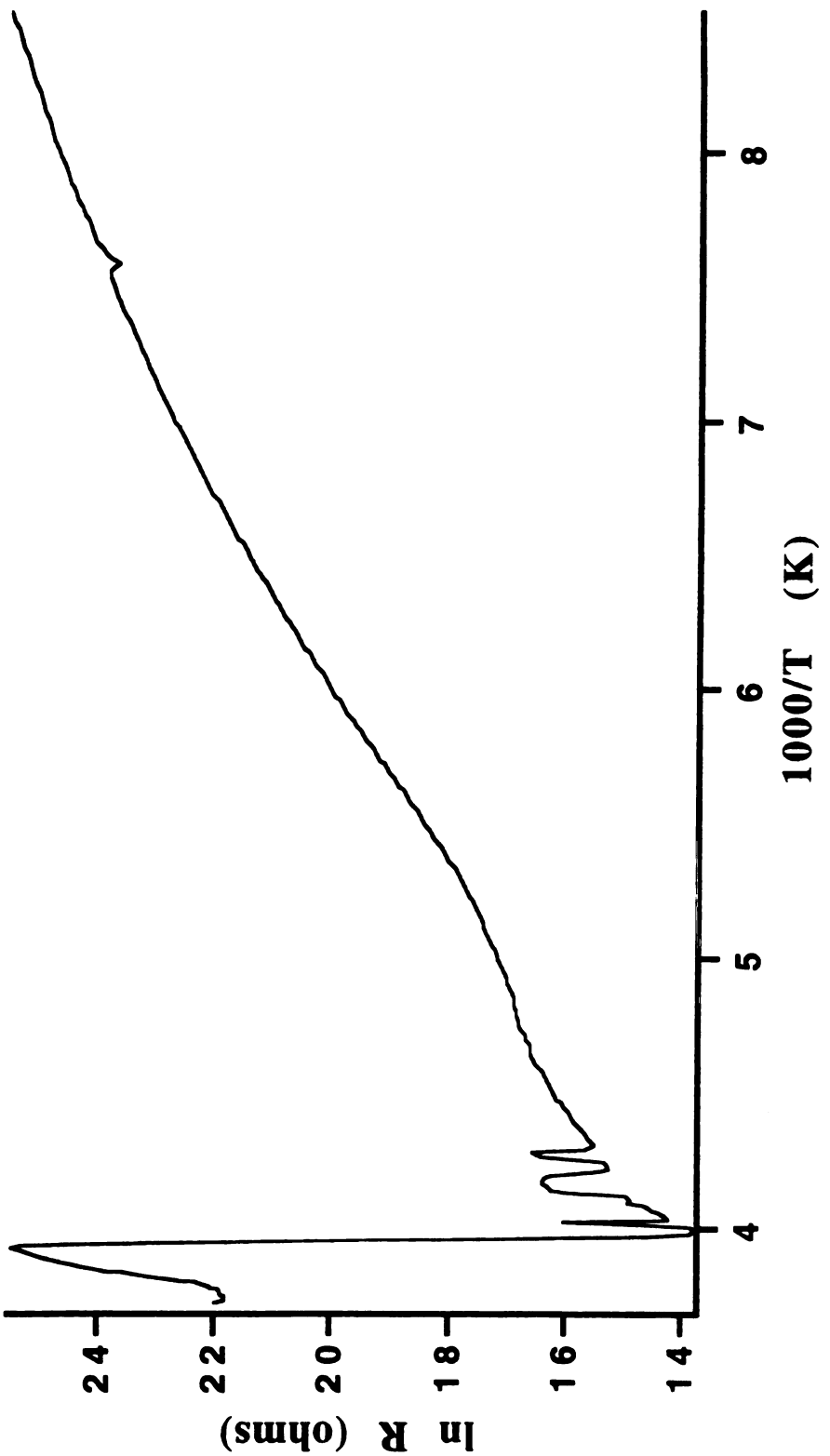

Figure 4. Two-probe packed powder DC conductivity of $Li^{+}(C211)e^{-}$.

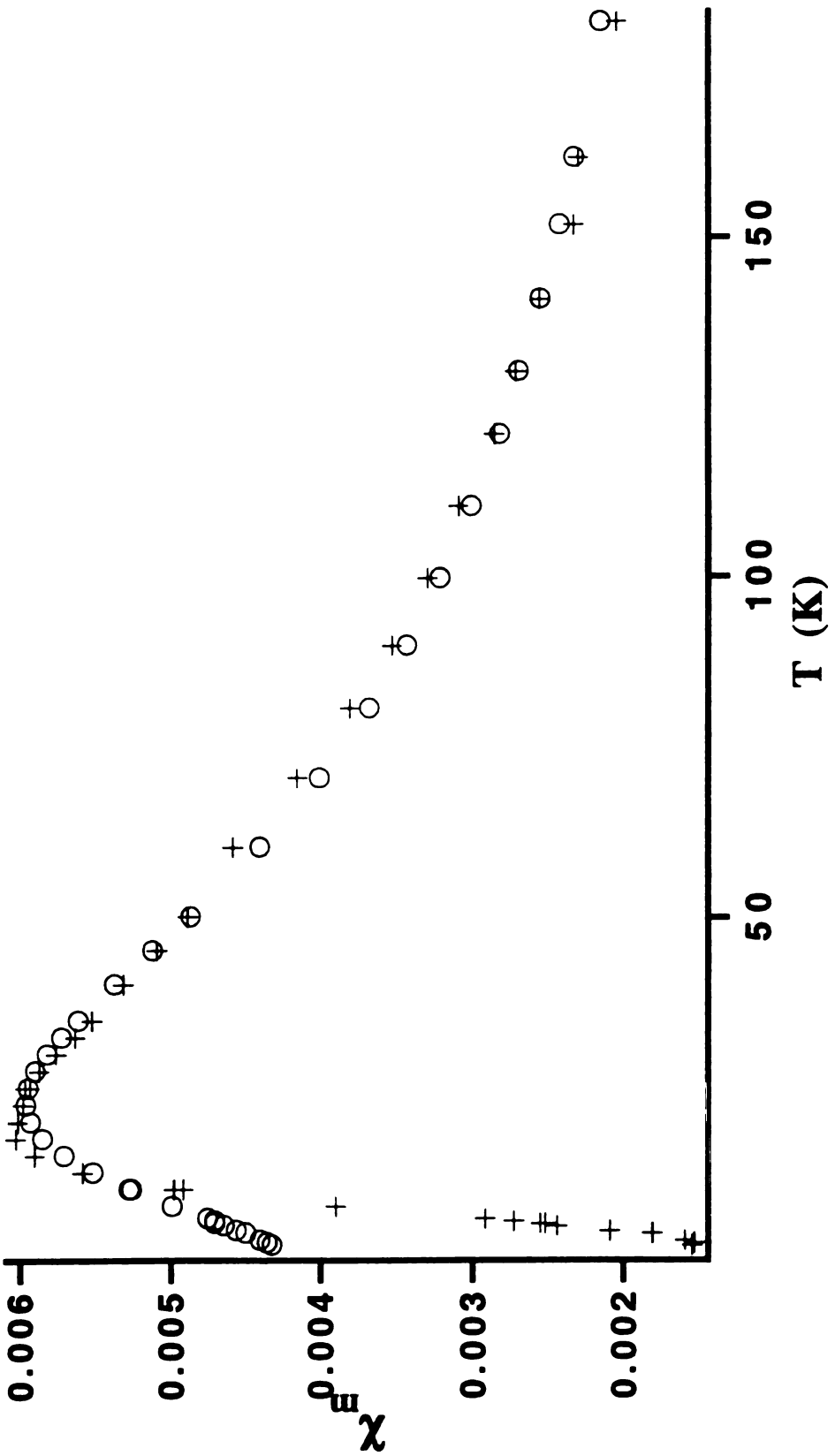

Figure 5. Molar magnetic susceptibility of $Li^{+}(C211)e^{-}$ (crosses) and fit to linear chain Heisenberg antiferromagnet model (circles).

zig-zag chains. The spin anisotropy is probably extremely small, as is the case for electrides in general[12-14] and was seen for rapidly precipitated samples of $(Li)_x(C211)$.[2] Therefore, the system is describable as a S = 1/2 linear-chain Heisenberg antiferromagnet (LCHA), whose spin Hamiltonian, neglecting the Zeeman interaction, can be written as

$$\mathcal{H} = -2J\sum_i \hat{S}_i\hat{S}_{i+1} \qquad (1)$$

where J is the interaction parameter coupling the ith spin with each of it two nearest neighbors. The temperature dependence of the susceptibility of LCHA's has not been solved as a closed form analytical expression, except in the case of the classical spin (S = ∞) in zero magnetic field.[15] Extrapolations of infinite chain behavior from finite size ring calculations have been published for the case of S = 1/2.[16] The results of these extrapolations have been fit to the analytical expression

$$\chi_m = \frac{Ng^2\beta^2}{kT}\left[\frac{0.25 + 0.14995x + 0.30094x^2}{1 + 1.9862x + 0.68854x^2 + 6.0626x^3}\right] \qquad (2)$$

where $x = kT/|J|$ and J is constrained to be negative (antiferromagnetic).[17,18] This equation, plus a temperature independent term to correct for temperature independent paramagnetism and the diamagnetism of inner shell electrons, was used to fit the data. As shown in Figure 5 (circles), with $|J|/k$ = -17.7, 86% of the expected spins accounted for (assuming g=2.0023) and a temperature independent correction of 5.7 x 10^{-4}, this model can reproduce the broad maximum in the susceptibility, but not the low temperature drop of the susceptibility toward zero. This is indicative that the magnetic interactions are one-dimensional, however, the large deviation at low temperatures indicates that the second nearest neighbor interactions are not negligible.

Examples of linear chain systems with competing first and second nearest neighbor interactions are rare. The Hamiltonian for a "ladderlike" system can be written, again neglecting the Zeeman term, as

$$H = -2J_1 \sum_i \hat{S}_i \hat{S}_{i+1} - 2J_2 \sum_i \hat{S}_i \hat{S}_{i+2} . \qquad (3)$$

Overlap of the trapped electrons in the channels is expected to be non-orthogonal; therefore, both the first and second nearest neighbor interactions are expected to be antiferromagnetic. If both interactions are antiferromagnetic, the nearest neighbor interactions, which tend to align them antiparallel, are opposed by the second nearest neighbor interactions, which tend to align them parallel (Figure 6). Systems which are governed by such Hamiltonians are expected to display a wide variety of magnetic phase behavior.[19,20] Unfortunately, analytical solutions for this Hamiltonian have not been found; in fact, extrapolations to infinite length from exact numerical calculations on finite chains fail to converge.[21]

In spite of the problems of complete analysis of the susceptibility, we can in fact construct a reasonable model of the electride that yields a tractable Hamiltonian. Our first model of the magnetic interactions was as an antiferromagnetically coupled infinite chain. It is well known that such a system is unstable with respect to dimerization,[22] in fact, so much so that structural distortions, known as spin-Peierls transitions, can occur to accommodate the dimerizations.[23] The existence of antiferromagnetic second nearest neighbor interactions would magnify this effect, increasing the likelihood of a lattice dimerization. In the case of most materials, the interacting spins are anchored at lattice sites and dimerization requires rearrangements which are energetically unfavorable. Spin-Peierls transitions occur in materials which can undergo elastic distortions with an increase in lattice free energy that is smaller than the decrease in magnetic free energy resulting from the pairing. In electrides, the magnetic species are trapped electrons and thus deformation

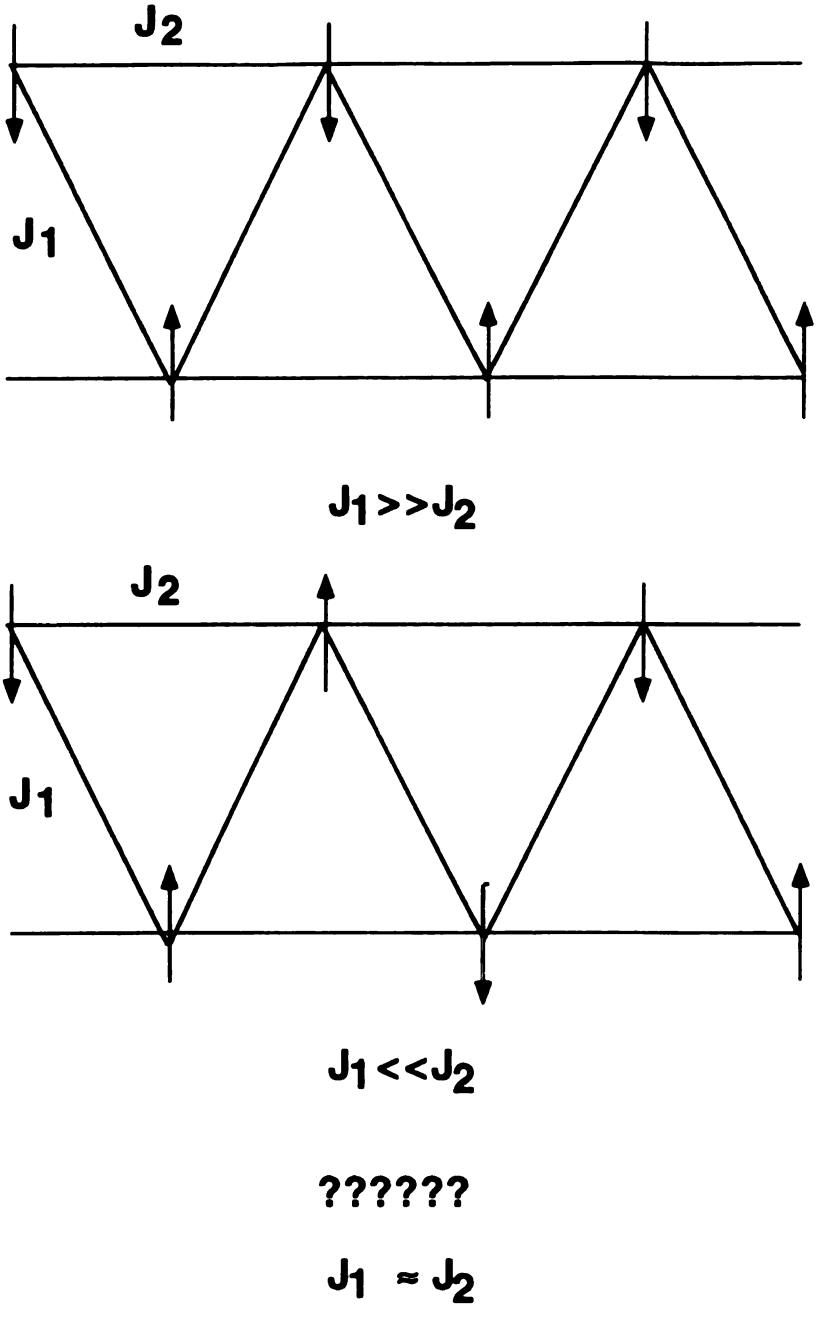

Figure 6. Schematic illustrating the spin interactions in zig-zag chains. When the nearest and second nearest neighbor are of similar magnitude, they "compete"; the result of this competition is not known a priori.

does not necessitate structural transformation; electron polarization would be sufficient. Partial withdrawal of electron density from the smaller channels would result in an increase in the kinetic energy of the trapped electrons, however, this could be counterbalanced by a decrease in magnetic free energy. The relocation of this charge density would require an increase in the coupling within the larger channels. Partial dimerization, such as that depicted in Figure 7, might lower the net energy of the system. Some distortion of the lattice may accompany these polarizations, but structural rearrangement is not required. The dimerization of the lattice would result in the opening of a gap between the ground state and the first excited state as shown in Figure 8. This type of behavior is qualitatively consistent with the measured susceptibility, since in a dimerized system the susceptibility would tend to zero at 0 K as observed, whereas a uniform chain would have a net susceptibility at 0 K.

If the spin chains were dimerized, one would expect the system to behave as a linear chain with alternating coupling parameters. The Hamiltonian of such a system can be written as

$$H = -2J\sum_{i=1}^{n/2}[\hat{S}_{2i}\hat{S}_{2i-1} + \alpha\hat{S}_{2i}\hat{S}_{2i+1}] \qquad (4)$$

where J is the exchange parameter between a spin and one of its nearest neighbors along the chain and αJ is the exchange parameter between it and its other nearest neighbor. Although this model has not been solved analytically, infinite limit extrapolations of numerical calculations of finite size rings and convenient fitting expressions based on these calculations have been published.[24] The published expression is

$$\chi_m = \frac{Ng^2\beta^2}{kT}\left[\frac{[A(\alpha)]+[B(\alpha)]X+[C(\alpha)]X^2}{1+[D(\alpha)]X+[E(\alpha)]X^2+[F(\alpha)]X^3}\right] \qquad (5)$$

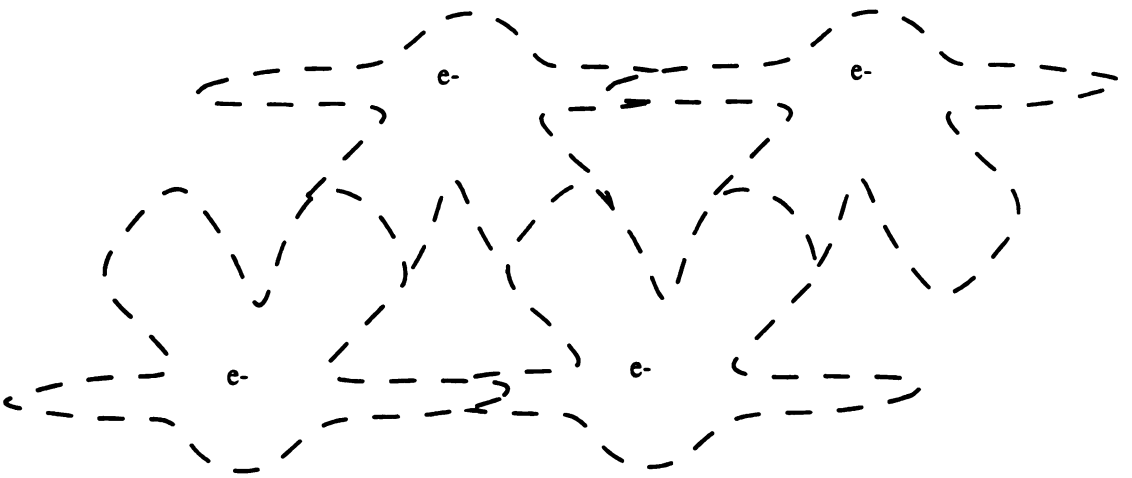

undimerized

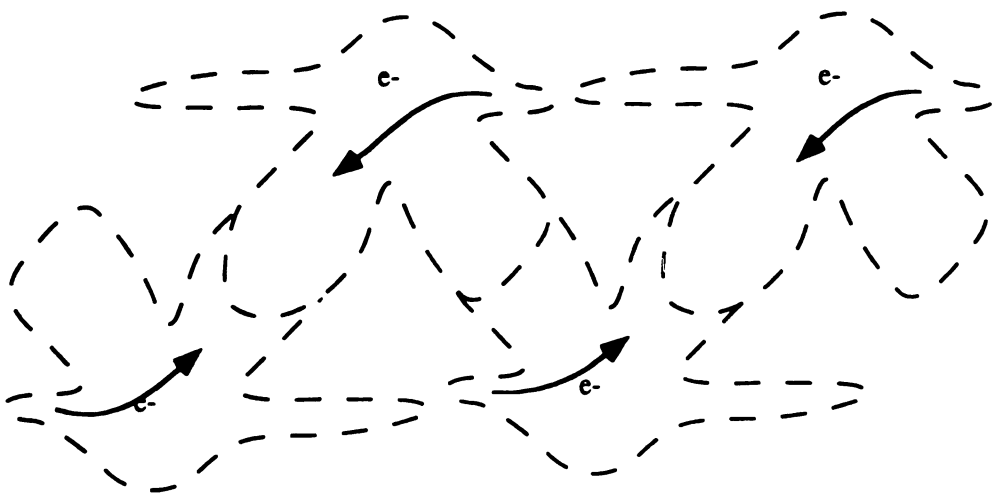

dimerized

Figure 7. Representation of possible electron withdrawal from the smaller channels to form a dimerized chain.

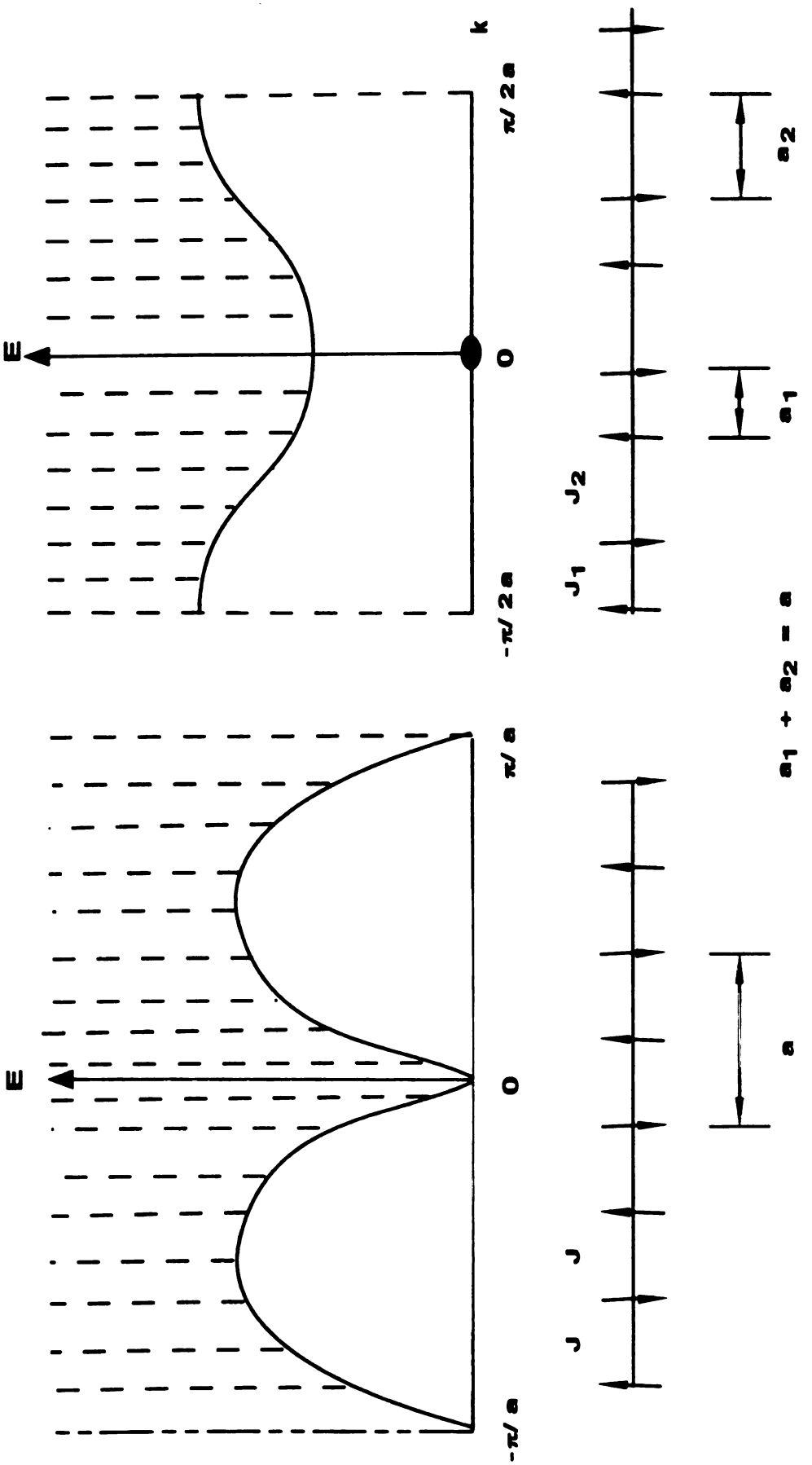

Figure 8. Diagram showing the creation of an energy gap by dimerization of an infinite one-dimensional chain. The filled circle at k=0 for the dimerized chain represents the ground state

where $X = |J|/kT$ and is valid for $X < 2$. The constants A through F are given functions[24] of α and take on values which depend on whether α is larger than or less than 0.4. Nonlinear least squares fitting of the susceptibility data resulted in excellent agreement (see Figure 9) with α =0.90(3), $|J|/k$ = -18.0(2) K, a temperature independent correction of 5.2(8) x 10^{-4} and 87(3)% of the expected free spins. The fitting was limited to data above 9 K due to the limited range of applicability of equation 5. Below 9 K, the data are in qualitative accord with what would be expected from an alternating chain, except instead of falling monotonically toward zero at 0 K, they appear to level out and perhaps rise near 2 K. This might be the result of a small concentration of isolated trapped electrons, which should obey the Curie law. To test this theory, a small Curie law correction was made , varying the percentage of impurity by eye to force the susceptibility to tend to zero. The data were then re-fit by equation 5, again resulting in an excellent fit (Figure 10) with α =0.86(2), $|J|/k$ = -18.9(2) K, a temperature independent correction of 4.9(8) x 10^{-4}, 87(3)% of the expected free spins and the impurity correction set at ~ 0.5% unpaired spins.

The value of the alternation parameter demonstrates that only a slight alternation of the coupling parameters is necessary to account for the susceptibility behavior. However, while the data are in accord with an alternating chain model, there is reason for skepticism. If the chains really do dimerize via electron polarization, the chains would probably dimerize progressively as temperature is lowered, as is the case in the aforementioned spin-Peierls transition, rather than the temperature independent dimerization assumed by the model. The susceptibility behavior of a spin-Peierls system is similar to that of a alternating chain; behaving as a uniform chain model until a critical temperature (T_{SP}) at which point the spins progressively dimerize until the maximum alternation of the chain is reached at 0 K. The small alternation needed by the alternating chain model to fit the data would then merely be an artifact of the limited fitting range and not at all indicative of the maximum alternation.

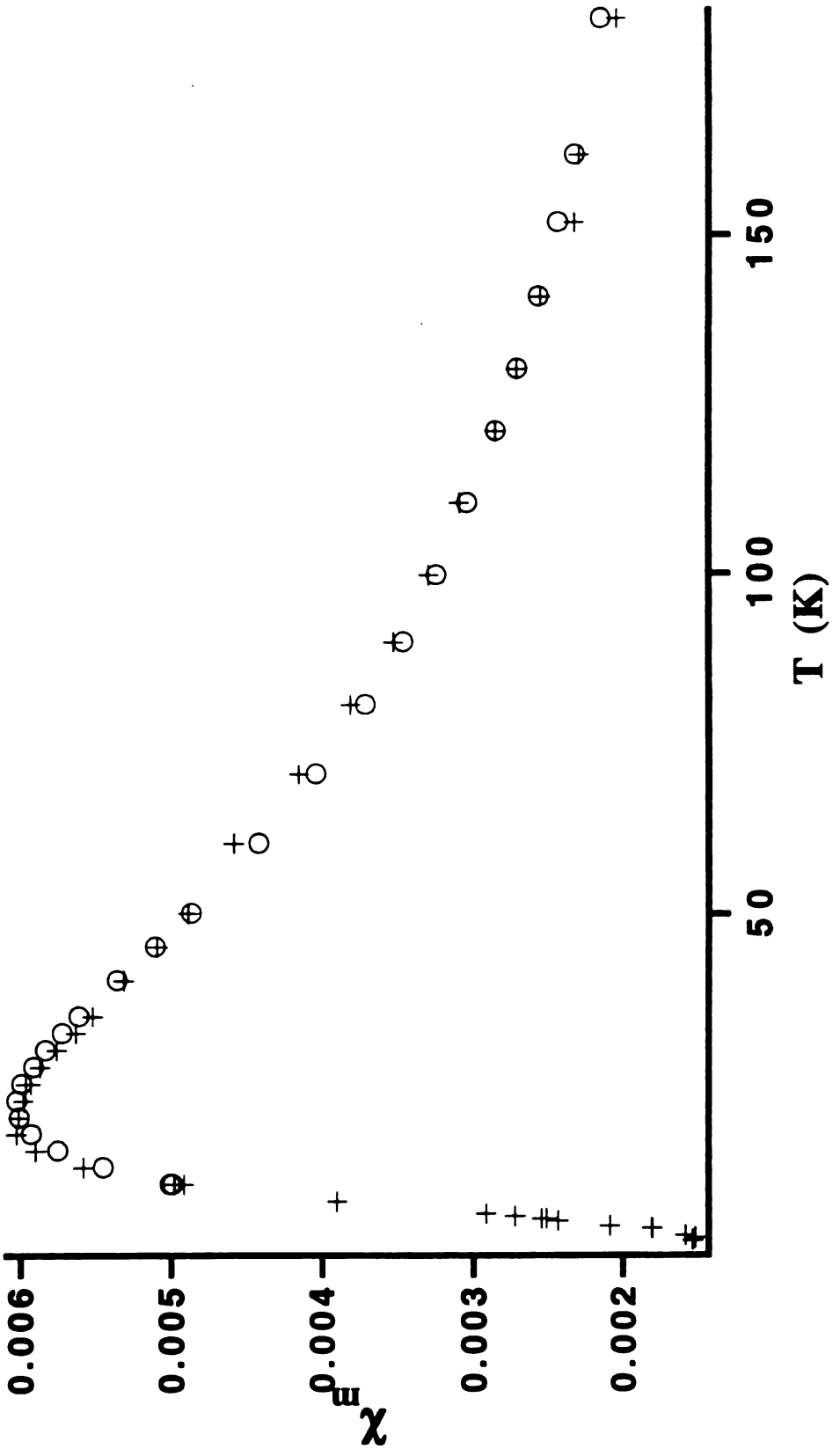

Figure 9. Fit of the magnetic susceptibility to the alternating linear chain Heisenberg antiferromagnet model.

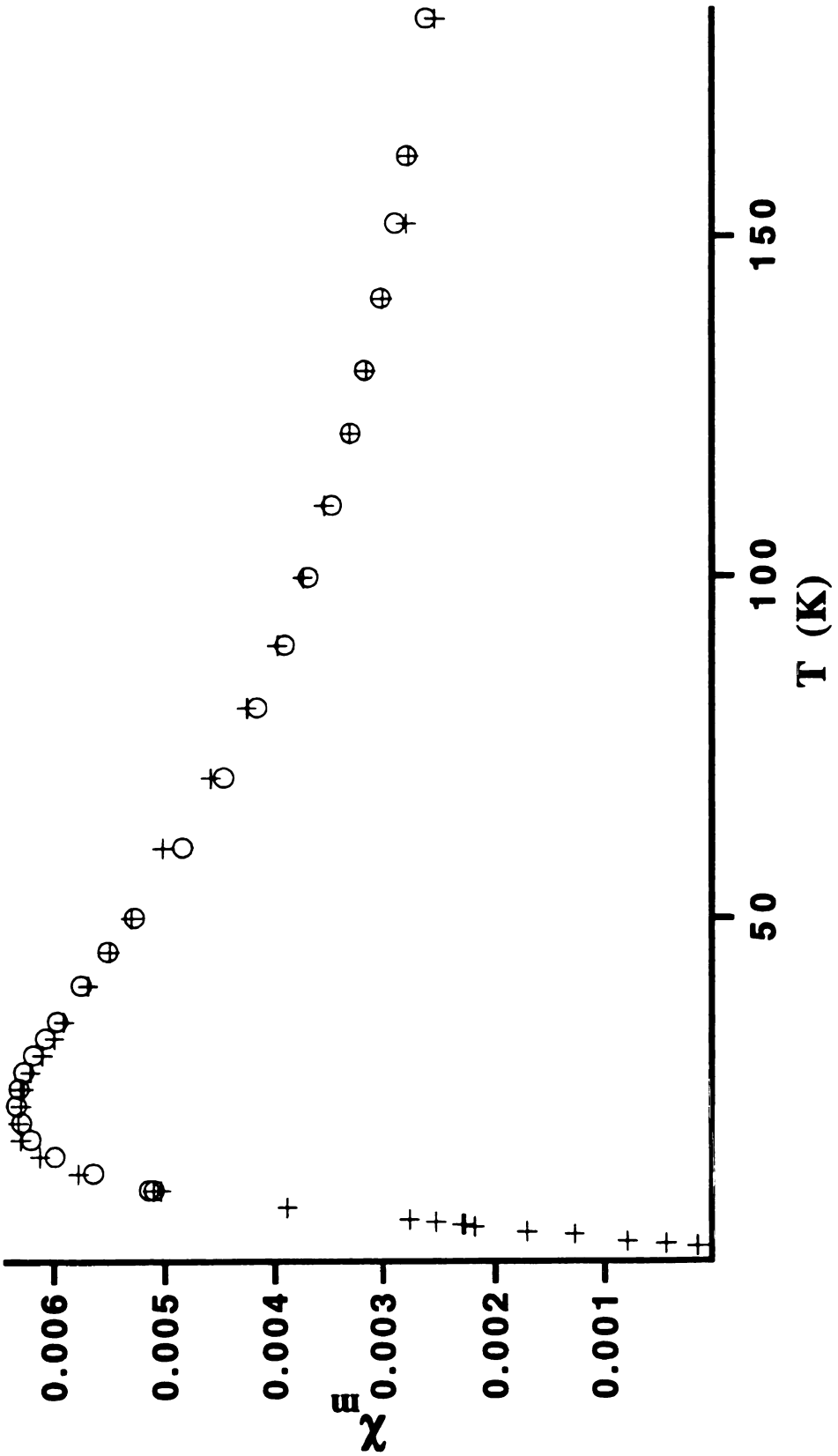

Figure 10. Fit of the magnetic susceptibility data to the alternating linear chain Heisenberg antiferromagnet model with correction for the Curie tail. Note the intercept at T = 0 appears to be zero after subtraction of the tail.

It is not clear, however, that this electride is describable as a spin-Peierls system since there is no obvious "knee" in the data at T_{sp}.[23] However, this may be an artifact of our attempt to fit the high temperature data to a simple linear chain rather than including the second nearest neighbor interactions. The excellent fit of the simple chain model as low as T = 22 K and the relative sizes of the channels strongly indicate the predominance of nearest neighbor interactions. If the second nearest neighbor interactions were negligible and a spin-Peierls distortion occurred, one would expect the susceptibility to drop sharply to zero at the temperature (T_{sp}) below which the uniform linear chain model no longer fits. In the present case, the susceptibility actually rises slightly and then drops toward zero. This could, however, be due to the second nearest neighbor interactions which would tend to increase the moment over that seen in the simple linear chain, as can be seen from Figure 6. The effect of the nearest neighbor coupling can be estimated by a mean field correction to the uniform chain model

$$\chi_m = \chi_H / (1 - 2zJ' \chi_H / Ng^2\beta^2) \qquad (6)$$

where χ_H is the susceptibility due to the nearest neighbor interactions (equation 2), J' is the interaction parameter coupling between a spin and its z next nearest neighbors. Fitting only for $T \geq T(\chi_{max})$ yields the fit shown in Figure 11. This fit assumes a stochiometric number of unpaired electrons with the free electron g value, an impurity tail of ~ 0.5% unpaired spins (the tail has a negligible effect on the fitting results but does force the susceptibility to tend to zero at 0 K) and yields $J/k = -17.1(4)$, $J'/k = -10(2)K$ and a temperature independent correction of 0.00038(3) as the adjustable parameters. The inset of Figure 11 clearly shows the existence of a "knee" in the data at ~ 12.5 K. Although the mean field approximation is of questionable validity since the condition $J >> J'$ is not met, the values of the coupling parameters should serve as rough estimates and verify the antiferromagnetic nature of both the nearest and next-nearest neighbor interactions.

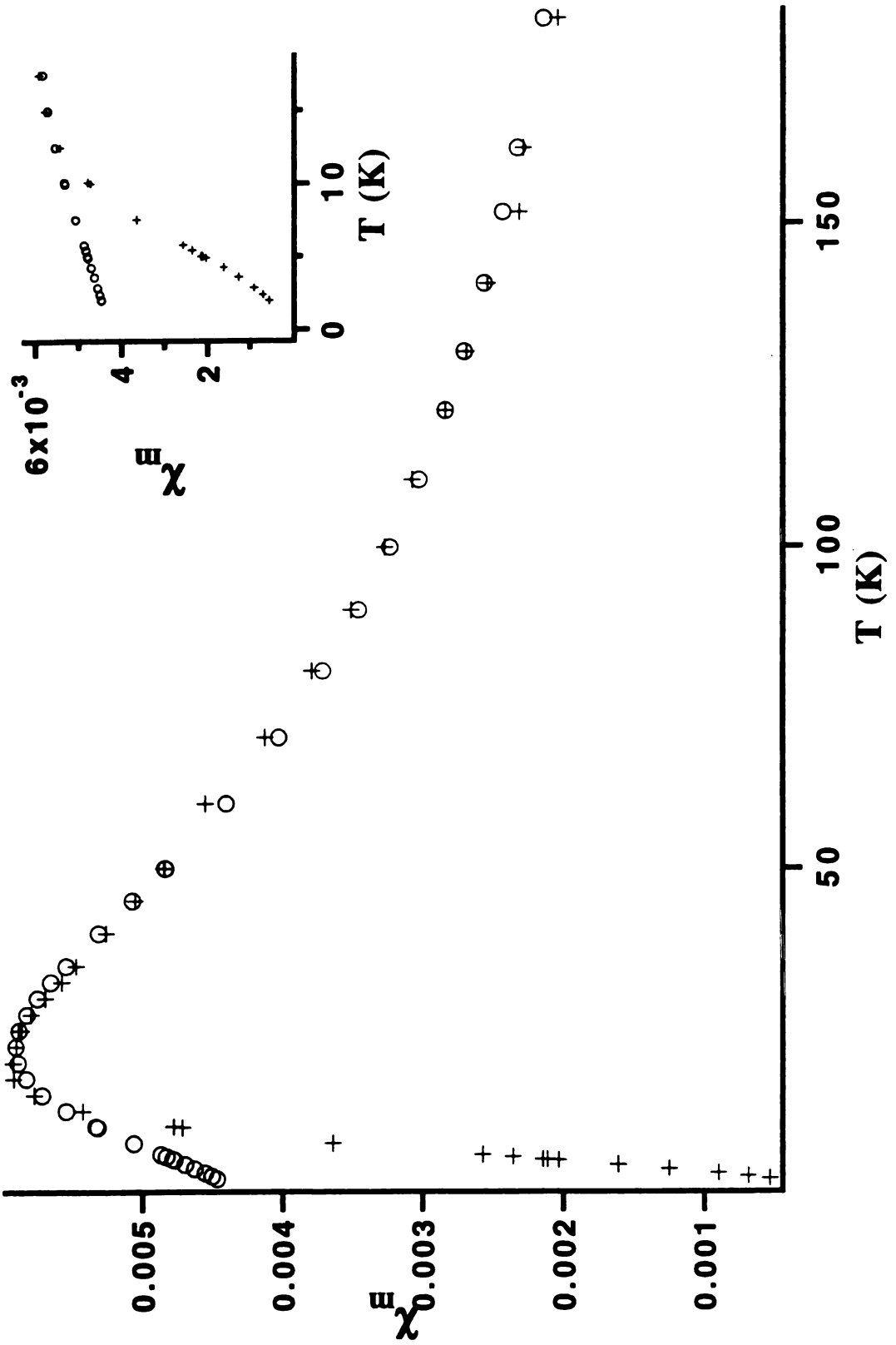

Figure 11. Fit of the linear chain Heisenberg antiferromagnetic model with a mean field correction. Note the "knee" in the data at approximately 12.5 K (inset).

Furthermore, the calculation suggests that there is indeed a spin-Peierls transition with a critical temperature T_{sp} of approximately 12.5 K. The magnitude of the magnetic gap created by the spin-Peierls transition at T = 0 K ($2\Delta(0)$) can be estimated from the relation[23]

$$\Delta(0) = 1.76T_{sp} \tag{7}$$

to be 44 K. This value, like those of the coupling parameters, must be viewed as a rough estimate. More precise values must await solutions to the low lying states of the ladderlike Hamiltonian.

II.F.6 NMR

When $Li^+(C211)e^-$ is carefully handled to avoid decomposition, its magic angle spinning (MAS) ^7Li NMR spectra exhibit a single resonance. The temperature dependence of the shift, shown in Figure 12, is largely the result of a contact (Knight) shift due to the interaction of the cation with the electride electrons. The unpaired electron contact density at the cation nucleus, $\langle|\psi(0)|^2\rangle$, is related to the contact (Knight) shift, $K(T)$, by

$$K(T) = (\frac{8\pi}{3N_{av}})\langle|\psi(0)|^2\rangle\chi(T) \tag{8}$$

where χ(T) is the electronic contribution to the magnetic susceptibility and all other symbols have their usual meanings.[25] Knowing both the Knight shift and the magnetic susceptibility allows one to calculate $\langle|\psi(0)|^2\rangle$, which can then be used to calculate the fractional atomic character defined as

$$F = \langle|\psi(0)|^2\rangle \Big/ \langle|\psi(0)|^2\rangle_{atom}. \tag{9}$$

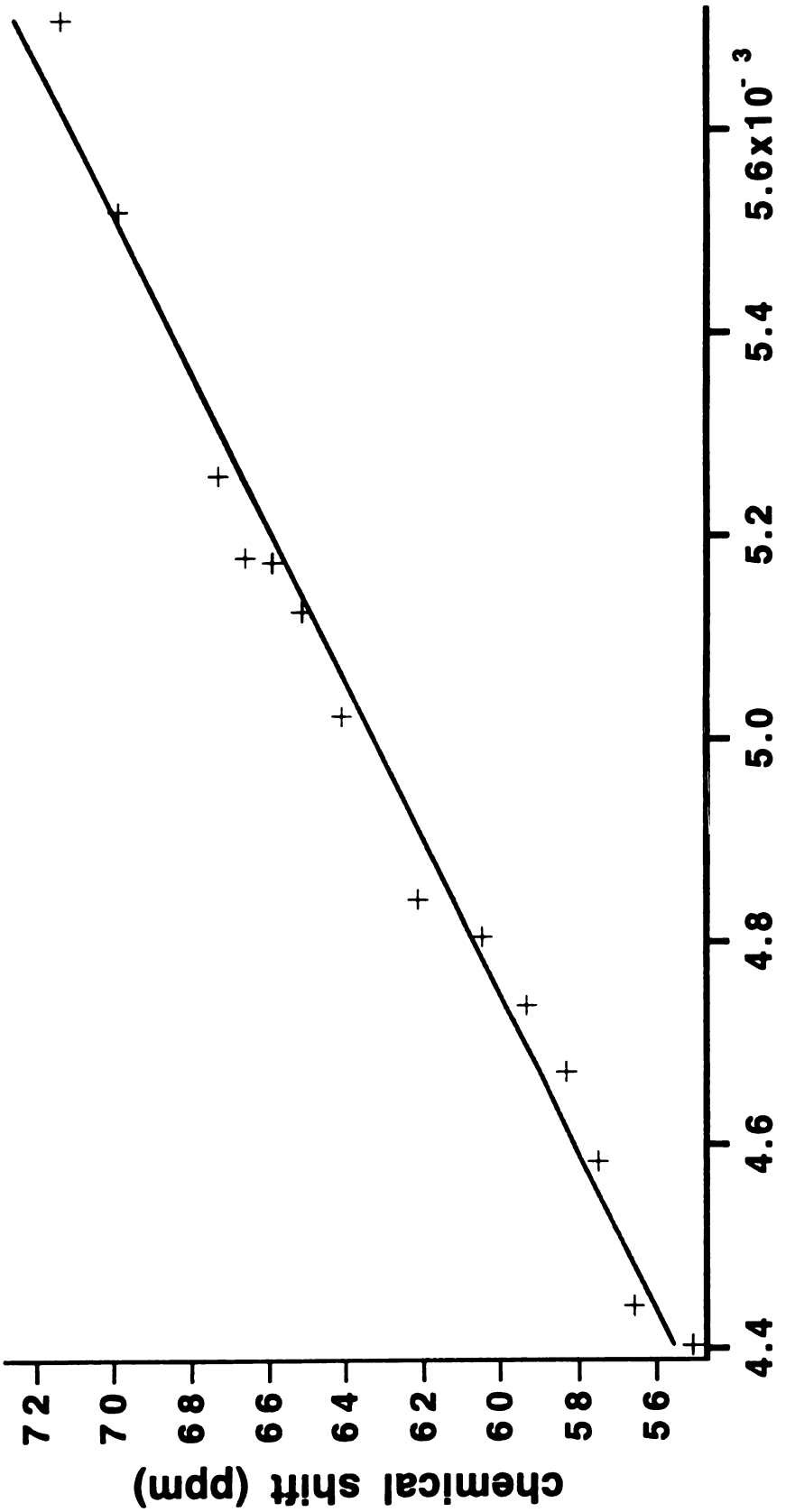

Figure 12. The ^{7}Li NMR chemical shift plotted against reciprocal temperature. The solid line is a fit by equation 10.

The electron density at the nucleus for an isolated gaseous lithium atom, $\langle|\psi(0)|^2\rangle_{atom}$, has been estimated to be $1.56\times10^{24} e\cdot cm^{-3}$.[26] Both the magnetic susceptibility and the chemical shift are inversely proportional to temperature in the region for which NMR data were obtained. The chemical shift (in ppm) fits the equation

$$\sigma(T) = \sigma(\infty) + K(T) = -1 + (1.30\times10^4)/T \qquad (10)$$

as shown in Figure 12. The value of the chemical shift at infinite temperature ($\sigma(\infty) = -1 \pm 2 ppm$) is in excellent agreement with the ^{7}Li shifts of lithium-211 complexes in solution.[27] The magnetic susceptibility at 181.75 K is 0.002049. The fractional atomic character of the excess electron calculated from the above data and equations 8-10 is 0.16%. This value is slightly less than that observed for lithium impurity donors in a silicon host matrix.[28] The large atomic character, compared to that of other electrides, is probably due to leakage of the electrons' wave functions into the cation through the rather open faces between long (two oxygen) and short (one oxygen) arms of the complexant.

II.F.7 Conclusions

Polycrystalline $Li^+(C211)e^-$ samples prepared by slow crystallization have magnetic properties which are consistent with the channel and cavity structure determined by single crystal X-ray crystallography. The magnetic interactions are consistent with a ladderlike Heisenberg linear chain with antiferromagnetic nearest and next-nearest neighbor interactions. The elasticity of the electron density in the cavities and channels allows the system to relax from the ladderlike chain structure with competing interactions to a dimerized chain through a spin-Peierls transition. $Li^+(C211)e^-$ is one of very few ladderlike structures known and, to our knowledge, the only one which possesses sufficient structural elasticity to undergo a spin-Peierls transition. It is indeed a rare

compound and the magnetic properties deserve further inspection. However, experimental studies of this compound must be accompanied by a theoretical study of the ladderlike Hamiltonian so that a more complete analysis of the data can be achieved.

The impetus to further characterize this electride goes beyond its unique magnetic properties. The original paper on $(Li)_x(C211)$ powders and films suggested that the properties of the materials were highly dependent on their stochiometry.[2] There is some evidence that this may be true even for samples crystallized from solution. For example, the data files of Margaret Faber, contain a set of susceptibility data labeled Li_2C211 and that are similar to that published for $(Li)_{0.6}(C211)$ powders.[2] The data displayed a broad, low maximum and fit well to a LCHA model (equation 2) as shown in Figure 13 with J/k = -49.8(5) K. Curiously enough, the magnitude of the susceptibility could be accounted for by only 8% of the electrons expected in a stochiometric electride. It may be that this $Li^+(C211)e^-$ is polymorphic or that lithium can be doped into the structure of the electride. The second explanation is rather attractive since lithium is small and may be easily accommodated in the cavities or channels of the structure. The ability to dope this electride with excess lithium might provide a valuable method by which to "tune" its electrical, optical and magnetic properties. Further study of the stochiometry dependence of the properties of the Li_xC211 system seems warranted.

II.F.8 Acknowledgments

This research was supported by NSF Solid State Chemistry Grants DMR 87-14751 and DMR 90-17292 and by the Michigan State University Center for Fundamental Materials Research.

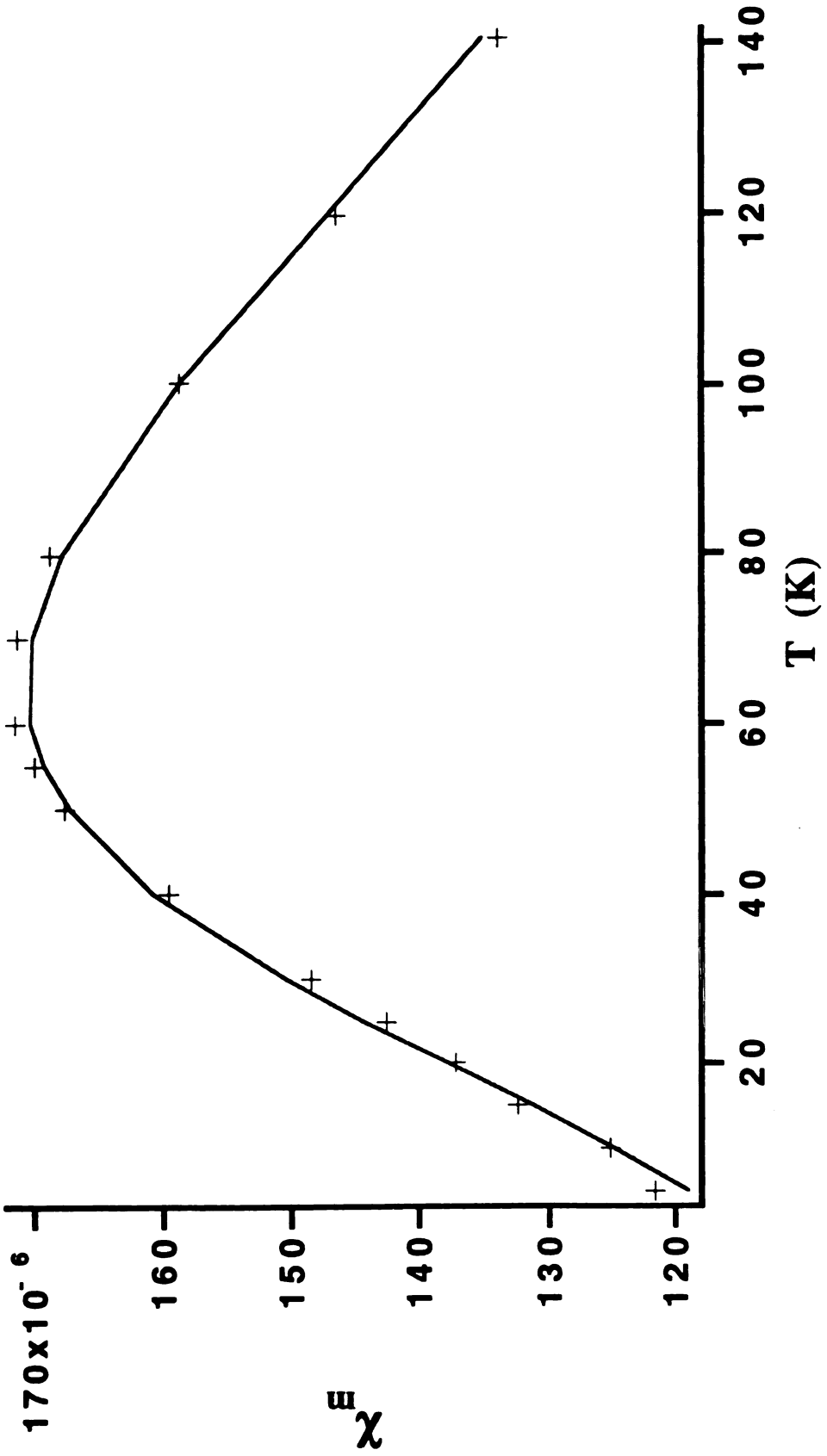

Figure 13. Fit of Margret Faber's magnetic susceptibility data labled Li2(C211) to linear chain Heisenberg antiferromagnetic model.

II.F.9 References

(1) Overney, G.; Nagy, T. F.; Wagner, M. J.; Dye, J. L. , *to be submitted to Angew. Chem. Int. Ed. Engl.*

(2) Landers, J. S.; Dye, J. L.; Stacy, A.; Sienko, M. J. *J. Phys. Chem.* **1981**, *85*, 1096.

(3) VanEck, B.; Le, L. D.; Issa, D.; Dye, J. L. *Inorg. Chem.* **1982**, *21*, 1966.

(4) Dye, J. L. *J. Phys. Chem.* **1980**, *84*, 1084.

(5) Dye, J. L. *J. Phys. Chem.* **1984**, *88*, 3842.

(6) Dye, J. L. *Pure & Appl. Chem.* **1989**, *61*, 1555.

(7) Moeggenborg, K. J. Ph.D. Dissertation, Mich. State Univ., East Lansing., **1990**.

(8) Moeggenborg, K. J.; Papaioannou, J.; Dye, J. L. *Chem. Mater.* **1991**, *3*, 514.

(9) English, A. D. *J. Magn. Reson.* **1984**, *57*, 491.

(10) Singh, D. J.; Krakauer, H.; Haas, C.; Pickett, W. E. *Nature* **1993**, *365*, 39.

(11) Kim, J. Ph.D. Dissertation, Michigan State Univ., East Lansing, **1989**.

(12) Shin, D.-H.; Ellaboudy, A. S.; Dye, J. L.; DeBacker, M. G. *J. Phys. Chem.* **1991**, *95*, 7085.

(13) Shin, D. H. Ph.D. Dissertation, Michigan State University, East Lansing, **1992**.

(14) Shin, D. H.; Dye, J. L.; Budil, D. E.; Earle, K. A.; Freed, J. H. *J. Phys. Chem.* **1993**, *97*, 1213.

(15) Fisher, M. E. *Amer. J. Phys.* **1964**, *32*, 343.

(16) Bonner, J. C.; Fisher, M. E. *Phys. Rev.* **1964**, *135*, A640.

(17) Estes, W. E.; Gavel, D. P.; Hatfield, W. E.; Hodgson, D. *Inorg. Chem.* **1978**, *17*, 1415.

(18) Hall, J. W. Ph.D. Dissertation, University of North Carolina, Chapel Hill, 1977.

(19) Hatfield, W. E. *J. Appl. Phys.* **1981**, *52*, 1985.

(20) Bonner, J. C. In *Magneto-Structural Correlations in Exchange Coupled Systems*; R. D. W. et. al., Ed.; D. Reidel Publishing Company: Dordrecht, Holland, 1985; pp 157.

(21) Ananthakrishna, G.; Weiss, L. F.; Foyt, D. C.; Klein, D. J. *Pyysica* **1976**, *81B*, 275.

(22) Peierls, R. E. *Quantum Theory of Solids*; Oxford University Press: London, **1955**.

(23) Bray, J. W.; Interrante, L. V.; Jacobs, I. S.; Bonner, J. C. In *Extended Linear Chain Compounds*; J. S. Miller, Ed.; Plenum Press: New York, **1983**; Vol. 3; pp 353.

(24) Hall, J. W.; Marsh, W. E.; Weller, R. R.; Hatfield, W. E. *Inorg. Chem.* **1981**, *20*, 1033.

(25) Knight, W. D. *Phys. Rev.* **1944**, *76*, 1259.

(26) O'Reilly, D. E. *J. Chem. Phys.* **1964**, *41*, 3729.

(27) Cahen, Y. M.; Dye, J. L.; Popov, A. I. *J. Phys. Chem.* **1975**, *79*, 1289.

(28) Catterall, R.; Edwards, P. P. *Chem. Phys. Lett.* **1976**, *43*, 122.

II.G $K^+(C222)e^-$: An Alternating Linear Chain Heisenberg Antiferromagnet

The following section was written with the intention that it be combined for publication with the work of James Hendrickson which is mentioned herein.

II.G.1 Introduction

More than 15 years have passed since the first report of the properties of $K^+(C222)e^-$, a study of the optical spectra of thin films.[1] Ten years later, in 1988, its structure was solved by single crystal x-ray diffraction and published.[2,3] However, the electrical and magnetic properties of this electride, although studied extensively for powder samples, are still poorly understood.[2,4,5] Measurements of the power absorption of powder samples[2,6] and optical spectra of thin films[6] suggest that it is metallic. However, powder and pressed pellet DC conductivity and impedence spectroscopy measurements show that its has a positive, albeit extremely small, temperature coefficient, characteristic of activated conductivity.[2,4,5] The sign of the temperature coefficient could, however, be entirely due to grain boundary effects so the measurements do not rule out metallic behavior. The unresolved questions about the interpretation of the properties and the unusual nature of the structure (described below) of $K^+(C222)e^-$ warranted the re-examination of the electrical and magnetic properties which follows.

II.G.2 Structure

The local structure of the complexed potassium cation in $K^+(C222)e^-$ is qualitatively as one might expect; the cation is encapsulated by the cryptand. The unusual feature of the structure of this electride is that the packing of the complexed cations leaves

pairs of cavities in the lattice. The "dumbell-shaped" cavity pairs are similar to those found to be the anionic sites of anion pairs in $K^+(C222)K^-$ and $Rb^+(C222)Rb^-$.[7] These cavities, which serve as the trapping sites of the electride electrons, and the interconnecting channels between these cavities, are displayed in the series of isosurfaces which comprise Figure 1.[8] As the allowable distance to the nearest atom is decreased (Figure 1, parts A-C), thinner interconnecting channels become visible. It is clear from these isosurfaces that the cavity and channel structure can be described as infinite chains of cavity dimers which are connected to other chains within a plane by long, narrow channels. Figure 1, part D, shows that the channels between these planes are negligible.

II.G.3 Magnetic Susceptibility

The data from one of the two published runs of the temperature dependence of the magnetic susceptibility were available and are shown in Figure 2.[2] The susceptibility shows a low-temperature rise which was attributed to preparation-dependent uncorrelated impurity electrons (a "Curie tail"). After subtraction of the tail, which could be accounted for by about 1% unpaired electrons, the susceptibility is seen to rise with increasing temperature. This was interpreted as being due to either thermally induced electron-pair dissociation or population of a triplet state with an estimated pairing energy of 0.05 - 0.10 eV. No attempts to fit the data to a model of the probable interactions were reported.

From the cavity and channel structure described above and qualitative data analysis, the most obvious model of the magnetic interactions to attempt to fit would be a simple model of antiferromagnetically interacting isolated spin-pairs. In general, electride spin anisotropies are expected to be and are found to be small.[9-11]; the pairing interactions are thus expected to be governed by the Heisenberg (isotropic) Hamiltonian. The Hamiltonian for the system can thus be writen as

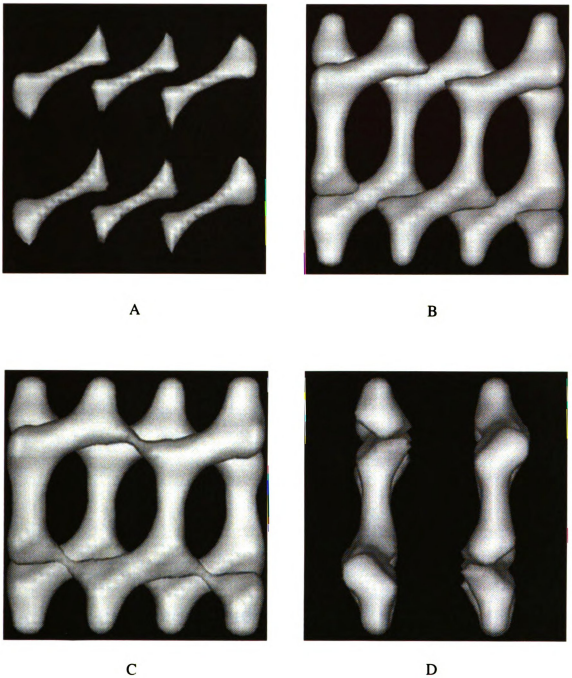

Figure 1. Isosurfaces of $K^{+}C222e^{-}$

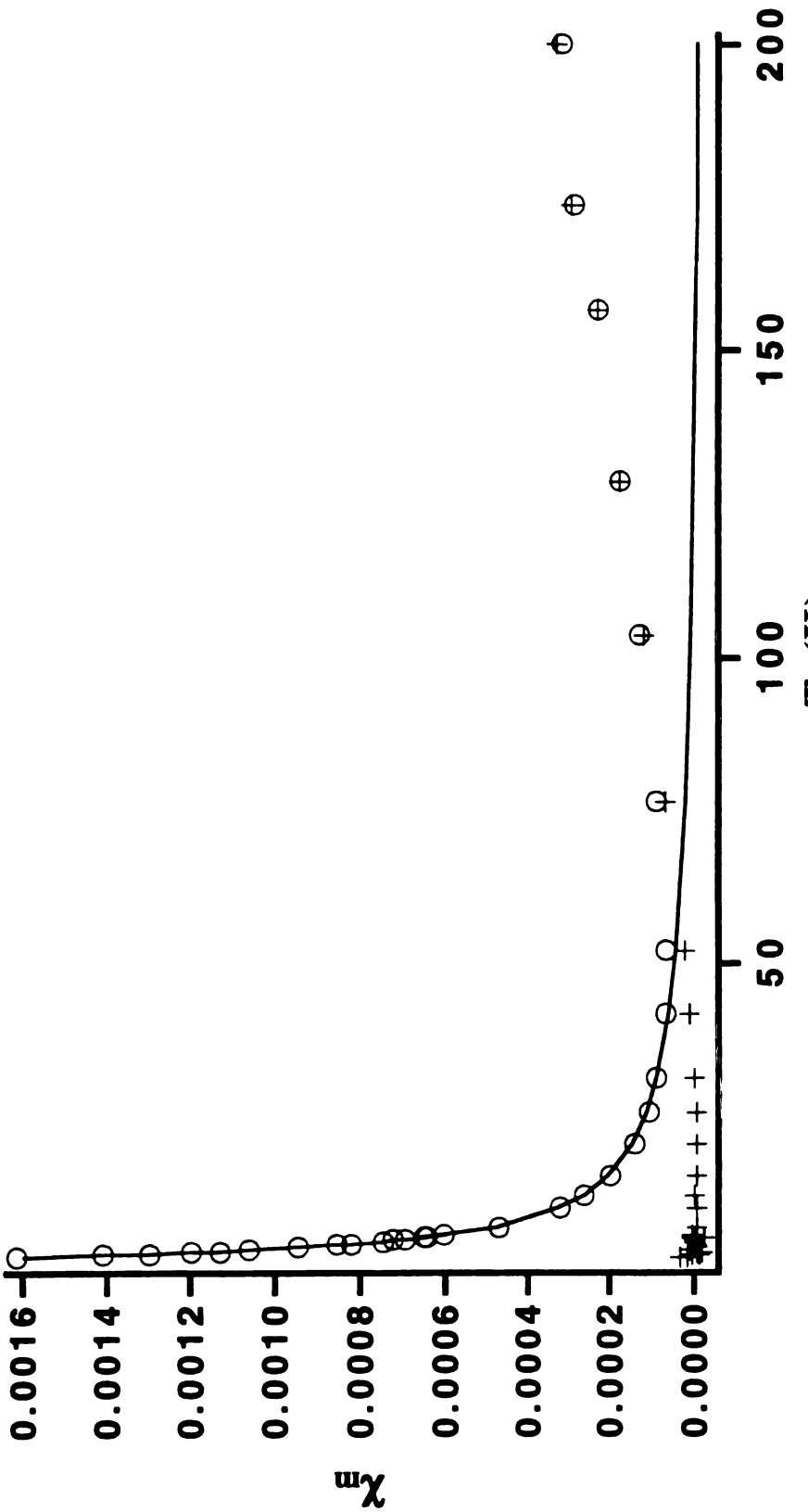

Figure 2. Molar electronic susceptibility (circles); fit of low temperature "Curie tail" (solid line); net susceptibility after tail subtraction (crosses).

$$\mathcal{H} = g\mu_B \hat{S}_z \vec{H}_z - 2J\hat{S}_1 \bullet \hat{S}_2 \qquad (1)$$

where the first term is the Zeeman interaction in a field $\vec{H}_z$ applied along the z-axis, $\hat{S}_z$ is the z-component of the total spin of the electron pair and the second term is the isotropic exchange interaction between the two spins. Antiferromagnetic interactions governed by this Hamiltonian result in a ground state singlet and an excited state triplet, separated by an energy of $-2J$. The magnetic susceptibility per mole of electride electrons for isolated S=1/2 spin pairs, as calculated from the Van Vleck[12] equation and commonly refered to as the "Bleany-Bowers equation",[13] is given by

$$\chi_m = (\frac{Ng^2\mu_B^2}{kT})[3 + \exp(-2J/kT)]. \qquad (2)$$

In addition to the susceptibility due to the spin pairs, one must also account for uncorrelated paramagnetic impurities as well as temperature independent paramagnetism (TIP), arising from mixing of excited states into the ground state singlet, and diamagnetism due to the interaction of paired electrons with the field. The paramagnetic impurities can be corrected for by assuming their susceptibility follows the Curie law (a "Curie tail")

$$\chi_{para} = \frac{Ng^2\mu_B^2}{3kT} S(S+1) \qquad (3)$$

where $Ng^2\mu_B^2 S(S+1)/3k$ is refered to as the Curie constant (C). Since both the TIP and diamagnetism are small and temperature independent, they can be corrected for by the addition of a term D making the measured susceptibility

$$\chi = \chi_m + \chi_{para} + D. \qquad (4)$$

Non-linear least squares fitting by this equation resulted in poor agreement with the measured susceptibility as seen in Figure 3. From this it is apparent that a more sophisticated analysis is necessary.

The most obvious modification of the susceptibility model would be to allow inter-pair coupling of the spins. The channels that connect the spin pairs are slightly longer than the intrapair channels but non-orthogonal overlap of the trapped electrons' wave functions down these channels could contribute a second antiferromagnetic interaction. This model is that of a spin = 1/2 alternating linear chain Heisenberg antiferromagnetic (ALCHA), whose Hamiltonian (excluding the Zeeman term) is

$$\mathcal{H} = -2J\sum_{i=1}^{n/2}[\hat{S}_{2i}\hat{S}_{2i-1} + \alpha\hat{S}_{2i}\hat{S}_{2i+1}] \qquad (5)$$

where J is the exchange parameter between a spin and one of its nearest neighbors along the chain and αJ is the exchange parameter between it and its other nearest neighbor. Although this model has not been solved analytically, infinite limit extrapolations of numerical calculations of finite size rings and convenient fitting expressions based on these calculations have been published.[14] The published expression is

$$\chi_m = \frac{Ng^2\beta^2}{kT}\left[\frac{[A(\alpha)]+[B(\alpha)]X+[C(\alpha)]X^2}{1+[D(\alpha)]X+[E(\alpha)]X^2+[F(\alpha)]X^3}\right] \qquad (6)$$

where $X = |J|/kT$ and is valid for $X < 2$. The constants A through F are given functions[14] of α and take on values which depend on whether α is larger than or less than 0.4. A non-linear leasts squares fit of the low temperature (T < 30 K) data to a "Curie tail" and a temperature independent correction was first subtracted from the data leaving a net susceptibility which increased smoothly with temperature from zero at 0 K. These data were then fit by equation 6 as shown in Figure 4. The very limited range of applicability

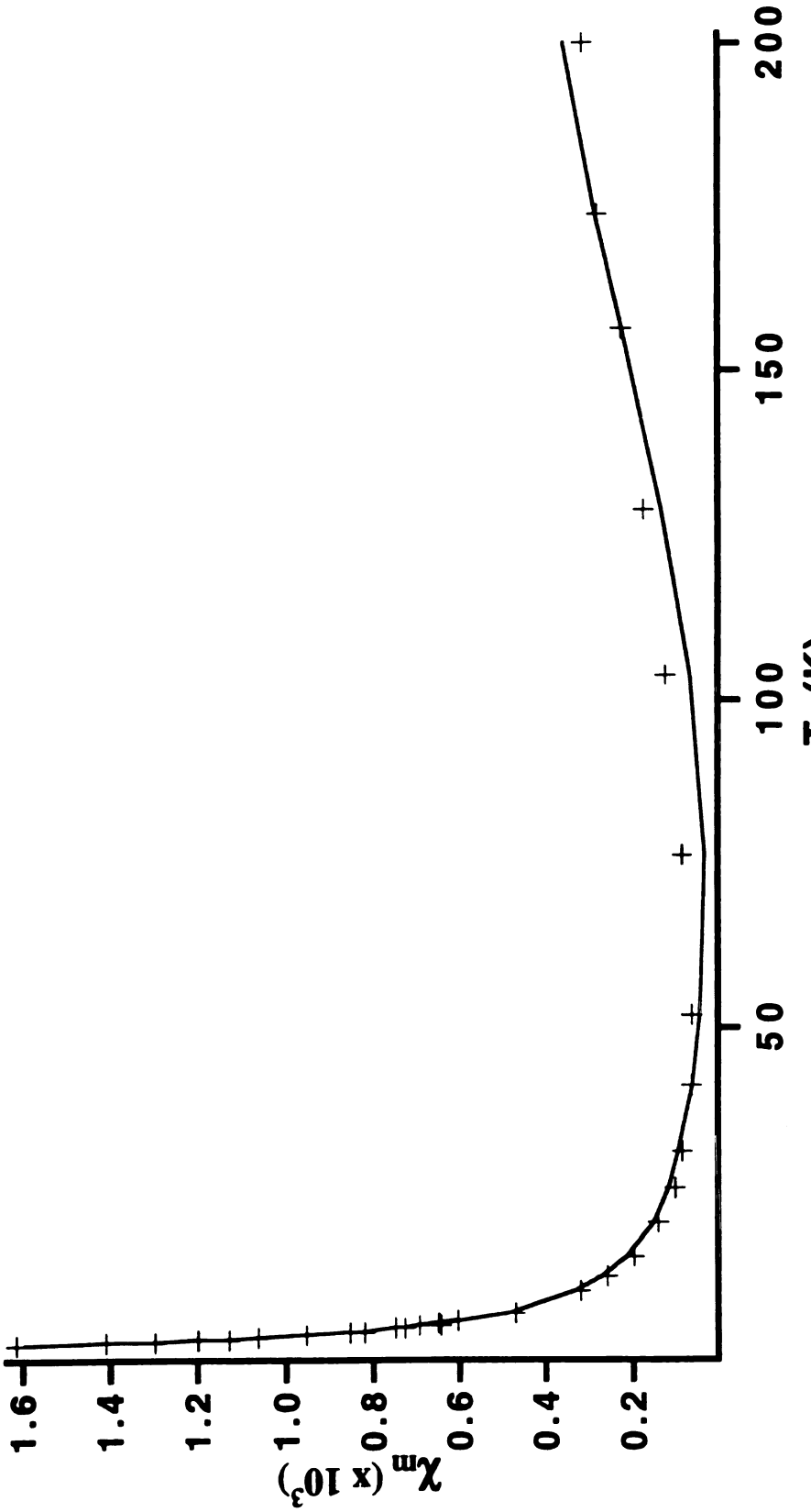

Figure 3. Fit of magnetic susceptibility to a spin pair model (equation 2).

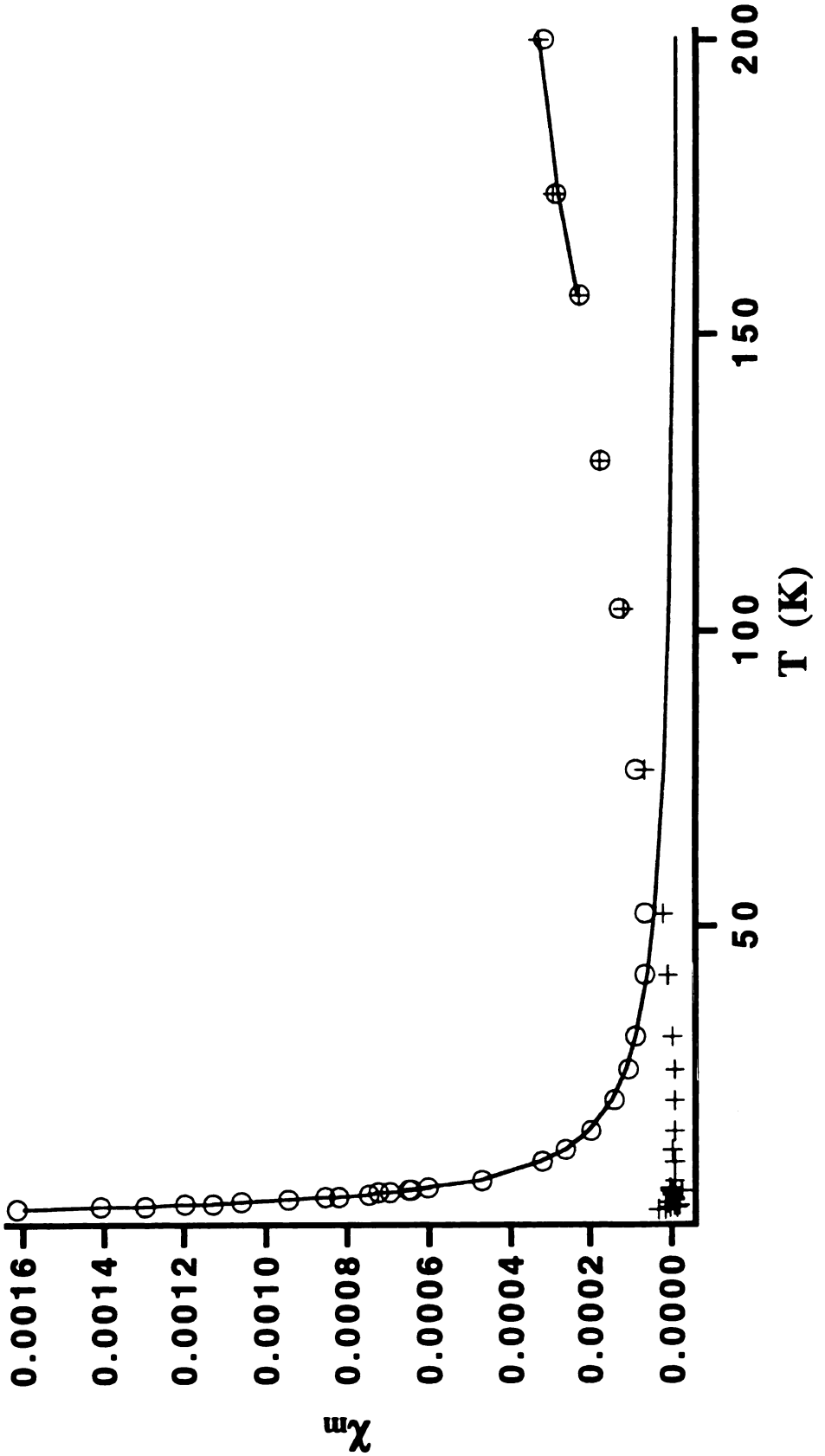

Figure 4. Molar electronic susceptibility (circles); fit of low temperature "Curie tail" (solid line); net susceptibility after tail subtraction (crosses); fit to ALCHA model (high temperature solid line).

due to the condition $X < 2$ and the variation shown at high temperatures in the two published runs made it clear that the susceptibility should be carefully re-run to higher temperatures with a higher data density, which I did. The measured susceptibility and the fit to the data is shown in Figure 5 with $\alpha = 0.85(1)$ and $|J|/k = 412(2)K$. It is clear from this treatment that although the data are limited, they are in good accord with the behavior expected from the channel and cavity structure of this electride.

II.G.4 Electrical Conductivity

Initial DC conductivity studies were made on pressed powders over a temperature range of 103 to 153 K.[2] These measurements showed semiconductor-like behavior and a bandgap of ~ 0.04 eV. More recently, pressed pellet DC conductivity and impedence conductivity studies, over the temperature range of 85 to 230 K, concluded that the bandgap was 0.055 eV up to ~ 135 K at which point it sharply rose to 0.086 eV.[4] This analysis was based on the assumption that $K^+(C222)e^-$ is a conventional semiconductor whose resistivity obeys the equation

$$\rho = \rho_o \exp(E_a / kT) \qquad (7)$$

where $2E_a$ is the bandgap. A logarithmic plot of the resistivity against inverse temperature should result in a straight line. A plot of the low frequency intercepts of the four-probe IS arcs clearly shows not one, but two straight line sections (Figure 6). It was suggested that the change in slope might be caused by either a change from extrinsic conductivity due to defect electrons to intrinsic conductivity or a reversible transition to a phase with a larger bandgap. An alternative way to fit the temperature dependence of the conductivity would be using the more general expression

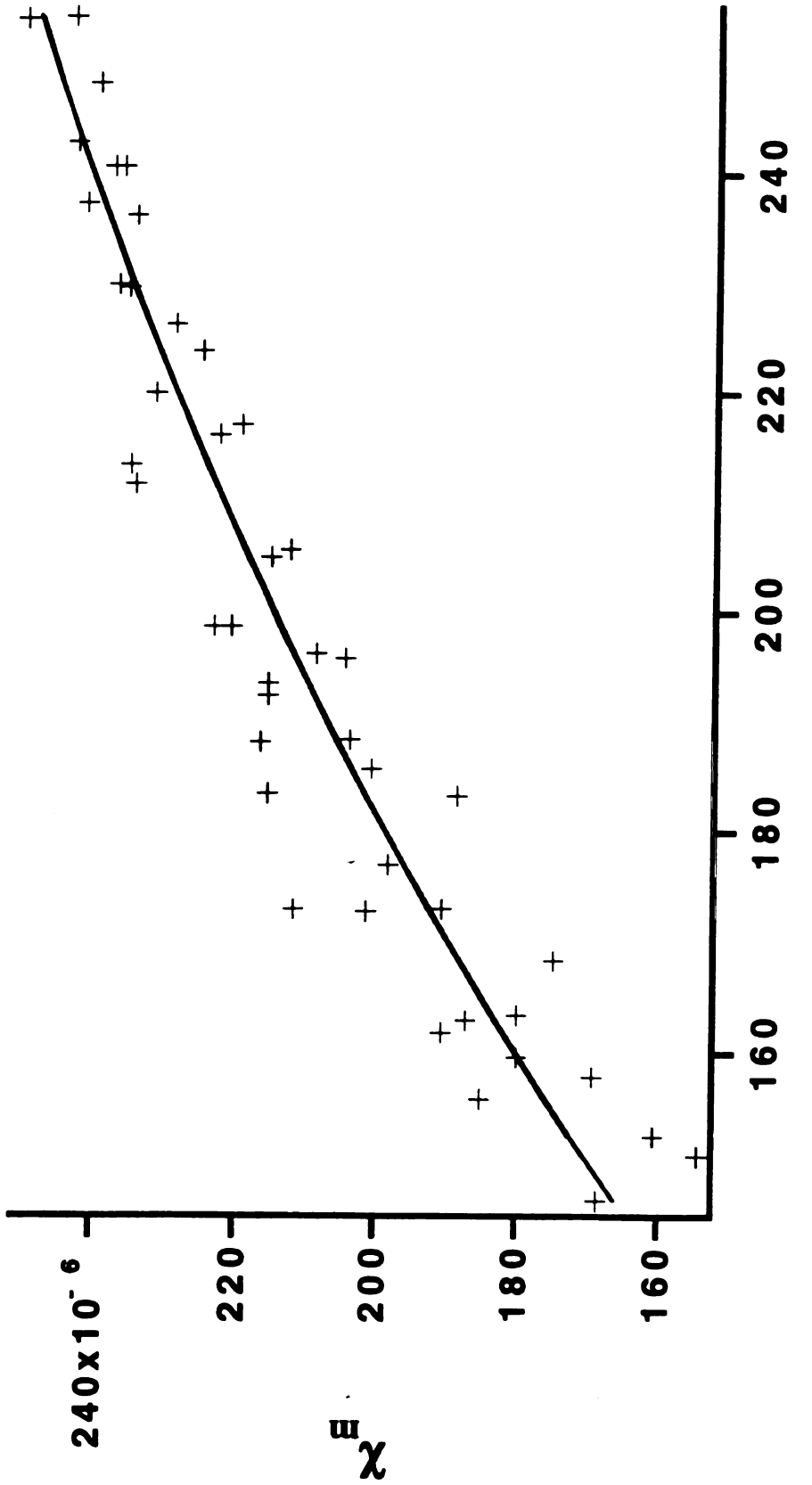

Figure 5. High temperature fit to ALCHA model (solid line).

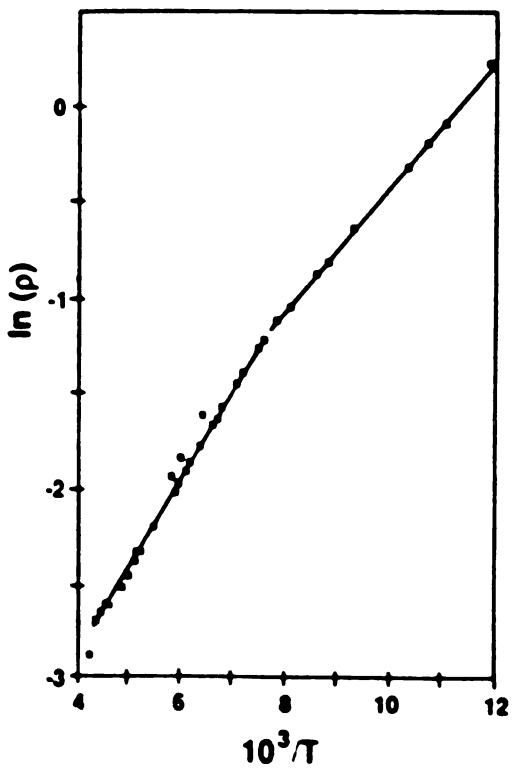

Figure 6. Previously published (reference 5) fit of the temperature dependence of the low frequency intercept of 4-probe IS arcs showing two straight line regions.

$$\rho = \rho_o \exp[(T_o / T)^n] \qquad (8)$$

where the definition of T_o depends on the conduction mechanism and the value of n (1 > n > 0) is indicative of the mechanism. Values of $n = 0.23(2)$, $T_o = 8.28(8) \times 10^6 K$ and $\rho_o = 5(4) \times 10^{-7} \Omega \cdot cm$ were determined from a non-linear least squares fitting of 4-probe DC conductivity data (which are nearly identical to the IS data) by equation 2 (Figure 7). The value of n suggests that the conduction is due to a variable range three dimensional hopping mechanism.[15,16] In this model, the theoretical value of n is 0.25 and T_O is inversely proportional to the localization length of the electronic states responsible for the conductivity. Fitting the data with the value of n held constant at the theoretical value of 0.25 results in an excellent fit with $\rho_o = 1.249(7) \times 10^{-6} \Omega \cdot cm$ and $T_o = 2.76(2) \times 10^6 K$ as shown in Figure 8.

II.G.5 Discussion

It has been suggested that $K^+(C222)e^-$ might be a metal. While it is clear that a hopping model provides a much better fit of the data, could this be due to activated hopping between the metallic grains or strands? Such a model would require a non-vanishing density of states at the Fermi level. If this were the case, one would expect the bulk magnetic susceptibility to exhibit Pauli paramagnetism and thus have a non-zero moment at 0 K. Fitting of the susceptibility indicates that there is a gap at the Fermi level at 0 K; thus the material is not a simple metal.

If the observed conductivity is truely due to activated hopping, how can one rationalize this within the cavity and channel model? Under this model, one would not expect metallic behavior since the lattice is best discribed as a dimerized chain, which leads to a gap at the Fermi level (Figure 9).[17] Hopping from one singly filled cavity to another to create an electron pair within a single cavity seems highly unlikely; Coulombic

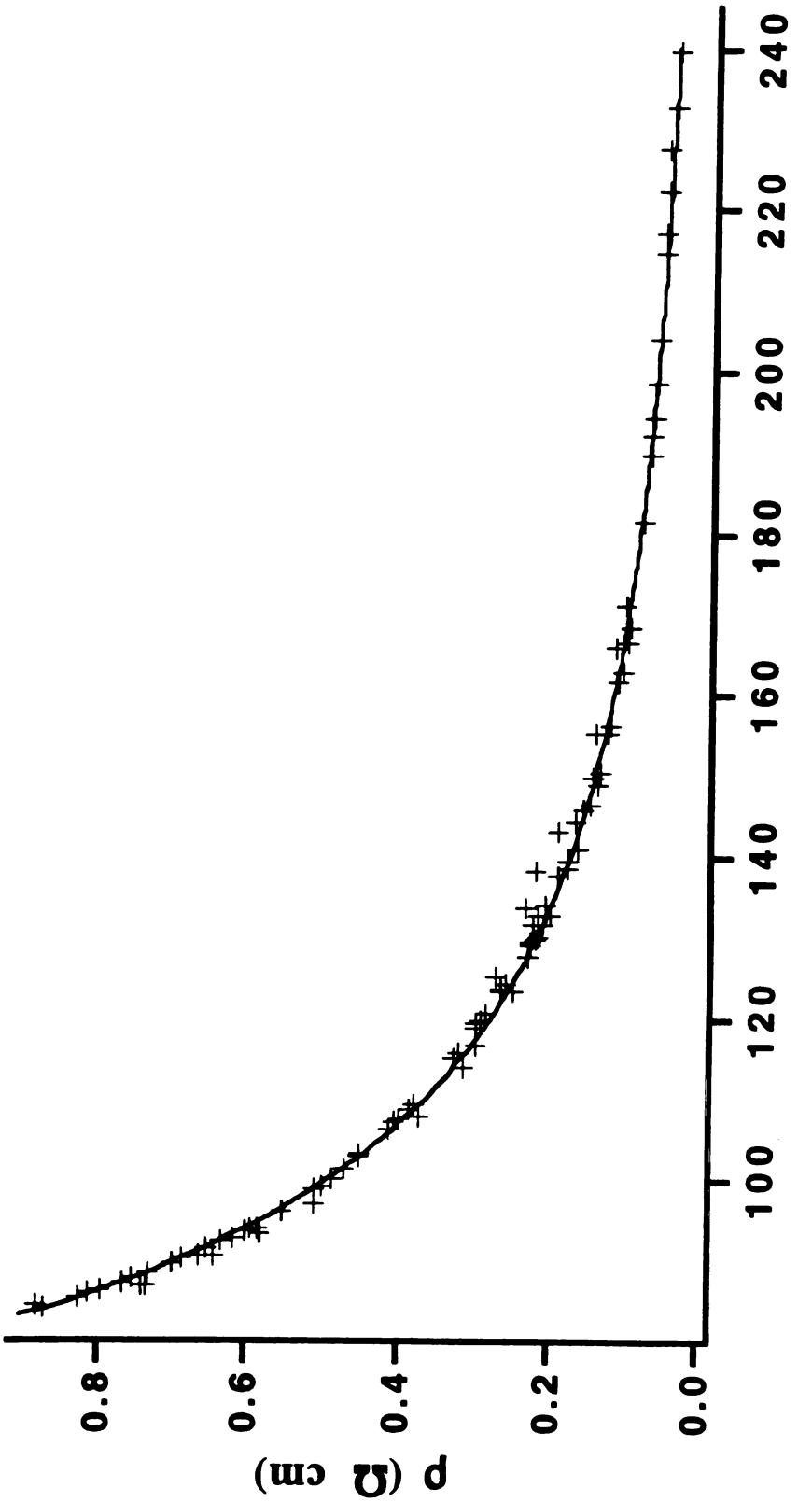

Figure 7. Fit of 4-probe conductivity data to equation 8.

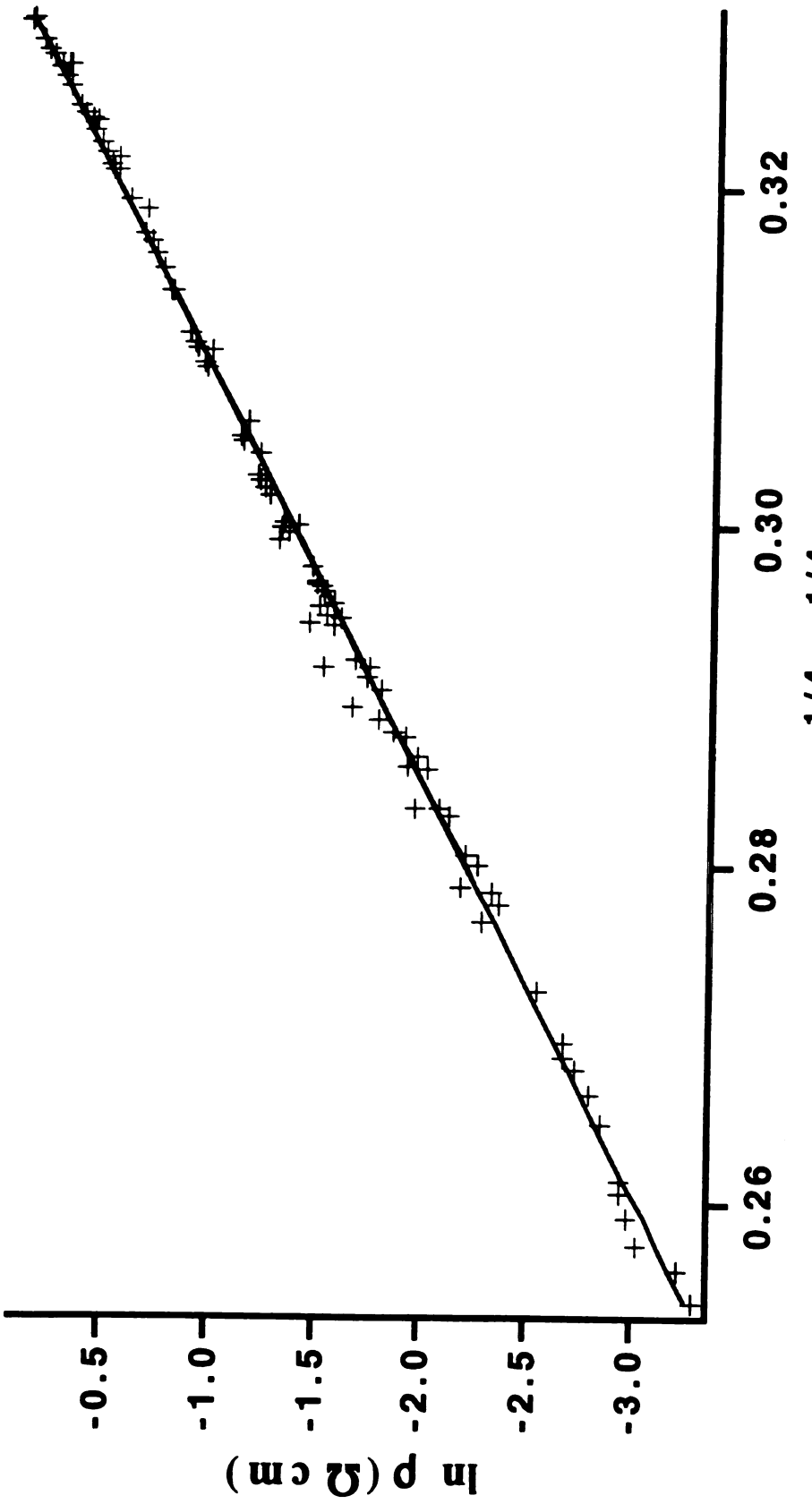

Figure 8. Fit of 4-probe conductivity data to 3-D hopping model.

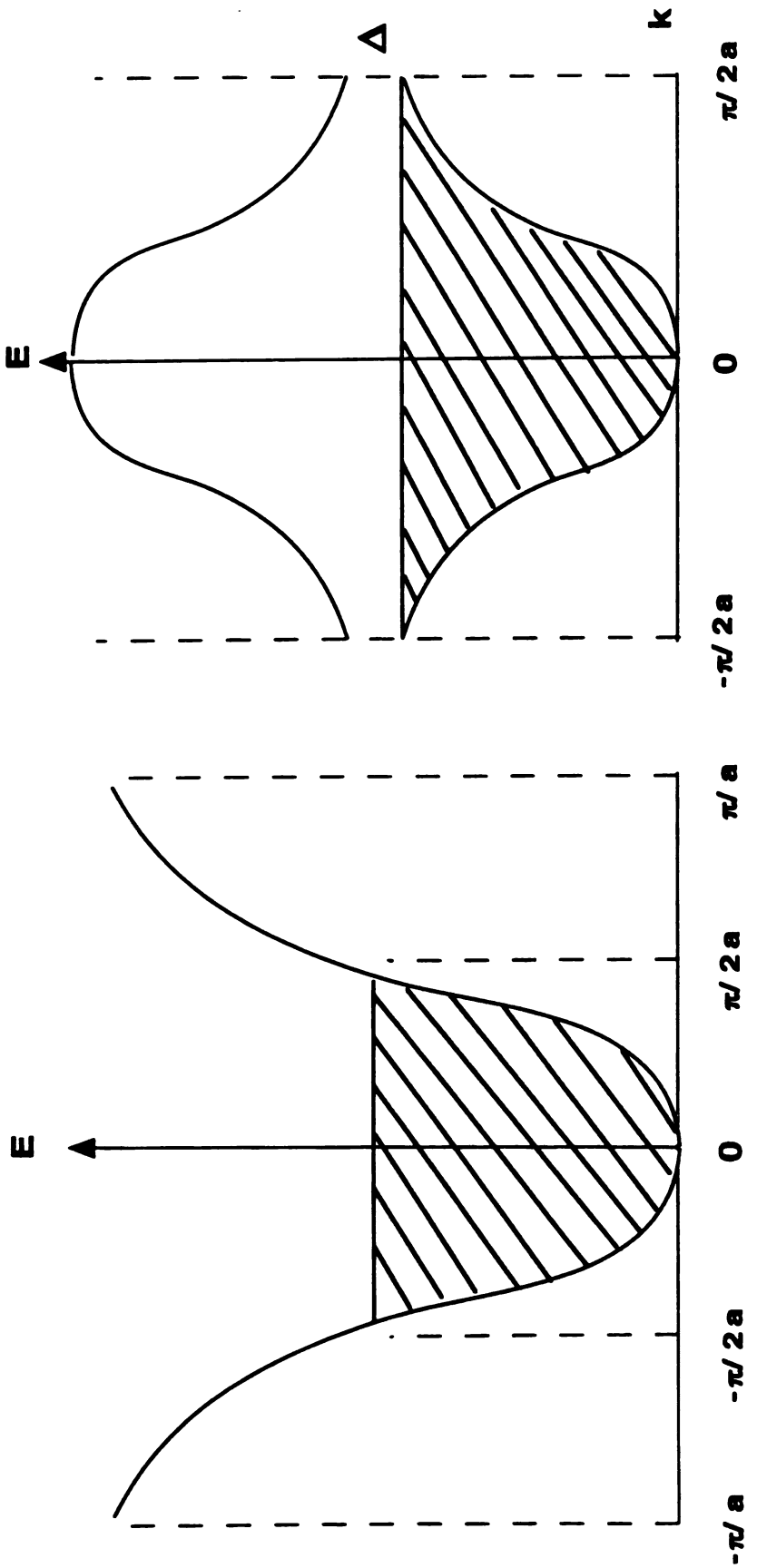

Figure 9. Schematic of the energy dispersion for a half-filled band of a uniform chain (left) and that of a dimerized chain (right) illustrating the instability of the formere with respect to the latter and the gap in the energy spectrum of the latter.

repulsions are probably extremely large. LDA calculations on $Cs^+(15C5)_2e^-$, which has cavities of similar size, indicate that the Coulombic repulsions are large even in the absence of a dimerized lattice.[18] The presence of electride electron vacancies (empty cavities or "holes"), however, would drastically alter the situation. The "defect" electrons, defined as those trapped in sites with a vacant nearest neighbor cavity, would be localized states near the Fermi level that are randomly distributed in energy and space as required by the hopping mechanism. The extension of the wavefunctions of the defect electrons into the channels makes the network of channels a natural one- or two-dimensional path for variable length hops. Thus, one- or two-dimensional hopping can easily be explained by the cavity and channel structure.

The fit to a three-dimensional hopping model might seem to be in conflict with the cavity and channel structure, which is one- or two-dimensional. However, in materials where the hopping probability is highly anisotropic, hops in the other dimension(s) will be made when lattice imperfections are encountered. If the total length of these hops is on the order of the length of hopping within a single "perfect" segment, the macroscopic hopping will appear three-dimensional.[15] While there are no significant channels between the two-dimensional layers of cavities, off plane hopping might be facilitated by the complexed potassium since the trapped electrons in adjacent planes will have a small density on these cations. It should also be pointed out that the temperature range and precision of the data are both limited enough to make the assignment of the conductivity to a three- rather than a two-dimensional model tenuous. The theoretical value of n in equation 8 for the variable range hopping models is 1/(d+1), where d is the dimensionality.[16] A fit to the two-dimensional model is also quite good as can be seen in Figure 10, with linear least-square fitting parameters of $\rho_o = 2.30(1)\times 10^{-5}\Omega\cdot cm$ and $T_o = 1.063(7)\times 10^5 K$.

If the predominant conduction mechanism is hopping of defect electrons, the conductivity of any single sample should depend on the number of these defects. Recently, a simultaneous study of the optical spectra and conductivity of vapor-deposited thin films

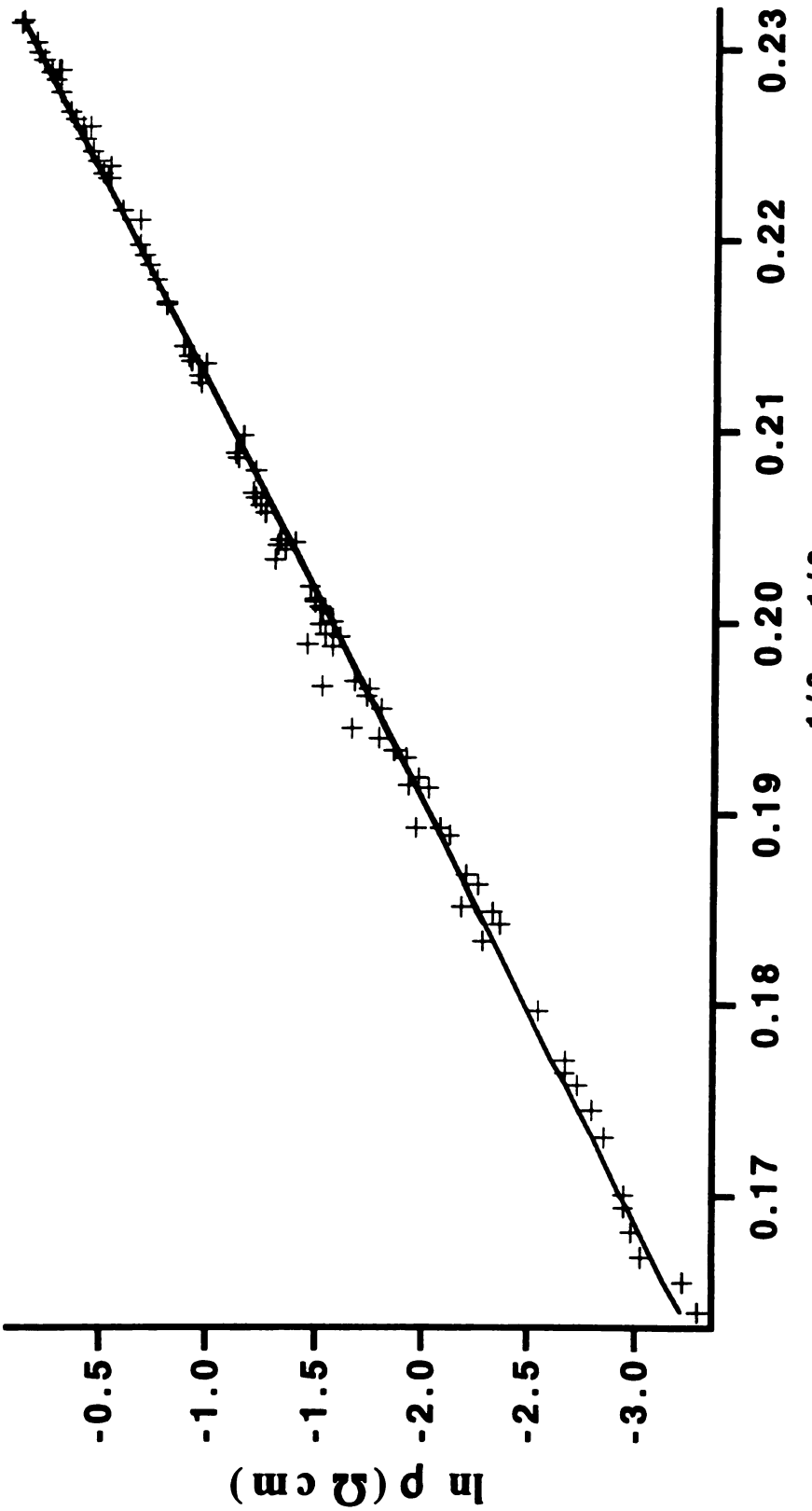

Figure 10. Fit of the conductivity data to a 2-D hopping model.

indicated that this could be true.[19] It was found that the conductivity of a sample increased during partial decomposition. This study did not show whether the increase in temperature to above 240 K, which was employed to cause slow decomposition, could create the increase in defect electrons necessary to validate the hopping model.

To verify that the cycling could indeed create these defects, the magnetic susceptibility of a polycrystalline sample was measured before and after cycling the temperature above 240, 250, and 260 K (Figure 11). The increase in the "Curie tail", from ~ 0.29 to ~ 0.38 to ~ 0.85%, upon thermal cycling is indicative of the creation of paramagnetic "defect" electrons. The invariance of the high temperature susceptibility (until catastrophic sample decomposition above 260 K) indicates that the sample is largely unaffected by these "defects". Reduction of individual cryptands, similar to the reduction of crowns seen in other alkalides and electrides,[20] could result in the production of two holes and two unpaired electrons per reduced cryptand, possibly leaving the channel and cavity structure largely intact. These electrons and holes would constitute the defects near the Fermi level necessary for the hopping model and would increase the conductivity as seen experimentally.

II.G.6 Conclusions

$K^+(C222)e^-$ is probably not a metal, except perhaps in the sense that the carrier density may be only weakly temperature dependent. Magnetic susceptibility and conductivity studies suggest that the conduction is probably due to two- or three-dimensional variable-range hopping of defect electrons. The "pure" electride may, in fact, be an insulator due to strong Coulombic repulsions. The electride electrons are trapped in pairs; however these pairs have significant interpair interactions to form antiferromagnetically coupled chains with weaker interchain interactions within a plane and negligible interplane interactions. These results are all consistent with the

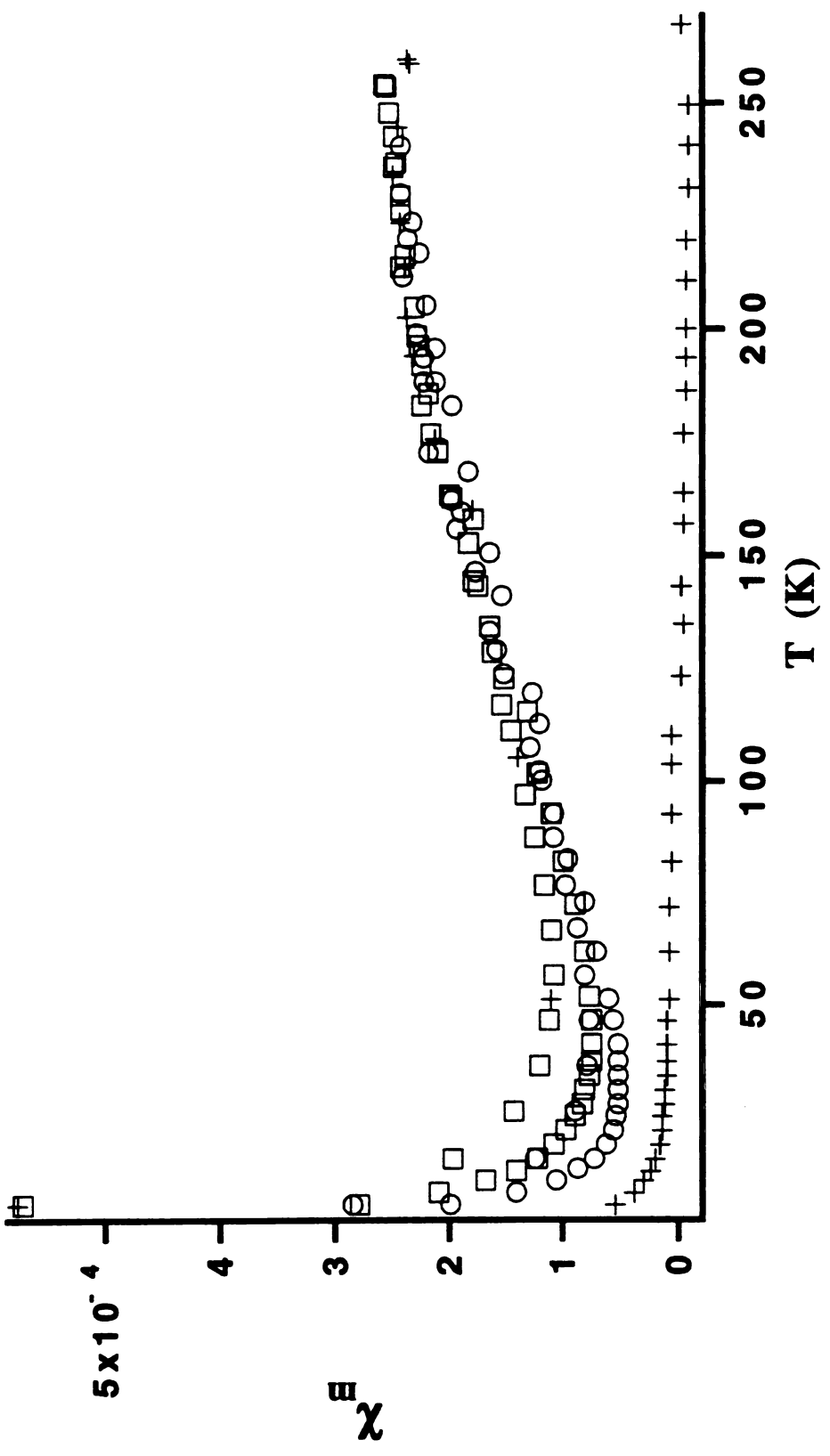

Figure 11. Magnetic susceptibility data showing the growth of defects caused by thermal cycling; circles - first run to 240 K, squares - subsequent run to 250 K, crosses - final run, sample decomposed above 260 K.

structure of the cavities and channels in which the electride electrons are presumed to reside.

II.G.7 Acknowledgments

This research was supported by NSF Solid State Chemistry Grants DMR 87-14751 and DMR 90-17292 and by the Michigan State University Center for Fundamental Materials Research.

II.G.8 References

(1) Dye, J. L.; Yemen, M. R.; DaGue, M. G.; Lehn, J. *J. Chem. Phys.* **1978**, *68*, 1665.

(2) Huang, R. H.; Faber, M. K.; Moeggenborg, K. J.; Ward, D. L.; Dye, J. L. *Nature* **1988**, *331*, 599.

(3) Ward, D. L.; Huang, R. H.; Dye, J. L. *Acta Crystallogr.* **1988**, *C44*, 1374.

(4) Moeggenborg, K. J. Ph.D. Dissertation Thesis, Mich. State Univ., East Lansing., **1990**.

(5) Moeggenborg, K. J.; Papaioannou, J.; Dye, J. L. *Chem. Mater.* **1991**, *3*, 514.

(6) DaGue, M. G.; Landers, J. S.; Lewis, H. L.; Dye, J. L. *Chemical Physical Letters* **1979**, *66*, 169.

(7) Huang, R. H.; Ward, D. L.; Dye, J. L. *J. Am. Chem. Soc.* **1989**, *111*, 5707-5708.

(8) Overney, G.; Nagy, T. F.; Wagner, M.; Dye, J. L. , *submitted to Angew. Chem. Int. Ed. Engl.*

(9) Shin, D.-H.; Ellaboudy, A. S.; Dye, J. L.; DeBacker, M. G. *J. Phys. Chem.* **1991**, *95*, 7085.

(10) Shin, D. H. Ph.D. Dissertation Thesis, Michigan State University, East Lansing, **1992**.

(11) Shin, D. H.; Dye, J. L.; Budil, D. E.; Earle, K. A.; Freed, J. H. *J. Phys. Chem.* **1993**, *97*, 1213.

(12) Van Vleck, J. H. *The Theory of Electric and Magnetic Susceptibilities*; Oxford University Press: Oxfork, **1932**.

(13) Bleaney, B.; Bowers, K. D. *Proc. Roy. Soc. (London)* **1952**, *A214*, 451.

(14) Hall, J. W.; Marsh, W. E.; Weller, R. R.; Hatfield, W. E. *Inorg. Chem.* **1981**, *20*, 1033.

(15) Mott, N. F. *Phil. Mag.* **1969**, *19*, 835.

(16) Brenig, W.; Dohler, G. H.; Heyszenau, H. *Phil. Mag.* **1973**, *27*, 1093.

(17) Peierls, R. E. *Quantum Theory of Solids*; Oxford University Press: London, 1955.

(18) Singh, D. J.; Krakauer, H.; Haas, C.; Pickett, W. E. *Nature* **1993**, *365*, 39.

(19) Hendrickson, J. E. Ph.D. Dissertation Thesis, Mich. State Univ., East Lansing., **1994**.

(20) Cauliez, P. M.; Jackson, J. E.; Dye, J. L. **1991**, *32*, 5039.

III STATIC POLYCRYSTALLINE MAGNETIC SUSCEPTIBILITY AND 4-PROBE SINGLE CRYSTAL CONDUCTIVITY STUDIES OF $[Ru(bpy)_3]^0$

The following chapter is in the form of a paper that has been submitted to *The Journal of the American Society*. I am solely responsible for the writing of this manuscript entitled "Static polycrystalline magnetic susceptibility and 4-probe single crystal conductivity studies of $[Ru(bpy)_3]^0$". I am also personally responsible for all the data and analysis included in this paper. The samples were supplied by my co-authors Eduardo Pérez-Cordero, Rosanna Buigas and Professor Luis Echegoyen. Professor Dye was involved in the planning and interpretation of the results and provided editorial assistance.

III.A Introduction

The synthesis of crown ethers[1] by Pederson in 1967 and cryptands[2] by Lehn in 1969 ignited the still exploding field of macrocyclic host-guest chemistry. These complexants and those synthesized subsequently have been used to make a myriad of expanded metal cations and entirely new classes of salts. Two such salts, alkalides and electrides, consist of complexed alkali metal cations charge-balanced by alkali metal anions or trapped electrons respectively.[3] The anionic electrons in electrides range from weakly coupled, localized electrons to strongly interacting ones and itinerant behavior. Closely related to electrides are electropositive metals that are complexed by organic complexants with low lying molecular acceptor levels. The charge transferred electrons are localized in these orbitals rather than in lattice vacancies. If the complexant allows for delocalization of the electron(s) over the complexant molecule, the charge neutral entity can be considered an "expanded atom".[4] This type of molecular species holds the

promise of bridging the gap between electrides and the closely related alkali metal doped fullerenes (M_xC_{60}), which have the highest recorded superconducting critical temperatures of any known molecular material.[5,6] Electrides and M_xC_{60} differ mainly in that electrides have no low-lying π^* orbitals into which the reducing electrons can delocalize. Bridging this gap with "expanded atoms" holds the promise of new and exciting electronic properties in view of the properties of the extreme members.

A compound which comes close to this description, refered to as a *cryptatium*, and depicted in Figure 1, has been synthesized and its crystal structure determined.[7] Its complexant, tris(bipyridine) cryptand,[8] can be considered to be three bipyridine ligands tethered at both ends. The electron released from the complexed sodium cation is localized in one of the bipyridine ligands. Complexation of a trivalent cation might result in a crystalline species of "expanded atoms" in which each "cryptand" captures three electrons.

The success of controlled-current electrocrystallization of cryptatium lead to the subsequent crystallization of single crystals of $[Ru(bpy)_3]^0$.[9] Powder or microcrystalline samples of this material had been previously reported and studied by EPR methods; however, no previous attempts at growth of single crystals had been reported.[10-12] $[Ru(bpy)_3]^0$ is of interest to us due to the obvious relationship of its ligands to *cryptatium* and its bi-reduced state. Numerous attempts to solve the structure by x-ray diffraction failed, presumably because of disorder, although it was possible to determine that the material possesses hexagonal symmetry. However, the molecular nature of the material permitted safe assumptions to be made about the likely structure of the complexed cation. We assume the local structure to be similar to that determined for $[Ru(bpy)_3](PF_6)_2$ (Figure 2),[13] with a propeller-like, six coordinate arrangement of the ligands and nearly octahedral coordination of the nitrogen atoms. The absence of counter-ions suggests that the molecules might be packed in the solid state with good intermolecular π^* overlap. If so, this material might be a good model for crystallized

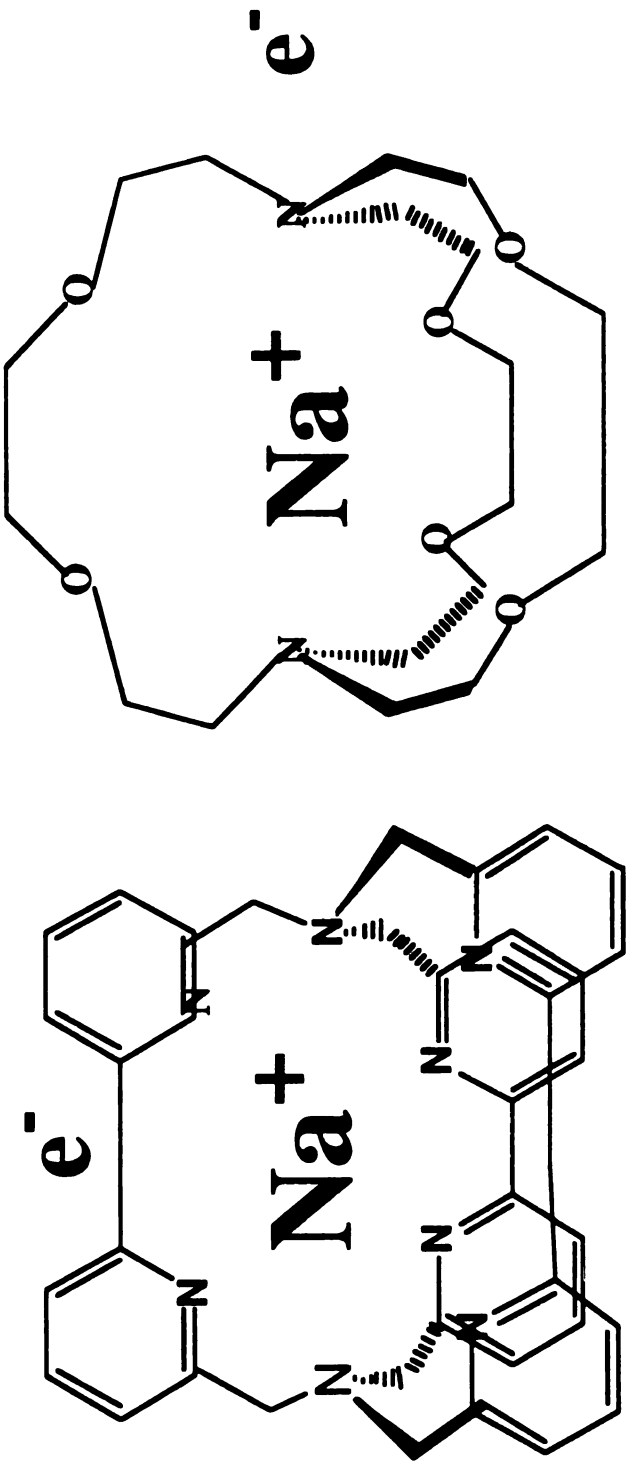

Figure 1. Schematic diagram of sodium cryptatium (left) with a sodium cryptate electride (right) included for comparision.

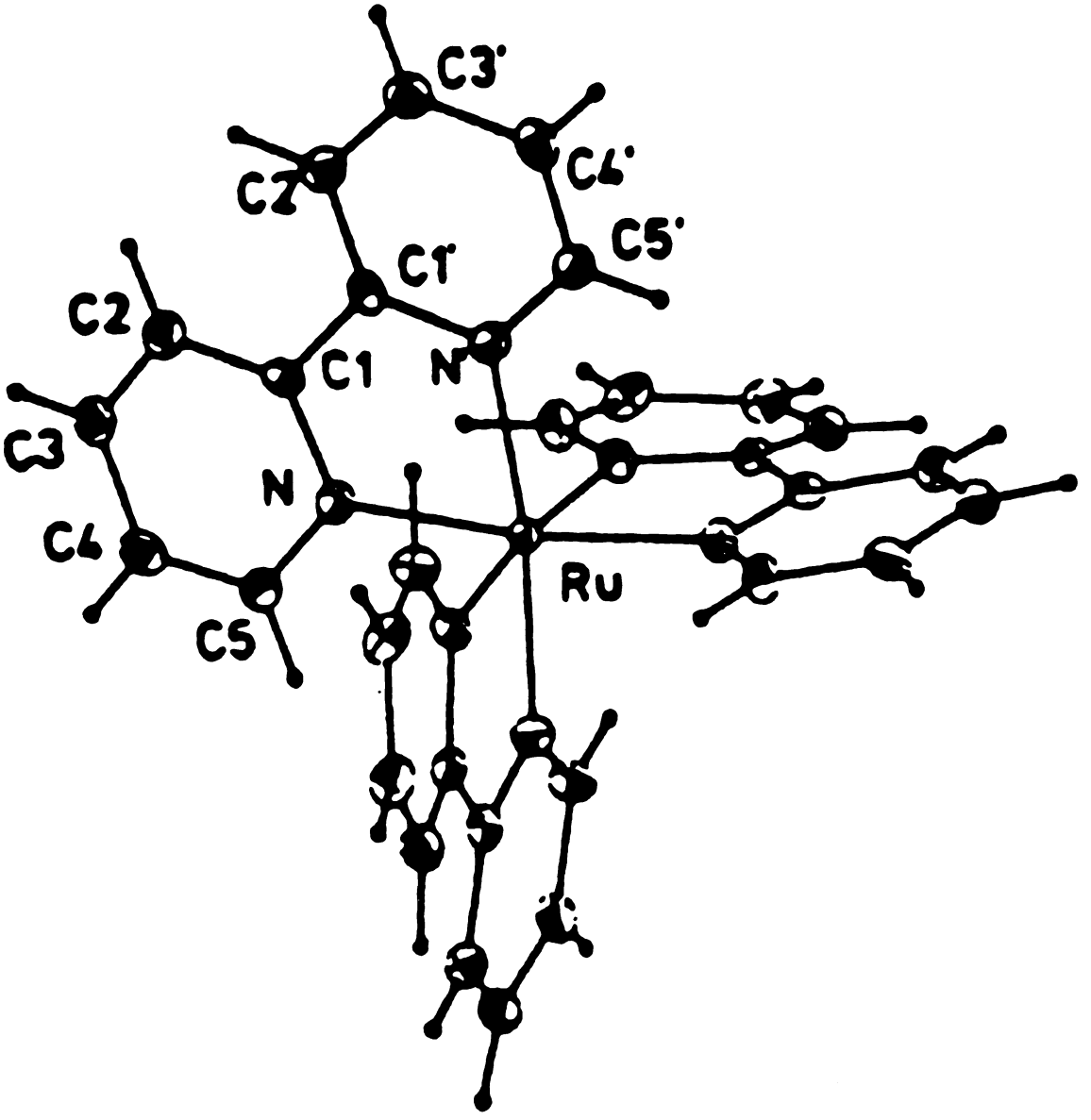

Figure 2. The local structure of $[Ru(bpy)_3]^{3+}$. This structure is virtually indistinguishable from the dipositive species. Reproduced, with permission from Biner, M., Bürgie, H., Ludi, A., Rohr, C. J. *J. Am. Chem. Soc.*, **1992**, *114*, 5197. Copyright © 1992 by the American Chemical Society.

"expanded atoms". This article reports the results of 4-probe single crystal conductivity and powder static magnetic susceptibility measurements.

III.B Experimental

Crystals of $[Ru(bpy)_3]^0$ were grown by reductive electrocrystallization methods described fully elsewhere.[7,9,14] Two Pt wires were used, one as the cathode and one as the anode. High vacuum was maintained during the controlled-current process (I = 7.5 mA) and 0.1 M tetrabutylammonium tetrafluorophosphate in acetonitrile was used as the solvent. Since they are air sensitive, manipulations of the harvested dark black-blue needle shaped crystals were always performed under inert atmosphere or high vacuum.

The magnetic susceptibility was measured from 1.5 to 390 K with a S.H.E. Corp. model 800 variable temperature SQUID susceptometer. The sample was pulverized into a fine powder with an agate mortar and pestle and loaded into an aluminum-silicon alloy holder in a helium filled glove box. The sample was then transferred to the SQUID under a helium atmosphere and cooled to 2 K in zero applied field. The temperature dependence of the susceptibility was measured in a 7 KG applied field. The small, nearly temperature independent paramagnetic susceptibility of the holder was subtracted after running the empty holder under the same conditions.

The DC conductivity was obtained by using a previously described crystal holder.[15] Measurements were made on a well-formed single crystal with hexagonal outer morphology (cross-section). Results with other crystals were qualitatively similar. The length of the crystal was 1.30(3) mm and its face-to-face width was 0.91(3) mm (numbers in parenthesis are uncertainties in the final digits). The crystal was selected in a helium filled glove box and transferred under helium to a pair of nitrogen filled glove bags. One of the glove bags was set-up inside the other; separate nitrogen gas supplies purged each so that the outer bag served as an antechamber. A dewar of liquid nitrogen was maintained inside the inner bag to minimize the humidity. Four gold wire leads (0.0127

mm diameter) were attached in a linear arrangement along one face of the crystal under a microscope with silver paint. The temperature was controlled by suspending the cell in a liquid nitrogen dewar above the liquid level. A positive pressure of flowing nitrogen was maintained in the dewar at all times. The temperature was measured with a copper-constantan thermocouple mounted in contact with the sample platform. After allowing the sample to come to thermal equilibrium, a DC current of 100 μA was supplied to the outermost leads and the voltage between the innermost was measured. The leads were then reversed and the measurement repeated. The two readings were averaged when determining the resistivity. Ohmic behavior was confirmed at each temperature by measurements at 10 μA. Two Keithley 617 electrometers were employed as the current source and voltammeter.

III.C Results and Discussion

The measured molar susceptibility is shown in Figure 3. The low temperature rise in susceptibility is qualitatively similar to that expected for uncorrelated impurities (a "Curie tail"). However, a Curie law fit is far from satisfactory. A much better fit of the 1.5 to 19 K data can be obtained by using

$$\chi_m = CT^n + D \qquad (1)$$

where C = 0.00200(4) (related to the concentration of spins as in the Curie law) and n = 0.59(5). The bulk diamagnetic correction, D, is -0.00027(6) which is reasonable when compared to that obtained from Pascal's constants (≈ - 0.000338), especially if one considers the possibility of a small temperature independent paramagnetic component.[16,17] This fit is shown in the inset of Figure 3. We are aware of only two theoretical explanations for such a sub-Curie law tail; the random exchange Heisenberg

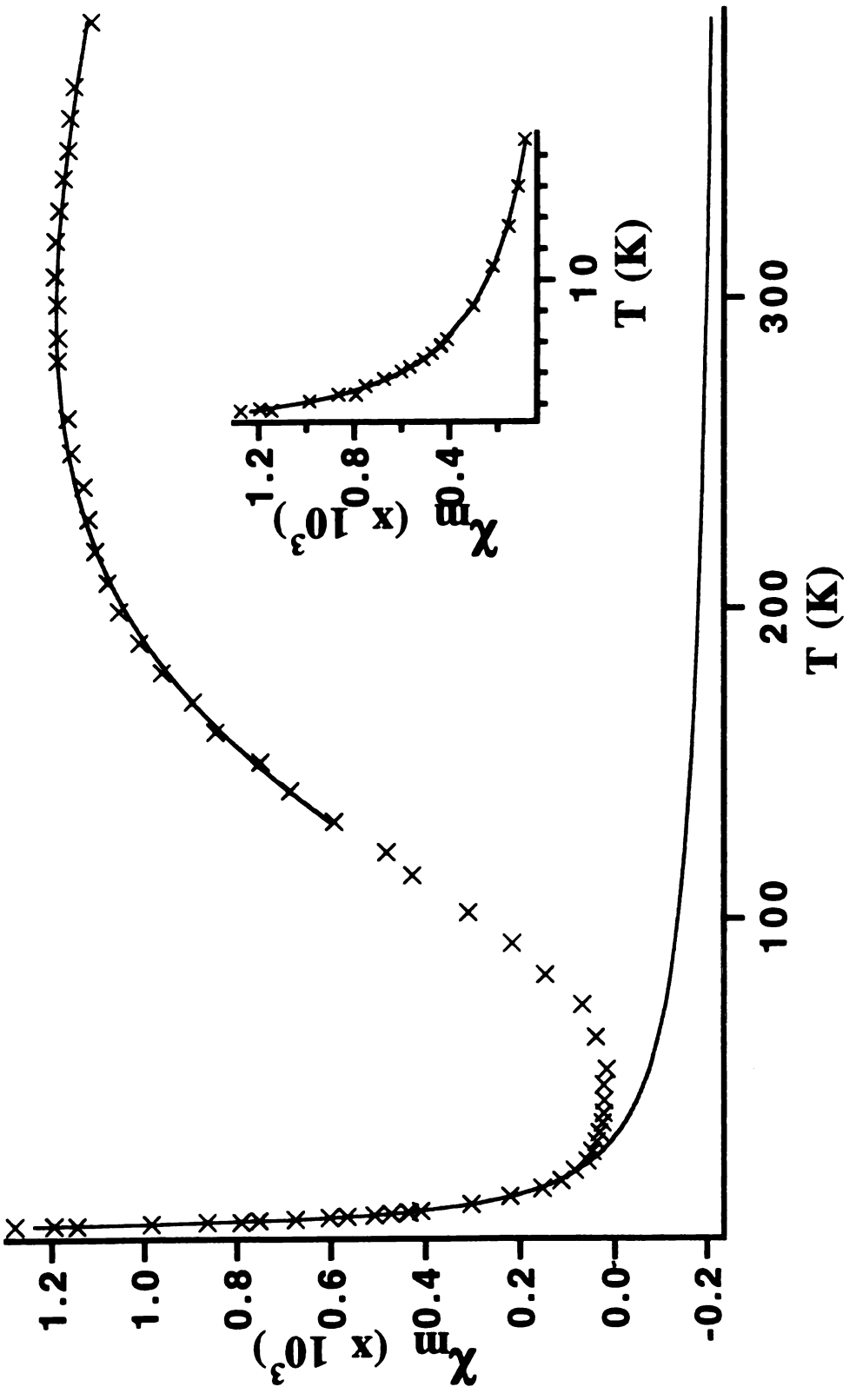

Figure 3. Temperature dependence of the magnetic susceptibility of[Ru(bpy)$_3$]^0 (crosses). The solid line extending from low temperature is the best fit to equation 6. The low temperature "sub-Curie" tail (crosses) is shown in the inset. The solid line represents the best fit to equation 1.

antiferromagnetic coupling (REHAC) model[18] and the interspersion of variable-length paramagnetic odd and diamagnetic even chain segments.[19] The REHAC model results in a sub-Curie temperature dependence due to random, weak exchange between paramagnetic sites. The chain segmentation model results in the same behavior but is due to the presence of paramagnetic, odd length segments. The probability of the occurrence of the weakly interacting spin subsystems required for sub-Curie law behavior is negligibly small in two and three dimensional systems.[18] This behavior strongly suggests a one dimensional exchange pathway.

After subtraction of the sub-Curie law tail, the susceptibility rises from zero as the temperature is increased and displays a broad maximum at about 300 K. Attempts were made to fit the susceptibility to simple spin pairing models.[17,20] Neither S=1 nor S=1/2 models could satisfactorily fit the data. The low temperature sub-Curie law tail and broad maxima in the susceptibility both strongly suggest one-dimensional chain behavior. It is not immediately apparent, however, whether an effective spin of 1 or 1/2 is more appropriate.

DeArmond, Hanck and co-workers have suggested, based on EPR data, that the two electrons in the HOMO of $[Ru(bpy)_3]^0$ are localized in the ligand π^* orbitals ($L\pi^*$) when the molecule is in solution and in the two metal $d\sigma^*$ orbitals in the solid state.[10-12] They make the assignment in the solid state based on a choice of the three configurations they see as most likely, assuming no significant orbital mixing; $(L_1\pi^*)^1(L_2\pi^*)^1$, $(L_1\pi^*)^1(d_1\sigma^*)^1$, and $(d_1\sigma^*)^1(d_2\sigma^*)^1$. They rule out the first configuration based on its lack of a reasonable mechanism to account for a large g-shift, from 1.995 (solution) to 2.23 (solid). The second configuration, while accounting for the broad (250 gauss) signal in the solid state, is dismissed; it was concluded that spin-spin and spin-orbit coupling would have an uncertain effect on the EPR spectrum. They argue that the third, metal based, configuration is correct since the isoelectronic Ni(II) species with strong exchange interactions display similar g-values and linewidths. The change

from a ligand based HOMO in solution to a metal based one in the solid, they conclude, is due to the small energy separation between the ligand π^* and the metal $d\sigma^*$ orbitals and to solvent stabilization of former. This would mean that $[Ru(bpy)_3]^o$ would be best represented as a S = 1 species in the solid state.

The conclusions of DeArmond, Hanck and co-workers yield a d^8 ground-state configuration. A pseudooctahedral environment is expected, leading to a $^3A_{2g}$ single-ion ground term and quenching of the orbital angular momentum. The general spin Hamiltonian, assuming a one-dimensional chain and neglecting all terms except single ion and nearest neighbor interactions, would be

$$H = H_{zee} + H_{D} + H_{HDVV} + H_{D\cdot M} + H_{A} + H_{bi} \qquad (2)$$

or

$$H = \sum_i (g_i \beta \hat{S}_i \vec{H} + \hat{S}_i \bullet D \bullet \hat{S}_i - 2J_{i,i+1}\hat{S}_i \bullet \hat{S}_{i+1} + D_{i,i+1} \bullet [\hat{S}_i \times \hat{S}_{i+1}] + \hat{S}_i \bullet \Gamma_{i,i+1} \bullet \hat{S}_{i+1} + j_{i,i+1}(\hat{S}_i \bullet \hat{S}_{i+1})^2) \qquad (3)$$

where the terms represent the field dependent Zeeman perturbation, the local distortion, the Heisenberg-Dirac-Van Vleck isotropic exchange, the Dzyaloshinsky-Moriya antisymmetric exchange, the anisotropic exchange, and the biquadratic splitting respectively.[17] The high temperature at which the maximum in susceptibility is reached strongly suggests that the isotropic exchange term dominates. The biquadratic splitting only affects the excited-state terms of an exchange-coupled ground state singlet; since these excited states are only populated at rather high temperatures in this system, kT is expected to be much larger than the interaction parameter. The magnitude of the anisotropic exchange can be approximated by $(1 - 2/g)^2 J$.[17] This interaction, using g = 2.23, is approximately 1% of the isotropic exchange and thus is negligible at high

temperatures. The antisymmetric exchange is similarly negligible, typically dominated even by the anisotropic exchange.[20] Local anisotropy is typically on the order of a few Kelvin. Neglecting the contributions of these terms should not significantly affect the determination of the isotropic exchange interaction if only the high temperature data are included in the fitting procedure.

The resulting Hamiltonian from the above analysis is simply that of a linear-chain Heisenberg antiferromagnet (LCHA). The temperature dependence of the susceptibility of LCHA's has not been solved as a closed form analytical expression, except in the case of the classical spin ($S = \infty$) in zero magnetic field.[21] Extrapolations of infinite chain behavior from finite size ring calculations have been published for the case of $S = 1/2$.[22] The results of these calculations are qualitatively similar; the susceptibility displays a broad maximum and a non-zero intercept at 0 K. For a number of years, it was assumed that LCHA's with other spin values would be qualitatively similar as well. It was further assumed that the quantitative behavior would vary systematically with spin, excluding the classical spin. More recently, Haldane[23] has published a conjecture which states that half-integer spin systems should be qualitatively similar to the spin 1/2 case but that all even integer spin systems will diverge from this behavior near T=0. Half-integer systems exhibit a finite zero K susceptibility, arising from their lack of an excitation gap between the ground state singlet and triplet excited states.[24] On the other hand, integer systems, according to Haldane, should have a gap in their energy spectra resulting in a susceptibility which vanishes exponentially as T approaches 0. The existence of the Haldane gap has been confirmed in the S=1 case by both experimental and numerical methods.[25,26]

The temperature dependence of the susceptibility of S=1 LCHA's has been studied by finite ring extrapolation methods.[27] The study did not extend down to temperatures low enough to observe the effects of the Haldane gap.[28] The results have been fit by the analytical expression[29]

$$\chi = \frac{N\beta^2 g^2}{kT}\left[\frac{2+0.0194X+0.777X^2}{3+4.346X+3.232X^2+5.834X^3}\right] \qquad (4)$$

where $X = 2|J|/kT$, and is valid for $X \leq 5$ (note that the factor of 2 difference in the definition of X between this paper and the published expression derives from the conventions used in the formulation of the respective Hamiltonians). This expression has been successfully used to fit the temperature dependence of S = 1 ACHA's which show the effects of the Haldane gap.[29,30] Non-linear least squares fits of this expression to the $[Ru(bpy)_3]^o$ data proved to be unsatisfactory. Even fitting only data below $X \approx 1$ resulted in systematic errors as shown in Figure 4. It is clear that the model is an inappropriate one with which to describe the magnetic properties of $[Ru(bpy)_3]^o$.

An alternative model of $[Ru(bpy)_3]^o$ is as a system with two ligand-localized unpaired electrons. Voltammetric results support such an assignment.[31] However, the electrons would probably have significant $d\sigma^*$ character as suggested by DeArmond, Hanck and Wertz.[32] A one dimensional chain structure could result from an antiferromagnetic intermolecular interaction of the ligand π^* orbitals. Thus, the $[Ru(bpy)_3]^o$ system could be considered one in which each electron is coupled both intramolecularly to the electron on one of the other ligands and intermolecularly to an electron on a neighboring molecule's ligand. This model is equivalent to that of a spin-1/2 alternating linear chain Heisenberg antiferromagnet (ALCHA), whose Hamiltonian (excluding the Zeeman term) is

$$H = -2J\sum_{i=1}^{n/2}[\hat{S}_{2i}\hat{S}_{2i-1} + \alpha\hat{S}_{2i}\hat{S}_{2i+1}] \qquad (5)$$

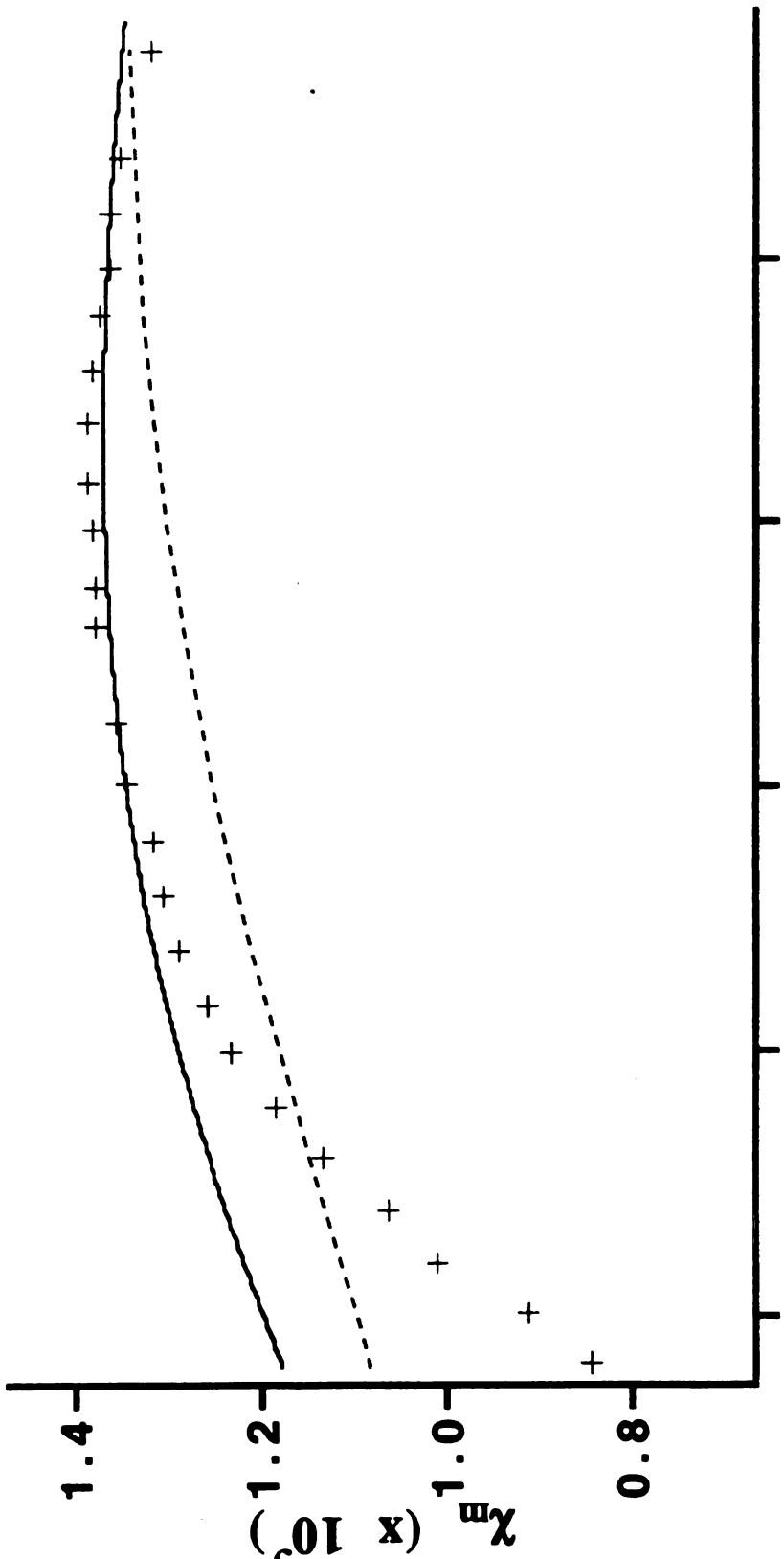

Figure 4. "Best" fits of the high temperature susceptibility data to a S=1 chain model (equation 4). The solid line was generated from a fit of the data between 239 to 390 K, showing systematic errors even over a limited temperature range. Theoretically, the line should fit the entire temperature range shown, however, as demonstrated by the dashed line, fitting this larger temperature range resulted in a much poorer fit due to the inability of the model to incorporate the necessary curvature.

where J is the exchange parameter between a spin and one of its nearest neighbors along the chain and αJ is the exchange parameter between it and its other nearest neighbor. Although this model has not been solved analytically, infinite limit extrapolations of numerical calculations of finite size rings and convenient fitting expressions based on these calculations have been published.[33] The published expression is

$$\chi_m = \frac{Ng^2\beta^2}{kT}\left[\frac{[A(\alpha)]+[B(\alpha)]X+[C(\alpha)]X^2}{1+[D(\alpha)]X+[E(\alpha)]X^2+[F(\alpha)]X^3}\right] \qquad (6)$$

where $X=|J|/kT$ and is valid for $X<2$. The constants A through F are given functions[33] of α and take on values which depend on whether α is larger than or less than 0.4. Nonlinear least squares fitting of the susceptibility data resulted in excellent agreement (see Figure 3) with α =0.40(3), $|J|/k$=238(3) K and g=2.20(4). Note the excellent agreement between the fitted magnetogyroscopic ratio (g) and that determined by DeArmond and co-workers from EPR spectra.[12] The intermolecular exchange parameter, $|J|/k$, refers to the intermolecular coupling while the intramolecular coupling (between the two ligand localized electrons on each $[Ru(bpy)_3]^0$ is αJ. This assignment is likely since, if the stronger coupling were intramolecular, the random distribution of exchange parameters required by the REHAC model would not be present and intramolecular spin dimerization as temperature decreased would result in a singlet ground state even for the chain ends. Therefore, the stronger coupling must be intermolecular in order to give rise to the observed sub-Curie tail.

In solution, $[Ru(bpy)_3]^0$ EPR results have been interpreted in terms of the spatially isolated orbital model.[10-12,32,34] Within this model, the ligand π^* orbitals are electronically isolated and filled independently upon successive reduction. DeArmond, Hanck and co-workers suggested that loss of solvent stabilization of these orbitals in the solid state results in the reordering of the orbitals such that the metal $d\sigma^*$ orbitals become the HOMO orbitals. They based their assignment of metal based HOMOs and

the resulting S=1 configuration on the assumption that there was no significant orbital mixing. This was probably not a good assumption, especially in light of the small energy separation between the metal $d\sigma^*$ and ligand π^* orbitals.[35,36] The loss of solvent stabilization may be responsible for reducing the energy gap between the metal $d\sigma^*$ and ligand π^* orbitals, but the susceptibility data presented here strongly suggest that the orbitals are not reordered. The observed g shift is probably due to additional $d\sigma^*$ character introduced into the ligand localized orbitals as they suggested in a later review.[32] This could be due to the loss of solvent stabilization resulting in narrowing of the energy gap or to crystal lattice interactions. The broad EPR lines are due to the strong spin-spin coupling in the solid state, a mechanism which can be especially effective in one-dimensional systems.[37,38] Thus, $[Ru(bpy)_3]^o$ is best considered under the spatially isolated orbital model even in the solid state.

The conductivity along the long axis (the 6-fold symmetric axis) of the crystal is displayed in Figures 5 and 6. It about two orders of magnitude less conductive than n-doped silicon at room temperature. Its conductivity increases with temperature as one might expect for a semiconductor. Fitting the data with a conventional semiconductor expression

$$\sigma = \sigma_0 \exp(-E_a/2kT) \qquad (7)$$

where E_a is the bandgap and all other symbols have their usual meanings, proved to be highly unsatisfactory, as shown in Figure 5 ($E_a/2$=0.029(1) eV). We therefore fit the data by the more general expression

$$\sigma = \sigma_0 \exp[-(T_0/T)^n] \qquad (8)$$

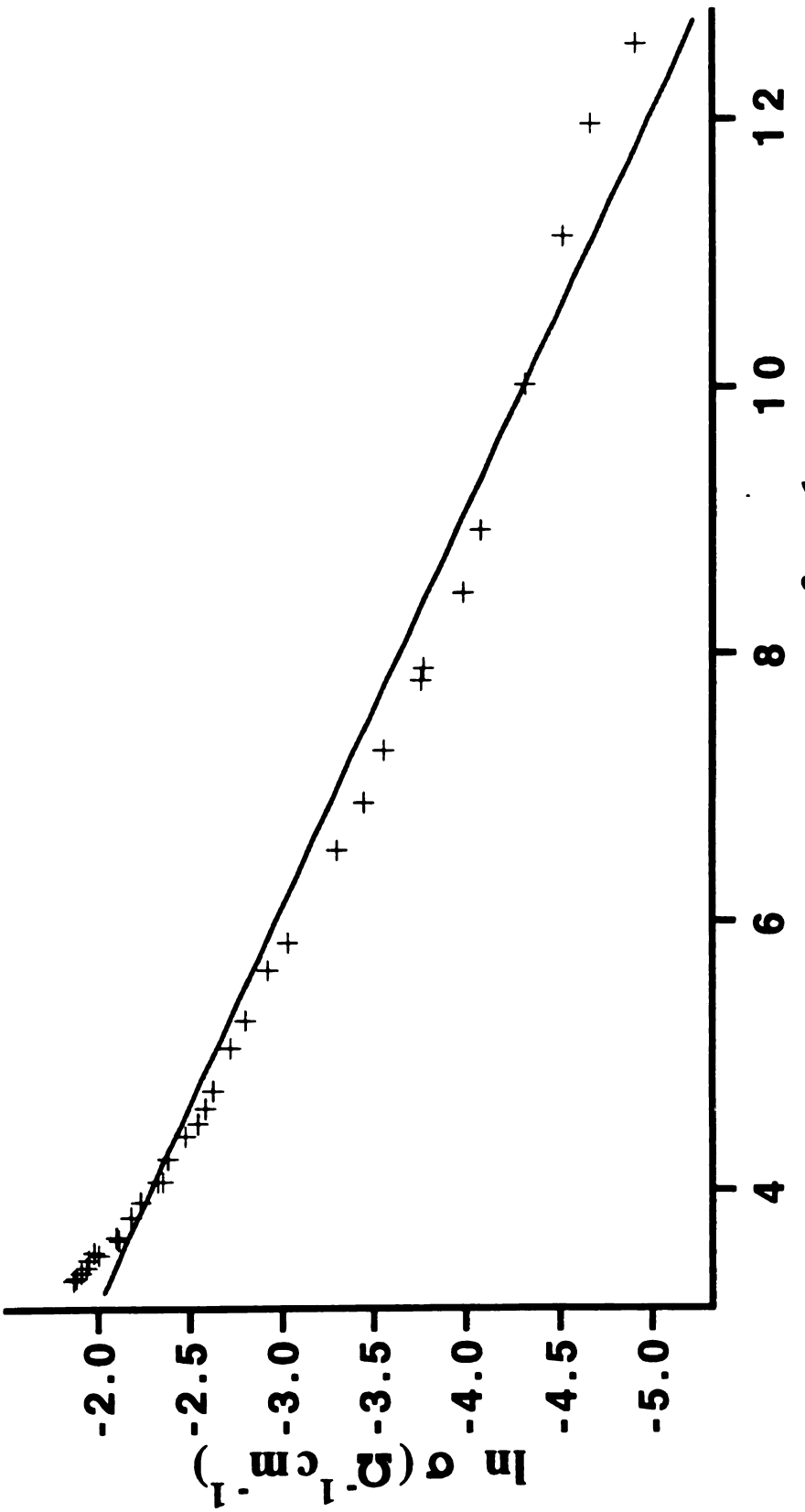

Figure 5. "Best" fit (solid line) of the temperature dependence of the conductivity with a conventional semiconductor expression (equation 7).

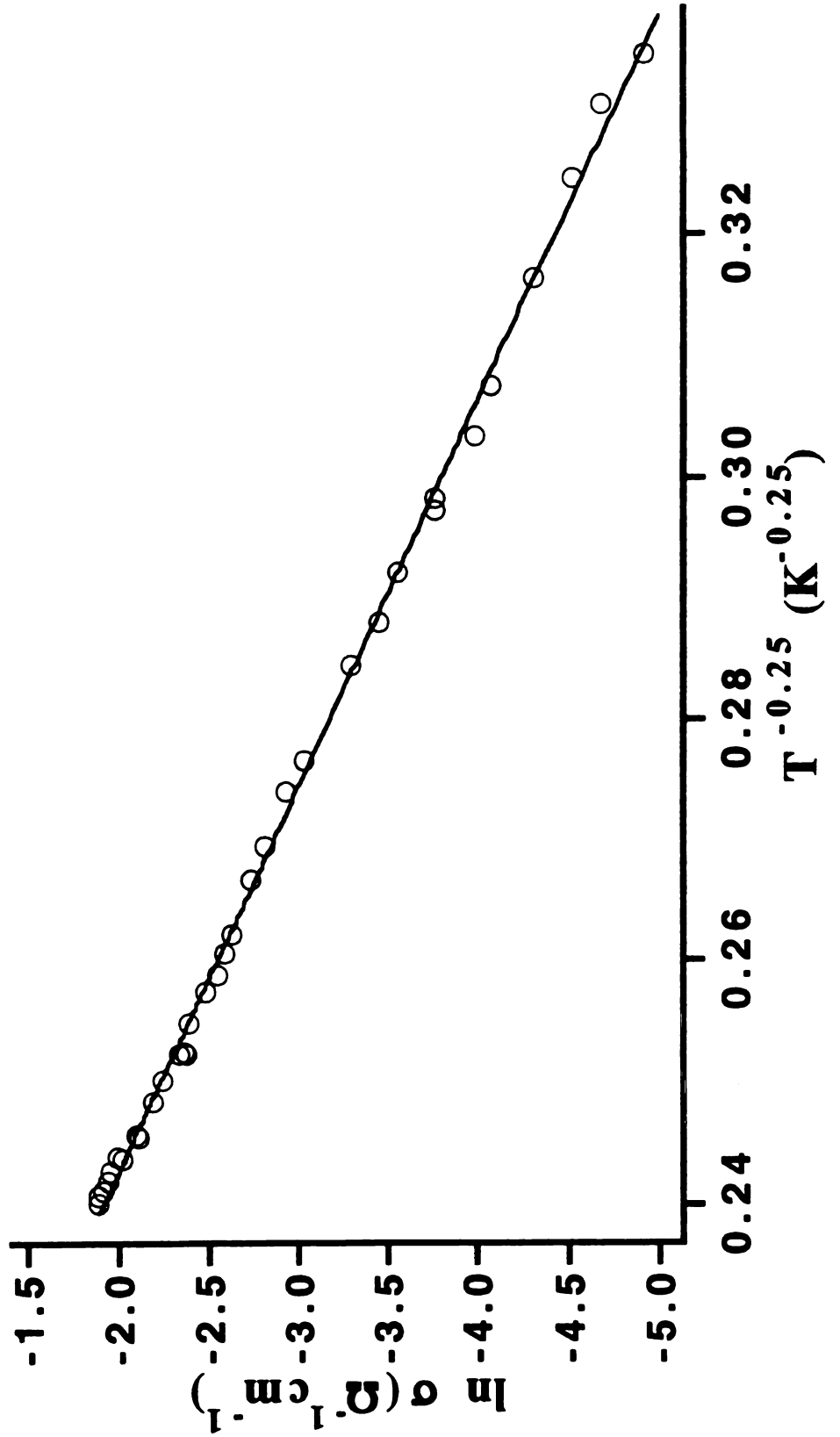

Figure 6. Fit (solid line) of the temperature dependence of the conductivity to a 3-D variable range hopping mechanism (see text).

where the definition of T_o depends on the conduction mechanism and the value of $0 < n < 1$ is indicative of this mechanism. This resulted in an excellent fit with fitting parameters of $\sigma_o = 4(1) \times 10^3\ \Omega^{-1}\ cm^{-1}$, $T_o = 5.44(5) \times 10^7$ K and n = 0.19(4). The value of n suggests that the conduction is due to a variable range three dimensional hopping mechanism.[39,40] In this model, the theoretical value of n is 0.25 and T_o is inversely proportional to the localization length of the electronic states responsible for the conductivity. This model was derived for materials with localized states near the Fermi level which are randomly distributed in energy and space. The fit of the data by it and our repeated failures to solve the structure of these seemingly well formed crystals by single crystal x-ray diffraction imply a certain degree of disorder. Fitting the data with the value of n held constant at the theoretical value of 0.25 results in an excellent fit with $\sigma_o = 278(3)\ \Omega^{-1}\ cm^{-1}$ and $T_o = 9.75(7) \times 10^5$ K as shown in Figure 6.

Hopping conductivity could result from jumps from occupied to unoccupied $L\pi^*$ and/or metal $d\sigma^*$ orbitals. Hopping between the ligands is expected; in solution fast electron hopping is responsible for broadening of the EPR line.[12] In the solid state, the alternating nature of the exchange path results in a splitting of the half-filled $L\pi^*$ band, creating a gap about the Fermi level with a filled lower band and an unfilled upper band.[41] The hopping mechanism invoked to explain our results assumes that this gap is much larger than kT and that the disordered localized states (the unoccupied $L\pi^*$ or $d\sigma^*$ orbitals) are near the Fermi level. Both conditions seem reasonable.

The difference in the dimensionality of the hopping conduction and the magnetic exchange paths is in no way contradictory. As stated above, the hopping is probably not between occupied sites in the chain. Even if the hopping conductivity is largely one-dimensional, if the total distance of all interchain hops is comparable to the length of a single chain the system would behave as a 3-D system.[39]

Within the ALCHA model of $[Ru(bpy)_3]^o$, we can speculate upon the nature of the disorder which is indicated by both our single crystal x-ray and conductivity results.

Localization of the two reducing electrons in two of the ligands should break the threefold symmetry, resulting in two of the three ligands having bond lengths which are shorter than the third. A similar reduction of molecular symmetry was seen in the case of cryptatium.[7] Such asymmetry might result in disorder in the crystal as the molecules may pack with occasional random orientation of the three ligands.

III.D Conclusions

The results of static magnetic susceptibility measurements of $[Ru(bpy)_3]^0$ are consistent with a model of ligand localization of the reductant electrons, although these HOMO orbitals are probably hybrids with significant metal $d\sigma^*$ character. While we could not solve the structure through single crystal crystallography, it seems likely that it can be characterized as "complexed" ruthenium cations whose ligand localized reductant electrons are moderately antiferromagnetically coupled. This interaction is probably mediated by the cation's e_g^* orbitals since the ligand-ligand angle is expected to be ~ 120^o, allowing for a nonorthogonal component of the overlap through the metal $d_{x^2-y^2}$ and d_{z^2} orbitals. These neutral molecules pack in close proximity, allowing for a strong intermolecular antiferromagnetic π^*-π^* overlap. This nearest neighbor interaction is unique so that each reductant electron is intermolecularly coupled strongly to but one other electron. Thus, the intra- and intermolecular interactions repeat through the lattice in a chainlike fashion, with, of course, breaks in the chain due to the occasional molecular misalignment.

Conductivity measurements with a 4-probe DC method show that the crystals are highly conducting along the needle axis. Conduction is probably through a variable-range three-dimensional hopping mechanism. It seems likely that the conduction path is composed of the empty $L\pi^*$ and/or metal $d\sigma^*$ orbitals.

This material represents another step toward the production of crystalline solids composed of "expanded atoms". The electrons released from the cation are localized in two of the bipyridine ligands rather than delocalized over the entire "complexant" so it does not truely represent an "expanded atom". It would be interesting to synthesize compounds in which all of the $L\pi^*$ orbitals were singly occupied. Delocalization of these electrons over the extended π^* orbital system would represent a bridge over the gap between electrides and alkali doped fullerenes.

III.E Acknowledgment

This research was supported by AFOSR Grant F49620-92-J-0523. We thank Rui H. Huang for his efforts in x-ray crystal structure determination. Eduardo Pérez-Cordero, Rosanna Buigas and Luis Echegoyen would like to thank the National Science Foundation (DMR-9119986) for generous support.

III.F References

(1) Pederson, C. J. *J. Am. Chem. Soc.* **1967**, *89*, 7017.

(2) Dietrich, B.; Lehn, J.; Sauvage, J. P. *Tetrahedron Lett.* **1969**, *34*, 2885.

(3) Wagner, M. J.; Dye, J. L. *Annu. Rev. Mater. Sci.* **1993**, *23*, 223.

(4) Lehn, J. M. *Pure & Appl. Chem.* **1977**, *49*, 857.

(5) Hebard, A. F.; Rosseinsky, M. J.; Haddon, R. C.; Murphy, D.; Glarum, S. H.; Plastra, T. T. M.; Ramirez, A. P.; Kortan, A. R. *Nature* **1991**, *350*, 600.

(6) Bensebaa, F.; Xiang, B.; Kevan, L. *J. Phys. Chem.* **1992**, *96*, 6118.

(7) Echegoyen, L.; DeCian, A.; Fischer, J.; Lehn, J. *Angew. Chem. Int. Ed. Engl.* **1991**, *30*, 838.

(8) Rodriguez-Ubis, J.; Alpha, B.; Plancherel, D.; Lehn, J. *Helv. Chim. Acta* **1984**, *67*, 2264.

(9) Echegoyen, L.; Xie, Q.; Perez-Cordero, E. *Pure Appl. Chem.* **1993**, *65*, 441.

(10) Morris, D. E.; Hanck, K. W.; DeArmond, M. K. *Inorg. Chem.* **1985**, *24*, 977.

(11) Moris, D. E.; Hanck, K. W.; DeArmond, M. K. *J. Am. Chem. Soc.* **1983**, *105*, 3032.

(12) Motten, A. G.; Hanck, K. W.; DeArmond, M. K. *Chem. Phys. Lett.* **1981**, *79*, 541.

(13) Biner, M.; Bürgi, H.; Ludi, A.; Rohr, C. J. *J. Am. Chem. Soc.* **1992**, *114*, 5197.

(14) Perez-Cordero, E.; Buigas, R.; Brady, N.; Echegoyen, L.; Arana, C.; Lehn, J.-M. *Helv. Chim. Acta* **in press.**

(15) Papaioannou, J.; Dye, J. L. *Rev. Sci. Instrum.* **1988**, *59*, 496.

(16) Carlin, R. L. *Magnetochemistry*; Springer-Verlag: Berlin Heildelberg, 1986.

(17) O'Connor, C. J. *Prog. Inorg. Chem.* **1982**, *29*, 203.

(18) Bulaevskii, L. N.; Zvarykina, A. V.; Karimov, Y. S.; Lyubovskii, B. B.; Shchegolev, I. F. *Sov. Phys. JETP* **1972**, *35*, 384.

(19) Soos, Z. G.; Bondeson, S. R. *Mol. Cryst. Liq. Cryst* **1982**, *85*, 19.

(20) Kahn, O. *Molecular Magnetism*; VCH Publishers, Inc.: New York, NY, 1993.

(21) Fisher, M. E. *Amer. J. Phys.* **1964**, *32*, 343.

(22) Bonner, J. C.; Fisher, M. E. *Phys. Rev.* **1964**, *135*, A640.

(23) Haldane, F. D. M. *Phys. Lett.* **1983**, *93 A*, 464.

(24) Anderson, P. W. *Phys. Rev.* **1952**, *86*, 694.

(25) Yamamoto, S.; Miyashita, S. *Phys. Rev. B* **1993**, *48*, 9528.

(26) Deisz, J.; Jarrell, M.; Cox, D. L. *Phys. Rev. B* **1993**, *48*, 10227.

(27) Weng, C. Y. Ph. D. Thesis, Carnegie Institute of Technology, 1968.

(28) Bonner, J. C. In *Magneto-Structural Correlations in Exchange Coupled Systems*; R. D. W. e. al., Ed.; D. Reidel Publishing Company: New York, 1985; pp 157-205.

(29) Meyer, A.; Gleizes, A.; Girerd, J. J.; Verdaguer, M.; Kahn, O. *Inorg. Chem.* **1982**, *21*, 1729.

(30) Avenel, O.; Xu, J.; Xia, J. S.; Xu, M.-F.; Andraka, B.; Lang, T.; Moyland, P. L.; Ni, W.; Signore, P. J. C.; van Woerkens, C. M.; Adams, E. D.; Ihas, G. G.; Meisel, M. W.; Nagler, S. E.; Sullivan, N. S.; Takano, Y.; Talham, D. R.; Goto, T.; Fujiwara, N. *Phys. Rev. B* **1992**, *46*, 8655.

(31) Saji, T.; Aoyagui, S., J. *Electroanal. Chem. Interfacial Electrochem.* **1975**, *63*, 31.

(32) DeArmond, K. M.; Hanck, K. W.; Wertz, D. W. *Coord. Chem. Rev.* **1985**, *64*, 65.

(33) Hall, J. W.; Marsh, W. E.; Weller, R. R.; Hatfield, W. E. *Inorg. Chem.* **1981**, *20*, 1033.

(34) DeArmond, M. K.; Carlin, C. M. *Coord. Chem. Rev.* **1981**, *36*, 325.

(35) Van Houten, J.; Watts, R. *J. Am. Chem. Soc.* **1976**, *98*, 4853.

(36) Durham, B.; Walsh, J.; Carter, C.; Meyer, T. *Inorg. Chem.* **1980**, *19*, 860.

(37) Hennessy, M. J.; McElwee, C. D.; Richards, P. M. *Phys. Rev. B* **1973**, *7*, 930.

(38) Dietz, R. E.; Merritt, F. R.; Dingle, R.; Hone, D.; Silbernagel, B. G.; Richards, P. M. *Phys. Rev. Letters* **1971**, *26*, 1186.

(39) Mott, N. F. *Phil. Mag.* **1969**, *19*, 835.

(40) Brenig, W.; Dohler, G. H.; Heyszenau, H. *Phil. Mag.* **1973**, *27*, 1093.

(41) Peierls, R. E. *Quantum Theory of Solids*; Oxford University Press: London, 1955.

IV CONCLUSIONS AND SUGGESTIONS FOR FUTURE WORK

In Chapter 1, evidence for correlated large amplitude "merry-go-round" motions of crown ether complexants in alkalides was presented. It is certainly reasonable to assume that the same type of motion takes place in crown ether electrides and perhaps aza-crown alkalides and electrides. A more complete understanding of these motions can be achieved by completing the inelastic neutron scattering experiments which I initiated with Dr. Dan Neumann at the National Institute of Standards and Technology (NIST). We have already completed measurements and spectral analysis of protonated $Cs^+(18\text{-crown-}6)_2e^-$. This electride was chosen because it shows a very interesting order/disorder transition which may be associated with crown motions as outlined in Chapter 2. Measurements of both the low temperature (ordered) and high temperature (disordered) phases have been completed. Measurements on the electride made with deuterated crowns will allow us to move closer to the elastic peak and further characterize the correlated molecular rotations of the crown ethers as well as confirm the higher momentum spectral assignments. Single crystal measurements will allow the full orientational analysis of the motions.

Another project which would build on the work of this thesis is the study of molecular motions in model salts which I started but did not have time to complete. $Cs^+(15\text{-crown-}5)_2I^-$ shows evidence of a first order phase transition at ~ 240 K as shown in Figure 1, in which its NMR powder pattern reveals a change in the symmetry of the chemical shift anisotropy from non-axial to nearly axial. $Cs^+(18\text{-crown-}6)_2I^-$ shows a transition from a single peak spectrum to a two peak spectrum (Figure 2). Understanding these easily handled compounds may lead to a better understanding of alkalides and electrides.

In Chapter 2, the physical characterization by NMR, static magnetic susceptibility, DSC, DC conductivity and impedance spectroscopy of four of the five electrides with

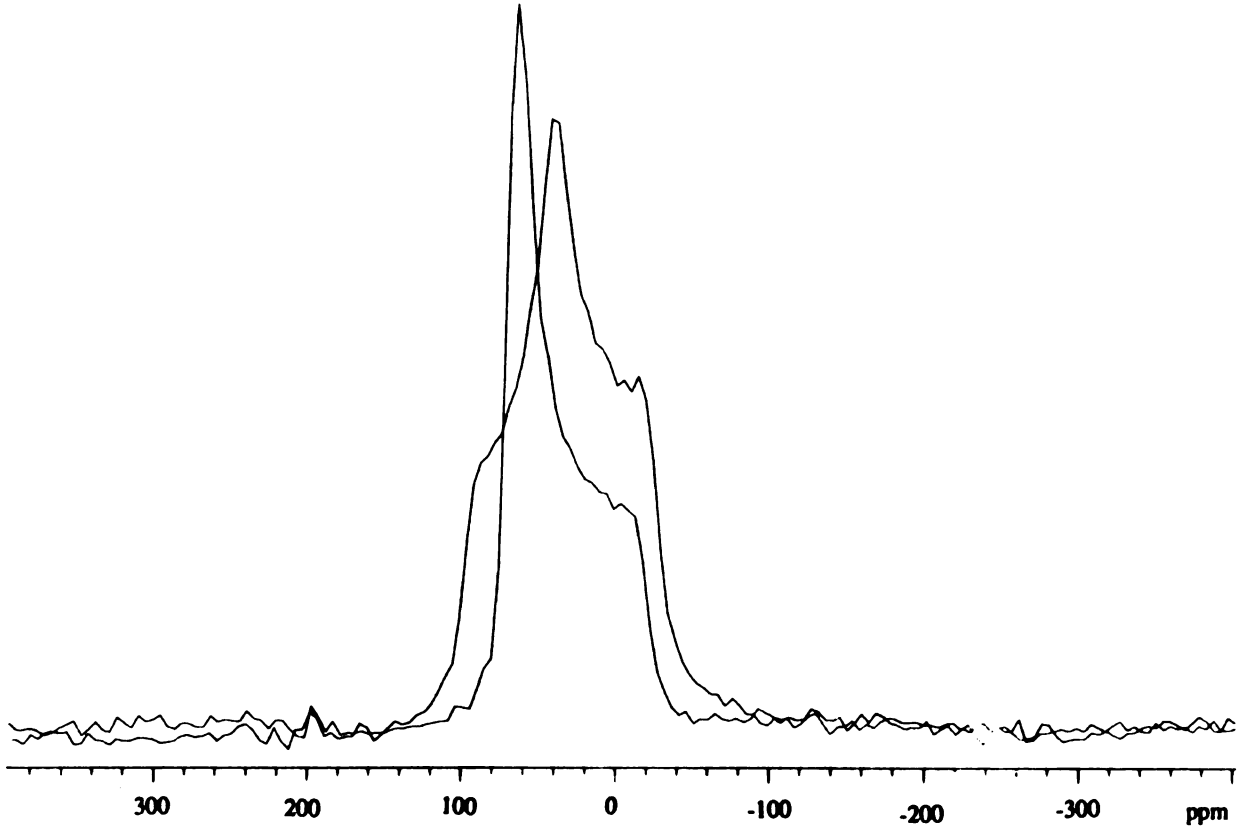

Figure 1. ^{133}Cs NMR powder patterns for $Cs^{+}(15\text{-crown-}5)_2I^{-}$. The nearly axial pattern was obtained at 243 K. The non-axial pattern was obtained at 233 K, however the transition between the two phases is sharp and fast, a similar spectrum could be obtained at ~235 K.

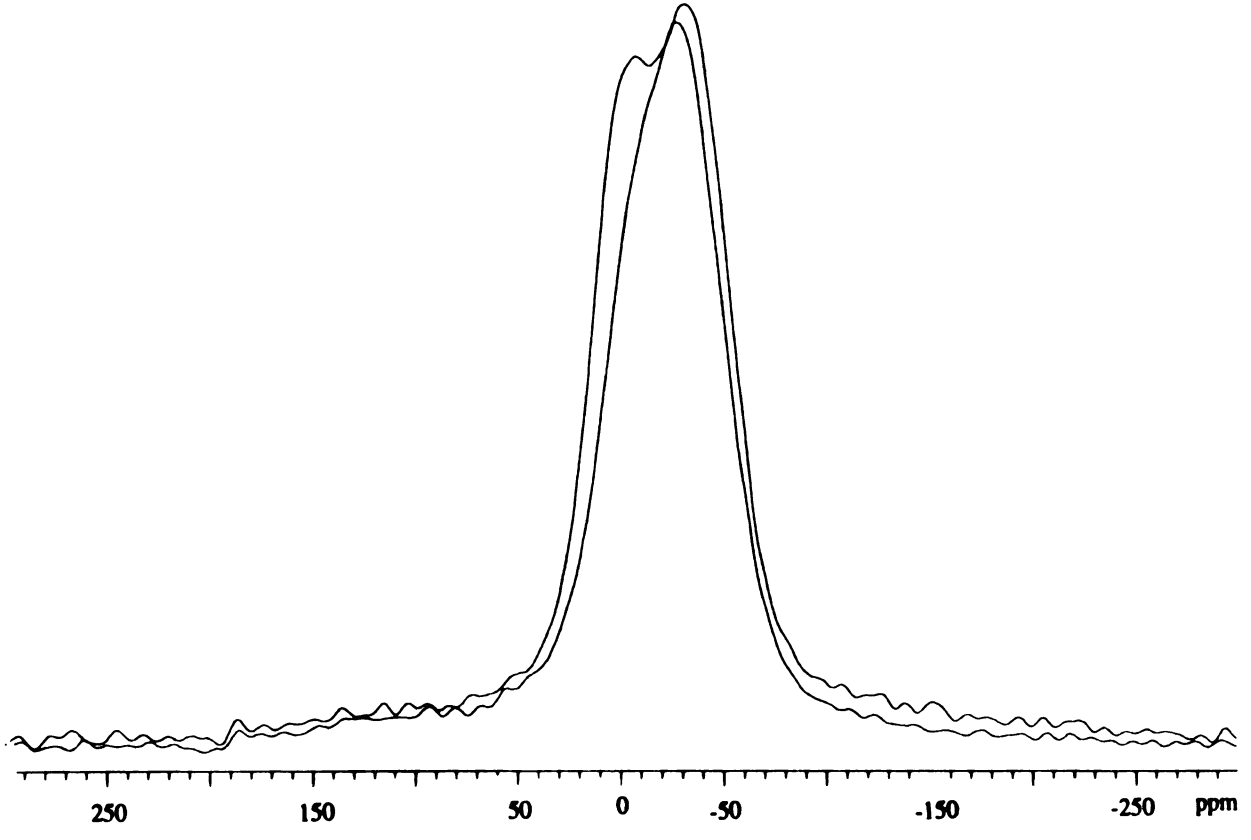

Figure 2. ^{133}Cs NMR powder patterns for $Cs^{+}(18\text{-crown-6})_2I^{-}$. The seemingly single peak spectrum was obtained at 202 K. A second peak appears as a shoulder and shifts paramagnetically with decreasing temperature. This shoulder is apparent in the superimposed spectrum which was obtained at ~194 K.

known crystal structures was presented. Correlations between the cavity and channel structure of these electrides and their magnetic and electrical properties were drawn. From this study, it can be concluded that in order to rationally engineer desired properties into an electride, one must be able to predict and control the cavity and channel structure. To further the understanding of electrides which Chapter 2 has established, I have initiated a collaboration with Dr. Julie Borchers at NIST to study the magnetic structure of Cs^+(18-crown-6)$_2e^-$. If the model of Cs^+(18-crown-6)$_2e^-$ established in Chapter 2 is correct, i.e. that it is a linear chain Heisenberg antiferromagnet, we should, in principle, be able to study the spin wave excitations. In addition, neutron diffraction can detect any 3-dimensional magnetic ordering or spin-Peierls transitions and equipment is available to cool down to the millikelvin regime, if necessary, in order to find either. Redetermination of the crystal structure at these temperatures by neutron diffraction will allow the mapping of the magnetic lattice onto the atomic lattice, possible providing irrefutable proof of the trapping locations of the excess electrons in electrides. Short of that goal would be to measure the form factor of the trapped electrons and from that derive the extent of the wave function in three dimensions which could then be compared to the trapping sites to check for consistency with the cavity and channel model of electrides. This type of study (and single crystal susceptibility measurements) should also be done with Cs^+(15-crown-5)$_2e^-$ and Li^+(C211)e^- due to their weaker interactions and the unique magnetic properties of the latter electride.

In order to fully utilize the abilities of neutron scattering and diffraction techniques, large single crystals of Cs^+(18-crown-6)$_2e^-$ synthesized with deuterated crown ethers must be grown. I have developed the techniques with which these crystals can be grown. Growing Cs^+(18-crown-6)$_2e^-$ by slow solvent evaporation techniques sometimes results in crystals on the millimeter scale. These crystals can be used as seed crystals in a saturated solution to grow even larger crystals. However, the extreme sensitivity of electrides has prevented researchers from using seeded solutions to grow alkalide and electride crystals. I

have designed specialized glassware to overcome these difficulties; a schematic of the crystallization cell is shown in Figure 3. The cell features two reaction vessels separated by a breakseal; this allows one to make a saturated solution in one vessel without exposing the seed crystal in the other to solvent. The use of the cell is simple; one loads polycrystalline material into chamber 1 (through the stopcock with a funnel, the sidearm is removed after cleaning) and the seed crystal into chamber 2 (a ladle made of aluminum foil filled with a small pool of liquid nitrogen and the crystal works well to place the crystal in the chamber). Of course, this must be done in a glove bag, fully immersing the cell in liquid nitrogen to ensure that the seed crystal does not undergo thermal disordering and to prevent decomposition of either material. Chamber 2 can be sealed with its own stopcock after evacuation of the entire cell to ~ 10^{-6} torr, allowing one to add solvent (dimethyl ether) and co-solvent (TMA) to make a saturated solution in chamber 1. After allowing time to ensure that the saturated solution (at -78° C) is in equilibrium, one can simply break the seal with the magnet (enclosed in glass) and pour it onto the seed crystal. Preferential growth of the electride on the seed crystal then ensures that a large crystal is obtained. Pouring off the last few milliliters of solvent left after the slow reduction, drying and washing the crystal with co-solvent (recommended only if a thin coating of complexant on the outer surface of the crystal is detrimental to the envisioned application) can then be followed by crystal recovery in a glovebag through the large side arm. This procedure can be done recursively using the recovered crystal as the seed if it is not large enough for the desired application. I have tested these techniques twice using a number (6-10) of small (<< $1mm^3$) crystals, each time resulting in preferential seed growth to yield crystals as large as ~ 2 x 2 x 3 mm in a period of a few days. With luck, larger starting seeds, or recursive seeding, it should be possible to grow centimeter scale crystals by this technique. This technique should be applicable to all alkalides and electrides, making the study of their single crystal properties more generally feasible.

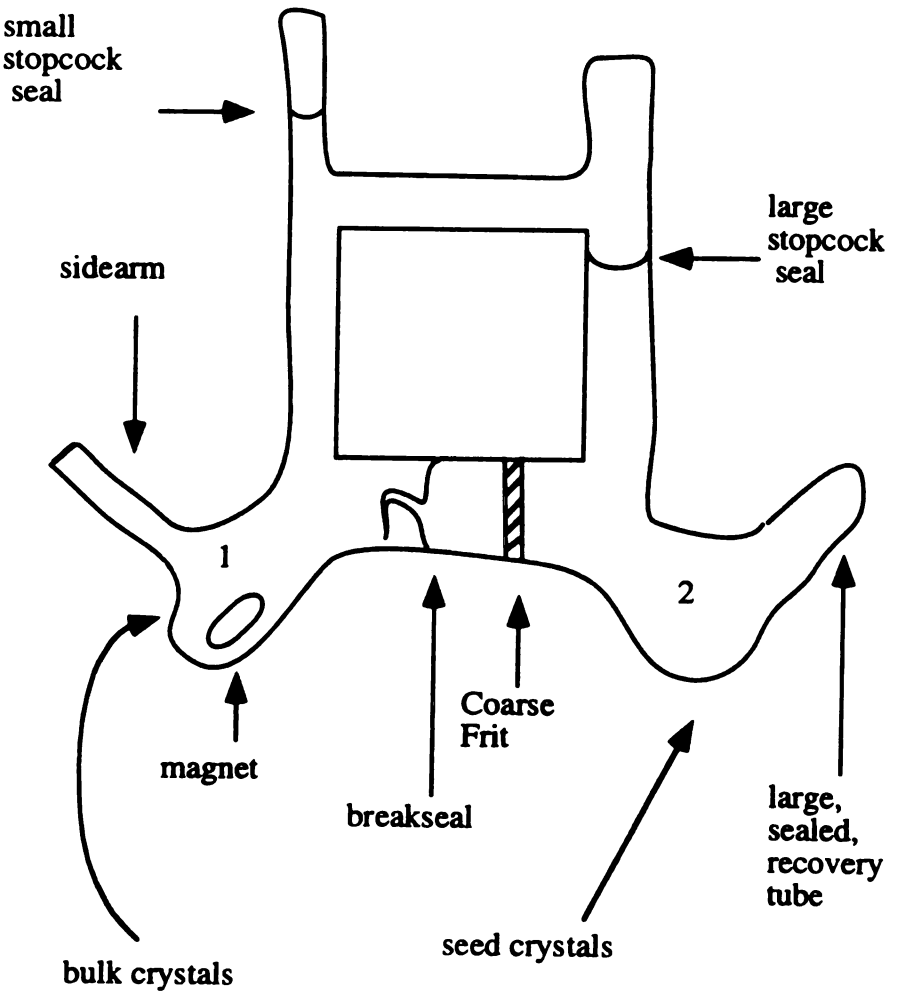

Figure 3. Recrystallization cell.

The final chapter of this thesis is the first study to be completed within a new thrust area of this laboratory; that is, production and characterization of "pseudo-buckyballs". This class of materials is comprised of electropositive metals complexed by complexants with low lying π^* states into which the released electron can delocalize, similar to the way alkali metals donate an electron to the π^* orbitals of "buckyballs". When the electrons are fully delocalized over the complexant, the material could be considered "expanded atoms" and provide a link between electrides and alkali metal doped buckyballs. Judging from the properties of the extreme members of this class of materials, they promise to be novel materials. The study of $[Ru(bpy)_3]^o$ is a first step towards achieving the goal of the production of these "expanded atoms". The study presented in chapter 3 should be followed by a similar study of the related compound $[Os(bpy)_3]^o$. Both preliminary four-probe conductivity measurements (which I made) and published physical characterization (see references and in chapter 3) indicate that the physical properties of the iron analog are very similar to those of $[Ru(bpy)_3]^o$. On the other hand, the energy separation between ligand π^* and the metal $d\sigma^*$ orbitals is much larger in the osmium analog. This promises to limit, or even virtually eliminate, the $d\sigma^*$ mixing in the HOMO's, perhaps leading to more delocalization of the HOMO electrons and perhaps itinerant behavior. This would make the material an "expanded metal".

Alkalides, electrides and the closely related "pseudo-buckyballs" are fascinating materials which have seen only limited exploration over a very few years. They are much like liquid crystals in their high temperature molecular dynamical behavior. Their electrical properties range from insulating to highly conducting by a hopping mechanism, not unlike conductive polymers. Their magnetic properties range from uncorrelated to strongly antiferromagnetic with low dimensional coupling, competing interactions and intriguing magnetic phase behavior such as spin-Peierls transitions. At the other end of this range of materials, alkali metal doped buckyballs, superconductivity has been observed. Because only a few of the vast number of possible materials of this class have been studied, it is

reasonable to expect that materials with even more exciting properties are awaiting discovery. With the present lack of research effort in this area, it truly represents one of the "Frontiers of Science". Such a wide open frontier reminds one of the great western United States before the land rush of the 1800's; an unlimited wealth of possibilities with few vying for the right to claim discovery.

BIBLIOGRAPHY

BIBLIOGRAPHY

(1) Edwards, P. P. *Adv. Inorg.Chem. RadioChem.* **1982**, *25*, 135.

(2) Pedersen, C. J. *J. Am. Chem. Soc.* **1967**, *89*, 7017.

(3) Dietrich, B.; Lehn, J.-M.; Sauvage, J. P. *Tetrahedron Lett.* **1969**, 2885.

(4) Wagner, M. J.; Dye, J. L. *Ann. Rev. Mat. Sci.* **1993**, *23*, 223.

(5) Wagner, M. J.; Dye, J. L. In *Molecular Recognition: Receptors for Cationic Guests*; G. W. Gokel, Ed.; Pergamon Press: in press; Vol. I.

(6) Dye, J. L. *Chemtracts-Inorganic Chemistry* **1993**, *5*, 243.

(7) Dawes, S. B.; Ward, D. L.; Huang, R. H.; Dye, J. L. *J. Am. Chem. Soc.* **1986**, *108*, 3534.

(8) Tehan, F. J.; Barnett, B. L.; Dye, J. L. *J. Am. Chem. Soc.* **1974**, *96*, 7203.

(9) Lehn, J. M. *Pure & Appl. Chem.* **1977**, *49*, 857.

(10) VanEck, B.; Le, L. D.; Issa, D.; Dye, J. L. *Inorg. Chem.* **1982**, *21*, 1966.

(11) Dye, J. L. *J. Phys. Chem.* **1980**, *84*, 1084.

(12) Dye, J. L. *J. Phys. Chem.* **1984**, *88*, 3842.

(13) Dye, J. L. *Pure & Appl. Chem.* **1989**, *61*, 1555.

(14) Singh, D. J.; Krakauer, H.; Haas, C.; Pickett, W. E. *Nature* **1993**, *365*, 39.

(15) Renscok, R.; Kaplan, T. A.; Harrison, J. F. *Phys. Rev. B.* **1993**, *submitted*,

(16) Rencsok, R.; Kaplan, T. A.; Harrison, J. F. *J. Chem. Phys.* **1993**, *98*, 9758.

(17) Overney, G.; Nagy, T. F.; Wagner, M. J.; Dye, J. L. , *to be submitted to Angew. Chem. Int. Ed. Engl.*